Optimised remote sensing methodologies for mapping and monitoring seagrass in southeastern Australian estuaries

James Patrick Simpson

A thesis submitted in fulfilment of the requirements for the degree of

Doctor of Philosophy

School of Geosciences

Faculty of Science

The University of Sydney

2026

This is to certify that the content of this thesis is my own work. This thesis has not been submitted for any other degree or purpose.

I certify that the intellectual content of this thesis is the product of my own work, and that all assistance received in preparing this thesis and all sources have been acknowledged.

Jamie Simpson

30 June 2025

Author attribution statement

Chapter 3 is published as Simpson, J., Bruce, E., Davies, K.P. and Barber, P., 2022. A blueprint for the estimation of seagrass carbon stock using remote sensing-enabled proxies. *Remote Sensing*, *14*(15), p.3572. https://doi.org/10.3390/rs14153572. Conceptualization, J.S., E.B., and K.P.D.; investigation, J.S.; resources, E.B., P.B. and K.P.D.; writing—original draft preparation, J.S.; writing—review and editing, J.S., E.B., P.B. and K.P.D.; visualization, J.S., E.B. and P.B.; supervision, E.B., P.B. and K.P.D.; project administration, E.B. and K.P.D.; funding acquisition, E.B. All authors have read and agreed to the published version of the manuscript.

Chapter 4 is published as Simpson, J., Davies, K.P., Barber, P. and Bruce, E., 2024. Mapping fine-scale seagrass disturbance using bi-temporal UAV-acquired images and multivariate alteration detection. *Scientific reports*, *14*(1), p.19083. https://doi.org/10.1038/s41598-024-69695-8. J.S., K.P.D., E.B. and P.B. conceived and designed the study. J.S. and K.P.D. collected data. J.S. prepared the data and ran all data analysis, and K.P.D. supervised data analysis. J.S. prepared the manuscript, and K.P.D., E.B., and P.B. edited the manuscript. E.B. acquired funding for the project. All authors contributed extensively to the work presented.

Chapter 5 is in preparation for submission. J.S. co-designed this study with K.P.D, E.B., and P.B. J.S. and K.P.D. collected data, and J.S. carried out all data analysis, with supervision from K.D. J.S. drafted the chapter, and K.P.D., E.B., and P.B. provided intellectual input on the text. E.B. acquired funding.

Chapter 6 is in preparation for submission. J.S. co-designed this study with K.P.D, E.B., and P.B. J.S. and K.P.D. collected data, and J.S. carried out all data analysis. J.S. drafted the chapter, and K.P.D., E.B., and P.B. provided intellectual input on the text. E.B. acquired funding.

In addition to the authorship attribution statements above, in cases where I am not the corresponding author of a published item, permission to include the published material has been granted by the corresponding author.

As supervisor for the candidature upon which this thesis is based, I can confirm that the authorship attribution statements above are correct.

No content produced by generative AI tools has been used in the preparation of this thesis.

This research was supported by an Australian Government Research Training Program (RTP) fee offset, and the Australian Research Council, grant number IC170100023.

Acknowledgements

This thesis would never have seen the light of day without the support I received from many people around me. First and foremost, I thank my primary supervisor, Associate Professor Eleanor Bruce, whose mentorship, guidance, and wealth of knowledge have proved indispensable throughout my candidature. More than this, Eleanor has endless energy, positivity, and passion for her work, qualities that (I like to think) she has imparted to me. I also thank my co-supervisors Dr Kevin Davies, who provided invaluable technical advice, while also being affable, supportive, and always up for a chat; and Dr Paul Barber, who has been a consistent source of valuable suggestions, encouragement, and reminders to look at things from another angle.

My thanks also go to the ARC Training Centre for CubeSats, UAVs and their Applications for funding my project, and my CUAVA colleagues for remaining interested as I prattled on about seagrass. Thanks especially to Iver Cairns for his leadership, and to Robert Steel and Reign MacMillan for their organisational skills.

My fieldwork was supported immensely by Jeremy Randle, who gave me the confidence to lead UAV field trips with ease. Various people from the School of Geosciences helped hugely with the administrative side of fieldwork, most notably Tom Savage and Dr Tiago Passos. Warren Brown and Ben Cuerel from Central Coast Council further assisted with work on my main field site. Fieldwork wouldn't have been possible at all without the people that volunteered to help me: Neil Berry, Matt Clements, Ellen Feltscheer, Gabija Posiunaite, Savannah McGuirk, Kate Whitton, and Yilin Wang.

Special thanks go to Dr Billy Haworth and Professor Elaine Baker, amazing mentors with whom I have been lucky to work throughout the last two years of my candidature.

I also thank my fellow PhD students, whose company made the whole experience far more enjoyable, especially Elizabeth Duncan, Nicola Perry, Alexandra Jones, Hannah Della Bosca, Elnaz Heidari, and Hojat Shirmard.

To my parents and my brother, for always being supportive of my academic pursuits, thank you from the bottom of my heart. To my partner Amy, for always being helpful, inspirational, smart, thoughtful, and fun to be around, thank you for being the best thing in my life. April, you're a good dog.

Abstract

Characterising the carbon sequestration capacity and economic value of seagrass has been challenging due to the geographical heterogeneity and temporal variability of seagrass beds. The ability to produce spatially dynamic and high-quality maps that represent biophysical characteristics of seagrass meadows is critical to accurately assessing their carbon sequestration potential. Field surveys can provide detailed information on biophysical indicators but cannot accurately capture differences within highly heterogeneous seagrass habitats. Remote sensing enables synoptic mapping of seagrass at meadow to regional scale.

The overarching objective of this research was to develop and assess new approaches that utilise emerging remote sensing techniques and technologies to detect biophysical characteristics of seagrass, with a focus on capturing spatial heterogeneity and temporal variability relevant to assessing seagrass carbon stock. The specific aims were to identify seagrass biophysical characteristics related to carbon stock that can be mapped with remote sensing, evaluate methods for mapping these characteristics with UAVs, assess the role of additional spectral bands, and upscale the detection of these characteristics to Sentinel-2 time-series data.

Selected biophysical characteristics of seagrass meadows were identified through a systematic review synthesising academic literature on drivers of seagrass carbon stock variation and seagrass remote sensing. Four key seagrass characteristics were identified: species, percent cover or above-ground biomass, spatial configuration, and temporal variability.

Detection of fine-scale, temporal changes in the spatial configuration of estuarine seagrass was explored using a novel application of Iteratively Reweighted Multivariate Alteration Detection (IR-MAD) an unsupervised change detection method not previously applied in coastal environments. This approach was effective for detecting changes in estuarine seagrass spatial configuration including anthropogenic disturbance events and subsequent seagrass recovery. Seagrass percent cover was mapped from UAV images using red-edge normalised difference index (RENDI), a spectral vegetation index using red-edge and red reflectance. This produced maps of

spatially variable percent cover at a very fine scale, characterising the spatial heterogeneity within the seagrass meadows. The RENDI methods developed and calibrated using ~5 cm resolution UAV images and detailed field quadrat sampling was then applied to Sentinel-2 time series. The upscaling of this method enabled a regional-scale study that mapped temporal variability of seagrass cover over nine NSW estuaries. This innovative approach to characterising seagrass percent cover variability provides new insight into geomorphic and geographical patterns in seagrass blue carbon potential.

The methods demonstrated here contribute to more accurate and detailed mapping and monitoring of ecologically and economically valuable seagrass ecosystems. This has important implications for producing spatially explicit models of seagrass carbon stock and sequestration capacity, allowing blue carbon financing to account for heterogeneous and variable seagrass beds.

Table of Contents

List of Figures

Chapter 1

Chapter 2

Chapter 3

Chapter 4

Chapter 5

Chapter 6

List of Tables

Chapter 2

Chapter 4

Chapter 5

Chapter 6

List of abbreviations

AGB	Above ground biomass
AOI	Area of Interest
BGB	Below ground biomass
CASI-2	Compact Airborne Spectrographic Imager 2
CCA	Canonical Correlation Analysis
C_{org}	Organic Carbon
LAI	Leaf Area Index
Landsat ETM+	Landsat Enhanced Thematic Mapper Plus
Landsat MSS	Landsat Multispectral Scanner
Landsat OLI	Landsat Operational Land Imager
Landsat TM	Landsat Thematic Mapper
LiDAR	Light Detection and Ranging
LULUCF	Land Use, Land Use Change, and Forestry
GEE	Google Earth Engine
GHG	Greenhouse gas
IPCC	Intergovernmental Panel on Climate Change
IR-MAD	Iteratively Reweighted Multivariate Alteration Detection
JM	Jeffreys-Matusita
LOOCV	Leave-one-out cross validation
MAD	Multivariate Alteration Detection
MAE	Mean absolute error
MNDWI	Modified Normalised Difference Water Index
NDC	Nationally Determined Contribution
NDI	Normalised Difference Index
NDTI	Normalised Difference Turbidity Index
NDVI	Normalised Difference Vegetation Index
NIR	Near Infrared

NSW	New South Wales
OBIA	Object-based image analysis
RENDI	Red-edge Normalised Difference Index
RGB	Red-Green-Blue
RMSE	Root mean square error
ROI	Region of Interest
SPOT	*Satellite pour l'Observation de la Terre*
UAV	Unoccupied Aerial Vehicle

Chapter 1

Introduction

1.1 Background

1.1.1 Seagrass

Seagrasses are a functional group of angiosperms adapted to marine conditions. They are the only true plants that can grow fully submerged in sea water, producing roots, stems, leaves, and flowers, like their terrestrial ancestors from which they evolved over 100 million years ago (den Hartog, 1970). Four families comprising approximately 70 species of seagrass are known, growing globally in the shallow waters of 191 countries in all continents except Antarctica (McKenzie et al., 2020). Though there are relatively few distinct seagrass species, different seagrasses exhibit large physiological differences (Figure 1), ranging from small species like *Halophila decipiens* which opportunistically colonises marine sediments with leaves a few centimetres long and a sparse rhizosphere, to large species like *Posidonia oceanica* which constructs rhizome mattes many metres thick in the Mediterranean Sea (den Hartog, 1970, Kuo and den Hartog, 2006). Seagrasses also exhibit a wide range of life cycles and are responsive to changes in their environment including shifts in water temperature, turbidity and hydrodynamics conditions (Kilminster et al., 2015; Figure 1).

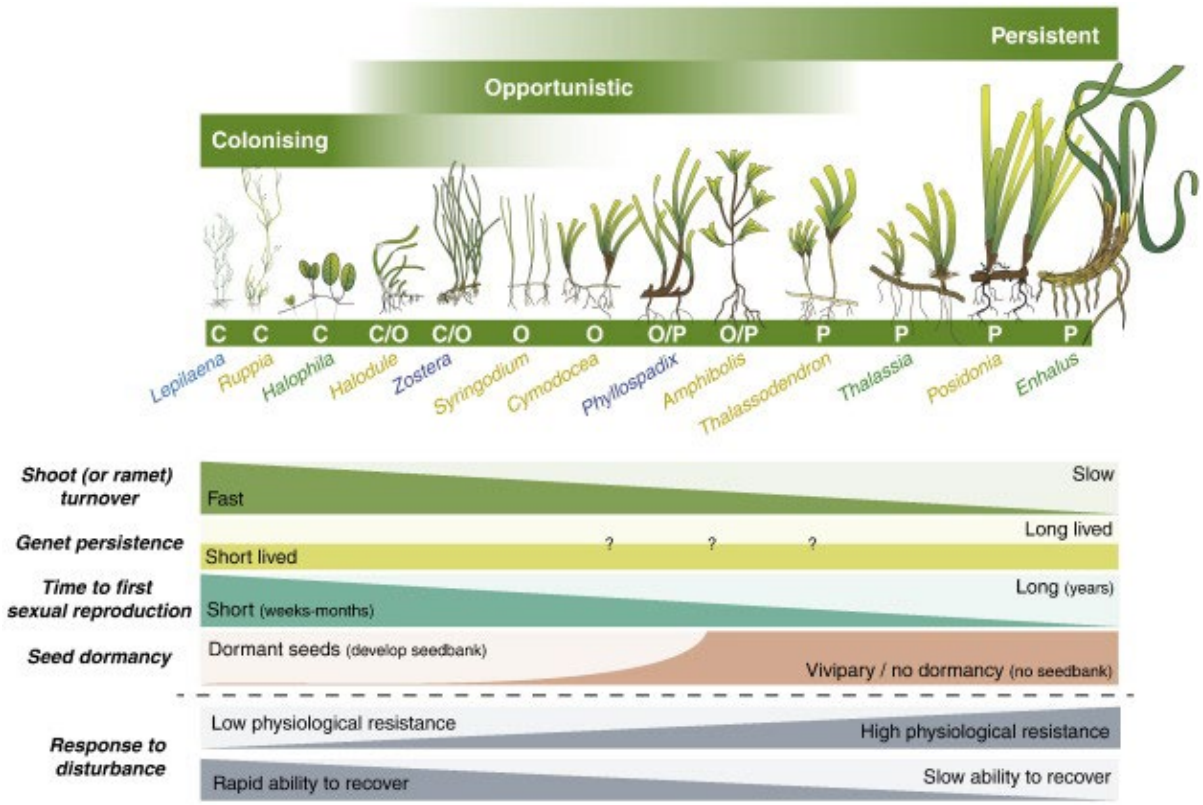

Figure 1. An outline of the range of seagrass morphologies, life cycles, and responses to environmental change and disturbance. Figure from Kilminster et al. 2015.

Seagrasses are ecologically important in coastal environments, regulating biogeochemical processes from local to global scales (Hemminga and Duarte, 2000). The high productivity of seagrasses results in densely vegetated meadows which play a fundamental role in supporting fish and invertebrate life, acting as habitat, breeding ground, food source, and protection from predation (Jackson et al., 2001, Boström et al., 2006). Other marine herbivores also rely on seagrass, most notably sea turtles and dugongs (Aragones, 1996). The roots and rhizomes of seagrass meadows stabilise surrounding sediments, reducing erosion, while seagrass leaves baffle suspended material, encouraging deposition and reducing resuspension (Widdows et al., 2008, Van Katwijk et al., 2010, Paul, 2018). Concurrently, this process purifies coastal waters, removing sediments and pollutants that may negatively impact other marine habitats (de los Santos et al., 2020). The high productivity of seagrass ecosystems and their tendency to collect organic material exported from nearby systems such as mangroves and tidal marshes leads to high rates of carbon burial in seagrass sediments (Mateo and Romero, 1997, Hemminga and Duarte, 2000, Duarte et al., 2010), further enhanced by

an environment that renders buried carbon relatively recalcitrant (Trevathan-Tackett et al., 2017).

Theorised through the lens of ecosystem services, seagrass ecosystem functions provide a wide array of financial and livelihood benefits to humans (Nordlund et al., 2016). Global estimates of seagrass financial value are not yet established with confidence, due to the difficulty of quantifying the services they provide (Dewsbury et al., 2016, Mehvar et al., 2018). Recent estimates of ecosystem services provided by seagrasses in the Mediterranean Sea estimate their total economic value at US$11.6 billion/year (Stamatiadou et al., 2025). It is well established that the ecosystem services provided by seagrasses are of considerable socio-economic importance to humans (Nordlund et al., 2018).

Seagrasses are subject to a multitude of primarily anthropogenic, cumulative stressors, leading to a global pattern of decline (Roca et al., 2016). Human activities lead to direct destruction of seagrass through dredging and construction, as well as input of excess sediment and nutrients into the coastal zone, which impedes photosynthesis by increasing turbidity and encouraging algal growth (Short and Wyllie-Echeverria, 1996). Global seagrass loss has been estimated at as high as 7% per year (Waycott et al., 2009), though more recent estimates suggest lower loss rates, accounting for restoration activities and natural recovery (Dunic et al., 2021). Global patterns of seagrass decline necessitate research that can contribute to more rigorous quantification of seagrass cover.

1.1.2 Blue carbon, seagrass conservation and restoration

Seagrass sediments contain 10% of all organic carbon in ocean sediments, despite occupying just 0.2% of global ocean area (Fourqurean et al., 2012). Carbon burial in seagrass meadows has been shown to be highly efficient, at a rate up to 40 times that of terrestrial forests (Serrano et al., 2021). This high rate is a result of high rates of leaf, root, and rhizome burial, as well as encouragement of sedimentation by seagrass leaves (Mazarrasa et al., 2018). The disproportionately high capacity of seagrass to sequester atmospheric carbon has led to their recognition as ‘blue carbon’ ecosystems along with

mangroves and salt marshes, and are proposed as a nature-based solution to the climate crisis (Macreadie et al., 2021).

Blue carbon financing offers a potential means to improve seagrass ecosystem health by funding conservation and restoration projects. The high sequestration rate coupled with large existing carbon stocks means that conservation of seagrass provides the dual benefit of drawing down atmospheric carbon while retaining existing stocks, leading to a possible equivalent mitigation benefit of 34.1 million tonnes of CO_2 per year (Griscom et al., 2017). Conversely, the global decline in seagrass is a twofold climate risk, as loss of seagrass meadows removes future sequestration potential while also leading to remineralisation of carbon stored in sediments (Krause et al., 2025). Restoration of degraded seagrass has been shown to increase carbon stocks and restore previously lost ecosystem services (Greiner et al., 2013, Thorhaug et al., 2017, Beheshti et al., 2022). Though operationalising blue carbon financing for seagrass restoration is challenging, it remains a high priority for the health of coastal areas (Ward et al., 2025).

The wide global variety of seagrass habitats and the range of seagrass physiologies limits the transferability of carbon estimates across different environments required for determining blue carbon potential. Above-ground seagrass biomass can vary between species by almost 500 times (Duarte and Chiscano, 1999). Krause et al. (2025) recently developed a global database demonstrating a greater than 100,000-fold disparity between highest and lowest overall carbon stock, including soil carbon, per hectare. Dissimilarity in seagrass carbon stock largely arises from interspecific differences in biomass and abundance, and variance in environmental drivers between seagrass meadows, including hydrological energy, temperature, and soil microbial environment (Mateo et al., 2006, Lavery et al., 2013, Samper-Villarreal et al., 2016, Howard et al., 2021, Fourqurean et al., 2023). Even across different parts of the same seagrass meadow, seagrass carbon stocks can differ by up to 50 times (Juma et al., 2020, Ricart et al., 2020), largely due to differences in input of allochthonous carbon from suspended material across environments (Mazarrasa et al. 2018). Despite this high heterogeneity, estimates of seagrass carbon stock for greenhouse emissions reporting and related work frequently use simple estimates based on seagrass area multiplied by regional or global

carbon stock factors, rather than developing spatially explicit models of carbon stock (UNEP, 2020).

1.1.3 Seagrass mapping and monitoring

Mapping seagrass is challenging due to its large geographical range, variable physical properties, and the difficulty of detecting seagrass in deep or turbid environments (McKenzie et al., 2020). Consequently, seagrass maps are derived from multiple sources, including field observations, optical and acoustic remote sensing data, and habitat modelling outputs (Kirkman, 1996, Hossain et al., 2014, Jayathilake and Costello, 2018, Gumusay et al., 2019, Beca-Carretero et al., 2020), and are considered incomplete on a global scale (McKenzie et al., 2020). Where maps of seagrass are available, they are often limited to capturing extent (Duarte et al., 2025). However, mapping the distribution and biophysical characteristics of seagrass beyond spatial extent is a prerequisite for valuing ecosystem services, as well as providing information for conservation and restoration by providing historical points of comparison for future seagrass change (Nordlund et al., 2016, Dalby et al., 2023).

The resource requirements for long-term monitoring of any coastal habitat are high, and as a result methods for seagrass monitoring are even less established than mapping (Pham et al., 2019). Monitoring programs such as Seagrass-Watch, which involves a citizen science approach to field monitoring (McKenzie et al., 2000) have been successful in providing a baseline understanding of natural seagrass variability and response to human and climate stressors (Jones et al., 2018). Field monitoring is required for understanding change and variability in seagrass meadows due to its superior accuracy, thematic resolution, and statistical power for determining change compared to remote sensing methods (Schultz et al., 2015). However, given the high heterogeneity within seagrass meadows, and the potential for seagrasses in similar environments to response to anthropogenic disturbance in different ways, broader-scale monitoring approaches are also required (Traganos et al., 2018).

For mapping seagrass meadows with large coverage and capturing habitat heterogeneity (Duarte et al., 2025, Krause et al., 2025) and accurate methods of long-term seagrass monitoring (Pham et al., 2019), remote sensing methods are a logical source of data.

Remote sensing plays a large and increasing role in seagrass mapping and monitoring as it offers synoptic data observations at recurrent time intervals (Pham et al., 2019, Veettil et al., 2020). However, remote sensing of seagrass environments is inherently limited by the spatial, spectral, and temporal resolution of remote sensing data, as well as the unique challenges associated with detecting underwater targets (Roelfsema et al., 2013). New developments in remote sensing technology have enabled improvements in seagrass mapping, such as very high-resolution satellite images and hyperspectral data (Mumby and Edwards, 2002, Pu et al., 2012, Pu and Bell, 2017). As emergent remote sensing technologies, such as sensors integrated into CubeSats, become available possibilities for improving accuracy and thematic resolution of seagrass maps will continue to develop.

1.1.4 Optical remote sensing of seagrass

Above-water remote sensing is the dominant source of imaging data for mapping and monitoring seagrass ecosystems (Veettil et al., 2020). Other types of remote sensing approaches used include side-scan sonar and bathymetric LiDAR (Pan et al., 2016, Greene et al., 2018). Below-water imaging provides very high-resolution images of the benthic surface, but spatial coverage is restricted to small areas and requires intensive fieldwork or specialised equipment such as remotely operated submersibles (Marre et al., 2020). Due to the routine, freely available, and spatially comprehensive nature of optical data captured with above-water platforms, this is currently the most suitable approach. To understand the potential for emerging remote sensing technologies for capturing seagrass heterogeneity and variability, the physical constraints for optical sensing in coastal environments must first be considered.

Photosynthesising vegetation reflects light in characteristic ways that allow detection by optical remote sensing. Remote sensing of photosynthetic vegetation relies on the characteristic absorption of visible light in photosynthetically active wavelengths (approximately 400-700 nm) and the scattering of light in near-infrared wavelengths (750-1400 nm). Spectral vegetation indices (such as the Normalised Difference Vegetation Index or NDVI; Rouse Jr et al., 1973) exploit this contrast in reflectance between the red and near-infrared wavelengths to detect and characterise vegetation in remotely sensed images. However, attenuation of light by water varies by wavelength,

and the near-infrared light required for derivation of NDVI is extinguished by water almost immediately (Kirk, 1977, Kirk, 1994). Water over subtidal seagrass meadows thus constrains the available wavelengths for optical remote sensing to those that penetrate water and impacts the reflected signals of available wavelengths (Figure 2). The other constituents of the water column, including dissolved or suspended material, are another consideration, as they also reflect and scatter light, interfering with retrieval of benthic reflectance (Phinn et al., 2018). Light also refracts and reflects at the air-water interface, further complicating signal retrieval (Phinn et al., 2018).

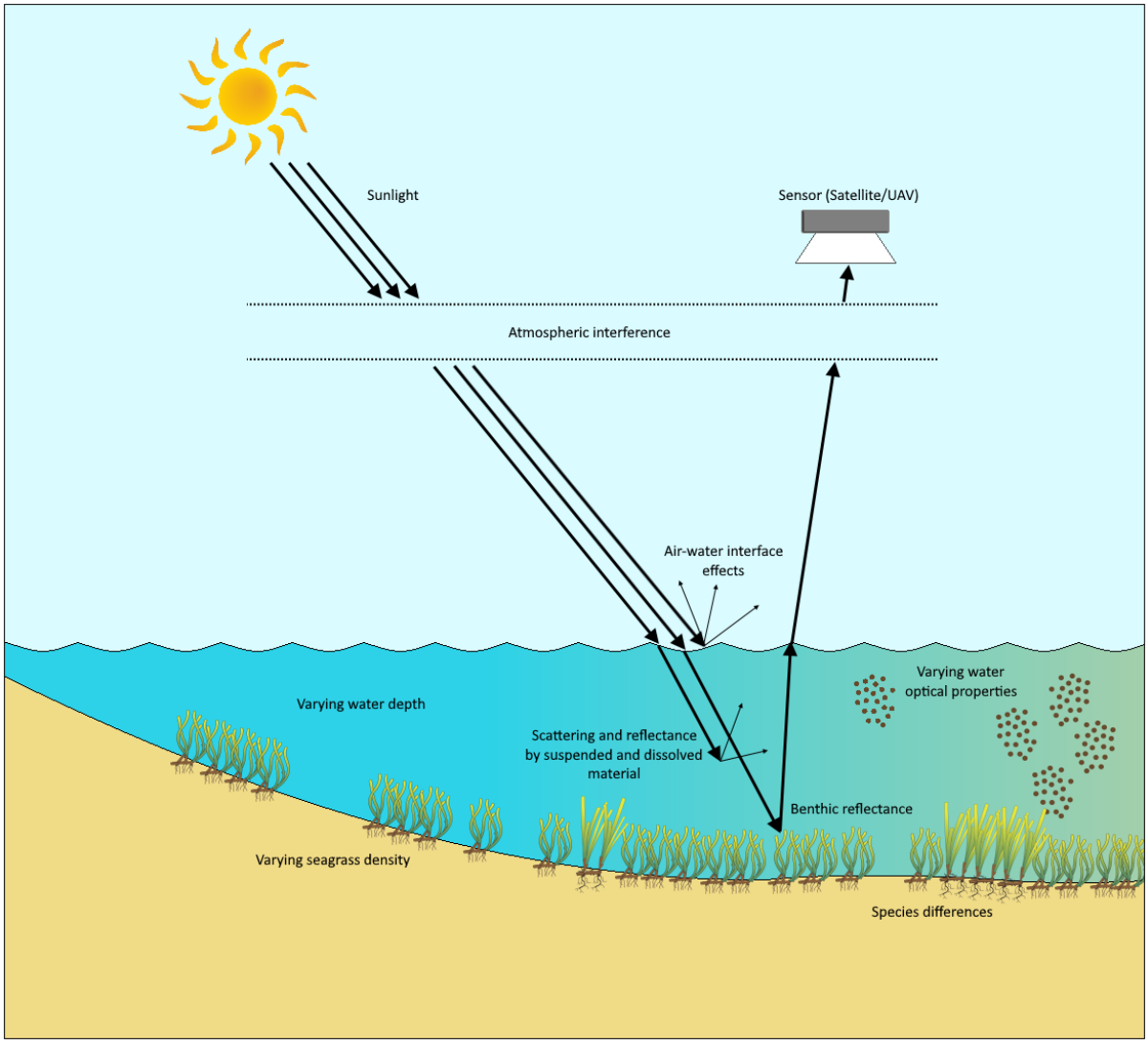

Figure 2. A simplified representation of light interaction with shallow water environments, and factors that need to be considered in remote sensing of seagrass. Adapted from Phinn et al. 2018.

Despite the confounding effects of the water column and the atmosphere, assuming some component of the light reaching a sensor is reflected from the benthos, information about benthic cover may be derived. However, this requires corrections for

atmosphere and water column effects. Satellite and UAV products are generally calibrated to surface reflectance to reduce solar illumination and atmospheric effects, but water column corrections are not routinely applied to publicly available data products such as Sentinel-2 images. Though there are some particularities to atmospheric interference over coastal areas due to differences in atmospheric composition compared to inland areas, this issue is outside the scope of this thesis and existing atmospheric correction approaches have been used where required.

Numerous approaches to water column correction have been developed, each with different data requirements and applications (Zoffoli et al., 2014). One set of commonly applied approaches utilises image-based measurements of reflectance over varying depth and consistent cover to derive depth-invariant ratios of bands (Lyzenga, 1978, Lyzenga, 1981, Tassan, 1996, Conger et al., 2006). These band ratio approaches only produce secondary variables and do not provide spectral information or corrected benthic reflectance. Other models rely on depth and a diffuse attenuation coefficient that represents all absorption and scattering in the water column, which can be used to estimate benthic reflectance based on the assumption that light is exponentially attenuated in water inferred from the Beer-Lambert Law (Maritorena et al., 1994, Vahtmäe et al., 2020). Depth and attenuation coefficients can be measured *in situ* or estimated from images with a variety of techniques (Bierwirth et al., 1993, Stumpf et al., 2003). Other more complex models parameterise the optical properties of water separately (Lee et al., 1999) or simulate the underwater environment to use a look-up table approach (Louchard et al., 2003, Mobley et al., 2005). Unlike band ratio methods, model- and simulation-based approaches to water column correction allow for derivation of actual estimates of benthic reflectance. Model- and simulation-based approaches are valuable as they provide estimates of actual reflectances from benthic cover, which maintain relationships between spectral band reflectances and can be used to derive secondary variables such as vegetation indices.

Under certain circumstances, water column correction may not be necessary. Theoretically, if water was of a consistent depth and constitution across an entire image, the effect of the water column on retrieved reflectances would also be consistent, and any difference in reflectance between pixels would be caused by differences in benthic

cover. In practice, when variation in reflectance caused by differences in benthic cover is greater than that caused by differences in water depth or optical properties, water column correction may be unnecessary (Lyons et al., 2011).

Selecting an approach to reduce the confounding effects of the water column for seagrass mapping must therefore consider the geography and hydrology of the study site, as well as the availability of ancillary data to perform corrections. For instance, in temperate estuarine settings, though water is generally shallow, water optical properties can change substantially in response to inputs of sediment or other material. The ideal case of a fully parameterised model with sufficient *in situ* data to account for the multiple sources of interference is not practical for large-scale mapping. Monitoring of seagrass is further complicated as the model parameters of water depth and optical properties may change between image captures due to tides and turbidity events respectively. This necessitates parameterising models and performing corrections on each image individually.

1.1.5 Emergent remote sensing techniques and technologies

New developments in the last decade have created opportunities for seagrass remote sensing. Sensors mounted on unoccupied aerial vehicles (UAVs), or drones, offer a way to capture data at a previously unprecedented spatial resolution for a relatively low cost (Joyce et al., 2023). The spatial resolution offered by UAV-mounted sensors can provide more information on seagrass heterogeneity than lower-resolution sensors, with complete coverage not available through field surveys alone (James et al., 2020, Riniatsih et al., 2021, Price et al., 2022). Flexibility in UAV flight planning allows timing of remote sensing data collection with low tide and good conditions (Elma et al., 2024).

Though red-green-blue (RGB) cameras can be used for seagrass mapping (Tahara et al., 2022), many UAV sensors, designed primarily for precision agriculture, like the Micasense Red-Edge MX Dual camera system (Micasense, Seattle, USA), produce images with better spectral resolutions than most multispectral remote sensing data. In the context of nearshore environments which limit available wavelengths, improved spectral resolution has the potential to identify new remote sensing variables or indices which can capture key seagrass reflectance features (Pu et al., 2013, Pu et al., 2015).

Recent advancements in satellite remote sensing platforms have also created new opportunities for seagrass research. Sentinel-2, first launched in 2015, has rapidly become the preferred data source for seagrass mapping due to its improved spatial, spectral, and temporal resolution compared to Landsat (Kovacs et al., 2018, Kohlus et al., 2020). Processing techniques for satellite data have also been significantly improved due to cloud geoprocessing platforms like Google Earth Engine (GEE; Gorelick et al., 2017) and the Open Data Cube (Ross et al., 2017). These platforms make it relatively straightforward to map seagrass using large remote sensing data sets in ways previously very time-consuming using desktop software (Traganos et al., 2018).

1.2 Geographical setting

1.2.1 New South Wales Estuaries

The coast of New South Wales (NSW), along the east and southeast of Australia, faces the Tasman Sea (Figure 3). It includes a range of estuarine environments, primarily barrier estuaries and drowned river valleys that are wave-dominated with diurnal tidal regimes with ranges up to about 2 m (Kench, 1999). NSW estuaries are at various stages of sedimentary infilling depending on their evolutionary maturity, associated with a clear progression in hydrological, sedimentological, and ecological regimes (Roy, 1984, Roy et al., 2001). Parts of the NSW coast are heavily urbanised, especially around Sydney, Wollongong, and Newcastle, and most of the state's population lives within 10 km of the coast, with population density rapidly decreasing inland (Chen and McAneney, 2006). Outside of these urban centres, population is generally low, and some estuaries are protected from development by being included in or surrounded by National Parks (Thom et al., 2023).

Figure 3. Location of New South Wales within Australia, and the coast of New South Wales with key urban centres marked.

1.2.2 Estuarine seagrass in New South Wales

NSW has a relatively low overall seagrass area compared to other states, partly due to growth being limited to sheltered estuarine areas by the high wave energy of the east-facing coast (Macreadie et al., 2018). However, within estuaries seagrasses are common, with at least one species mapped in 112 of the 179 estuaries in the state (NSW DCCEEW, 2010).

Seven species of seagrass across three genera are found in NSW estuaries. *Zostera muelleri* (syn. *Z. capricorni, Z. mucronata, Z. novozelandica*) is the most dominant eastern Australian seagrass, present in almost all NSW estuaries that support seagrass, from fringes of drowned river valleys to saline coastal lagoons (Macreadie et al., 2018). *Z. muelleri* is a mid-sized colonising species with strap-like leaves up to ~80 cm long (den Hartog, 1970) that forms heterogeneous meadows that can vary considerably in extent and arrangement over time in response to variation in environmental conditions and anthropogenic disturbance (Kerr and Strother, 1990, York et al., 2013, Wendländer et al., 2019).

Posidonia australis is a less common seagrass species in NSW with its range not extending as far north as *Z. muelleri*. It is recognised as endangered in heavily developed estuaries north of Port Hacking, near Sydney (NSW Department of Primary Industries,

2012). *P. australis* is larger, slower growing, and generally forms denser, more persisting meadows than *Z. muelleri*, generally in more open, deeper embayments and estuaries (West et al., 1985, Creese et al., 2009, Macreadie et al., 2018). *P. australis* is not prone to significant changes over short time periods and is very slow to recover from disturbance (Meehan and West, 2000, Kilminster et al., 2015).

Four species of the genus *Halophila* (*H. decipiens, H. australis, H. ovalis, and H. minor)* are also found in NSW waters (Macreadie et al., 2018). *Halophila spp.* grow small, paddle-shaped leaves on a wide variety of substrates in a range of conditions, from shallow saline lagoons to deep water (den Hartog, 1970, Macreadie et al., 2018). It follows an opportunistic life cycle, quickly colonising bare areas with a shallow, sparse rhizosphere (Kilminster et al., 2015).

The research sites in this thesis were selected from NSW estuaries for two main reasons. First, NSW estuarine seagrass is well mapped from aerial photography, with considerable existing data on historical and current extent available (NSW Department of Primary Industries, 2023), allowing for informed decisions about study site locations. Second, there is a relative lack of satellite remote sensing studies focusing on temperate estuarine seagrass compared to other coastal environments.

The seagrass species of focus for this study was *Z. muelleri* due to its dominance in NSW, heterogeneous growth patterns, and high variability. *P. australis* was also present at four estuaries (Wallis Lake, Brisbane Water, Lake Macquarie, Merimbula Lake) but was generally restricted to small, deeper areas within those estuaries. *Halophila spp.* is also periodically present in many NSW estuaries but tends to be relatively too small in patch size, sparse, and ephemeral to be mapped using remote sensing in these areas. Due to the relatively small area of *P. australis* and difficulty in detecting *Halophila spp.*, these species have not been explicitly accounted for in the current research.

1.3 Research Aims

This research was informed by the need for more comprehensive seagrass mapping in temperate estuarine environments, addressing the common limitation of existing approaches that often represent seagrass extent without accurately capturing spatio-temporal dynamics. Recent developments in remote sensing technology, including

UAV-mounted sensors, inclusion of additional spectral bands in multispectral data products, and remote sensing innovation enabled through CubeSat missions, provides a timely opportunity to investigate new methods for enhancing estuarine seagrass mapping. The overarching objective of this research was to develop new approaches that utilise emerging remote sensing techniques and technologies to detect biophysical characteristics of seagrass, with a focus on capturing spatial heterogeneity and temporal variability relevant to assessing seagrass carbon stock. This was achieved through the following four specific aims:

Aim 1: Identify key biophysical characteristics of seagrass that relate to carbon stock and sequestration that can be derived using satellite- and UAV-acquired remote sensing. The identified characteristics inform **Aims 2**, **3**, and **4**.

Aim 2: Develop and evaluate appropriate methods for using UAV-mounted sensors to map and monitor seagrass cover and spatial configuration (**Aim 1**) in estuarine environments at very fine spatial resolution.

Aim 3: Explore the potential for additional spectral bands, including coastal blue and red-edge bands available in contemporary and planned remote sensing platforms, to improve the mapping of seagrass cover and spatial configuration (**Aim 1**).

Aim 4: Assess whether the methods developed for mapping seagrass cover (**Aim 2** and **Aim 3**) can be upscaled for larger geographical areas across different estuaries to map temporal variability of seagrass cover.

1.4 Thesis outline

This work is presented as a thesis with publications, consisting of seven chapters (Figure 4). Background literature and knowledge gaps presented in this chapter are expanded in Chapter 2 to establish the rationale for this research. Chapter 3-6 are independent but interlinked research chapters, two published, and two in preparation. The discussion chapter (Chapter 7) draws together the key findings that have emerged from the research and returns to the original research problem.

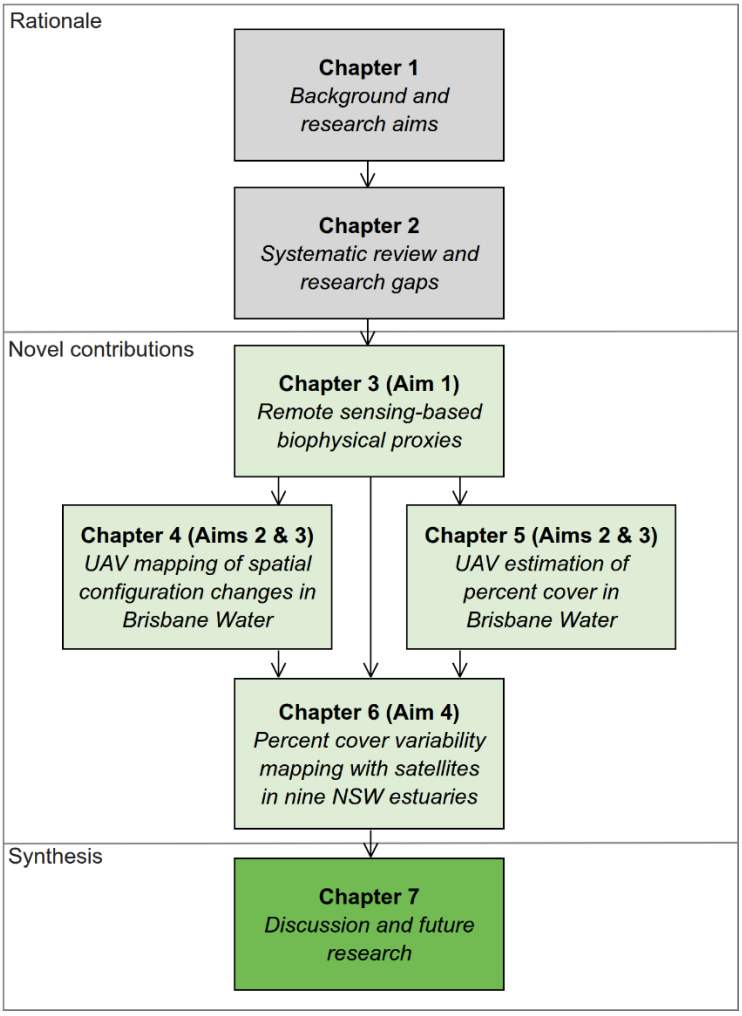

Figure 4. Structure of this thesis, including primary focus of each chapter, corresponding research aims, and field sites used.

Chapter 2 establishes the foundation for enhancing the application of seagrass remote sensing by critically reviewing existing methodologies. This review was used to refine the identified research gaps and provide the broader academic context for the research.

Chapter 3 examines seagrass spatial ecology as it relates to heterogeneity and variability of carbon stock with remote sensing technology to identify "biophysical proxies" or seagrass biophysical characteristics that can be related to carbon stock and measurable using remote sensing (**Aim 1**). The biophysical proxies identified in this chapter form the theoretical basis for the remaining work.

Chapter 4 applies a novel unsupervised change detection method (Iteratively Reweighted Multivariate Alteration Detection; IR-MAD), to UAV-captured images of seagrass meadows. This approach is evaluated for its ability to rapidly and efficiently

capture changes in seagrass spatial arrangement and density between image dates at a very high resolution (<8 cm) to address **Aim 2**. Chapter 4 contributes to **Aim 3** by assessing the relevance of spectral resolution to identifying change in seagrass meadows.

Chapter 5 addresses **Aim 2** by focusing on mapping seagrass percent cover using UAV images. Seagrass spectra derived from water-column corrected UAV images are used to develop a spectral vegetation index that exploits red-edge reflectance (**Aim 3**) which is correlated linearly with, and can predict, seagrass percent cover. This chapter presents methods for mapping percent cover as a continuous variable, rather than discrete classes, to capture heterogeneity within seagrass meadows.

Chapter 6 applies the spectral vegetation index developed in Chapter 5 to satellite remote sensing data in addressing **Aim 4**. The findings presented in Chapters 4 and 5 inform the design and development of a dynamic seagrass variability mapping method, based on time series Sentinel-2 data.

Chapter 7 synthesises and critically discusses the research findings, identifying key overarching themes emerging from the thesis linked to the original research aims. These results are evaluated in relation to their implications for seagrass carbon stock assessment and broader seagrass management strategies. The chapter concludes by exploring the relevance of this research for further inquiry in the context of recent and expected developments in the field of coastal remote sensing.

References

ARAGONES, L. V. 1996. Dugongs and green turtles: grazers in the tropical seagrass ecosystem. PhD Thesis. James Cook University, Townsville, Australia.

BECA-CARRETERO, P., VARELA, S. & STENGEL, D. B. 2020. A novel method combining species distribution models, remote sensing, and field surveys for detecting and mapping subtidal seagrass meadows. Aquatic Conservation: Marine and Freshwater Ecosystems, 30, 1098-1110.

BEHESHTI, K. M., WILLIAMS, S. L., BOYER, K. E., ENDRIS, C., CLEMONS, A., GRIMES, T., WASSON, K. & HUGHES, B. B. 2022. Rapid enhancement of multiple ecosystem services following the restoration of a coastal foundation species. Ecological Applications, 32, e02466.

BIERWIRTH, P., LEE, T. & BURNE, R. 1993. Shallow sea-floor reflectance and water depth derived by unmixing multispectral imagery. Photogrammetric Engineering and Remote Sensing, 59.

BOSTRÖM, C., JACKSON, E. L. & SIMENSTAD, C. A. 2006. Seagrass landscapes and their effects on associated fauna: a review. Estuarine, Coastal and shelf science, 68, 383-403.

CHEN, K. & MCANENEY, J. 2006. High-resolution estimates of Australia's coastal population. Geophysical research letters, 33.

CONGER, C. L., HOCHBERG, E. J., FLETCHER, C. H. & ATKINSON, M. J. 2006. Decorrelating remote sensing color bands from bathymetry in optically shallow waters. IEEE transactions on Geoscience and Remote Sensing, 44, 1655-1660.

CREESE, R., GLASBY, T., WEST, G. & GALLEN, C. 2009. Mapping the habitats of NSW estuaries. Nelson Bay: Industry & Investment NSW.

DALBY, O., PUCINO, N., TAN, Y. M., JACKSON, E. L., MACREADIE, P. I., COLEMAN, R. A., YOUNG, M. A., IERODIACONOU, D. & SHERMAN, C. D. 2023. Identifying spatio-temporal trends in seagrass meadows to inform future restoration. Restoration Ecology, 31, e13787.

DE LOS SANTOS, C. B., OLIVÉ, I., MOREIRA, M., SILVA, A., FREITAS, C., LUNA, R. A., QUENTAL-FERREIRA, H., MARTINS, M., COSTA, M. M. & SILVA, J. 2020. Seagrass meadows improve inflowing water quality in aquaculture ponds. Aquaculture, 528, 735502.

DEN HARTOG, C. 1970. The sea-grasses of the world, Amsterdam, North Holland Publishing Co.

DEWSBURY, B. M., BHAT, M. & FOURQUREAN, J. W. 2016. A review of seagrass economic valuations: gaps and progress in valuation approaches. Ecosystem Services, 18, 68-77.

DUARTE, C. M., APOSTOLAKI, E. T., SERRANO, O., STECKBAUER, A. & UNSWORTH, R. K. 2025. Conserving seagrass ecosystems to meet global biodiversity and climate goals. Nature Reviews Biodiversity, 1-16.

DUARTE, C. M. & CHISCANO, C. L. 1999. Seagrass biomass and production: a reassessment. Aquatic Botany, 65, 159-174.

DUARTE, C. M., MARBÀ, N., GACIA, E., FOURQUREAN, J. W., BEGGINS, J., BARRÓN, C. & APOSTOLAKI, E. T. 2010. Seagrass community metabolism: Assessing the carbon sink capacity of seagrass meadows. Global Biogeochemical Cycles, 24, n/a-n/a.

DUNIC, J. C., BROWN, C. J., CONNOLLY, R. M., TURSCHWELL, M. P. & CÔTÉ, I. M. 2021. Long-term declines and recovery of meadow area across the world's seagrass bioregions. Global Change Biology, 27, 4096-4109.

ELMA, E., GAULTON, R., CHUDLEY, T. R., SCOTT, C. L., EAST, H. K., WESTOBY, H. & FITZSIMMONS, C. 2024. Evaluating UAV-based multispectral imagery for mapping an intertidal seagrass environment. Aquatic Conservation: Marine and Freshwater Ecosystems, 34, e4230.

FOURQUREAN, J. W., CAMPBELL, J. E., RHOADES, O. K., MUNSON, C. J., KRAUSE, J. R., ALTIERI, A. H., DOUGLASS, J. G., HECK JR, K. L., PAUL, V. J. & ARMITAGE, A. R. 2023. Seagrass abundance predicts surficial soil organic carbon stocks across the range of Thalassia testudinum in the Western North Atlantic. Estuaries and coasts, 46, 1280-1301.

FOURQUREAN, J. W., DUARTE, C. M., KENNEDY, H., MARBÀ, N., HOLMER, M., MATEO, M. A., APOSTOLAKI, E. T., KENDRICK, G. A., KRAUSE-JENSEN, D. & MCGLATHERY, K. J. 2012. Seagrass ecosystems as a globally significant carbon stock. Nature Geoscience, 5, 505-509.

GORELICK, N., HANCHER, M., DIXON, M., ILYUSHCHENKO, S., THAU, D. & MOORE, R. 2017. Google Earth Engine: Planetary-scale geospatial analysis for everyone. Remote sensing of Environment, 202, 18-27.

GREENE, A., RAHMAN, A. F., KLINE, R. & RAHMAN, M. S. 2018. Side scan sonar: A cost-efficient alternative method for measuring seagrass cover in shallow environments. Estuarine, Coastal and Shelf Science, 207, 250-258.
GREINER, J. T., MCGLATHERY, K. J., GUNNELL, J. & MCKEE, B. A. 2013. Seagrass restoration enhances "blue carbon" sequestration in coastal waters. PLoS One, 8, e72469.
GRISCOM, B. W., ADAMS, J., ELLIS, P. W., HOUGHTON, R. A., LOMAX, G., MITEVA, D. A., SCHLESINGER, W. H., SHOCH, D., SIIKAMÄKI, J. V. & SMITH, P. J. 2017. Natural climate solutions. Proceedings of the National Academy of Sciences, 114, 11645-11650.
GUMUSAY, M. U., BAKIRMAN, T., TUNEY KIZILKAYA, I. & AYKUT, N. O. 2019. A review of seagrass detection, mapping and monitoring applications using acoustic systems. European Journal of Remote Sensing, 52, 1-29.
HEMMINGA, M. A. & DUARTE, C. M. 2000. Seagrass ecology, Cambridge University Press.
HOSSAIN, M. S., BUJANG, J. S., ZAKARIA, M. H. & HASHIM, M. 2014. The application of remote sensing to seagrass ecosystems: an overview and future research prospects. International Journal of Remote Sensing, 36, 61-114.
HOWARD, J. L., LOPES, C. C., WILSON, S. S., MCGEE-ABSTEN, V., CARRIÓN, C. I. & FOURQUREAN, J. W. 2021. Decomposition rates of surficial and buried organic matter and the lability of soil carbon stocks across a large tropical seagrass landscape. Estuaries and Coasts, 44, 846-866.
JACKSON, E. L., ROWDEN, A. A., ATTRILL, M. J., BOSSEY, S. J. & JONES, M. B. 2001. The importance of seagrass beds as a habitat for fishery species. Oceanography and marine biology, 39, 269-304.
JAMES, D., COLLIN, A., HOUET, T., MURY, A., GLORIA, H. & LE POULAIN, N. 2020. Towards Better Mapping of Seagrass Meadows using UAV Multispectral and Topographic Data. Journal of Coastal Research, 95.
JAYATHILAKE, D. R. & COSTELLO, M. J. 2018. A modelled global distribution of the seagrass biome. Biological Conservation, 226, 120-126.
JONES, B. L., UNSWORTH, R. K., MCKENZIE, L. J., YOSHIDA, R. L. & CULLEN-UNSWORTH, L. C. 2018. Crowdsourcing conservation: The role of citizen science in securing a future for seagrass. Marine pollution bulletin, 134, 210-215.
JOYCE, K. E., FICKAS, K. C. & KALAMANDEEN, M. 2023. The unique value proposition for using drones to map coastal ecosystems. Cambridge prisms: coastal futures, 1, e6.
JUMA, G. A., MAGANA, A. M., MICHAEL, G. N. & KAIRO, J. G. 2020. Variation in seagrass carbon stocks between tropical estuarine and marine mangrove-fringed creeks. Frontiers in Marine Science, 7, 696.
KENCH, P. S. 1999. Geomorphology of Australian estuaries: review and prospect. Australian Journal of Ecology, 24, 367-380.
KERR, E. & STROTHER, S. 1990. Seasonal changes in standing crop of Zostera muelleri in south-eastern Australia. Aquatic Botany, 38, 369-376.
KILMINSTER, K., MCMAHON, K., WAYCOTT, M., KENDRICK, G. A., SCANES, P., MCKENZIE, L., O'BRIEN, K. R., LYONS, M., FERGUSON, A., MAXWELL, P., GLASBY, T. & UDY, J. 2015. Unravelling complexity in seagrass systems for management: Australia as a microcosm. Sci Total Environ, 534, 97-109.
KIRK, J. 1977. Attenuation of light in natural waters. Marine and Freshwater Research, 28, 497-508.
KIRK, J. T. 1994. Light and photosynthesis in aquatic ecosystems, Cambridge University Press.
KIRKMAN, H. 1996. Baseline and monitoring methods for seagrass meadows. Journal of Environmental Management, 47, 191-201.
KOHLUS, J., STELZER, K., MÜLLER, G., SMOLLICH, S. J. E., COASTAL & SCIENCE, S. 2020. Mapping seagrass (Zostera) by remote sensing in the Schleswig-Holstein Wadden Sea. 238, 106699.
KOVACS, E., ROELFSEMA, C., LYONS, M., ZHAO, S. & PHINN, S. 2018. Seagrass habitat mapping: how do Landsat 8 OLI, Sentinel-2, ZY-3A, and Worldview-3 perform? Remote Sensing Letters, 9, 686-695.
KRAUSE, J. R., CAMERON, C., ARIAS-ORTIZ, A., CIFUENTES-JARA, M., CROOKS, S., DAHL, M., FRIESS, D. A., KENNEDY, H., LIM, K. E. & LOVELOCK, C. E. 2025. Global seagrass carbon stock variability and emissions from seagrass loss. Nature Communications, 16, 1-9.
KUO, J. & DEN HARTOG, C. 2006. Seagrass Morphology, Anatomy, and Ultrastructure. In: LARKUM, A. W. D., ORTH, R. J. & DUARTE, C. M. (eds.) Seagrasses: Biology, ecology and conservation. Dordrecht: Springer.

LAVERY, P. S., MATEO, M.-Á., SERRANO, O. & ROZAIMI, M. 2013. Variability in the carbon storage of seagrass habitats and its implications for global estimates of blue carbon ecosystem service. PloS one, 8, e73748.

LEE, Z., CARDER, K. L., MOBLEY, C. D., STEWARD, R. G. & PATCH, J. S. 1999. Hyperspectral remote sensing for shallow waters: 2. Deriving bottom depths and water properties by optimization. Applied Optics, 38, 3831-3843.

LOUCHARD, E. M., REID, R. P., STEPHENS, F. C., DAVIS, C. O., LEATHERS, R. A. & T. VALERIE, D. 2003. Optical remote sensing of benthic habitats and bathymetry in coastal environments at Lee Stocking Island, Bahamas: A comparative spectral classification approach. Limnology and oceanography, 48, 511-521.

LYONS, M., PHINN, S. & ROELFSEMA, C. 2011. Integrating Quickbird Multi-Spectral Satellite and Field Data: Mapping Bathymetry, Seagrass Cover, Seagrass Species and Change in Moreton Bay, Australia in 2004 and 2007. Remote Sensing, 3, 42-64.

LYZENGA, D. R. 1978. Passive remote sensing techniques for mapping water depth and bottom features. Applied Optics, 17, 379-383.

LYZENGA, D. R. 1981. Remote sensing of bottom reflectance and water attenuation parameters in shallow water using aircraft and Landsat data. International Journal of Remote Sensing, 2, 71-82.

MACREADIE, P. I., COSTA, M. D., ATWOOD, T. B., FRIESS, D. A., KELLEWAY, J. J., KENNEDY, H., LOVELOCK, C. E., SERRANO, O., DUARTE, C. M. J. N. R. E. & ENVIRONMENT 2021. Blue carbon as a natural climate solution. 1-14.

MACREADIE, P. I., SULLIVAN, B., EVANS, S. M. & SMITH, T. M. 2018. Biogeography of Australian Seagrasses: NSW, Victoria, Tasmania and Temperate Queensland. Seagrasses of Australia: Structure, ecology and conservation, 31-59.

MARITORENA, S., MOREL, A. & GENTILI, B. 1994. Diffuse reflectance of oceanic shallow waters: Influence of water depth and bottom albedo. Limnology and Oceanography, 39, 1689-1703.

MARRE, G., DETER, J., HOLON, F., BOISSERY, P. & LUQUE, S. 2020. Fine-scale automatic mapping of living Posidonia oceanica seagrass beds with underwater photogrammetry. Marine Ecology Progress Series, 643, 63-74.

MATEO, M. & ROMERO, J. 1997. Detritus dynamics in the seagrass Posidonia oceanica: elements for an ecosystem carbon and nutrient budget. Marine Ecology Progress Series, 151, 43-53.

MATEO, M. A., CEBRIAN, J., DUNTON, K. & MUTCHLER, T. 2006. Carbon Flux in Seagrass Ecosystems. In: LARKUM, A. W. D., ORTH, R. J. & DUARTE, C. M. (eds.) Seagrasses: Biology, Ecology and Conservation. The Netherlands: Springer.

MAZARRASA, I., SAMPER-VILLARREAL, J., SERRANO, O., LAVERY, P. S., LOVELOCK, C. E., MARBA, N., DUARTE, C. M. & CORTES, J. 2018. Habitat characteristics provide insights of carbon storage in seagrass meadows. Mar Pollut Bull, 134, 106-117.

MCKENZIE, L., LONG, L., COLES, R. & RODER, C. 2000. Seagrass-Watch: Community based monitoring of seagrass resources. Biologia marina mediterranea, 7, 393-396.

MCKENZIE, L. J., NORDLUND, L. M., JONES, B. L., CULLEN-UNSWORTH, L. C., ROELFSEMA, C. & UNSWORTH, R. K. F. 2020. The global distribution of seagrass meadows. Environmental Research Letters, 15.

MEEHAN, A. J. & WEST, R. J. 2000. Recovery times for a damaged Posidonia australis bed in south eastern Australia. Aquatic Botany, 67, 161-167.

MEHVAR, S., FILATOVA, T., DASTGHEIB, A., DE RUYTER VAN STEVENINCK, E. & RANASINGHE, R. 2018. Quantifying economic value of coastal ecosystem services: a review. Journal of marine science and engineering, 6, 5.

MOBLEY, C. D., SUNDMAN, L. K., DAVIS, C. O., BOWLES, J. H., DOWNES, T. V., LEATHERS, R. A., MONTES, M. J., BISSETT, W. P., KOHLER, D. D. & REID, R. P. 2005. Interpretation of hyperspectral remote-sensing imagery by spectrum matching and look-up tables. Applied Optics, 44, 3576-3592.

MUMBY, P. J. & EDWARDS, A. J. 2002. Mapping marine environments with IKONOS imagery: enhanced spatial resolution can deliver greater thematic accuracy. Remote Sensing of Environment, 82, 248-257.

NORDLUND, L., KOCH, E. W., BARBIER, E. B. & CREED, J. C. 2016. Seagrass Ecosystem Services and Their Variability across Genera and Geographical Regions. PLoS One, 11, e0163091.

NORDLUND, L. M., JACKSON, E. L., NAKAOKA, M., SAMPER-VILLARREAL, J., BECA-CARRETERO, P. & CREED, J. C. 2018. Seagrass ecosystem services–What's next? Marine Pollution Bulletin, 134, 145-151.

NSW DEPARTMENT OF CLIMATE CHANGE, E., THE ENVIRONMENT AND WATER 2010. Estuaries. State Government of NSW.

NSW DEPARTMENT OF PRIMARY INDUSTRIES 2012. Endangered populations in NSW Factsheet: Posidonia australis. In: INDUSTRIES, N. D. O. P. (ed.). Sydney: NSW Department of Primary Industries.

NSW DEPARTMENT OF PRIMARY INDUSTRIES, N. S. W. G. 2023. NSW Estuarine Macrophytes 2023.

PAN, Z., GLENNIE, C., FERNANDEZ-DIAZ, J. C. & STAREK, M. 2016. Comparison of bathymetry and seagrass mapping with hyperspectral imagery and airborne bathymetric lidar in a shallow estuarine environment. International Journal of Remote Sensing, 37, 516-536.

PAUL, M. 2018. The protection of sandy shores–can we afford to ignore the contribution of seagrass? Marine Pollution Bulletin, 134, 152-159.

PHAM, T. D., XIA, J., HA, N. T., BUI, D. T., LE, N. N. & TEKEUCHI, W. 2019. A Review of Remote Sensing Approaches for Monitoring Blue Carbon Ecosystems: Mangroves, Seagrassesand Salt Marshes during 2010(-)2018. Sensors (Basel), 19.

PHINN, S., ROELFSEMA, C., KOVACS, E., CANTO, R., LYONS, M., SAUNDERS, M. & MAXWELL, P. 2018. Mapping, monitoring and modelling seagrass using remote sensing techniques. Seagrasses of Australia: Structure, ecology and conservation, 445-487.

PRICE, D. M., FELGATE, S. L., HUVENNE, V. A., STRONG, J., CARPENTER, S., BARRY, C., LICHTSCHLAG, A., SANDERS, R., CARRIAS, A. & YOUNG, A. 2022. Quantifying the intra-habitat variation of seagrass beds with unoccupied aerial vehicles (UAVs). Remote Sensing, 14, 480.

PU, R. & BELL, S. 2017. Mapping seagrass coverage and spatial patterns with high spatial resolution IKONOS imagery. International Journal of Applied Earth Observation and Geoinformation, 54, 145-158.

PU, R., BELL, S. & ENGLISH, D. 2015. Developing Hyperspectral Vegetation Indices for Identifying Seagrass Species and Cover Classes. Journal of Coastal Research, 313, 595-615.

PU, R., BELL, S., MEYER, C., BAGGETT, L. & ZHAO, Y. 2012. Mapping and assessing seagrass along the western coast of Florida using Landsat TM and EO-1 ALI/Hyperion imagery. Estuarine, Coastal and Shelf Science, 115, 234-245.

PU, R., BELL, S. J. I. J. O. P. & SENSING, R. 2013. A protocol for improving mapping and assessing of seagrass abundance along the West Central Coast of Florida using Landsat TM and EO-1 ALI/Hyperion images. 83, 116-129.

RICART, A. M., YORK, P. H., BRYANT, C. V., RASHEED, M. A., IERODIACONOU, D. & MACREADIE, P. I. 2020. High variability of Blue Carbon storage in seagrass meadows at the estuary scale. Scientific reports, 10, 5865.

RINIATSIH, I., AMBARIYANTO, A., YUDIATI, E., REDJEKI, S. & HARTATI, R. Monitoring the seagrass ecosystem using the unmanned aerial vehicle (UAV) in coastal water of Jepara. IOP Conference Series: Earth and Environmental Science, 2021. IOP Publishing, 012075.

ROCA, G., ALCOVERRO, T., KRAUSE-JENSEN, D., BALSBY, T. J. S., VAN KATWIJK, M. M., MARBÀ, N., SANTOS, R., ARTHUR, R., MASCARÓ, O. & FERNÁNDEZ-TORQUEMADA, Y. 2016. Response of seagrass indicators to shifts in environmental stressors: a global review and management synthesis. Ecological Indicators, 63, 310-323.

ROELFSEMA, C., KOVACS, E. M., SAUNDERS, M. I., PHINN, S., LYONS, M. & MAXWELL, P. 2013. Challenges of remote sensing for quantifying changes in large complex seagrass environments. Estuarine, Coastal and Shelf Science, 133, 161-171.

ROSS, J., KILLOUGH, B., DHU, T. & PAGET, M. 2017. Open Data Cube and the committee on earth observation satellites data cube initiative. IAC.

ROUSE JR, J., HAAS, R., SCHELL, J. & DEERING, D. Monitoring vegetation systems in the Great Plains with ERTS. Third ERTS-1 symposium: The Proceedings of a Symposium Held by Goddard Space Flight center, 1973 Washington, DC. 309.

ROY, P. 1984. New South Wales estuaries: their origin and evolution. In: THOM, B. (ed.) Coastal Geomorphology in Australia. Sydney: Academic Press.

ROY, P., WILLIAMS, R., JONES, A., YASSINI, I., GIBBS, P., COATES, B., WEST, R., SCANES, P., HUDSON, J. & NICHOL, S. 2001. Structure and function of south-east Australian estuaries. Estuarine, coastal and shelf science, 53, 351-384.

SAMPER-VILLARREAL, J., LOVELOCK, C. E., SAUNDERS, M. I., ROELFSEMA, C. & MUMBY, P. J. 2016. Organic carbon in seagrass sediments is influenced by seagrass canopy complexity, turbidity, wave height, and water depth. Limnology and Oceanography, 61, 938-952.

SCHULTZ, S. T., KRUSCHEL, C., BAKRAN-PETRICIOLI, T. & PETRICIOLI, D. 2015. Error, power, and blind sentinels: the statistics of seagrass monitoring. PloS one, 10, e0138378.

SERRANO, O., GÓMEZ-LÓPEZ, D. I., SÁNCHEZ-VALENCIA, L., ACOSTA-CHAPARRO, A., NAVAS-CAMACHO, R., GONZÁLEZ-CORREDOR, J., SALINAS, C., MASQUE, P., BERNAL, C. A. & MARBÀ, N. 2021. Seagrass blue carbon stocks and sequestration rates in the Colombian Caribbean. Scientific Reports, 11, 1-12.

SHORT, F. T. & WYLLIE-ECHEVERRIA, S. 1996. Natural and human-induced disturbance of seagrasses. Environmental conservation, 23, 17-27.

STAMATIADOU, V., MAZARIS, A. D. & KATSANEVAKIS, S. 2025. Meta-analysis and mapping of the monetary value of Mediterranean seagrass ecosystem services. Ecosystem Services, 72, 101704.

STUMPF, R. P., HOLDERIED, K. & SINCLAIR, M. 2003. Determination of water depth with high-resolution satellite imagery over variable bottom types. Limnology and Oceanography, 48, 547-556.

TAHARA, S., SUDO, K., YAMAKITA, T. & NAKAOKA, M. 2022. Species level mapping of a seagrass bed using an unmanned aerial vehicle and deep learning technique. PeerJ, 10, e14017.

TASSAN, S. 1996. Modified Lyzenga's method for macroalgae detection in water with non-uniform composition. International Journal of Remote Sensing, 17, 1601-1607.

THOM, B., HUDSON, J. & DEAN-JONES, P. 2023. Estuary contexts and governance models in the new climate era, New South Wales, Australia. Frontiers in Environmental Science, 11, 1127839.

THORHAUG, A., POULOS, H. M., LÓPEZ-PORTILLO, J., KU, T. C. & BERLYN, G. P. 2017. Seagrass blue carbon dynamics in the Gulf of Mexico: Stocks, losses from anthropogenic disturbance, and gains through seagrass restoration. Science of the total environment, 605, 626-636.

TRAGANOS, D., AGGARWAL, B., POURSANIDIS, D., TOPOUZELIS, K., CHRYSOULAKIS, N. & REINARTZ, P. 2018. Towards Global-Scale Seagrass Mapping and Monitoring Using Sentinel-2 on Google Earth Engine: The Case Study of the Aegean and Ionian Seas. Remote Sensing, 10.

TREVATHAN-TACKETT, S. M., SEYMOUR, J. R., NIELSEN, D. A., MACREADIE, P. I., JEFFRIES, T. C., SANDERMAN, J., BALDOCK, J., HOWES, J. M., STEVEN, A. D. & RALPH, P. J. 2017. Sediment anoxia limits microbial-driven seagrass carbon remineralization under warming conditions. FEMS Microbiology Ecology, 93, fix033.

UNEP 2020. Out of the blue: The value of seagrasses to the environment and to people. Nairobi.

VAHTMÄE, E., KUTSER, T. & PAAVEL, B. 2020. Performance and Applicability of Water Column Correction Models in Optically Complex Coastal Waters. Remote Sensing, 12.

VAN KATWIJK, M., BOS, A., HERMUS, D. & SUYKERBUYK, W. 2010. Sediment modification by seagrass beds: Muddification and sandification induced by plant cover and environmental conditions. Estuarine Coastal and Shelf Science, 89, 175-181.

VEETTIL, B. K., WARD, R. D., LIMA, M. D. A. C., STANKOVIC, M., HOAI, P. N. & QUANG, N. X. 2020. Opportunities for seagrass research derived from remote sensing: A review of current methods. Ecological Indicators, 117.

WARD, M., DIBBLE, C., MILLINGTON-DRAKE, M., LYNCH, J., MCGLATHERY, K., LILLEY, R. J., STRONG, A. L. & WEDDING, L. M. 2025. Management approach matters: meeting seagrass recovery and carbon mitigation goals. npj Ocean Sustainability, 4, 18.

WAYCOTT, M., DUARTE, C. M., CARRUTHERS, T. J., ORTH, R. J., DENNISON, W. C., OLYARNIK, S., CALLADINE, A., FOURQUREAN, J. W., HECK JR, K. L. & HUGHES, A. R. 2009. Accelerating loss of seagrasses across the globe threatens coastal ecosystems. Proceedings of the national academy of sciences, 106, 12377-12381.

WENDLÄNDER, N. S., LANGE, T., CONNOLLY, R. M., KRISTENSEN, E., PEARSON, R. M., VALDEMARSEN, T. & FLINDT, M. R. 2019. Assessing methods for restoring seagrass (Zostera muelleri) in Australia's subtropical waters. Marine and Freshwater Research, 71, 996-1005.

WEST, R., THOROGOOD, C. & WALFORD, T. 1985. An estuarine inventory for New South Wales, Australia, Department of Agriculture New South Wales.

WIDDOWS, J., POPE, N. D., BRINSLEY, M. D., ASMUS, H. & ASMUS, R. M. 2008. Effects of seagrass beds (Zostera noltii and Z. marina) on near-bed hydrodynamics and sediment resuspension. Marine Ecology Progress Series, 358, 125-136.

YORK, P. H., GRUBER, R. K., HILL, R., RALPH, P. J., BOOTH, D. J. & MACREADIE, P. I. 2013. Physiological and morphological responses of the temperate seagrass Zostera muelleri to multiple stressors: investigating the interactive effects of light and temperature. PloS one, 8, e76377.

ZOFFOLI, M. L., FROUIN, R. & KAMPEL, M. J. S. 2014. Water column correction for coral reef studies by remote sensing. 14, 16881-16931.

Chapter 2

Satellite-based remote sensing of seagrass: A systematic literature review

This chapter is not written for publication as a paper.

This chapter contributes to addressing **Aim 1** by surveying existing approaches to remote sensing of seagrass.

2.1 Introduction

Seagrasses create heterogeneous, often extensive beds in coastal areas globally. They grow in a range of different environments, from open coasts to shallow, saline lagoons. Due to their large global range, high heterogeneity, and the challenges involved in field surveys, seagrass habitats are frequently mapped using remote sensing. The repeatable, synoptic coverage provided by remote sensing, especially satellite remote sensing, allows for large scale mapping and monitoring of seagrass that would not be feasible with field surveys alone (Duffy et al., 2019). Unlike terrestrial vegetation, seagrass is often submerged under water, limiting optical remote sensing to wavelengths that penetrate the water column. Consequently, the selection of analytical techniques requires careful consideration, as water depth and turbidity significantly interfere with the remote sensing signal (Kirk, 1994, Veettil et al., 2020).

Satellite-based remote sensing is important for characterising blue carbon in seagrass habitats, as acquiring data on the extent and characteristics of seagrass beds, as well as changes over time, is a requirement for mapping and monitoring overall carbon stocks (Araya-Lopez et al., 2023). Seagrass beds can be highly heterogeneous and vary spatially in species composition and density in response to differences in environmental conditions such as light availability and wave energy (Bell et al., 1999, Collier et al., 2007, Uhrin and Turner, 2018). Though field surveys can capture more detailed information about seagrass characteristics, remote sensing is uniquely positioned to map seagrass across heterogeneous landscapes (Schütt et al., 2025). The current knowledge gap in the approaches for capturing the inherently variable and

heterogeneous nature of seagrass beds represents a significant barrier to advancing global understanding of seagrass blue carbon (Duarte et al., 2025, Krause et al., 2025), highlighting the need for improved remote sensing methodologies that account for spatio-temporal change.

This review examined existing approaches to satellite remote sensing of seagrass to develop a critical understanding of methodologies relating to sensors, analytical techniques, and the seagrass biophysical variables included in mapping applications. The review was based on academic publications which use satellite remote sensing data to produce maps that include seagrass. Though excluded from the systematic review, a brief overview of remote sensing of seagrass using data captured with Unoccupied Aerial Vehicles (UAVs) is included in this chapter due to the relevance of these platforms to the methods applied in later chapters.

2.2 Methods

A systematic review of literature published on or before 30 April 2022 was conducted to develop a synopsis of methodologies applied to optical remote sensing of seagrass habitats. The following search terms were entered into Web of Science and Scopus, and the results deduplicated: (“Seagrass” OR “submerged aquatic vegetation”) AND (“remote sensing” OR “remotely sensed” OR “satellite” OR “earth observation” OR “Landsat” OR “WorldView” OR “PlanetScope” OR “QuickBird” OR “IKONOS” OR “Sentinel-2”). Only academic journal articles were included in the search. A total of 1119 studies were identified after deduplication. The abstracts of these studies were reviewed, and articles that did not map seagrass using remote sensing data were excluded. The full texts of the remaining articles were examined to ensure that they met all the following criteria:

- Optical satellite remote sensing data was used to map at least one biophysical characteristic of seagrass;
- A clearly described methods section was present;
- Manual image interpretation was not the exclusive method employed.

Based on these criteria, 203 papers were retained and analysed. The methods used in these papers were summarised in terms of the site location, the analytical method, the biophysical variable(s) assessed, and the sensor used to capture the data (Table 1).

Table 1. Examples of aspects of seagrass remote sensing methodologies summarised in the surveyed literature before 30 April 2022.

Aspect	Examples
Field site	Moreton Bay, Australia; Thermaikos Gulf, Greece
Primary method	Object-based classification, regression of NDVI against field biomass measurements
Target biophysical variable	Extent, species, biomass
Sensor	Landsat ETM+, IKONOS

2.3 Results of the review

2.3.1 Field sites

The literature contained examples of seagrass remote sensing in every continent except Antarctica (Table 2, Figure 1), ranging in latitude from 36° S (Tauranga Harbour, New Zealand; Ha et al., 2020) to 59° N (Pakri, Estonia; Vahtmäe et al., 2021). The sites were distributed disproportionately between continents, ranging from only three in South America to 67 in Asia (Table 2). A total of 97 study sites were in the tropics (defined as 23.5° S to 23.5° N), 87 study sites were north of 23.5° N, and 19 study sites were south of 23.5° S (Figure 1).

Table 2. Regional summary of locations of satellite seagrass remote sensing studies identified in the academic literature published before 30 April 2022.

Region	Sites
Africa	19
Asia	67
Middle East	5
Europe	28
North America and Caribbean	57
Oceania and Pacific	25
South America	3

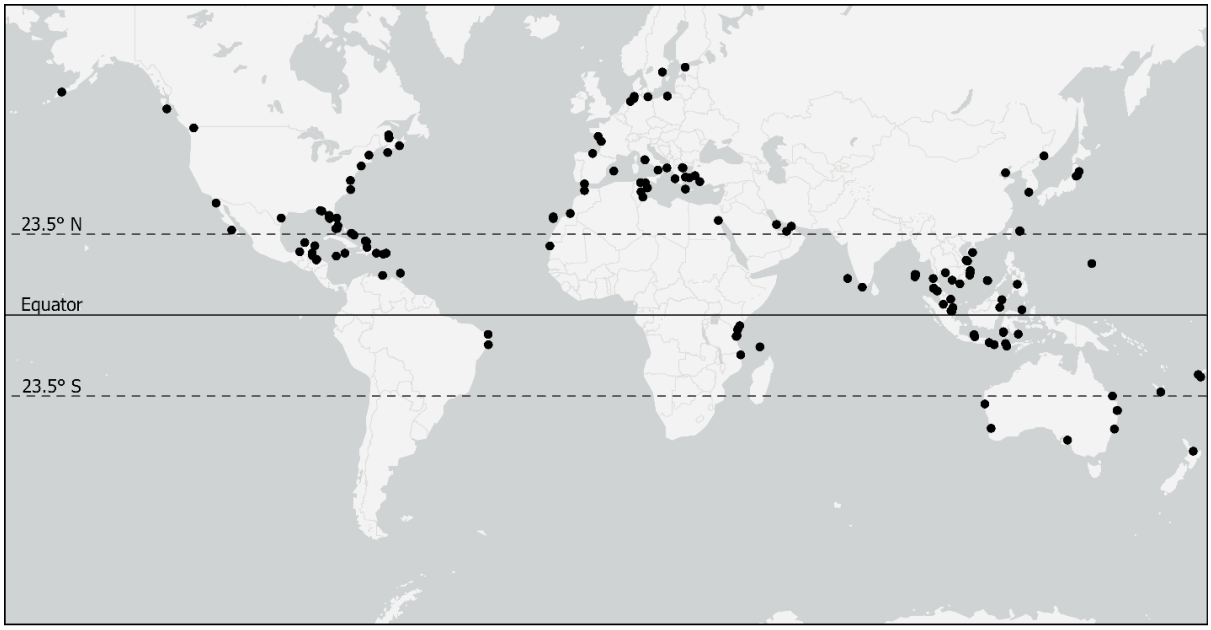

Figure 1. Locations of satellite seagrass remote sensing publications identified in the academic literature published before 30 April 2022.

A total of 24 studies used field sites in Oceania and the South Pacific, including 17 in Australia. There were only six unique sites studied in Australia: Moreton Bay, Queensland (12 studies); Heron Reef, Queensland; Wallis Lake, NSW; the shoreline near Adelaide, SA; Rottnest Island, WA; and Shark Bay, WA. The Australian sites represent a range of different seagrass habitats, including tropical reefs (Heron Reef; Roelfsema et al., 2018), temperate coasts (Adelaide; Fernandes et al., 2022), and two east coast wave-dominated barrier estuaries (Moreton Bay; e.g. Phinn et al., 2008, Wallis Lake; Dekker et al., 2005).

2.3.2 Primary method

The primary method used to map seagrass biophysical characteristics varied across the 203 papers analysed. These methods were grouped into five broad categories: unsupervised pixel-based classification, supervised pixel-based classification, supervised object-based classification, regression, and other (i.e. less common methods e.g. radiative transfer model inversion and time series analysis). The cumulative total of published studies by method category showed that a large proportion of studies favoured supervised pixel-based classification as the primary method (Figure 2). The following sections explore the most common methods used in more detail.

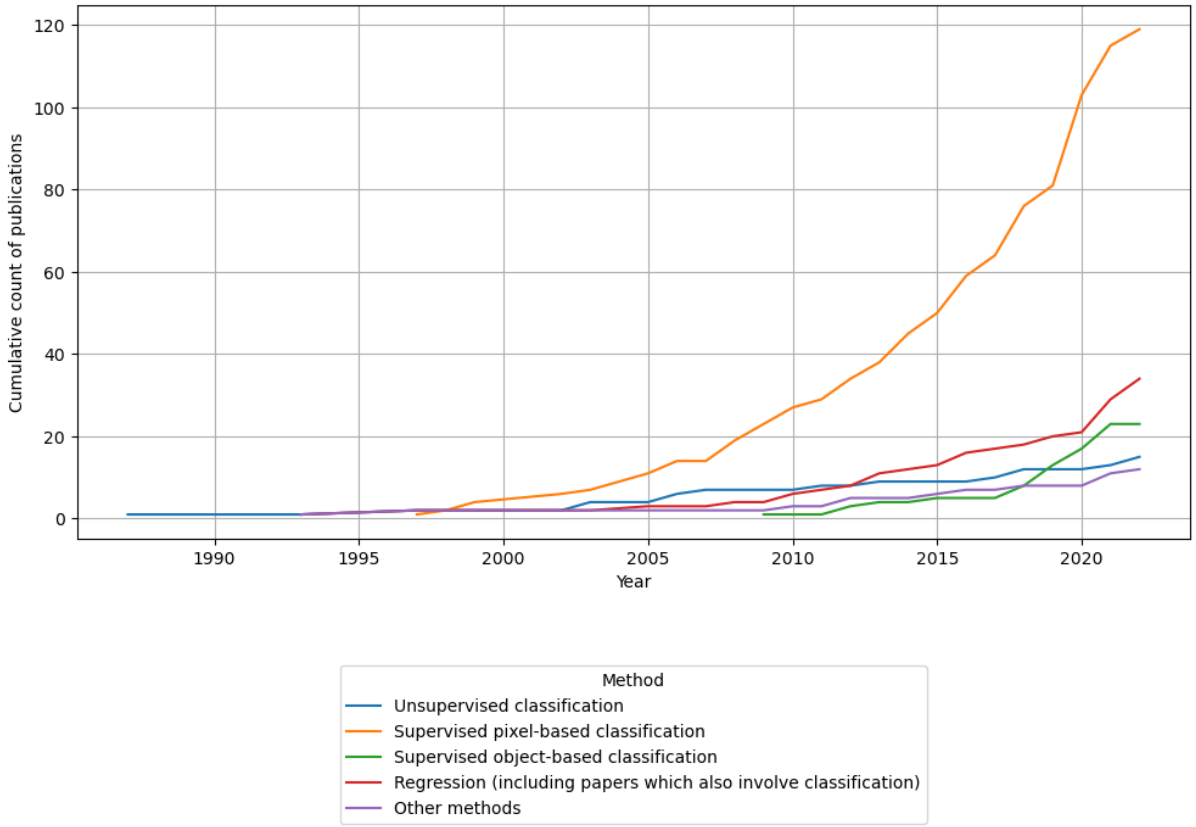

Figure 2. Cumulative total of academic publications on seagrass remote sensing before 30 April 2022, grouped by primary analytical method. Note that 2022, the last year in the series, was incomplete and only includes four months of data.

2.3.2.1 Unsupervised classification and supervised pixel-based classification

Benthic cover mapping using remote sensing is dominated by pixel-based classification in a similar manner to terrestrial mapping applications. Pixel-based classification places pixels into discrete categories (or labels) based on spectral information. The earliest publication identified in the literature search used unsupervised classification techniques to map seagrass cover (Ackleson and Klemas, 1987), and the range of approaches to pixel-based classification was found to widen considerably over time. Numerous seagrass characteristics have been mapped using pixel-based classification (primarily supervised), ranging from relatively simple binary classifications of seagrass extent (e.g. Fornes et al., 2006) to mapping complex multi-species benthic habitats (e.g. Cajica et al., 2020). The discrete mapping output produced by pixel-based classification approaches were used to differentiate identified categories in the study site, such as dominant species (Dekker et al., 2005, e.g. Wicaksono and Lazuardi, 2021, Haro et al., 2022); however, pixel-based classification were also widely used to map stratified

quantitative variables with the most frequent being percentage of seagrass cover (e.g. Wabnitz et al., 2008, Roelfsema et al., 2009, León-Pérez et al., 2019).

Pixel-based classification techniques are relatively straightforward to implement and produce outputs that are readily interpreted and suitable for assessing accuracy. However, exclusive use of spectral information is limited in its capacity to identify meaningful differences in benthic cover that do not produce significantly different spectral signals (Thorhaug et al., 2007). Some pixel-based classifications have accounted for this, improving classifications by incorporating textural datasets derived from spectral information, such as variance (Mumby and Edwards, 2002, Pu and Bell, 2017, Marcello et al., 2018, Kohlus et al., 2020). Others have incorporated entirely separate non-spectral datasets such as bathymetry into the classification process (Wicaksono et al., 2019, Poursanidis et al., 2021).

2.3.2.2 Supervised object-based classification

Object-based classification uses context and spatial relationships in addition to spectral information to categorise groups of pixels (Blaschke et al., 2000) and is capable of mapping vegetation properties with greater accuracy than pixel-based approaches (Blaschke, 2010). The value of object-based approaches relative to pixel-based approaches increases further with higher spatial resolution imagery (Blaschke, 2010). A total of 23 studies identified used object-based classification, 18 of which were published from 2018 onwards (Figure 2).

Urbański et al. (2009) was the earliest study in this review using object-based classification to map seagrass patches across multiple spatial scales, based on an established typology of seagrass landscape patterns (Robbins and Bell, 1994). Object-based approaches have since been used to produce high accuracy maps of seagrass species and percent cover classes. Roelfsema et al. (2014) found that an object-based approach to classifying high resolution IKONOS, WorldView-2 and QuickBird imagery produced higher accuracy results compared to pixel-based classification for mapping of both species composition and percentage cover. Incorporation of bathymetric data into object-based classification routines has also been used to increase overall accuracy (Li et al., 2019, Rende et al., 2020), possibly due to the natural variation in seagrass

characteristics over depth gradients (Collier et al., 2007). The relatively higher accuracy of object-based classification in identifying seagrass landscape patterns suggests that it may be more effective than pixel-based approaches for meaningfully capturing data across heterogeneous seagrass environments. However, outputs from object-based classifications are still necessarily stratified rather than continuous and cannot fully capture gradients of seagrass change over space.

2.3.2.3 Regression analysis

Regression analysis uses an empirical model to relate quantitative field measurements with remote sensing data and is an alternative to classification for continuous variables (e.g. seagrass percent cover). The continuous outputs from regression analysis can produce outputs which more realistically reflect variation across heterogeneous landscapes (Southworth et al., 2004). Regression analysis appears consistently throughout the reviewed literature, first used in the context of seagrass remote sensing by Armstrong (1993), who successfully predicted seagrass biomass from Landsat TM images. In total, 30 of the 203 studies identified used regression analysis to estimate at least one seagrass biophysical characteristic. The dependent variables used in regression analyses were percent cover (e.g. Amran and Rappe, 2010), Leaf Area Index (LAI) (e.g. Wicaksono and Hafizt, 2013) and biomass (e.g. Lyons et al., 2015). Like image classification, regression analysis approaches to seagrass mapping required considerable field data that was site-specific and representative.

While terrestrial remote sensing studies most frequently use spectral vegetation indices (e.g. NDVI) as the independent variable in a regression analysis (Liang and Wang, 2019), attenuation of near-infrared light in the water column limits this in analysis of intertidal seagrass beds (Zoffoli et al., 2020). For subtidal seagrass meadows, independent variables used for regression analysis included single bands (e.g. Phinn et al., 2008), depth-invariant indices (e.g. Mumby et al., 1997), multispectral indices calculated from water-penetrating bands (e.g. Borfecchia et al., 2013), and hyperspectral indices (e.g. Pu and Bell, 2013, Borfecchia et al., 2019).

Regression analysis was often used in addition to pixel-based classification to extract further information from satellite data. For example, classification was used for the

delineation of seagrass presence, so only relevant image data was included in a subsequent regression analysis (Phinn et al., 2008). In some studies, with more detailed classification outputs, such as maps of dominant species, separate models were created where significant interspecific biomass variations are present (Knudby and Nordlund, 2011, Roelfsema et al., 2014). Lyons et al. (2015) found that stratifying relationships between image data and biomass based on species differences significantly improved the predictive strength of regressions.

2.3.2.4 Other methods

A small number of studies (6%) used other methods that did not fall into the above categories, most notably radiative transfer model inversion and time series analysis. Studies that use radiative transfer model inversion for seagrass mapping developed models which incorporated benthic cover, optical properties of the water column, and water depth, and then applied the model to predict reflectances with different arrangements of parameters (Hedley et al., 2009, Hedley et al., 2016). Inversion of this model allows for measured reflectances to be used to predict the relevant parameters, including seagrass cover, based on pre-calculated look-up tables or successive approximation.

Time-series based analysis of remote sensing images to extract seagrass biophysical characteristics was utilised in three studies. Using this technique, seasonal patterns in seagrass reflectance were demonstrated in Florida Bay (Stumpf et al., 1999) and non-seasonal trajectories of seagrass change were mapped in the Caribbean (Michalek et al., 1993). More advanced time series analysis methods were used to develop maps of annual seagrass extent in New Brunswick, Canada, showing considerable variability over time in an estuarine environment (Leblanc et al., 2021). These studies demonstrated not only the value in measuring seagrass biophysical characteristics from a time series of images, but also the high variability in seagrass habitats that necessitates consideration of change.

2.3.3 Target biophysical characteristics

Multiple biophysical characteristics of seagrass meadows were mapped in the identified studies ranging from simple maps showing seagrass extent to per-pixel estimates of

percent cover, biomass, Leaf Area Index (LAI) and primary productivity (Table 3). A total of 96 of the 203 studies mapped seagrass extent only. Discrete percent cover or density classes were mapped in 67 studies, while a total of eight studies mapped percent cover as a continuous variable. Different seagrass species were distinguished in 31, biomass was estimated in 22, LAI was estimated in nine, and primary productivity was estimated in four. These totals include 16 studies where 2-4 variables were estimated for the same sites.

2.3.3.1 Extent

Seagrass meadow extent was the only variable mapped in almost 50% of studies. Mapping extent only was found to be useful for regional scale studies, where detailed field data was not available or field data collection was not feasible (Bouvet et al., 2003, Hogrefe et al., 2014, Topouzelis et al., 2018). Likewise, retrospective change detection studies, where historical field data was unavailable, were frequently limited to mapping extent (e.g. Tsujimoto et al., 2016, Tin et al., 2020). Though maps of extent are potentially useful for some applications, such as design of marine protected areas (Torres-Pulliza et al., 2013), they do not capture the heterogeneity of seagrass environments in relation to species composition and density. Simple extent mapping may be appropriate for largely homogeneous areas and is valuable as a preliminary step for delineating seagrass meadows prior to further analysis (e.g. Koedsin et al., 2016, Vahtmäe et al., 2021).

2.3.3.2 Discrete percent cover/density classes

The abundance or density of seagrass meadows frequently varies continuously along environmental gradients and in patchy meadows (Bell et al., 1999, Collier et al., 2007, van der Heide et al., 2010). Despite this, 89% of the studied papers which produced estimates of seagrass abundance used pixel or object-based classification techniques to create discrete abundance maps. Over 90% of the discrete percent cover mapping papers used two to four classes of percent cover.

Though Landsat TM and ETM+ imagery was used by some researchers to successfully map cover classes (e.g. Calleja et al., 2017), studies which compare multiple sensors tended to show improved accuracy results with higher resolution images. Higher

accuracies across all classes have been reported when using hyperspectral satellite or aerial images compared to satellite multispectral data (Phinn et al., 2008, Pu and Bell, 2013). QuickBird-2 has been used to successfully map seagrass percent cover when Landsat TM was not sufficient (Yang and Yang, 2009), and Sentinel-2 data has provided better accuracy results compared to Landsat TM (Kohlus et al., 2020).

Meyer et al. (2012) compared two classification schema for seagrass percent cover: one with two classes (<25% and 25-100%), and one with three (<25%, 25-75% and >75%). Classification accuracies were consistently lower across seagrass classes when the intermediate class was added. A similar study also achieved high overall accuracy (92-96%) with three classes, but low to moderate accuracy (66-79%) with five (Pu et al., 2012). A clear pattern is apparent across studies that map seagrass cover where intermediate or sparse classes are relatively inaccurate. Wabnitz et al. (2008) could not successfully differentiate between medium and dense seagrass. Many other studies report low to very low classification accuracy values for sparse seagrass classes (Pu et al., 2014, Zharikov et al., 2018, Li et al., 2019, Su and Huang, 2019, Strydom et al., 2020). Additionally, confusion between cover classes was a common issue (Pasqualini et al., 2005, Lyons et al., 2011, Roelfsema et al., 2014). Consequently, some researchers conclude that, if possible, mapping of seagrass cover as a continuous variable may be of greater value (Lyons et al., 2011). However, in the absence of other more rigorous techniques and field data to support continuous estimates of seagrass cover, discrete mapping seagrass cover classes was shown to be successful in some circumstances, especially with high resolution images and four or fewer classes.

2.3.3.3 Continuous mapping of percent cover, LAI, biomass, and primary productivity

Continuous mapping of seagrass characteristics was considerably less popular than discrete classification. A total of 33 studies were identified which used satellite remote sensing data to map cover, LAI, biomass, or primary productivity as continuous variables in seagrass habitats. These variables are typically estimated based on the same remote sensing-derived value or values, such as spectral bands or a vegetation index, as an independent variable. Accordingly, these variables are considered together here.

Different remote sensing-derived measurements and indices have been used as independent variables in regression analyses. Depth Invariant Indices (Lyzenga, 1978) were found to have moderate to good predictive power for biomass and percent cover (Armstrong, 1993, Mumby et al., 1997, Schweizer et al., 2005, Amran and Rappe, 2010, Fauzan et al., 2017), as did the modified Bottom Reflectance Index (Misbari and Hashim, 2016). NDVI has been used to accurately predict seagrass cover and biomass, but this was only possible in intertidal meadows due to the absence of an overlying water column (Barillé et al., 2010, Zoffoli et al., 2020). For subtidal seagrass meadows, a wide range of vegetation indices have been tested. Bramante et al. (2018) used a function of the coastal blue and red bands of WorldView-2, which was found to have a statistically significant relationship with seagrass biomass (R^2 = 0.55, $p<0.001$). Using multiple linear regression based on normalized differences of visible bands from Landsat OLI data had similarly significant results (Borfecchia et al., 2019). Hyperspectral bands from EO-1 Hyperion data in the visible and red-edge have also been shown to improve model predictions for seagrass mapping in estuarine environments (Pu et al., 2012). These studies demonstrate the effectiveness of spectral indices for predicting continuous variables such as percent cover, especially in shallow, submerged seagrass environments, such as estuaries.

2.3.3.4 Species

Seagrass species maps were produced in 31 of the identified studies. This is often possible due to differences in morphology and leaf colour between species, though in some circumstances they can be too similar to differentiate (Fyfe, 2003, Thorhaug et al., 2007). Though spectral differences between seagrass species are identifiable, species mapping is often a trade-off between accuracy and thematic resolution. Mumby et al. (1997) designed three classification schemas based on field surveys and the Bray-Curtis similarity index (Bray and Curtis, 1957). The most complex schema included 13 classes, including mixed classes, macroalgae, and coral. This classification returned low accuracy with this complex schema (37% overall accuracy at most). Higher overall accuracies of 73% and 67% for Landsat TM and SPOT XS images respectively were only achieved with a simplified four class schema, including all seagrass as a single class. Classifying at the same high thematic resolution has also been attempted with IKONOS

images, achieving 41% overall accuracy using spectral information only, and 50% when incorporating textural data (Mumby and Edwards, 2002).

Phinn et al. (2008) used pixel-based classification with QuickBird-2 imagery to map seagrass species assemblages in Moreton Bay, Queensland, Australia, with a schema of eight classes (five monospecific, three mixed species). They reported an overall accuracy of only 23% for the species map, though a comparative classification using CASI-2 airborne hyperspectral imagery performed only slightly better (28% overall accuracy). A later study at the same site reported considerably better results, also using pixel-based classification and QuickBird-2 imagery, but with only five species classes (four monospecific, one mixed) (Lyons et al., 2011). Object-based classification and a five-class schema applied to QuickBird-2, IKONOS and WorldView-2 data also showed good results (Roelfsema et al., 2014). The authors reported overall accuracies between 68-83% (average 77%) using the OBIA method (Roelfsema et al., 2014). The improved accuracy that OBIA and textural data offers demonstrates that non-spectral information can enhance species classification results to produce more accurate high thematic resolution maps.

2.3.4 Sensors

A total of 33 different satellite sensors were utilized for mapping biophysical properties of seagrass in the reviewed literature, though only nine sensors were used in at least five publications (Figure 3). The earliest study identified in this review compared Landsat TM and MSS images (Ackleson and Klemas, 1987), and since then, a further 48 studies have used Landsat TM images, 39 used Landsat ETM+ images, and 36 used Landsat OLI images. The temporal continuity of the Landsat program makes it particularly well-suited for the analysis of long-term seagrass change (Dekker et al., 2005, Yang and Yang, 2009, Knudby et al., 2010, Lyons et al., 2012, Blakey et al., 2015, Vo et al., 2020). The open-access and availability of Landsat data contribute to its efficacy across a range of applications. However, the ~30m spatial resolution of Landsat has been identified as a limiting factor in some seagrass environments (Phinn et al., 2008, Lyons et al., 2015), which frequently vary at a scale finer than a single 30 m Landsat pixel.

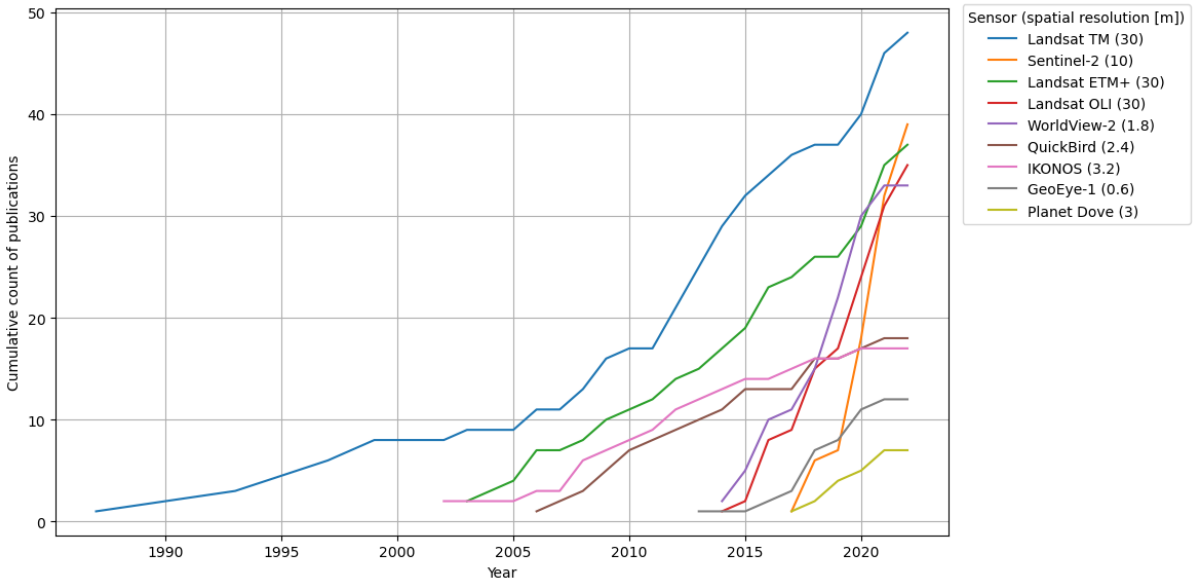

Figure 3. Cumulative total of publications using the nine most common sensors identified in the literature. Note that 2022, the last year in the series, was incomplete and only includes four months of data.

An increasing preference towards very high spatial resolution sensors can be identified in the literature. WorldView-2 (33 studies), IKONOS (18 studies), and QuickBird (17 studies) provided new options for higher spatial resolution mapping of seagrass. Comparisons between Landsat TM and IKONOS images have consistently shown that the higher spatial resolution IKONOS images produce more accurate maps, regardless of classification schema complexity (Mumby and Edwards, 2002, Pu and Bell, 2017).

Sentinel-2, though medium spatial resolution of 10-20 m, has rapidly become the most common platform for seagrass remote sensing. Sentinel-2 was used in 39 studies despite only having been launched in 2015 and was the most used sensor in 2018, 2020, 2021, and 2022. Sentinel-2 has the benefit of being freely available through the European Space Agency Copernicus programme, enabling large-scale seagrass studies at an improved spatial resolution from Landsat's 30 m (Traganos and Reinartz, 2018). Additionally, Sentinel-2 offers additional spectral bands which are not available in data from legacy satellite sensors such as Landsat TM/ETM+. The Sentinel-2 coastal blue band has been shown to increase the maximum depth at which seagrass can be detected (Poursanidis et al., 2019). Even with Sentinel-2 imagery resampled to 30 m pixels, it has demonstrated higher overall accuracies than Landsat TM and ETM+ images, which have fewer bands in the visible and red-edge range (Strydom et al., 2020). Multispectral

sensors with additional visible bands provide enhanced spectral information for improving seagrass mapping accuracy.

2.4 UAV remote sensing

UAV remote sensing has more recently become a viable option for mapping seagrass, though relatively few studies were published before the April 2022 date of this systematic review. Pixel- and object-based classification applied to UAV-captured images was used to map extent of seagrass meadows (Nahirnick et al., 2019, James et al., 2020, Hobley et al., 2021, Sneep et al., 2024), percent cover classes (Hamad et al., 2022), and species compositions (Tahara et al., 2022, Elma et al., 2024). The maps produced from UAV images were shown to provide detailed spatial information on fine-scale features within seagrass meadows such as small patches and boat propeller scars (Karang et al., 2024). UAV images were also used for continuous mapping of seagrass biophysical characteristics (Chand and Bollard, 2021, Akinaga et al., 2025), as the very high resolution of the images was found to be effective for capturing intra-habitat heterogeneity (Price et al., 2022). Some studies have further advanced UAV-based seagrass mapping by incorporating other datasets, such as bathymetric data (James et al., 2020, Ekelund et al., 2024). An additional application of UAV-acquired images was to train algorithms for processing satellite remote sensing data (Carpenter et al., 2022, Wicaksono et al., 2024). The approaches used in these studies were generally comparable to satellite remote sensing, though with much finer spatial resolution data, which allowed for resolution of very small features and heterogeneity at very fine scales.

The high spatial resolution of UAV images therefore makes them well-suited to characterising heterogeneity. UAVs can also capture variability in seagrass habitats by repeating flights at the same location (James et al., 2025). However, to produce reliable change information, the conditions at flight times must be considered, especially tidal height (Prystay et al., 2023, Elma et al., 2024). Reliably detecting change could also be supported with application of water column correction techniques, although this is uncommon in published studies using UAV data, and no studies were identified that applied water column corrections for seagrass mapping. However, the physical principles on which water column correction methods are based are as applicable to

UAV data as other sources. Common water column correction methods such as Depth Invariant Indices and algebraic methods have been successfully applied to UAV images in contexts such as coral reef mapping (Muslim et al., 2019, Cornet & Joyce, 2021, Zaki et al., 2022). With the correct planning and processing methods to account for variations in environmental conditions, repeated UAV surveys provide viable opportunities for time series seagrass mapping.

2.5 Discussion and conclusions

Seagrass mapping sites are globally distributed but are clustered in certain regions, namely Southeast Asia, the Caribbean Sea, and the Mediterranean Sea. Approximately half of the reviewed seagrass mapping research has occurred in the tropics, and seagrass mapping in the northern hemisphere is more common than the southern hemisphere. Though this is partly a function of the distribution of seagrass, which is found globally but concentrated in the tropics (Jayathilake and Costello, 2018), it also reflects regional bias in seagrass mapping research. Most seagrass mapping sites reported in the scientific literature are reefs and coastal meadows in the tropics and Europe, while only four studies involved temperate southern hemisphere estuarine sites.

Multiple remote sensing methods were used to map seagrass biophysical characteristics. Species classification was largely successful for multi-species meadows, even in tropical areas with many species (Knudby and Nordlund, 2011). Distinguishing between species based on morphology offers another viable approach when individual species are not separable (Wicaksono et al., 2021). Seagrass species maps were further improved beyond standard pixel-based classification outputs with methods such as object-based classification and machine learning classifiers. Classification of discrete cover classes was also a common approach to characterizing seagrass with satellite remote sensing data but frequently resulted in lower classification accuracies due to interclass confusion, especially for intermediate classes between bare substrate and dense seagrass (Pasqualini et al., 2005, Lyons et al., 2011, Roelfsema et al., 2014). There is a clear need for new remote sensing methods that can accurately estimate seagrass percent cover, especially for heterogeneous meadows.

A key challenge common to studies that involve the continuous measurement of seagrass characteristics was identifying remote sensing variables that can be used to predict subtidal seagrass percent cover, LAI, or related variables. This is because near infra-red reflectance, which is commonly used in terrestrial and intertidal contexts, is not viable for submerged sites due to its rapid attenuation by water. Various multispectral remote sensing values have been tested for this purpose, including a single green band (Fauzan et al., 2017) and vegetation indices based on visible bands (Borfecchia et al., 2013). Studies using hyperspectral data for estimating seagrass abundance suggest that, with the correct spectral information, new indices could be developed based on blue, red, and red-edge reflectance (Pu and Bell, 2013, Pu and Bell, 2017). Continuous estimates of seagrass cover have the potential to capture detail on seagrass cover as it varies spatio-temporally across heterogeneous seagrass meadows, but this is understudied.

More recent platforms which offer improved spatial resolution over Landsat (e.g. Sentinel-2) have led to more accurate seagrass mapping, as they were found to capture heterogeneity in seagrass habitats occurring over fine spatial scales. There has been rapid adoption of Sentinel-2 for seagrass mapping, likely because it compares well to Landsat in terms of spatial, spectral, and temporal resolution. The additional spectral data in the coastal blue and red-edge captured by Sentinel-2 have shown promise for improving efficacy of seagrass detection (Poursanidis et al., 2019, Strydom et al., 2020), but predicting continuous variations in seagrass cover density using vegetation indices derived from Sentinel-2 data is an understudied area of inquiry.

Remote sensing using UAV-captured images has the potential to contribute significantly to characterising seagrass heterogeneity at fine scales. Satellite images are generally of a medium spatial resolution which can mask heterogeneity, especially those that are freely available such as Sentinel-2 (10 m) and Landsat (30 m). Recent advancements in UAV platforms provide a timely opportunity to assess the efficacy of UAV data in mapping and monitoring of seagrass at very fine spatial scales. UAV-mounted multispectral sensors that offer more than three visible spectral bands including red-edge bands, mostly developed for precision agriculture applications,

present an opportunity to further examine the role of spectral resolution in estuarine seagrass mapping.

Satellite remote sensing of seagrass is a rapidly expanding research field with global applications across diverse coastal settings. However, most satellite remote sensing studies of seagrass focus on the characterisation of extent, species, or discrete percent cover classes with limited analysis of spatio-temporal seagrass dynamics. Variability and heterogeneity in estuarine seagrass meadows is relatively understudied using remote sensing techniques, even though the condition of estuarine seagrass is an important indicator of overall estuarine health (Corbett et al., 2004, Purvaja et al., 2018). Emerging developments in remote sensing, including high resolution satellite images, sensors capturing data in additional spectral regions (e.g. red-edge), and UAV-mounted sensors, show considerable potential for improving the accuracy and resolution of estuarine seagrass mapping. These developments have the potential to enable accurate detection of continuous gradients in heterogeneous seagrass meadows, and fine-scale monitoring of seagrass temporal variability and change.

References

ACKLESON, S. & KLEMAS, V. 1987. Remote sensing of submerged aquatic vegetation in lower Chesapeake Bay: A comparison of Landsat MSS to TM imagery. *Remote Sensing of Environment,* 22, 235-248.

AKINAGA, T., SAITO, M., ONODERA, S.-I. & HYODO, F. 2025. UAV visual imagery-based evaluation of blue carbon as seagrass beds on a tidal flat scale. *Remote Sensing Applications: Society and Environment,* 37, 101430.

AMRAN, M. A. & RAPPE, R. A. J. B. 2010. Estimation of seagrass coverage by depth invariant indices on quickbird imagery. 17, 42-50.

ARAYA-LOPEZ, R., DE PAULA COSTA, M. D., WARTMAN, M. & MACREADIE, P. I. 2023. Trends in the application of remote sensing in blue carbon science. *Ecology and Evolution,* 13, e10559.

ARMSTRONG, R. A. 1993. Remote sensing of submerged vegetation canopies for biomass estimation. *International Journal of Remote Sensing,* 14, 621-627.

BARILLÉ, L., ROBIN, M., HARIN, N., BARGAIN, A. & LAUNEAU, P. 2010. Increase in seagrass distribution at Bourgneuf Bay (France) detected by spatial remote sensing. *Aquatic Botany,* 92, 185-194.

BELL, S. S., ROBBINS, B. D. & JENSEN, S. L. 1999. Gap dynamics in a seagrass landscape. *Ecosystems,* 2, 493-504.

BLAKEY, T., MELESSE, A. & HALL, M. O. 2015. Supervised classification of benthic reflectance in shallow subtropical waters using a generalized pixel-based classifier across a time series. *Remote Sensing,* 7, 5098-5116.

BLASCHKE, T. 2010. Object based image analysis for remote sensing. *ISPRS Journal of Photogrammetry and Remote Sensing,* 65, 2-16.

BLASCHKE, T., LANG, S., LORUP, E., STROBL, J., ZEIL, P. J. E. I. F. P., POLITICS & PUBLIC, T. 2000. Object-oriented image processing in an integrated GIS/remote sensing environment and perspectives for environmental applications. 2, 555-570.

BORFECCHIA, F., CONSALVI, N., MICHELI, C., CARLI, F. M., COGNETTI DE MARTIIS, S., GNISCI, V., PIERMATTEI, V., BELMONTE, A., DE CECCO, L. & BONAMANO, S. J. I. J. O. R. S. 2019. Landsat 8 OLI satellite data for mapping of the Posidonia oceanica and benthic habitats of coastal ecosystems. 40, 1548-1575.

BORFECCHIA, F., DE CECCO, L., MARTINI, S., CERIOLA, G., BOLLANOS, S., VLACHOPOULOS, G., VALIANTE, L. M., BELMONTE, A. & MICHELI, C. 2013. Posidonia oceanica genetic and biometry mapping through high-resolution satellite spectral vegetation indices and sea-truth calibration. *International Journal of Remote Sensing,* 34, 4680-4701.

BOUVET, G., FERRARIS, J. & ANDRÉFOUËT, S. 2003. Evaluation of large-scale unsupervised classification of New Caledonia reef ecosystems using Landsat 7 ETM+ imagery. *Oceanologica Acta,* 26, 281-290.

BRAY, J. R. & CURTIS, J. T. 1957. An ordination of the upland forest communities of southern Wisconsin. *Ecological Monographs,* 27, 326-349.

CAJICA, A. K. O., HINOJOSA-ARANGO, G., GARZA-PÉREZ, J. R. & RIOJA-NIETO, R. 2020. Seascape metrics, spatio-temporal change, and intensity of use for the spatial conservation prioritization of a Caribbean marine protected area. *Ocean & Coastal Management,* 194, 105265.

CALLEJA, F., GALVAN, C., SILIO-CALZADA, A., JUANES, J. A. & ONDIVIELA, B. 2017. Long-term analysis of Zostera noltei: A retrospective approach for understanding seagrasses' dynamics. *Mar Environ Res,* 130, 93-105.

CARPENTER, S., BYFIELD, V., FELGATE, S. L., PRICE, D. M., ANDRADE, V., COBB, E., STRONG, J., LICHTSCHLAG, A., BRITTAIN, H. & BARRY, C. 2022. Using unoccupied aerial vehicles (UAVs) to map seagrass cover from Sentinel-2 imagery. *Remote Sensing,* 14, 477.

CHAND, S. & BOLLARD, B. 2021. Low altitude spatial assessment and monitoring of intertidal seagrass meadows beyond the visible spectrum using a remotely piloted aircraft system. *Estuarine, Coastal and Shelf Science,* 255, 107299.

COLLIER, C. J., LAVERY, P. S., MASINI, R. J. & RALPH, P. J. J. M. E. P. S. 2007. Morphological, growth and meadow characteristics of the seagrass Posidonia sinuosa along a depth-related gradient of light availability. 337, 103-115.

CORBETT, C. A., DOERING, P. H., MADLEY, K. A., OTT, J. A. & TOMASKO, D. A. 2004. Using seagrass coverage as an indicator of ecosystem condition. *Estuarine indicators.* CRC Press.

CORNET, V. J. & JOYCE, K. E. 2021. Assessing the potential of remotely-sensed drone spectroscopy to determine live coral cover on Heron Reef. *Drones,* 5(2), 29.

DEKKER, A. G., BRANDO, V. E. & ANSTEE, J. M. 2005. Retrospective seagrass change detection in a shallow coastal tidal Australian lake. *Remote Sensing of Environment,* 97**,** 415-433.

DUARTE, C. M., APOSTOLAKI, E. T., SERRANO, O., STECKBAUER, A. & UNSWORTH, R. K. 2025. Conserving seagrass ecosystems to meet global biodiversity and climate goals. *Nature Reviews Biodiversity***,** 1-16.

DUFFY, J. E., BENEDETTI-CECCHI, L., TRINANES, J., MULLER-KARGER, F. E., AMBO-RAPPE, R., BOSTRÖM, C., BUSCHMANN, A. H., BYRNES, J., COLES, R. G., CREED, J., CULLEN-UNSWORTH, L. C., DIAZ-PULIDO, G., DUARTE, C. M., EDGAR, G. J., FORTES, M., GONI, G., HU, C., HUANG, X., HURD, C. L., JOHNSON, C., KONAR, B., KRAUSE-JENSEN, D., KRUMHANSL, K., MACREADIE, P., MARSH, H., MCKENZIE, L. J., MIESZKOWSKA, N., MILOSLAVICH, P., MONTES, E., NAKAOKA, M., NORDERHAUG, K. M., NORLUND, L. M., ORTH, R. J., PRATHEP, A., PUTMAN, N. F., SAMPER-VILLARREAL, J., SERRAO, E. A., SHORT, F., PINTO, I. S., STEINBERG, P., STUART-SMITH, R., UNSWORTH, R. K. F., VAN KEULEN, M., VAN TUSSENBROEK, B. I., WANG, M., WAYCOTT, M., WEATHERDON, L. V., WERNBERG, T. & YAAKUB, S. M. 2019. Toward a Coordinated Global Observing System for Seagrasses and Marine Macroalgae. *Frontiers in Marine Science,* 6.

EKELUND, A., WADDINGTON, A., HARRIS, S. D., HOWE, W., DERSELL, C., JOSEFSSON, E., OLSZEWSKI, J., TINGÅKER, T., YANG, E. & DUARTE, C. M. 2024. High-resolution, precision mapping of seagrass blue carbon habitat using multi-spectral imaging and aerial LiDAR. *Estuarine, Coastal and Shelf Science,* 304**,** 108832.

ELMA, E., GAULTON, R., CHUDLEY, T. R., SCOTT, C. L., EAST, H. K., WESTOBY, H. & FITZSIMMONS, C. 2024. Evaluating UAV-based multispectral imagery for mapping an intertidal seagrass environment. *Aquatic Conservation: Marine and Freshwater Ecosystems,* 34**,** e4230.

FAUZAN, M. A., KUMARA, I. S., YOGYANTORO, R., SUWARDANA, S., FADHILAH, N., NURMALASARI, I., APRIYANI, S. & WICAKSONO, P. 2017. Assessing the capability of Sentinel-2A data for mapping seagrass percent cover in Jerowaru, East Lombok. *Indonesian Journal of Geography,* 49**,** 195-203.

FERNANDES, M. B., HENNESSY, A., LAW, W. B., DALY, R., GAYLARD, S., LEWIS, M. & CLARKE, K. 2022. Landsat historical records reveal large-scale dynamics and enduring recovery of seagrasses in an impacted seascape. *Science of the Total Environment,* 813**,** 152646.

FORNES, A., BASTERRETXEA, G., ORFILA, A., JORDI, A., ÁLVAREZ, A., TINTORÉ, J. J. I. J. O. P. & SENSING, R. 2006. Mapping Posidonia oceanica from IKONOS. 60**,** 315-322.

FYFE, S. 2003. Spatial and temporal variation in spectral reflectance: Are seagrass species spectrally distinct? *Journal of Limnology and Oceanography,* 48**,** 464-479.

HA, N. T., MANLEY-HARRIS, M., PHAM, T. D. & HAWES, I. 2020. A Comparative Assessment of Ensemble-Based Machine Learning and Maximum Likelihood Methods for Mapping Seagrass Using Sentinel-2 Imagery in Tauranga Harbor, New Zealand. *Remote Sensing,* 12.

HAMAD, I. Y., STAEHR, P. A., RASMUSSEN, M. B. & SHEIKH, M. 2022. Drone-Based Characterization of Seagrass Habitats in the Tropical Waters of Zanzibar. *Remote Sensing* [Online], 14.

HARO, S., JESUS, B., OIRY, S., PAPASPYROU, S., LARA, M., GONZÁLEZ, C. & CORZO, A. 2022. Microphytobenthos spatio-temporal dynamics across an intertidal gradient using Random Forest classification and Sentinel-2 imagery. *Science of The Total Environment,* 804**,** 149983.

HEDLEY, J., ROELFSEMA, C. & PHINN, S. R. J. R. S. O. E. 2009. Efficient radiative transfer model inversion for remote sensing applications. 113**,** 2527-2532.

HEDLEY, J., RUSSELL, B., RANDOLPH, K. & DIERSSEN, H. 2016. A physics-based method for the remote sensing of seagrasses. *Remote Sensing of Environment,* 174**,** 134-147.

HOBLEY, B., AROSIO, R., FRENCH, G., BREMNER, J., DOLPHIN, T. & MACKIEWICZ, M. 2021. Semi-supervised segmentation for coastal monitoring seagrass using RPA imagery. *Remote Sensing,* 13**,** 1741.

HOGREFE, K. R., WARD, D. H., DONNELLY, T. F. & DAU, N. 2014. Establishing a baseline for regional scale monitoring of eelgrass (Zostera marina) habitat on the lower Alaska Peninsula. *Remote Sensing,* 6**,** 12447-12477.

JAMES, D., COLLIN, A., BOUET, A., PERETTE, M., DIMEGLIO, T., HERVOUET, G., DUROZIER, T., DUTHION, G. & LEBAS, J.-F. 2025. Multi-Temporal Drone Mapping of Coastal Ecosystems in Restoration: Seagrass, Salt Marsh, and Dune. *Journal of Coastal Research,* 113**,** 524-528.

JAMES, D., COLLIN, A., HOUET, T., MURY, A., GLORIA, H. & LE POULAIN, N. 2020. Towards Better Mapping of Seagrass Meadows using UAV Multispectral and Topographic Data. *Journal of Coastal Research,* 95.

JAYATHILAKE, D. R. M. & COSTELLO, M. J. 2018. A modelled global distribution of the seagrass biome. *Biological Conservation,* 226**,** 120-126.

KARANG, I., PRAVITHA, N. L. P. R., NUARSA, I. W., BASHEER AHAMMED, K. & WICAKSONO, P. 2024. High-resolution seagrass species mapping and propeller scars detection in Tanjung Benoa, Bali through UAV imagery. *Journal of Ecological Engineering,* 25.

KIRK, J. T. 1994. *Light and photosynthesis in aquatic ecosystems*, Cambridge university press.

KNUDBY, A., NEWMAN, C., SHAGHUDE, Y. & MUHANDO, C. 2010. Simple and effective monitoring of historic changes in nearshore environments using the free archive of Landsat imagery. *International Journal of Applied Earth Observation and Geoinformation,* 12**,** S116-S122.

KNUDBY, A. & NORDLUND, L. 2011. Remote sensing of seagrasses in a patchy multi-species environment. *International Journal of Remote Sensing,* 32**,** 2227-2244.

KOEDSIN, W., INTARARUANG, W., RITCHIE, R. J. & HUETE, A. 2016. An integrated field and remote sensing method for mapping seagrass species, cover, and biomass in southern Thailand. *Remote Sensing,* 8**,** 292.

KOHLUS, J., STELZER, K., MÜLLER, G., SMOLLICH, S. J. E., COASTAL & SCIENCE, S. 2020. Mapping seagrass (Zostera) by remote sensing in the Schleswig-Holstein Wadden Sea. 238**,** 106699.

KRAUSE, J. R., CAMERON, C., ARIAS-ORTIZ, A., CIFUENTES-JARA, M., CROOKS, S., DAHL, M., FRIESS, D. A., KENNEDY, H., LIM, K. E. & LOVELOCK, C. E. 2025. Global seagrass carbon stock variability and emissions from seagrass loss. *Nature Communications,* 16**,** 1-9.

LEBLANC, M.-L., LAROCQUE, A., LEBLON, B., HANSON, A. & HUMPHRIES, M. M. 2021. Using Landsat time-series to monitor and inform seagrass dynamics: a case study in the Tabusintac estuary, New Brunswick, Canada. *Canadian Journal of Remote Sensing,* 47**,** 65-82.

LEÓN-PÉREZ, M. C., HERNÁNDEZ, W. J. & ARMSTRONG, R. A. J. J. O. C. R. 2019. Characterization and distribution of seagrass habitats in a Caribbean nature reserve using high-resolution satellite imagery and field sampling. 35**,** 937-947.

LI, J., SCHILL, S. R., KNAPP, D. E. & ASNER, G. P. J. R. S. 2019. Object-based mapping of coral reef habitats using planet dove satellites. 11**,** 1445.

LIANG, S. & WANG, J. 2019. *Advanced remote sensing: terrestrial information extraction and applications*, Academic Press.

LYONS, M., PHINN, S. & ROELFSEMA, C. 2011. Integrating Quickbird Multi-Spectral Satellite and Field Data: Mapping Bathymetry, Seagrass Cover, Seagrass Species and Change in Moreton Bay, Australia in 2004 and 2007. *Remote Sensing,* 3**,** 42-64.

LYONS, M., ROELFSEMA, C., KOVACS, E., SAMPER-VILLARREAL, J., SAUNDERS, M., MAXWELL, P. & PHINN, S. 2015. Rapid monitoring of seagrass biomass using a simple linear modelling approach, in the field and from space. *Marine Ecology Progress Series,* 530**,** 1-14.

LYONS, M. B., PHINN, S. R. & ROELFSEMA, C. M. 2012. Long term land cover and seagrass mapping using Landsat and object-based image analysis from 1972 to 2010 in the coastal environment of South East Queensland, Australia. *ISPRS Journal of Photogrammetry and Remote Sensing,* 71**,** 34-46.

LYZENGA, D. R. 1978. Passive remote sensing techniques for mapping water depth and bottom features. *Applied Optics,* 17**,** 379-383.

MARCELLO, J., EUGENIO, F., MARTÍN, J. & MARQUÉS, F. J. R. S. 2018. Seabed mapping in coastal shallow waters using high resolution multispectral and hyperspectral imagery. 10**,** 1208.

MEYER, C. A., PU, R. J. E. M. & ASSESSMENT 2012. Seagrass resource assessment using remote sensing methods in St. Joseph Sound and Clearwater Harbor, Florida, USA. 184**,** 1131-1143.

MICHALEK, J. L., WAGNER, T. W., LUCZKOVICH, J. J. & STOFFLE, R. W. 1993. Multispectral change vector analysis for monitoring coastal marine environments. *Photogrammetric Engineering and Remote Sensing,* 59**,** 381-384.

MISBARI, S. & HASHIM, M. 2016. Change detection of submerged seagrass biomass in shallow coastal water. *Remote Sensing,* 8**,** 200.

MUMBY, P., GREEN, E., EDWARDS, A. & CLARK, C. J. M. E. P. S. 1997. Measurement of seagrass standing crop using satellite and digital airborne remote sensing. 159**,** 51-60.

MUMBY, P. J. & EDWARDS, A. J. 2002. Mapping marine environments with IKONOS imagery: enhanced spatial resolution can deliver greater thematic accuracy. *Remote Sensing of Environment,* 82**,** 248-257.

MUSLIM, A. M, CHONG, W. S., SAFUAN, C. D. M., KHALIL, I. & HOSSAIN, M. S. 2019. Coral Reef Mapping of UAV: A Comparison of Sun Glint Correction Methods. *Remote Sensing,* 11(20), 2422.

NAHIRNICK, N. K., RESHITNYK, L., CAMPBELL, M., HESSING-LEWIS, M., COSTA, M., YAKIMISHYN, J. & LEE, L. 2019. Mapping with confidence; delineating seagrass habitats using Unoccupied Aerial Systems (UAS). *Remote Sensing in Ecology and Conservation,* 5**,** 121-135.

PASQUALINI, V., PERGENT-MARTINI, C., PERGENT, G., AGREIL, M., SKOUFAS, G., SOURBES, L. & TSIRIKA, A. J. R. S. O. E. 2005. Use of SPOT 5 for mapping seagrasses: An application to Posidonia oceanica. 94**,** 39-45.

PHINN, S., ROELFSEMA, C., DEKKER, A., BRANDO, V. & ANSTEE, J. 2008. Mapping seagrass species, cover and biomass in shallow waters: An assessment of satellite multi-spectral and airborne hyper-spectral imaging systems in Moreton Bay (Australia). *Remote Sensing of Environment,* 112**,** 3413-3425.

POURSANIDIS, D., TRAGANOS, D., REINARTZ, P. & CHRYSOULAKIS, N. 2019. On the use of Sentinel-2 for coastal habitat mapping and satellite-derived bathymetry estimation using downscaled coastal aerosol band. *International Journal of Applied Earth Observation and Geoinformation,* 80**,** 58-70.

POURSANIDIS, D., TRAGANOS, D., TEIXEIRA, L., SHAPIRO, A. & MUAVES, L. 2021. Cloud-native seascape mapping of Mozambique' s Quirimbas National Park with Sentinel-2. *Remote Sensing in Ecology and Conservation,* 7**,** 275-291.

PRICE, D. M., FELGATE, S. L., HUVENNE, V. A., STRONG, J., CARPENTER, S., BARRY, C., LICHTSCHLAG, A., SANDERS, R., CARRIAS, A. & YOUNG, A. 2022. Quantifying the intra-habitat variation of seagrass beds with unoccupied aerial vehicles (UAVs). *Remote Sensing,* 14**,** 480.

PRYSTAY, T. S., ADAMS, G., FAVARO, B., GREGORY, R. S. & LE BRIS, A. 2023. The reproducibility of remotely piloted aircraft systems to monitor seasonal variation in submerged seagrass and estuarine habitats. *Facets,* 8**,** 1-22.

PU, R. & BELL, S. 2013. A protocol for improving mapping and assessing of seagrass abundance along the West Central Coast of Florida using Landsat TM and EO-1 ALI/Hyperion images. *ISPRS Journal of Photogrammetry and Remote Sensing,* 83**,** 116-129.

PU, R. & BELL, S. 2017. Mapping seagrass coverage and spatial patterns with high spatial resolution IKONOS imagery. *International Journal of Applied Earth Observation and Geoinformation,* 54**,** 145-158.

PU, R., BELL, S. & MEYER, C. 2014. Mapping and assessing seagrass bed changes in Central Florida's west coast using multitemporal Landsat TM imagery. *Estuarine, Coastal and Shelf Science,* 149**,** 68-79.

PU, R., BELL, S., MEYER, C., BAGGETT, L. & ZHAO, Y. 2012. Mapping and assessing seagrass along the western coast of Florida using Landsat TM and EO-1 ALI/Hyperion imagery. *Estuarine, Coastal and Shelf Science,* 115**,** 234-245.

PURVAJA, R., ROBIN, R., GANGULY, D., HARIHARAN, G., SINGH, G., RAGHURAMAN, R. & RAMESH, R. 2018. Seagrass meadows as proxy for assessment of ecosystem health. *Ocean & coastal management,* 159**,** 34-45.

RENDE, S. F., BOSMAN, A., DI MENTO, R., BRUNO, F., LAGUDI, A., IRVING, A. D., DATTOLA, L., GIAMBATTISTA, L. D., LANERA, P., PROIETTI, R. J. J. O. M. S. & ENGINEERING 2020. Ultra-High-Resolution Mapping of Posidonia oceanica (L.) Delile Meadows through Acoustic, Optical Data and Object-based Image Classification. 8**,** 647.

ROBBINS, B. D. & BELL, S. S. 1994. Seagrass landscapes: a terrestrial approach to the marine subtidal environment. *Trends in Ecology & Evolution,* 9**,** 301-304.

ROELFSEMA, C., KOVACS, E., ROOS, P., TERZANO, D., LYONS, M. & PHINN, S. 2018. Use of a semi-automated object based analysis to map benthic composition, Heron Reef, Southern Great Barrier Reef. *Remote Sensing Letters,* 9**,** 324-333.

ROELFSEMA, C., PHINN, S., UDY, N. & MAXWELL, P. 2009. An integrated field and remote sensing approach for mapping seagrass cover, Moreton Bay, Australia. *Journal of Spatial Science,* 54**,** 45-62.

ROELFSEMA, C. M., LYONS, M., KOVACS, E. M., MAXWELL, P., SAUNDERS, M. I., SAMPER-VILLARREAL, J. & PHINN, S. R. 2014. Multi-temporal mapping of seagrass cover, species and

biomass: A semi-automated object based image analysis approach. *Remote Sensing of Environment,* 150, 172-187.
SCHÜTT, E. M., UHL, F., SCHUBERT, P. R., REUSCH, T. B. & OPPELT, N. 2025. Mapping subtidal seagrass in the turbid Baltic Sea: Rethinking satellite sensor selection using a sensor-agnostic pipeline. *Science of Remote Sensing*, 100243.
SCHWEIZER, D., ARMSTRONG, R. & POSADA, J. 2005. Remote sensing characterization of benthic habitats and submerged vegetation biomass in Los Roques Archipelago National Park, Venezuela. *International Journal of Remote Sensing,* 26, 2657-2667.
SNEEP, A., DEVILLERS, R., ROBERT, K., LE BRIS, A. & EDINGER, E. 2024. Mapping and Characterizing Eelgrass Meadows Using UAV Imagery in Placentia Bay and Trinity Bay, Newfoundland and Labrador, Canada. *Sustainability,* 16, 3471.
SOUTHWORTH, J., MUNROE, D., NAGENDRA, H. J. A., ECOSYSTEMS & ENVIRONMENT 2004. Land cover change and landscape fragmentation—comparing the utility of continuous and discrete analyses for a western Honduras region. 101, 185-205.
STRYDOM, S., MURRAY, K., WILSON, S., HUNTLEY, B., RULE, M., HEITHAUS, M., BESSEY, C., KENDRICK, G. A., BURKHOLDER, D. & FRASER, M. W. 2020. Too hot to handle: unprecedented seagrass death driven by marine heatwave in a World Heritage Area. *Global Change Biology,* 26, 3525-3538.
STUMPF, R., FRAYER, M., DURAKO, M. & BROCK, J. 1999. Variations in water clarity and bottom albedo in Florida Bay from 1985 to 1997. *Estuaries,* 22, 431-444.
SU, L. & HUANG, Y. 2019. Seagrass resource assessment using worldview-2 imagery in the redfish bay, Texas. *Journal of Marine Science and Engineering,* 7, 98.
TAHARA, S., SUDO, K., YAMAKITA, T. & NAKAOKA, M. 2022. Species level mapping of a seagrass bed using an unmanned aerial vehicle and deep learning technique. *PeerJ,* 10, e14017.
THORHAUG, A., RICHARDSON, A. & BERLYN, G. 2007. Spectral reflectance of the seagrasses: Thalassia testudinum, Halodule wrightii, Syringodium filiforme and five marine algae. *International Journal of Remote Sensing,* 28, 1487-1501.
TIN, H. C., UYEN, N. T., HIEU, D. V., NI, T. N., TU, N. H. & SAIZEN, I. 2020. Decadal dynamics and challenges for seagrass beds management in Cu Lao Cham Marine Protected Area, Central Vietnam. *Environment, Development and Sustainability,* 22, 7639-7660.
TOPOUZELIS, K., MAKRI, D., STOUPAS, N., PAPAKONSTANTINOU, A. & KATSANEVAKIS, S. 2018. Seagrass mapping in Greek territorial waters using Landsat-8 satellite images. *International Journal of Applied Earth Observation and Geoinformation,* 67, 98-113.
TORRES-PULLIZA, D., WILSON, J. R., DARMAWAN, A., CAMPBELL, S. J., ANDRÉFOUËT, S. J. O. & MANAGEMENT, C. 2013. Ecoregional scale seagrass mapping: A tool to support resilient MPA network design in the Coral Triangle. 80, 55-64.
TRAGANOS, D. & REINARTZ, P. 2018. Mapping Mediterranean seagrasses with Sentinel-2 imagery. *Mar Pollut Bull,* 134, 197-209.
TSUJIMOTO, R., TERAUCHI, G., SASAKI, H., SAKAMOTO, S. X., SAWAYAMA, S., SASA, S., YAGI, H. & KOMATSU, T. 2016. Damage to seagrass and seaweed beds in Matsushima Bay, Japan, caused by the huge tsunami of the Great East Japan Earthquake on 11 March 2011. *International Journal of Remote Sensing,* 37, 5843-5863.
UHRIN, A. V. & TURNER, M. G. 2018. Physical drivers of seagrass spatial configuration: the role of thresholds. *Landscape Ecology,* 33, 2253-2272.
URBAŃSKI, J., MAZUR, A. & JANAS, U. 2009. Object-oriented classification of QuickBird data for mapping seagrass spatial structure. *Oceanological and Hydrobiological Studies,* 38, 27-43.
VAHTMÄE, E., KOTTA, J., LÕUGAS, L. & KUTSER, T. 2021. Mapping spatial distribution, percent cover and biomass of benthic vegetation in optically complex coastal waters using hyperspectral CASI and multispectral Sentinel-2 sensors. *International Journal of Applied Earth Observation and Geoinformation,* 102, 102444.
VAN DER HEIDE, T., BOUMA, T. J., VAN NES, E. H., VAN DE KOPPEL, J., SCHEFFER, M., ROELOFS, J. G., VAN KATWIJK, M. M. & SMOLDERS, A. J. 2010. Spatial self-organized patterning in seagrasses along a depth gradient of an intertidal ecosystem. *Ecology,* 91, 362-369.
VEETTIL, B. K., WARD, R. D., LIMA, M. D. A. C., STANKOVIC, M., HOAI, P. N. & QUANG, N. X. 2020. Opportunities for seagrass research derived from remote sensing: A review of current methods. *Ecological Indicators,* 117.

VO, T.-T., LAU, K., LIAO, L. M. & NGUYEN, X.-V. 2020. Satellite image analysis reveals changes in seagrass beds at Van Phong Bay, Vietnam during the last 30 years. *Aquatic Living Resources,* 33**,** 4.

WABNITZ, C. C., ANDRÉFOUËT, S., TORRES-PULLIZA, D., MÜLLER-KARGER, F. E. & KRAMER, P. A. 2008. Regional-scale seagrass habitat mapping in the Wider Caribbean region using Landsat sensors: Applications to conservation and ecology. *Remote Sensing of Environment,* 112**,** 3455-3467.

WICAKSONO, P., ARYAGUNA, P. A. & LAZUARDI, W. 2019. Benthic Habitat Mapping Model and Cross Validation Using Machine-Learning Classification Algorithms. *Remote Sensing,* 11.

WICAKSONO, P. & HAFIZT, M. 2013. Mapping seagrass from space: Addressing the complexity of seagrass LAI mapping. *European Journal of Remote Sensing,* 46**,** 18-39.

WICAKSONO, P., HAFIZT, M., HARAHAP, S. D. & NANDIKA, M. R. 2024. Integrating Sentinel-2 and PlanetScope Image with Drone-based Seagrass Data for Seagrass Percent Cover Mapping. *IOP Conference Series: Earth and Environmental Science,* 1291.

WICAKSONO, P. & LAZUARDI, W. 2021. Assessment of PlanetScope images for benthic habitat and seagrass species mapping in a complex optically shallow water environment. *Fine Resolution Remote Sensing of Species in Terrestrial and Coastal Ecosystems.* Routledge.

YANG, D. & YANG, C. 2009. Detection of seagrass distribution changes from 1991 to 2006 in Xincun Bay, Hainan, with satellite remote sensing. *Sensors,* 9**,** 830-44.

ZAKI, N. H. M., CHONG, W. S., MUSLIM, A. M., REBA, M. N. M. & HOSSAIN, M. S. 2022. Assessing optimal UAV-data pre-processing workflows for quality ortho-image generation to support coral reef mapping. *Geocarto International.* 37(25), 10556-10580.

ZHARIKOV, V., BAZAROV, K. Y., EGIDAREV, E. & LEBEDEV, A. 2018. Application of Landsat data for mapping higher aquatic vegetation of the Far East Marine Reserve. *Oceanology,* 58**,** 487-496.

ZOFFOLI, M. L., GERNEZ, P., ROSA, P., LE BRIS, A., BRANDO, V. E., BARILLÉ, A.-L., HARIN, N., PETERS, S., POSER, K., SPAIAS, L., PERALTA, G. & BARILLÉ, L. 2020. Sentinel-2 remote sensing of Zostera noltei-dominated intertidal seagrass meadows. *Remote Sensing of Environment,* 251.

Chapter 3

A blueprint for the estimation of seagrass carbon stock using remote sensing-enabled proxies

This chapter is published as Simpson, J., Bruce, E., Davies, K.P. and Barber, P., 2022. A blueprint for the estimation of seagrass carbon stock using remote sensing-enabled proxies. *Remote Sensing*, *14*(15), p.3572. https://doi.org/10.3390/rs14153572. This text is a reproduction of the published paper. The original version of the paper is available in Appendix A.

This chapter addresses **Aim 1** by identifying key biophysical characteristics of seagrass that relate to carbon stock and sequestration and can be derived using remote sensing.

3.1 Introduction

The potential role of blue carbon as a natural climate mitigation strategy has prompted increased research focus on methods for monitoring coastal ecosystems (Macreadie et al., 2021). Although the ecological value of seagrass meadows is long established (Thayer et al., 1975), recognition of their value as important sinks in the global carbon cycle (Oreska et al., 2020) highlights the need for robust monitoring and reporting on greenhouse gas (GHG) offset projects (Campbell et al., 2022). Seagrasses contribute disproportionately to organic carbon (C_{org}) burial, sequestering 10% of oceanic buried C_{org} despite occupying less than 0.2% of ocean area (Fourqurean et al., 2012). Despite their relatively small global area compared to tropical, temperate and boreal forests, they sequester carbon at a comparable rate (McLeod et al., 2011). Seagrasses also influence water flows, cycle nutrients, form the base of food webs, and offer shelter for a range of marine species (Hemminga and Duarte, 2000), positioning them as providers of multiple ecosystem services beyond carbon sequestration (Nordlund et al., 2016, Unsworth et al., 2019). Development of methods to accurately map seagrass and produce robust estimates of seagrass carbon storage across large geographical areas is needed to improve global carbon monitoring schemes and support protection and restoration efforts crucial for maintaining ecosystem services.

The carbon sequestration capacity of seagrass is of critical interest in climate change mitigation and adaptation including emissions reporting, GHG abatement schemes and offset projects (Oreska et al., 2020, Macreadie et al., 2021). Protocols for accurate quantification of seagrass carbon stock in the field have been developed (Howard et al., 2014), and incorporated into some national GHG inventories (UNEP, 2020). However, high inter- and intra-habitat variability in seagrass carbon stock and burial rates (Lavery et al., 2013, Sanders et al., 2019, Ricart et al., 2020, Kim et al., 2022) suggests that regional-scale reporting would be strengthened by measurements which accurately capture this variability.

Satellite remote sensing has been used for continuous broad-scale monitoring of seagrass biomass and condition (Bramante et al., 2018, Poursanidis et al., 2021). Synoptic monitoring of coastal ecosystems by satellite remote sensing can provide vital spatial information about the ecological characteristics of seagrasses as they change over time, supporting coastal management and conservation (Topouzelis et al., 2018, Randazzo et al., 2021, McKenzie et al., 2022). To incorporate seagrass in quantitative climate change mitigation and adaptation strategies, robust methods are required to translate these satellite-derived ecological characteristics into metrics relevant to estimates of carbon stock and sequestration rates. This involves consideration of the ecological characteristics of seagrass meadows as they relate to carbon sequestration and the capabilities of current and future remote sensing platforms.

Although optical satellite remote sensing has been used to characterise the ecological characteristics of seagrass, direct measurement of seagrass carbon stock or sequestration rates using only remote sensing data is still not possible. Therefore, determining estimates of seagrass carbon stocks from remote sensing-based measurements requires an understanding of biophysical processes that underlie seagrass carbon sequestration, and the spatial, temporal and spectral scales relevant to those processes. Developing this understanding is important for identifying biophysical variables usable in carbon stock assessments which are measurable from remote observation platforms. Addressing this challenge requires developing and refining biophysical proxies for total carbon stock that can be derived from remote sensing data and understanding the limitations of current and next-generation remote sensing

platforms in sensing these proxies. Here we present a new perspective on the role of current and emerging remote sensing technologies for broad scale assessment of seagrass carbon stocks through the development of suitable proxy measures.

This review will establish a framework for developing methods for satellite remote sensing-enabled estimation of seagrass carbon stock. In Section 2, we provide background on the key challenges for carbon accounting in seagrass environments. In Section 3, we outline the biophysical processes operating within seagrass environments that drive carbon sequestration rates. In Sections 4 and 5, we carry out a literature review in order to identify viable methods for satellite remote sensing of seagrass biophysical characteristics. Based on this review, we consider a set of remote sensing proxies for carbon storage in seagrass which account for spatial heterogeneity and change over time. Finally, in Section 6, we relate these remote sensing proxies to current seagrass carbon accounting requirements, creating a blueprint for applying Tier 3 spatially explicit methods to seagrass carbon stock mapping and monitoring.

3.2 Background

Activities within the Land-Use, Land-Use Change and Forestry (LULUCF) sector, such as afforestation and habitat restoration, can provide cost-effective mechanisms for offsetting emissions, which play a key role in current and planned global climate change mitigation policy. Previous mitigation efforts of the LULUCF sector were generally focused on terrestrial forests and grasslands and omitted seagrass and other coastal ecosystems from national GHG inventories (Herr et al., 2012). The Intergovernmental Panel on Climate Change (IPCC) addressed this omission with the release of the Coastal Wetlands supplement to their guidelines on GHG inventories (IPCC, 2014). However, seagrass contributions to carbon emissions have remained underreported and were yet to be fully integrated into national inventories (UNEP, 2020, Ralph et al., 2018). National-level plans for climate change mitigation and adaptation, such as the Nationally Determined Contributions (NDCs) of parties to the Paris Agreement, continue to largely omit seagrass reporting. Of the 185 NDCs submitted by countries as of 2020, 64 included coastal wetlands, while only ten provided explicit reference to seagrasses (UNEP, 2020).

Accurate carbon accounting intersects with issues of seagrass conservation. Seagrass meadows are degrading globally, with a rate of loss possibly as high as 7% per year (Orth et al., 2006). Degradation of seagrass ecosystems represents a two-fold climate risk: reducing the capacity of blue carbon ecosystems to sequester carbon and provide co-benefits (Hopkinson et al., 2012), and increased emissions caused by stored C_{org} partially remineralising to become atmospheric CO_2 (Lovelock et al., 2017). Conversely, seagrass meadow restoration substantially increases carbon storage in the soil (Greiner et al., 2013, Oreska et al., 2020). A recent study estimated the combined possible mitigation benefit from avoided seagrass degradation and seagrass restoration to be 341 $TgCO_2$ equivalent y^{-1} (Griscom et al., 2017), based on a conservative global extent estimate (UNEP-WCMC and Short, 2021). Given the disproportionate carbon storage and high rate of change, incorporating seagrass conservation and restoration into national emissions reporting, GHG abatement schemes, and offset projects is critical to global climate mitigation efforts.

Accurate inclusion of seagrass ecosystems in carbon accounting estimates is currently limited by existing methodologies. Seagrass reporting in GHG inventories under the IPCC guidelines often employs Tier 1 or Tier 2 methods which rely on global and regional estimates of carbon stock respectively (IPCC, 2006). Tier 3 methods model carbon stocks using spatially explicit methods. Unlike terrestrial LULUCF inventory contributions, methods for Tier 3 reporting have not been established for seagrass ecosystems. Tier 3 approaches are intended to provide greater accuracy than Tier 1 or 2, and require a robust understanding of underlying processes, and identification of appropriate inputs for models of carbon stock over time (IPCC, 2019). The ability to accurately model carbon stocks in seagrass meadows is contingent upon capture of reliable, high resolution remote sensing data that can be used to represent biophysical characteristics of seagrass ecosystems relevant to carbon sequestration at ecologically appropriate spatiotemporal scales. Improving remote sensing methods for characterising seagrass ecosystems therefore forms a critical agenda for improving coastal carbon accounting mechanisms (Macreadie et al., 2014).

A key challenge for developing accurate Tier 3 representations of seagrass is the heterogeneous biophysical characteristics of these ecosystems. The contribution of

seagrasses toward carbon sequestration and co-benefits can vary geographically, and are influenced by biophysical characteristics and environmental conditions in ways that are still poorly understood (Miyajima et al., 2015, Dahl et al., 2016, Mazarrasa et al., 2017, Asplund et al., 2021). Spatial heterogeneity introduces uncertainty in quantifying ecosystem services in other contexts (Dong et al., 2015, Mattsson et al., 2016), and measurements of carbon stock across different seagrass environments frequently vary by a factor >20 (Lavery et al., 2013, Ewers Lewis et al., 2017). Spatially explicit Tier 3 models would need to capture spatio-temporal heterogeneity inherent in seagrass meadows to enable accurate emissions reporting.

Carbon stocks in seagrass, as in other environments, can be divided into pools, primarily above-ground biomass (AGB), below-ground biomass (BGB), and soil carbon. In seagrass ecosystems, the soil pool comprises as much as 98% of the total ecosystem carbon stock (Serrano et al., 2019). Studies have shown that carbon storage potential can be extremely high even in areas with low AGB, primary productivity and areal extent (Armitage and Fourqurean, 2016, Serrano et al., 2021). This is a barrier for optical remote sensing as only the above-ground components of the plant and soil background contribute to the optical signal, making estimation of total carbon stock from the optical signal challenging. Despite these challenges, the absorption of electromagnetic radiation by water limits the use of other remote sensing methods, such as microwave remote sensing, to targets above the surface of water. As many seagrass meadows are fully submerged, satellite-borne optical remote sensing is most promising for producing synoptic seagrass biophysical data; however, microwave remote sensing may contribute complementary information for seagrasses present in the intertidal zone.

Accurate and broad-scale seagrass mapping for carbon reporting requires the repeatable, synoptic coverage provided by satellite remote sensing, rigorously calibrated and validated through field-based verification (Duffy et al., 2019). However, the heterogeneity within seagrass meadows and the challenges associated with optical remote sensing of seagrass carbon stock limits the use of direct measurement of total carbon from space, necessitating the use of measurable biophysical “proxies” that can capture seagrass ecosystem heterogeneity and contribute to GHG inventories and carbon stock mapping. Appropriate proxies must reliably characterise overall carbon

stock and the associated spatial heterogeneity and be measurable with optical remote sensing by satellite. It is also critical that the limitations of remotely-sensed proxies for mapping overall carbon stock in seagrass meadows are clearly understood and described to provide accurate estimates of seagrass carbon stock and account for bias.

3.3 Processes and drivers of carbon sequestration in seagrass meadows

Understanding the biophysical processes which drive seagrass carbon sequestration is key to identifying suitable remote sensing proxies to ensure that approaches to development of total carbon stock estimation methods have ecological relevance. Mazarrasa et al. (Mazarrasa et al., 2018) identified three processes which contribute to carbon stock in the soil pool: biomass accumulation (especially below-ground), allochthonous C_{org} sedimentation, and efficient burial of C_{org} (Figure 1).

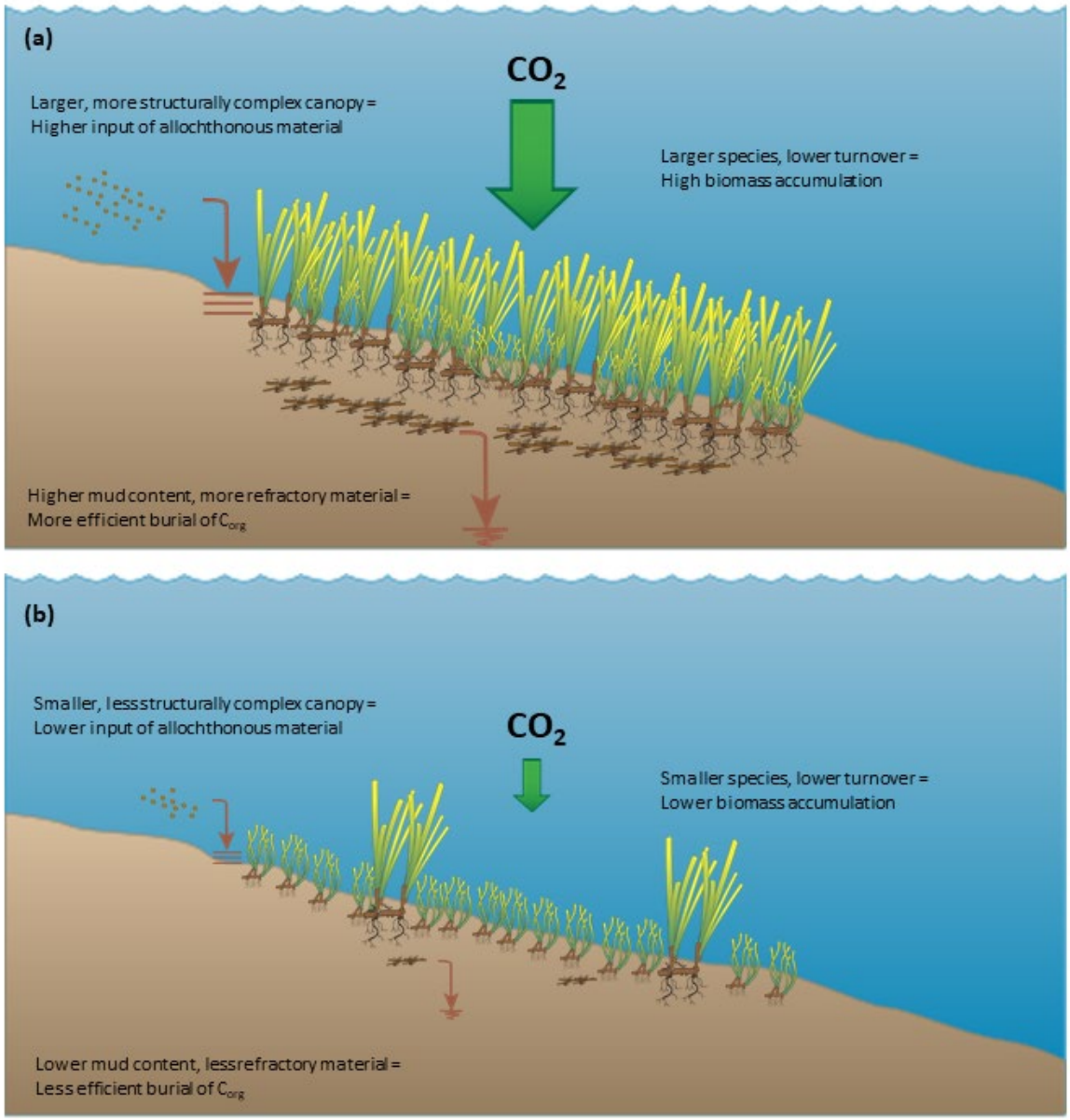

Figure 1. Three key processes in accumulation of seagrass carbon stock: biomass accumulation, input of allochthonous material, and efficient burial of Corg, and examples of the biophysical characteristics which drive higher (a) and lower (b) carbon stocks.

3.3.1 Biomass accumulation and autochthonous contributions to C_{org} stocks

Biomass accumulation is closely linked to the species composition of seagrass meadows, as seagrasses display large interspecific differences in biomass. For example, AGB can vary from 2.3 g m^{-2} (*Halophila stipulacea*) to 1005 g m^{-2} (*Amphibolis antarctica*) (Duarte and Chiscano, 1999), due to significant differences in shoot and leaf morphology. BGB varies similarly between species, with larger species tending to show both higher biomass and higher BGB to AGB ratios (Duarte and Chiscano, 1999). Certain species, most notably *Posidonia oceanica*, produce particularly large mattes of root and rhizome

material (Pergent et al., 1994). Intraspecies variations in biomass have also been identified, occurring across environmental gradients, including nutrient availability, light availability, salinity and temperature (Lirman and Cropper, 2003, Ferdie and Fourqurean, 2004, Collier et al., 2008, Serrano et al., 2014). The higher BGB to AGB ratio of morphologically larger seagrasses is important for carbon sequestration as roots and rhizomes are composed of more refractory material than shoots, are less prone to export via herbivory or physical disturbance, and are already located within the anoxic soils which facilitate long term C_{org} storage (Harrison, 1989, Hemminga et al., 1991, Fourqurean and Schrlau, 2003, Mateo et al., 2006, Trevathan-Tackett et al., 2017). Morphologically larger seagrasses trend towards higher carbon storage (Lavery et al., 2013, Rozaimi et al., 2013, Stankovic et al., 2017, Serrano et al., 2018), and have higher relative contribution of autochthonous compared to allochthonous inputs into the carbon stock (Bañolas et al., 2020, Mazarrasa et al., 2021).

The life cycles of seagrasses also show considerable interspecies variations. Smaller, colonizing species may exhibit full life cycles on the scale of months, while larger persistent species can take many years (Kilminster et al., 2015). This is an important factor influencing carbon sequestration, as the lower turnover rates of persistent species lead to high biomass accumulation (Mazarrasa et al., 2018). However, seagrass life cycles can also vary intraspecifically depending on environmental conditions (Thayer et al., 1984, Walker et al., 2001). The variation is significant enough that the same species can form both enduring and transitory meadows under different conditions (Duarte, 1989, Kilminster et al., 2015). These changing environmental conditions can follow annual cycles, or be related to shorter or longer-term changes caused by fluctuations in dynamic environments or major disturbance events such as storms (Kilminster et al., 2015). Though the relationship between persistence and carbon storage is established (Mazarrasa et al., 2018), there has been limited investigation of intraspecific variation in seagrass life cycle or meadow form and its relationship to carbon sequestration.

3.3.2 Input of allochthonous C_{org} into the ecosystem

Input of allochthonous C_{org} is controlled both by biophysical characteristics of seagrass meadows and environmental conditions. Seagrass canopies influence the local hydrodynamic environment, increasing sedimentation and decreasing resuspension

(Mateo et al., 2006, Fonseca and Fisher, 1986, Gambi et al., 1990, France and Holmquist, 1997). Morphologically larger species and mixed species meadows form canopies with higher complexity, which more effectively encourage sedimentation as they reduce water velocity and baffle sediments (Potouroglou et al., 2017, Mazarrasa et al., 2018). Higher density meadows also have a larger impact on local flow rates and sedimentation (Van Katwijk et al., 2010, Widdows et al., 2008). Input of allochthonous C_{org} is therefore influenced by the same set of biotic factors as biomass accumulation (Mazarrasa et al., 2018). However, unlike biomass accumulation, which is indirectly shaped by abiotic factors that determine seagrass growth patterns, the input of allochthonous C_{org} is more heavily influenced by abiotic factors, especially those relating to sediment. Capture of allochthonous C_{org} by seagrass meadows first requires a sediment source, therefore source sediment characteristics including density, grain size, and C_{org} content influence carbon stocks (Dahl et al., 2016, Serrano et al., 2016b, Gullström et al., 2017, Lima et al., 2020). Geomorphic setting also influences input of allochthonous C_{org} into the seagrass ecosystem. Small species in high-energy coastal settings have less capacity to capture sediment, while low-energy estuarine settings are associated with higher amounts of sedimentary C_{org} accumulation (Serrano et al., 2016a, Mazarrasa et al., 2021). Although relationships between canopy complexity and supply of allochthonous C_{org} appear to exist (Samper-Villarreal et al., 2016), this relationship is complicated by the abiotic factors which influence sedimentation rate and sediment C_{org} content.

The spatial arrangement of the seagrass landscape is an additional dimension that influences input of allochthonous C_{org} into seagrass carbon stocks. Continuous meadows capture sediment more effectively than meadows fragmented into patches (Oreska et al., 2017, Ricart et al., 2017). Carbon stocks within a patch tend to increase with distance from the patch edge (Ricart et al., 2015). The arrangement of gaps in seagrass meadows relative to the direction of water flow may also impact sedimentation, as flow attenuation will differ with variations in gap shape and arrangement (Adhitya et al., 2014, El Allaoui et al., 2016). The broader coastal landscape is also important, as proximal ecosystems that are highly productive such as mangroves can contribute C_{org} to seagrass sediments (Chen et al., 2017, Hemminga et al., 1994). Similarly, the presence of nearby barrier reefs can drive the input of allochthonous C_{org} by reducing local wave

energy (Guerra-Vargas et al., 2020). Input of allochthonous C_{org} is therefore driven by the complex interactions of biotic and abiotic characteristics acting across varying spatial scales.

3.3.3 Efficient burial of C_{org}

The burial efficiency of C_{org} determines the amount of organic material that will remain in the soil in the long term after being introduced through the processes of biomass accumulation and allochthonous sedimentation. This is influenced by conditions which lead to relatively high levels of recalcitrance, therefore lower levels of degradation into atmospheric CO_2, in organic material in the soil. An anoxic soil environment, high mud content, and a large proportion of more refractory material such as roots and rhizomes are conducive to higher burial efficiency (Mazarrasa et al., 2018). Seagrasses increase mud concentration in the soil by capturing fine sediments, in turn encouraging anoxic conditions and seagrass tissue recalcitrance (Serrano et al., 2020). The proportion of refractory material is linked to its origin, as autochthonous material tends to be more refractory than allochthonous. The efficient burial of C_{org} is therefore in part driven by the same conditions which lead to high biomass accumulation (morphologically larger, persistent species) and high input of allochthonous C_{org} (high rates of sedimentation and C_{org}-rich sediments).

3.3.4 Summary: processes and drivers of seagrass carbon stocks

The drivers of seagrass carbon sequestration are complex. Larger, more persistent species lead to higher carbon stocks, especially when meadows are dense and less fragmented. This applies to both autochthonous and allochthonous components of total carbon stock, though the latter is more influenced by geomorphic setting and source sediment properties. Estimation of carbon stocks therefore requires an understanding of the species composition and morphology, the spatial arrangement of seagrass meadows, patterns of spatiotemporal change, and the broader coastal landscape context in which the meadow is situated.

Although larger seagrass species have consistently higher C_{org} stocks, other drivers of carbon sequestration can act in highly variable ways depending upon context (Mazarrasa et al., 2021). The complexity of the relationships between drivers and carbon

stocks highlights the need to account for key biophysical characteristics, their variability and heterogeneity, as well as environmental setting in the mapping of seagrass carbon stocks.

3.4 Review method

A literature review was carried out to generate a library of established remote sensing methods to ascertain what biophysical characteristics have been measured in the past, how they were measured, and any technical limitations on their measurement. Studies to include in this library were identified through a systematic literature search.

Many remote sensing studies characterize seagrass without explicit reference to carbon stock or sequestration. For this reason the search terms did not include reference to carbon, instead focusing on the subject (seagrass) and the method (satellite remote sensing). The following search terms were entered into Web of Science and Scopus: ("Seagrass" OR "submerged aquatic vegetation") AND ("remote sensing" OR "remotely sensed" OR "satellite" OR "earth observation" OR "Landsat" OR "WorldView" OR "PlanetScope" OR "QuickBird" OR "IKONOS" OR "Sentinel-2"). The search was limited to academic journal articles published in English and studies published on or before 30 April 2022.

After deduplication, 1119 records were identified. The abstracts of these studies were examined and irrelevant records excluded. The full texts of the remaining studies were reviewed to ensure they:

1. contained a clearly described and repeatable method;
2. used optical satellite remote sensing data to attempt to measure at least one biophysical characteristic of seagrass;
3. did not exclusively use manual image interpretation techniques.

A total of 204 studies fulfilled these criteria and were used to create the database of seagrass remote sensing methods, including a record of different methodological techniques and contextual information such as study site location.

3.5 Identifying remote sensing proxies for seagrass carbon stock: possibilities and challenges

Levels of carbon stock within seagrass meadows are influenced by biomass accumulation, the input of allochthonous C_{org}, and efficient burial of C_{org} (Mazarrasa et al., 2018); and the biophysical and environmental drivers of those processes. In this section, we examine potential remote sensing proxies for improving the measurement of seagrass carbon stocks and evaluate direct monitoring of blue carbon potential from space. Although recent modelling has highlighted the complexity of the relationships between potential remote proxies and seagrass carbon stock (Asplund et al., 2021, Mazarrasa et al., 2021, Alemu et al., 2022), identification of proxies that can be measured from space, and an assessment of the limitations of such an approach is an important first step in conceiving a holistic remote sensing-enabled methodology for spatially explicit mapping of seagrass carbon stock.

3.5.1 Meadow characteristics and dynamics as proxy indicators of carbon stock

3.5.1.1 Aboveground Biomass (AGB)

Direct estimates of AGB, as well as the related biophysical metrics of percent cover and Leaf Area Index (LAI), have been widely used in studies characterising seagrass using satellite remote sensing (Ackleson and Klemas, 1987, Phinn et al., 2008, Roelfsema et al., 2009, Lyons et al., 2012, Pu et al., 2012, Wicaksono and Hafizt, 2013) Approaches applied include discrete mapping of percent cover classes (e.g. (Wabnitz et al., 2008, Roelfsema et al., 2009)) and regression-based estimates of AGB on a per-pixel basis (e.g. (Wicaksono and Hafizt, 2013, Lyons et al., 2015)). Although AGB contributes as little as 2% of total carbon stock in seagrass ecosystems (Serrano et al., 2019), AGB is closely related to both BGB and soil carbon (Stankovic et al., 2018, Samper-Villarreal et al., 2016). The importance of seagrass productivity and canopy complexity in carbon sequestration and the viability of remote sensing-based measurements of AGB and related characteristics highlight the potential of seagrass AGB as a remote sensing-based proxy for carbon stock.

The challenge in identifying the ideal approach for deriving estimates of seagrass AGB as a proxy for carbon stock is the selection of remote sensing methods that are both

ecologically appropriate and capable of producing accurate results. From the three interrelated metrics described above, percent cover is more easily derived from remote sensing data compared to LAI and AGB, as it contributes more directly to the remote sensing signal. In comparison, LAI and AGB estimates are more limited, especially in dense seagrass meadows, due to saturation of the remote sensing signal (Zoffoli et al., 2020, Pu et al., 2012, Borfecchia et al., 2013). Because AGB incorporates information about the three-dimensional volume of plants it is the most abstracted of these three metrics from the remote sensing signal (Pu et al., 2013). However, percent cover is less directly related to the accumulation of biomass and capture of allochthonous C_{org} than AGB and therefore a less direct proxy for overall carbon stock.

In the case of intertidal seagrass beds, the periodic absence of the water column provides additional remote sensing options for characterising seagrass AGB. Access to wavelengths of light which are highly attenuated by water makes common vegetation indices which rely upon near infrared reflectance, including the Normalised Difference Vegetation Index (NDVI), viable in intertidal environments (Barillé et al., 2010, Zoffoli et al., 2020). Additionally, recent research has suggested that Synthetic Aperture Radar (SAR) data improves the accuracy of seagrass mapping, including AGB estimates, by providing information on surface structure which complements optical remote sensing data (Müller et al., 2016, Ha et al., 2021). These approaches may also be applicable for seagrass beds which are emergent but not fully intertidal. These studies suggest that AGB estimates could be approached differently for intertidal and subtidal seagrass.

An important additional methodological consideration is whether to map AGB in discrete classes or as continuous values. As seagrass density can vary over light availability gradients (Bach et al., 1998, Collier et al., 2007), a continuous measurement would be more ecologically appropriate (Lyons et al., 2011). Remote sensing-derived estimates of AGB are likely to be an important proxy for total carbon stock, but their effective use requires a deeper understanding of methodological complexities to identify sensor properties data analysis techniques which can most accurately and reliably produce AGB estimates.

3.5.1.2 Meadow species composition

Species composition is an important consideration for the effective use of AGB-based carbon stock proxies. Significant differences in morphology and AGB to BGB ratio among seagrass species (Duarte and Chiscano, 1999) suggest that classification of seagrasses by species could enhance the accuracy of satellite derived prediction of overall carbon stock. Although species composition is not a reliable direct proxy for carbon stock, it can complement AGB data and improve remote sensing-enabled carbon stock estimates.

Many species of seagrass are spectrally separable (Fyfe, 2003, Phinn et al., 2008), and are therefore distinguishable using optical satellite remote sensing. However, spectral differences between seagrass species are often subtle (Thorhaug et al., 2007), and epiphytic growth can interfere with spectral separability (Dekker et al., 2005). Beyond the spectral properties of individual leaves, the morphology of shoots can also impact their detection. Traganos and Reinartz (Traganos et al., 2018, Traganos and Reinartz, 2018) mapped two morphologically distinct species (*Posidonia oceanica* and *Cymodocea nodosa*) using Sentinel-2 (Traganos et al., 2018) and RapidEye (Traganos and Reinartz, 2018) satellite images. Sentinel-2 has a broader spectral range compared to RapidEye with data captured in a shorter wavelength coastal blue band. In both cases *P. oceanica* was classified more accurately than *C. nodosa*. When the narrower spectral range RapidEye images were used, the difference was considerable with an accuracy of 89-92% for *P. oceanica* and 50-61% for *C. nodosa*. These results suggest that although smaller species are more difficult to map accurately, a broader spectral range has the potential to improve detection. Methods that incorporate non-spectral data such as secondary textural characteristics or object-based approaches are effective in classifying species, even in relatively species-rich tropical areas (Mumby and Edwards, 2002, Roelfsema et al., 2014, Kovacs et al., 2018). These approaches may offer a useful alternative for overcoming spectral similarity and other species classification challenges such as turbidity which can impact on the spectral information.

3.5.1.3 Intra-annual variation in seagrass growth

Seagrass meadows exhibit intra-annual, seasonal variation in AGB (Gilbert and Clark, 1981, Duarte, 1989) and at the extremes of habitat suitability, shoots can be completely absent for months of the year when water temperatures are outside the habitable range (Santamaría-Gallegos et al., 2000). This is particularly relevant when using AGB as a proxy for carbon stock, because despite seasonal variability in seagrass growth, soil carbon and total carbon stock are more temporally stable (Samper-Villarreal et al., 2018). Traditionally, biomass assessments were recommended during the peak growing season (McComb et al., 1981). However, significant intraspecific differences in seagrass phenology can exist even with minor differences in environmental conditions. This is further complicated in mixed meadows, where interspecific differences in phenology lead to biomass peaks at different times (de Boer, 2000). Given the complex factors dictating peak biomass and the apparent variability in the ratio of AGB to overall carbon stock, assessments at intra-annual timescales should be considered to ensure robustness when measuring AGB as a proxy for overall carbon stock. In addition, importance of regular monitoring will increase in the future as the environmental conditions which dictate seagrass phenology shift under changing climate conditions (Olsen et al., 2018).

3.5.2 Landscape ecology metrics and spatial characteristics as proxies for carbon stock

3.5.2.1 Landscape ecology metrics applied to seagrass meadows

The spatial structure and arrangement of seagrass meadows have been linked to rates of carbon burial, with studies showing that continuous seagrass meadows capture allochthonous C_{org} more effectively than fragmented meadows, leading to greater input of C_{org} into the sediments (Ricart et al., 2015, Ricart et al., 2017, Oreska et al., 2017). Landscape ecology metrics, which offer methods of quantifying the spatial arrangement of landscapes, may therefore provide a suitable remote sensing-based proxy for carbon stock across the seagrass landscape. Recognition of the system properties present in heterogeneous seascapes has prompted growing application of landscape ecology concepts and techniques to coastal and marine environments, including consideration

of spatial context, configuration, connectivity, and the effects of scale (Pittman et al., 2021).

Seagrass patches vary widely in size, often from 1-100 m in diameter (Robbins and Bell, 1994), however the spatial scales at which spatial configuration and fragmentation significantly affect carbon sequestration are not well established. Although seascape metrics could provide an effective indicator of potential carbon stock, there is a need to determine the appropriate spatio-temporal scale for adequately capturing the biophysical processes influencing the relationship between the spatial configuration of seagrass meadows and carbon sequestration (Costa et al., 2018).

The spatial, spectral and temporal resolution of remote sensing data products will determine the seascape metrics that can realistically be measured (Bell et al., 2007). Seascape metrics such as patch shape, area and edge length have been measured using aerial platforms (Hamylton and Spencer, 2011, Uhrin and Townsend, 2016, Uhrin and Turner, 2018) and patch complexity, connectivity and diversity have been quantified using high spatial resolution platforms, including GeoEye-1, IKONOS and SPOT 7 (Rioja-Nieto et al., 2013, Helmi et al., 2018, Cajica et al., 2020). Studies have demonstrated the importance of ultra-high spatial resolution imagery for mapping patch level fragmentation (Urbański et al., 2009, Pu and Bell, 2017), which may otherwise be masked in measures of overall seagrass density based on coarser spatial resolution imagery (Figure 2). Although there has been limited research linking landscape metrics and carbon stock using remote sensing data, modelling has shown that metrics related to heterogeneity and patch fragmentation are strong predictors of overall carbon stocks (Gullström et al., 2017, Asplund et al., 2021).

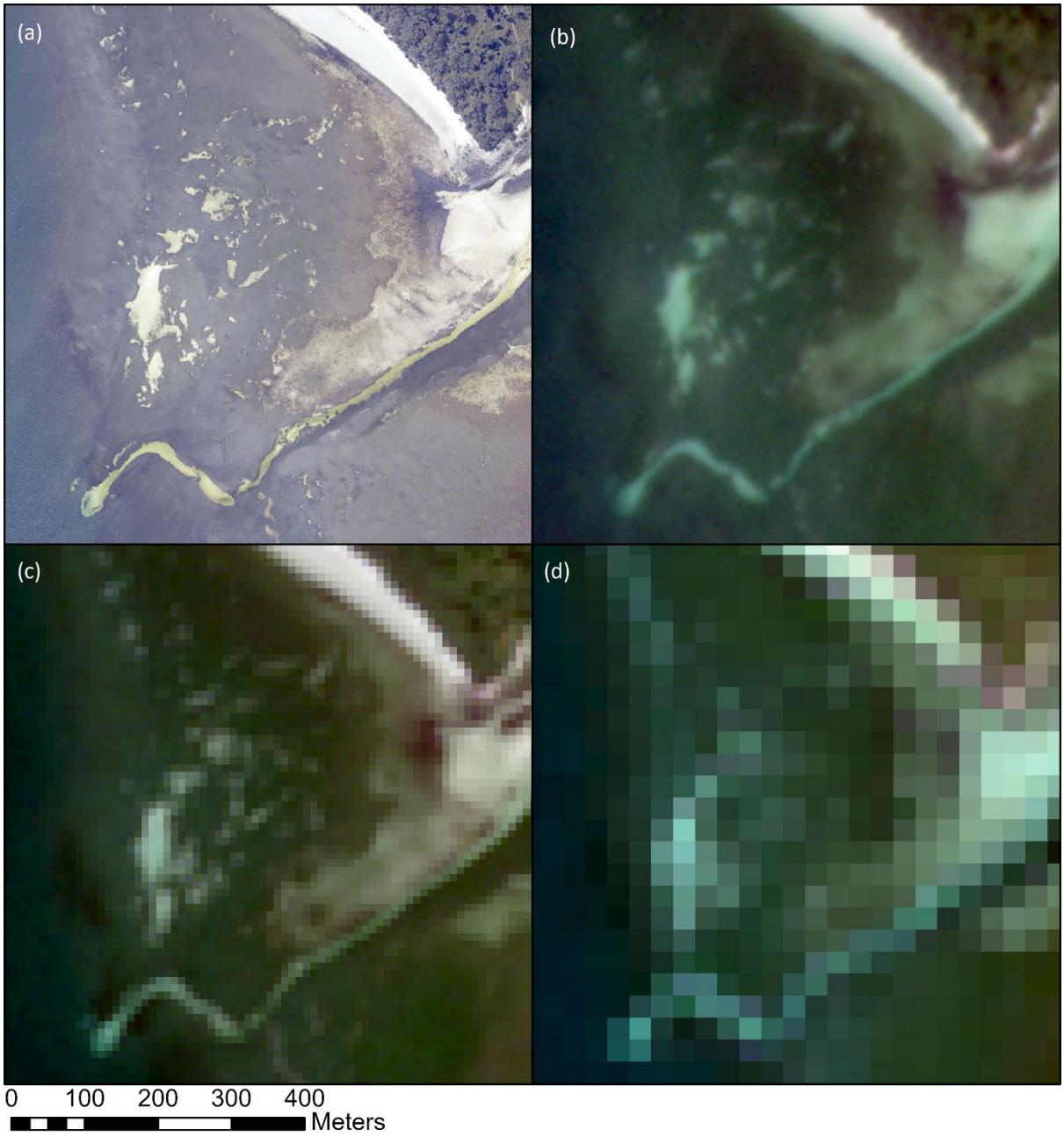

Figure 2. A patchy seagrass meadow in Jervis Bay NSW, Australia, displayed at four different spatial resolutions. This demonstrates the effect of image spatial resolution on the representation of spatial arrangement in seagrass ecosystems. Images sourced from (a) ArborCam aerial imagery (0.05m spatial resolution, captured October 15 2020), (b) PlanetScope (3m spatial resolution, captured October 14 2020), (c) Sentinel-2A (10m spatial resolution, captured October 12 2020), and (d) Landsat 8 OLI (30m spatial resolution, captured September 22 2020).

3.5.2.2 Landscape context

Local landscape context influences the quantity and carbon content of sediment deposits (Gullström et al., 2017, Ricart et al., 2020). In estuarine environments, seagrass meadows further inland and in areas less exposed to wave energy have higher sediment accretion rates, with studies showing carbon stocks decreasing along an oceanward

gradient (Ricart et al., 2020, Alemu et al., 2022). Additionally, proximity to ecosystems with high productivity and outflow of organic material, such as mangroves, is associated with increased carbon storage in seagrass meadows (Chen et al., 2017, Asplund et al., 2021).

Broad characterisations of geomorphic setting have been found to be insufficient for predicting seagrass total carbon stocks, suggesting that the influence of landscape context varies locally depending on factors such as sediment deposition rates and surrounding geology (Ewers Lewis et al., 2020, Mazarrasa et al., 2021). This is relevant for remote sensing-based estimates of carbon stock as it suggests that measuring seagrass characteristics alone, without landscape context, risks missing key variables. Further, Asplund et al. (Asplund et al., 2021) found that the predictive power of patch fragmentation metrics for estimating sedimentary C_{org} stock varied considerably between seagrass species. This work suggests that the effective use of landscape ecology-based proxies for seagrass carbon stock requires site specific understanding, including local landscape context and nearshore sedimentary environment.

3.5.3 Seagrass life history and phenological time series analysis

Carbon storage potential is also influenced by the temporal dynamics of seagrass meadows, a characteristic that can be detected using remote sensing-based change detection analysis. Enduring seagrass meadows have higher carbon stores than transitory meadows (Stankovic et al., 2021, Mazarrasa et al., 2018), highlighting the importance of seasonal and multi-decadal monitoring of vegetation cover. Change detection can support carbon stock assessments in two ways. First, through classification of life history (e.g. persistent/opportunistic/colonising, enduring/transitory; Kilminster et al., 2015) which would enable differentiation between areas which show significant intraspecies differences in life cycle (not measurable using single date or annual image capture, see Figure 3). Second, using temporal analysis to derive phenological metrics can assist in differentiating species where spectral separability is poor, an approach successfully applied in terrestrial contexts (Madonsela et al., 2017). Measures of intra-annual change and phenology have the potential to contribute directly as carbon storage proxies, or indirectly by supporting more accurate species classification.

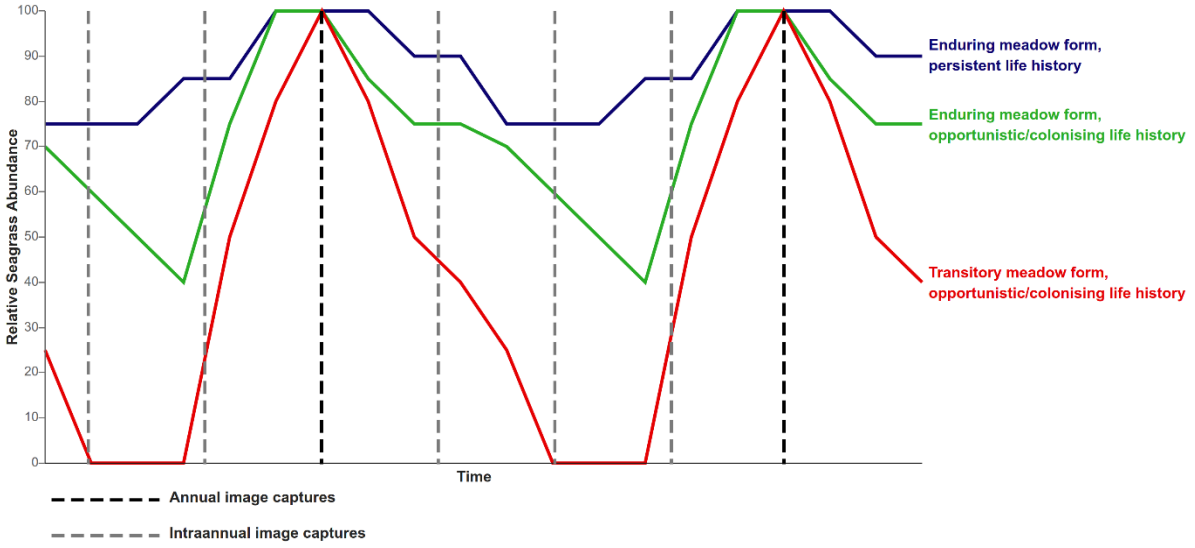

Figure 3. Conceptual comparison of different seagrass life cycles, highlighting the differences in representation between annual and intra-annual capture of remote sensing images. Indicative seagrass life cycles adapted from (Kilminster et al., 2015).

Multi-temporal remote sensing analysis of seagrass introduces challenges. Differences in water column properties (e.g. tidal level, turbidity) between image dates, or poor georegistration of mutitemporal images can introduce error when they are confused for changes in seagrass extent or biophysical properties (Lyons et al., 2013, Roelfsema et al., 2013).

Despite the dynamic nature of seagrass meadows, there is limited research on the use of remote sensing for characterising intra-annual variability, with most time series studies focused on longer-term change (Michalek et al., 1993, Shapiro and Rohmann, 2006, Blakey et al., 2015, Traganos and Reinartz, 2018). A relatively small number of studies have examined shorter term variation in seagrass using satellite remote sensing, often showing complex intra-annual dynamics (Lyons et al., 2013, Fauzan and Wicaksono, 2021, Krause et al., 2021). Given the potential significance of seagrass life cycle for carbon storage, further research is needed on the application of remote sensing for continuous capture of phenological patterns across seagrass meadows.

3.6 Enabling carbon stock estimates from space

Remote sensing-based proxies of seagrass carbon stocks should be informed by an understanding of the underlying biophysical processes and drivers of carbon sequestration. Satellite remote sensing is well placed to:

1. Estimate AGB and its heterogeneity across space;
2. Classify seagrass ecosystems by species composition or dominant species;
3. Characterise the spatial configuration and landscape context of seagrass ecosystems, and quantify these characteristics using landscape ecology metrics;
4. Capture intra-annual variability of seagrass species composition and AGB to monitor seagrass life cycles and temporal change (Figure 4).

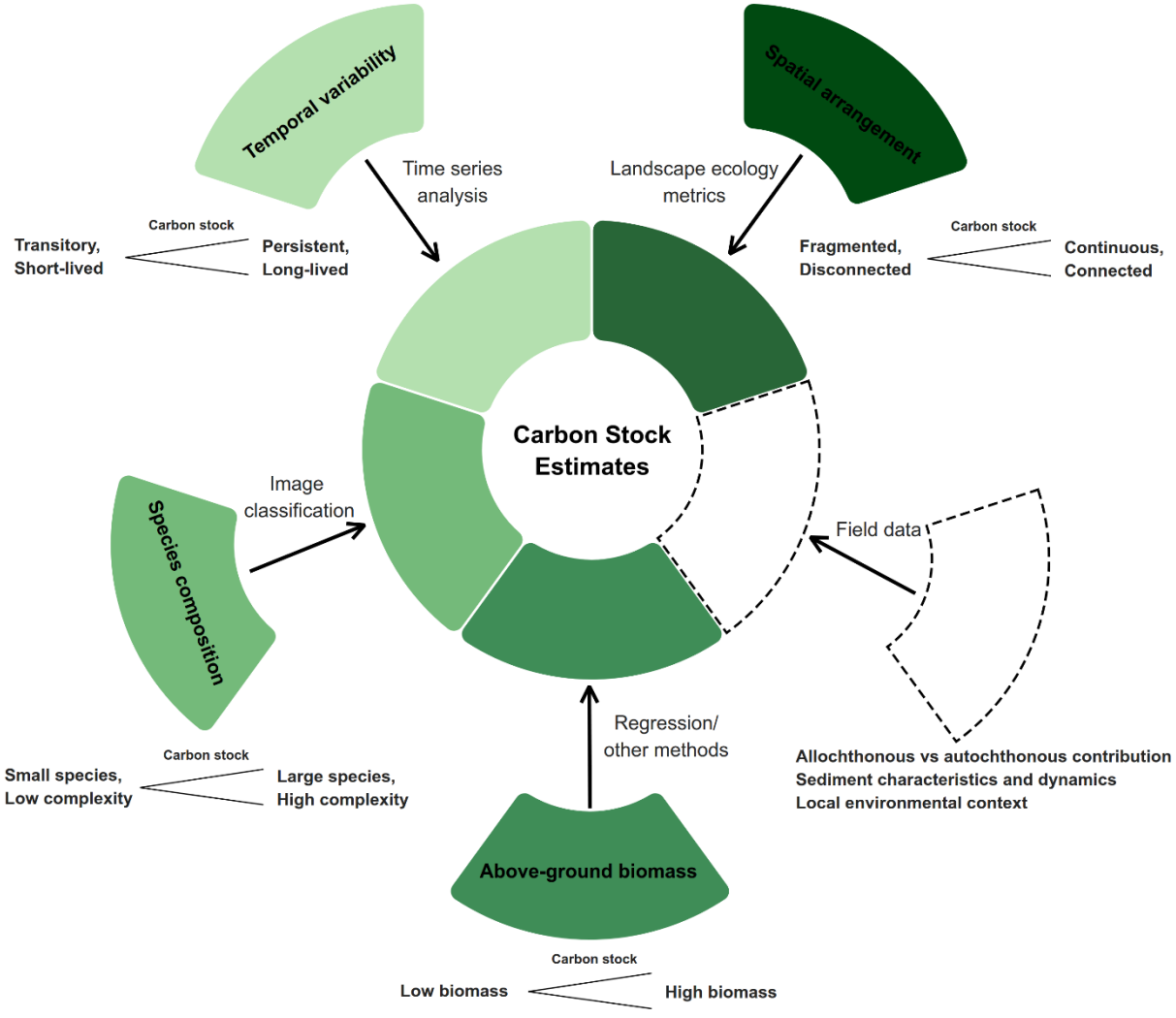

Figure 4. Potential proxies for estimating seagrass carbon stock. Filled in segments represent individual proxies measurable with remote sensing methods, while the dashed outline segment represents complementary field data for important variables not currently measurable using remote sensing.

However, the processes underlying seagrass carbon sequestration are complex, often non-linear in nature and abstracted from remote sensing signals. For example, while measurement of seagrass AGB can be detected via remote sensing, critical carbon accounting variables such as sediment properties, including grain size, sedimentation

rate and C_{org} content, cannot be directly measured from space. In many coastal settings, these sediment properties are the primary driver of carbon burial (Ricart et al., 2020), while in other environments seagrass properties, such as species composition, play an important role (Asplund et al., 2021). Accurate estimates must be verified, not only through *in situ* field validation of satellite data, but through incorporating knowledge of seascape context, sediment dynamics and the relative contributions of different biophysical processes. Characterising the relative contributions of allochthonous and autochthonous C_{org} to the seagrass carbon pool, the variation in these processes over space and time, and the sediment properties determining the efficiency of C_{org} burial is critical for deriving effective spatially explicit estimates of carbon stock to support carbon accounting (Figure 4).

3.7 Conclusions and future work

The globally significant contribution of seagrass ecosystems to carbon sequestration highlights the importance of rigorous methods to quantify carbon stock and stock change for incorporation into emissions reporting, GHG abatement schemes and offset projects. The processes involved in seagrass carbon sequestration are complex and require accurate characterization of key biophysical characteristics of the seagrass.

Future work to develop spatially explicit models of seagrass carbon stock should focus on determining reliable proxies of carbon stock which can be measured in a synoptic manner. Seagrass carbon stocks have been estimated using predictive modelling (Mazarrasa et al., 2021, Gullström et al., 2017, Asplund et al., 2021), and the inclusion of ecologically relevant remote sensing-based data can ensure that these models accurately capture the complexity and heterogeneity of seagrass ecosystems. This will support the effective use of remote sensing data by helping to identify the roles of local environmental processes in shaping carbon sequestration. Additionally, seagrass carbon stock estimation may be improved through optimising remote sensing data collection (e.g. sensor spatial, temporal and spectral properties) and data analysis (e.g. accuracy and thematic resolution of outputs). Addressing these priorities will improve spatially explicit carbon stock estimations in critical seagrass ecosystems.

References

ACKLESON, S. & KLEMAS, V. 1987. Remote sensing of submerged aquatic vegetation in lower Chesapeake Bay: A comparison of Landsat MSS to TM imagery. *Remote Sensing of Environment,* 22**,** 235-248.

ADHITYA, A., BOUMA, T., FOLKARD, A., VAN KATWIJK, M., CALLAGHAN, D., DE IONGH, H. & HERMAN, P. 2014. Comparison of the influence of patch-scale and meadow-scale characteristics on flow within seagrass meadows: a flume study. *Marine Ecology Progress Series,* 516**,** 49-59.

ALEMU, J. B., YAAKUB, S. M., YANDO, E. S., SAN LAU, R. Y., LIM, C. C., PUAH, J. Y. & FRIESS, D. A. 2022. Geomorphic gradients in shallow seagrass carbon stocks. *Estuarine, Coastal and Shelf Science,* 265**,** 107681.

ARMITAGE, A. R. & FOURQUREAN, J. W. 2016. Carbon storage in seagrass soils: long-term nutrient history exceeds the effects of near-term nutrient enrichment. *Biogeosciences,* 13**,** 313-321.

ASPLUND, M. E., DAHL, M., ISMAIL, R. O., ARIAS-ORTIZ, A., DEYANOVA, D., FRANCO, J. N., HAMMAR, L., HOAMBY, A. I., LINDERHOLM, H. W. & LYIMO, L. D. 2021. Dynamics and fate of blue carbon in a mangrove–seagrass seascape: influence of landscape configuration and land-use change. *Landscape Ecology,* 36**,** 1489-1509.

BACH, S. S., BORUM, J., FORTES, M. D. & DUARTE, C. M. J. M. E. P. S. 1998. Species composition and plant performance of mixed seagrass beds along a siltation gradient at Cape Bolinao, The Philippines. 174**,** 247-256.

BAÑOLAS, G., FERNÁNDEZ, S., ESPINO, F., HAROUN, R. & TUYA, F. 2020. Evaluation of carbon sinks by the seagrass Cymodocea nodosa at an oceanic island: Spatial variation and economic valuation. *Ocean & Coastal Management,* 187**,** 105112.

BARILLÉ, L., ROBIN, M., HARIN, N., BARGAIN, A. & LAUNEAU, P. 2010. Increase in seagrass distribution at Bourgneuf Bay (France) detected by spatial remote sensing. *Aquatic Botany,* 92**,** 185-194.

BELL, S. S., FONSECA, M. S. & STAFFORD, N. B. 2007. Seagrass ecology: new contributions from a landscape perspective. *SEAGRASSES: BIOLOGY, ECOLOGYAND CONSERVATION.* Springer.

BLAKEY, T., MELESSE, A. & HALL, M. O. 2015. Supervised classification of benthic reflectance in shallow subtropical waters using a generalized pixel-based classifier across a time series. *Remote Sensing,* 7**,** 5098-5116.

BORFECCHIA, F., DE CECCO, L., MARTINI, S., CERIOLA, G., BOLLANOS, S., VLACHOPOULOS, G., VALIANTE, L. M., BELMONTE, A. & MICHELI, C. 2013. Posidonia oceanica genetic and biometry mapping through high-resolution satellite spectral vegetation indices and sea-truth calibration. *International Journal of Remote Sensing,* 34**,** 4680-4701.

BRAMANTE, J. F., ALI, S. M., ZIEGLER, A. D. & SIN, T. M. 2018. Decadal biomass and area changes in a multi-species meadow in Singapore: application of multi-resolution satellite imagery. *Botanica Marina,* 61**,** 289-304.

CAJICA, A. K. O., HINOJOSA-ARANGO, G., GARZA-PÉREZ, J. R. & RIOJA-NIETO, R. 2020. Seascape metrics, spatio-temporal change, and intensity of use for the spatial conservation prioritization of a Caribbean marine protected area. *Ocean & Coastal Management,* 194**,** 105265.

CAMPBELL, A. D., FATOYINBO, T., CHARLES, S. P., BOURGEAU-CHAVEZ, L. L., GOES, J., GOMES, H., HALABISKY, M., HOLMQUIST, J., LOHRENZ, S., MITCHELL, C., MOSKAL, L. M., POULTER, B., QIU, H., DE SOUSA, C. H. R., SAYERS, M., SIMARD, M., STEWART, A. J., SINGH, D., TRETTIN, C., WU, J. H., ZHANG, X. S. & LAGOMASINO, D. 2022. A review of carbon monitoring in wet carbon systems using remote sensing. *Environmental Research Letters,* 17.

CHEN, G., AZKAB, M. H., CHMURA, G. L., CHEN, S., SASTROSUWONDO, P., MA, Z., DHARMAWAN, I. W. E., YIN, X. & CHEN, B. 2017. Mangroves as a major source of soil carbon storage in adjacent seagrass meadows. *Scientific Reports,* 7**,** 1-10.

COLLIER, C. J., LAVERY, P. S., MASINI, R. J. & RALPH, P. J. J. M. E. P. S. 2007. Morphological, growth and meadow characteristics of the seagrass Posidonia sinuosa along a depth-related gradient of light availability. 337**,** 103-115.

COLLIER, C. J., LAVERY, P. S., RALPH, P. J. & MASINI, R. J. 2008. Physiological characteristics of the seagrass Posidonia sinuosa along a depth-related gradient of light availability. *Marine Ecology Progress Series,* 353**,** 65-79.

COSTA, B., WALKER, B. K. & DIJKSTRA, J. A. 2018. Mapping and Quantifying Seascape Patterns. *In:* PITTMAN, S. J. (ed.) *Seascape Ecology.* Oxford: Wiley Blackwell.

DAHL, M., DEYANOVA, D., GUTSCHOW, S., ASPLUND, M. E., LYIMO, L. D., KARAMFILOV, V., SANTOS, R., BJORK, M. & GULLSTROM, M. 2016. Sediment Properties as Important Predictors of Carbon Storage in Zostera marina Meadows: A Comparison of Four European Areas. *PLoS One,* 11**,** e0167493.

DE BOER, W. F. 2000. Biomass dynamics of seagrasses and the role of mangrove and seagrass vegetation as different nutrient sources for an intertidal ecosystem. *Aquatic Botany,* 66**,** 225-239.

DEKKER, A. G., BRANDO, V. E. & ANSTEE, J. M. 2005. Retrospective seagrass change detection in a shallow coastal tidal Australian lake. *Remote Sensing of Environment,* 97**,** 415-433.

DONG, M., BRYAN, B. A., CONNOR, J. D., NOLAN, M. & GAO, L. 2015. Land use mapping error introduces strongly-localised, scale-dependent uncertainty into land use and ecosystem services modelling. *Ecosystem Services,* 15**,** 63-74.

DUARTE, C. M. 1989. Temporal biomass variability and production/biomass relationships of seagrass communities. *Marine Ecology Progress Series,* 51**,** 269-276.

DUARTE, C. M. & CHISCANO, C. L. 1999. Seagrass biomass and production: a reassessment. *Aquatic Botany,* 65**,** 159-174.

DUFFY, J. E., BENEDETTI-CECCHI, L., TRINANES, J., MULLER-KARGER, F. E., AMBO-RAPPE, R., BOSTRÖM, C., BUSCHMANN, A. H., BYRNES, J., COLES, R. G., CREED, J., CULLEN-UNSWORTH, L. C., DIAZ-PULIDO, G., DUARTE, C. M., EDGAR, G. J., FORTES, M., GONI, G., HU, C., HUANG, X., HURD, C. L., JOHNSON, C., KONAR, B., KRAUSE-JENSEN, D., KRUMHANSL, K., MACREADIE, P., MARSH, H., MCKENZIE, L. J., MIESZKOWSKA, N., MILOSLAVICH, P., MONTES, E., NAKAOKA, M., NORDERHAUG, K. M., NORLUND, L. M., ORTH, R. J., PRATHEP, A., PUTMAN, N. F., SAMPER-VILLARREAL, J., SERRAO, E. A., SHORT, F., PINTO, I. S., STEINBERG, P., STUART-SMITH, R., UNSWORTH, R. K. F., VAN KEULEN, M., VAN TUSSENBROEK, B. I., WANG, M., WAYCOTT, M., WEATHERDON, L. V., WERNBERG, T. & YAAKUB, S. M. 2019. Toward a Coordinated Global Observing System for Seagrasses and Marine Macroalgae. *Frontiers in Marine Science,* 6.

EL ALLAOUI, N., SERRA, T., COLOMER, J., SOLER, M., CASAMITJANA, X. & OLDHAM, C. 2016. Interactions between fragmented seagrass canopies and the local hydrodynamics. *PLoS One,* 11**,** e0156264.

EWERS LEWIS, C. J., CARNELL, P. E., SANDERMAN, J., BALDOCK, J. A. & MACREADIE, P. I. 2017. Variability and Vulnerability of Coastal 'Blue Carbon' Stocks: A Case Study from Southeast Australia. *Ecosystems,* 21**,** 263-279.

EWERS LEWIS, C. J., YOUNG, M. A., IERODIACONOU, D., BALDOCK, J. A., HAWKE, B., SANDERMAN, J., CARNELL, P. E. & MACREADIE, P. I. 2020. Drivers and modelling of blue carbon stock variability in sediments of southeastern Australia. *Biogeosciences,* 17**,** 2041-2059.

FAUZAN, M. A. & WICAKSONO, P. 2021. Characterizing Derawan seagrass cover change with time-series Sentinel-2 images. *Regional Studies in Marine Science,* 48**,** 102048.

FERDIE, M. & FOURQUREAN, J. W. 2004. Responses of seagrass communities to fertilization along a gradient of relative availability of nitrogen and phosphorus in a carbonate environment. *Limnology and Oceanography,* 49**,** 2082-2094.

FONSECA, M. S. & FISHER, J. S. 1986. A comparison of canopy friction and sediment movement between four species of seagrass with reference to their ecology and restoration. *Marine Ecology Progress Series,* 29**,** 5-22.

FOURQUREAN, J. W., DUARTE, C. M., KENNEDY, H., MARBÀ, N., HOLMER, M., MATEO, M. A., APOSTOLAKI, E. T., KENDRICK, G. A., KRAUSE-JENSEN, D. & MCGLATHERY, K. J. 2012. Seagrass ecosystems as a globally significant carbon stock. *Nature Geoscience,* 5**,** 505-509.

FOURQUREAN, J. W. & SCHRLAU, J. E. 2003. Changes in nutrient content and stable isotope ratios of C and N during decomposition of seagrasses and mangrove leaves along a nutrient availability gradient in Florida Bay, USA. *Chemistry and Ecology,* 19**,** 373-390.

FRANCE, R. L. & HOLMQUIST, J. G. 1997. Delta13C variability of macroalgae: effects of water motion via baffling by seagrasses and mangroves. *Marine Ecology Progress Series,* 149**,** 305-308.

FYFE, S. 2003. Spatial and temporal variation in spectral reflectance: Are seagrass species spectrally distinct? *Journal of Limnology and Oceanography,* 48**,** 464-479.

GAMBI, M. C., NOWELL, A. R. & JUMARS, P. A. 1990. Flume observations on flow dynamics in Zostera marina (eelgrass) beds. *Marine Ecology Progress Series***,** 159-169.

GILBERT, S. & CLARK, K. B. 1981. Seasonal variation in standing crop of the seagrass Syringodium filiforme and associated macrophytes in the northern Indian River, Florida. *Estuaries,* 4**,** 223-225.

GREINER, J. T., MCGLATHERY, K. J., GUNNELL, J. & MCKEE, B. A. 2013. Seagrass restoration enhances "blue carbon" sequestration in coastal waters. *PLoS One,* 8**,** e72469.

GRISCOM, B. W., ADAMS, J., ELLIS, P. W., HOUGHTON, R. A., LOMAX, G., MITEVA, D. A., SCHLESINGER, W. H., SHOCH, D., SIIKAMÄKI, J. V. & SMITH, P. J. 2017. Natural climate solutions. *Proceedings of the National Academy of Sciences,* 114**,** 11645-11650.

GUERRA-VARGAS, L. A., GILLIS, L. G. & MANCERA-PINEDA, J. E. 2020. Stronger Together: Do Coral Reefs Enhance Seagrass Meadows "Blue Carbon" Potential? *Frontiers in Marine Science,* 7**,** 628.

GULLSTRÖM, M., LYIMO, L. D., DAHL, M., SAMUELSSON, G. S., EGGERTSEN, M., ANDERBERG, E., RASMUSSON, L. M., LINDERHOLM, H. W., KNUDBY, A., BANDEIRA, S., NORDLUND, L. M. & BJÖRK, M. 2017. Blue Carbon Storage in Tropical Seagrass Meadows Relates to Carbonate Stock Dynamics, Plant–Sediment Processes, and Landscape Context: Insights from the Western Indian Ocean. *Ecosystems,* 21**,** 551-566.

HA, N. T., MANLEY-HARRIS, M., PHAM, T. D. & HAWES, I. J. I. J. O. R. S. 2021. The use of radar and optical satellite imagery combined with advanced machine learning and metaheuristic optimization techniques to detect and quantify above ground biomass of intertidal seagrass in a New Zealand estuary. 42**,** 4712-4738.

HAMYLTON, S. & SPENCER, T. 2011. Geomorphological modelling of tropical marine landscapes: Optical remote sensing, patches and spatial statistics. *Continental Shelf Research,* 31**,** S151-S161.

HARRISON, P. G. 1989. Detrital processing in seagrass systems: a review of factors affecting decay rates, remineralization and detritivory. *Aquatic Botany,* 35**,** 263-288.

HELMI, M., PURWANTO, W. A., SUBARDJO, P. & AYSIRA, A. 2018. Benthic Diversity Mapping and Analysis Base on Remote Sensing and Seascape Ecology Approach at Parang Islands, Karimunjawa National Park, Indonesia. *International Journal of Civil Engineering and Technology,* 9**,** 227-235.

HEMMINGA, M., HARRISON, P. & VAN LENT, F. 1991. The balance of nutrient losses and gains in seagrass meadows. *Marine Ecology Progress Series***,** 85-96.

HEMMINGA, M., SLIM, F., KAZUNGU, J., GANSSEN, G., NIEUWENHUIZE, J. & KRUYT, N. 1994. Carbon outwelling from a mangrove forest with adjacent seagrass beds and coral reefs (Gazi Bay, Kenya). *Marine Ecology Progress Series,* 106.

HEMMINGA, M. A. & DUARTE, C. M. 2000. *Seagrass ecology*, Cambridge University Press.

HERR, D., PIDGEON, E. & LAFFOLEY, D. D. A. 2012. *Blue carbon policy framework 2.0: based on the discussion of the International Blue Carbon Policy Working Group*, IUCN.

HOPKINSON, C. S., CAI, W.-J. & HU, X. 2012. Carbon sequestration in wetland dominated coastal systems—a global sink of rapidly diminishing magnitude. *Current Opinion in Environmental Sustainability,* 4**,** 186-194.

HOWARD, J., HOYT, S., ISENSEE, K., TELSZEWSKI, M. & PIDGEON, E. 2014. Coastal blue carbon: methods for assessing carbon stocks and emissions factors in mangroves, tidal salt marshes, and seagrasses.

IPCC 2006. *2006 IPCC Guidelines for National Greenhouse Gas Inventories, Prepared by the National Greenhouse Gas Inventories Programme,* Japan, IGES.

IPCC 2014. *2013 Supplement to the 2006 IPCC Guidelines for National Greenhouse Gas Inventories: Wetlands,* Switzerland, IPCC.

IPCC 2019. *2019 Refinement to the 2006 IPCC Guidelines for National Greenhouse Gas Inventories,* Switzerland, IPCC.

KILMINSTER, K., MCMAHON, K., WAYCOTT, M., KENDRICK, G. A., SCANES, P., MCKENZIE, L., O'BRIEN, K. R., LYONS, M., FERGUSON, A., MAXWELL, P., GLASBY, T. & UDY, J. 2015. Unravelling complexity in seagrass systems for management: Australia as a microcosm. *Sci Total Environ,* 534**,** 97-109.

KIM, S. H., SUONAN, Z., QIN, L.-Z., KIM, H., PARK, J.-I., KIM, Y. K., LEE, S., KIM, S.-G., KANG, C.-K. & LEE, K.-S. 2022. Variability in blue carbon storage related to biogeochemical factors in seagrass meadows off the coast of the Korean peninsula. *Science of the Total Environment,* 813**,** 152680.

KOVACS, E., ROELFSEMA, C., LYONS, M., ZHAO, S. & PHINN, S. 2018. Seagrass habitat mapping: how do Landsat 8 OLI, Sentinel-2, ZY-3A, and Worldview-3 perform? *Remote Sensing Letters,* 9**,** 686-695.

KRAUSE, J. R., HINOJOSA-CORONA, A., GRAY, A. B. & BURKE WATSON, E. 2021. Emerging Sensor Platforms Allow for Seagrass Extent Mapping in a Turbid Estuary and from the Meadow to Ecosystem Scale. *Remote Sensing,* 13**,** 3681.

LAVERY, P. S., MATEO, M. A., SERRANO, O. & ROZAIMI, M. 2013. Variability in the carbon storage of seagrass habitats and its implications for global estimates of blue carbon ecosystem service. *PLoS One,* 8**,** e73748.

LIMA, M. D. A. C., WARD, R. D. & JOYCE, C. B. 2020. Environmental drivers of sediment carbon storage in temperate seagrass meadows. *Hydrobiologia,* 847**,** 1773-1792.

LIRMAN, D. & CROPPER, W. P. 2003. The influence of salinity on seagrass growth, survivorship, and distribution within Biscayne Bay, Florida: field, experimental, and modeling studies. *Estuaries,* 26**,** 131-141.

LOVELOCK, C. E., ATWOOD, T., BALDOCK, J., DUARTE, C. M., HICKEY, S., LAVERY, P. S., MASQUE, P., MACREADIE, P. I., RICART, A. M. & SERRANO, O. 2017. Assessing the risk of carbon dioxide emissions from blue carbon ecosystems. *Frontiers in Ecology and the Environment,* 15**,** 257-265.

LYONS, M., PHINN, S. & ROELFSEMA, C. 2011. Integrating Quickbird Multi-Spectral Satellite and Field Data: Mapping Bathymetry, Seagrass Cover, Seagrass Species and Change in Moreton Bay, Australia in 2004 and 2007. *Remote Sensing,* 3**,** 42-64.

LYONS, M., ROELFSEMA, C., KOVACS, E., SAMPER-VILLARREAL, J., SAUNDERS, M., MAXWELL, P. & PHINN, S. 2015. Rapid monitoring of seagrass biomass using a simple linear modelling approach, in the field and from space. *Marine Ecology Progress Series,* 530**,** 1-14.

LYONS, M. B., PHINN, S. R. & ROELFSEMA, C. M. 2012. Long term land cover and seagrass mapping using Landsat and object-based image analysis from 1972 to 2010 in the coastal environment of South East Queensland, Australia. *ISPRS Journal of Photogrammetry and Remote Sensing,* 71**,** 34-46.

LYONS, M. B., ROELFSEMA, C. M. & PHINN, S. R. 2013. Towards understanding temporal and spatial dynamics of seagrass landscapes using time-series remote sensing. *Estuarine, Coastal and Shelf Science,* 120**,** 42-53.

MACREADIE, P. I., BAIRD, M. E., TREVATHAN-TACKETT, S. M., LARKUM, A. W. & RALPH, P. J. 2014. Quantifying and modelling the carbon sequestration capacity of seagrass meadows--a critical assessment. *Mar Pollut Bull,* 83**,** 430-9.

MACREADIE, P. I., COSTA, M. D., ATWOOD, T. B., FRIESS, D. A., KELLEWAY, J. J., KENNEDY, H., LOVELOCK, C. E., SERRANO, O. & DUARTE, C. M. 2021. Blue carbon as a natural climate solution. *Nature Reviews Earth & Environment*, 1-14.

MADONSELA, S., CHO, M. A., MATHIEU, R., MUTANGA, O., RAMOELO, A., KASZTA, Ż., VAN DE KERCHOVE, R. & WOLFF, E. 2017. Multi-phenology WorldView-2 imagery improves remote sensing of savannah tree species. *International Journal of Applied Earth Observation and Geoinformation,* 58, 65-73.

MATEO, M. A., CEBRIAN, J., DUNTON, K. & MUTCHLER, T. 2006. Carbon Flux in Seagrass Ecosystems. *In:* LARKUM, A. W. D., ORTH, R. J. & DUARTE, C. M. (eds.) *Seagrasses: Biology, Ecology and Conservation.* The Netherlands: Springer.

MATTSSON, E., OSTWALD, M., WALLIN, G. & NISSANKA, S. 2016. Heterogeneity and assessment uncertainties in forest characteristics and biomass carbon stocks: Important considerations for climate mitigation policies. *Land Use Policy,* 59, 84-94.

MAZARRASA, I., LAVERY, P., DUARTE, C. M., LAFRATTA, A., LOVELOCK, C. E., MACREADIE, P. I., SAMPER‐VILLARREAL, J., SALINAS, C., SANDERS, C. & TREVATHAN‐TACKETT, S. 2021. Factors determining seagrass Blue Carbon across bioregions and geomorphologies. *Global Biogeochemical Cycles*, e2021GB006935.

MAZARRASA, I., MARBÀ, N., GARCIA‐ORELLANA, J., MASQUÉ, P., ARIAS‐ORTIZ, A. & DUARTE, C. M. 2017. Effect of environmental factors (wave exposure and depth) and anthropogenic pressure in the C sink capacity of Posidonia oceanica meadows. *Limnology and Oceanography,* 62, 1436-1450.

MAZARRASA, I., SAMPER-VILLARREAL, J., SERRANO, O., LAVERY, P. S., LOVELOCK, C. E., MARBA, N., DUARTE, C. M. & CORTES, J. 2018. Habitat characteristics provide insights of carbon storage in seagrass meadows. *Mar Pollut Bull,* 134, 106-117.

MCCOMB, A., CAMBRIDGE, M., KIRKMAN, H. & KUO, J. 1981. The biology of Australian seagrasses. University of Western Australia Press.

MCKENZIE, L. J., LANGLOIS, L. A. & ROELFSEMA, C. M. 2022. Improving approaches to mapping seagrass within the Great Barrier Reef: From field to spaceborne earth observation. *Remote Sensing,* 14, 2604.

MCLEOD, E., CHMURA, G. L., BOUILLON, S., SALM, R., BJÖRK, M., DUARTE, C. M., LOVELOCK, C. E., SCHLESINGER, W. H. & SILLIMAN, B. R. 2011. A blueprint for blue carbon: toward an improved understanding of the role of vegetated coastal habitats in sequestering CO2. *Frontiers in Ecology and the Environment,* 9, 552-560.

MICHALEK, J. L., WAGNER, T. W., LUCZKOVICH, J. J. & STOFFLE, R. W. 1993. Multispectral change vector analysis for monitoring coastal marine environments. *Photogrammetric Engineering and Remote Sensing,* 59, 381-384.

MIYAJIMA, T., HORI, M., HAMAGUCHI, M., SHIMABUKURO, H., ADACHI, H., YAMANO, H. & NAKAOKA, M. 2015. Geographic variability in organic carbon stock and accumulation rate in sediments of East and Southeast Asian seagrass meadows. *Global Biogeochemical Cycles,* 29, 397-415.

MÜLLER, G., STELZER, K., SMOLLICH, S., GADE, M., ADOLPH, W., MELCHIONNA, S., KEMME, L., GEIßLER, J., MILLAT, G., REIMERS, H.-C. J. E. M. & ASSESSMENT 2016. Remotely sensing the German Wadden Sea—A new approach to address national and international environmental legislation. 188, 1-17.

MUMBY, P. J. & EDWARDS, A. J. 2002. Mapping marine environments with IKONOS imagery: enhanced spatial resolution can deliver greater thematic accuracy. *Remote Sensing of Environment,* 82, 248-257.

NORDLUND, L., KOCH, E. W., BARBIER, E. B. & CREED, J. C. 2016. Seagrass Ecosystem Services and Their Variability across Genera and Geographical Regions. *PLoS One,* 11, e0163091.

OLSEN, Y. S., COLLIER, C., OW, Y. X. & KENDRICK, G. A. 2018. Global Warming and Ocean Acidification: Effects on Australian Seagrass Ecosystems. *In:* LARKUM, A. W., KENDRICK, G.

A. & RALPH, P. J. (eds.) *Seagrasses of Australia: Structure, Ecology and Conservation.* Switzerland: Springer.

ORESKA, M. P., MCGLATHERY, K. J., AOKI, L. R., BERGER, A. C., BERG, P. & MULLINS, L. 2020. The greenhouse gas offset potential from seagrass restoration. *Scientific Reports,* 10**,** 1-15.

ORESKA, M. P. J., MCGLATHERY, K. J. & PORTER, J. H. 2017. Seagrass blue carbon spatial patterns at the meadow-scale. *PLoS One,* 12**,** e0176630.

ORTH, R. J., CARRUTHERS, T. J., DENNISON, W. C., DUARTE, C. M., FOURQUREAN, J. W., HECK, K. L., HUGHES, A. R., KENDRICK, G. A., KENWORTHY, W. J. & OLYARNIK, S. 2006. A global crisis for seagrass ecosystems. *Bioscience,* 56**,** 987-996.

PERGENT, G., ROMERO, J., PERGENT-MARTINI, C., MATEO, M.-A. & BOUDOURESQUE, C.-F. 1994. Primary production, stocks and fluxes in the Mediterranean seagrass Posidonia oceanica. *Marine Ecology Progress Series***,** 139-146.

PHINN, S., ROELFSEMA, C., DEKKER, A., BRANDO, V. & ANSTEE, J. 2008. Mapping seagrass species, cover and biomass in shallow waters: An assessment of satellite multi-spectral and airborne hyper-spectral imaging systems in Moreton Bay (Australia). *Remote Sensing of Environment,* 112**,** 3413-3425.

PITTMAN, S., YATES, K., BOUCHET, P., ALVAREZ-BERASTEGUI, D., ANDRÉFOUËT, S., BELL, S., BERKSTRÖM, C., BOSTRÖM, C., BROWN, C. & CONNOLLY, R. 2021. Seascape ecology: identifying research priorities for an emerging ocean sustainability science. *Marine Ecology Progress Series,* 663**,** 1-29.

POTOUROGLOU, M., BULL, J. C., KRAUSS, K. W., KENNEDY, H. A., FUSI, M., DAFFONCHIO, D., MANGORA, M. M., GITHAIGA, M. N., DIELE, K. & HUXHAM, M. 2017. Measuring the role of seagrasses in regulating sediment surface elevation. *Scientific Reports,* 7**,** 1-11.

POURSANIDIS, D., TRAGANOS, D., TEIXEIRA, L., SHAPIRO, A. & MUAVES, L. 2021. Cloud‐native seascape mapping of Mozambique's Quirimbas National Park with Sentinel‐2. *Remote Sensing in Ecology and Conservation,* 7**,** 275-291.

PU, R. & BELL, S. 2017. Mapping seagrass coverage and spatial patterns with high spatial resolution IKONOS imagery. *International Journal of Applied Earth Observation and Geoinformation,* 54**,** 145-158.

PU, R., BELL, S., MEYER, C., BAGGETT, L. & ZHAO, Y. 2012. Mapping and assessing seagrass along the western coast of Florida using Landsat TM and EO-1 ALI/Hyperion imagery. *Estuarine, Coastal and Shelf Science,* 115**,** 234-245.

PU, R., BELL, S. J. I. J. O. P. & SENSING, R. 2013. A protocol for improving mapping and assessing of seagrass abundance along the West Central Coast of Florida using Landsat TM and EO-1 ALI/Hyperion images. 83**,** 116-129.

RALPH, P. J., CROSSWELL, J., CANNARD, T. & STEVEN, A. D. 2018. Estimating seagrass blue carbon and policy implications: The Australian perspective. *Seagrasses of Australia.* Springer.

RANDAZZO, G., ITALIANO, F., MICALLEF, A., TOMASELLO, A., CASSETTI, F. P., ZAMMIT, A., D'AMICO, S., SALIBA, O., CASCIO, M. & CAVALLARO, F. 2021. WebGIS Implementation for Dynamic Mapping and Visualization of Coastal Geospatial Data: A Case Study of BESS Project. *Applied Sciences,* 11**,** 8233.

RICART, A. M., PÉREZ, M. & ROMERO, J. 2017. Landscape configuration modulates carbon storage in seagrass sediments. *Estuarine, Coastal and Shelf Science,* 185**,** 69-76.

RICART, A. M., YORK, P. H., BRYANT, C. V., RASHEED, M. A., IERODIACONOU, D. & MACREADIE, P. I. 2020. High variability of Blue Carbon storage in seagrass meadows at the estuary scale. *Scientific Reports,* 10**,** 1-12.

RICART, A. M., YORK, P. H., RASHEED, M. A., PÉREZ, M., ROMERO, J., BRYANT, C. V. & MACREADIE, P. I. 2015. Variability of sedimentary organic carbon in patchy seagrass landscapes. *Marine Pollution Bulletin,* 100**,** 476-482.

RIOJA-NIETO, R., BARRERA-FALCÓN, E., HINOJOSA-ARANGO, G. & RIOSMENA-RODRÍGUEZ, R. 2013. Benthic habitat β-diversity modeling and landscape metrics for the selection of priority

conservation areas using a systematic approach: Magdalena Bay, Mexico, as a case study. *Ocean & Coastal Management,* 82**,** 95-103.

ROBBINS, B. D. & BELL, S. S. 1994. Seagrass landscapes: a terrestrial approach to the marine subtidal environment. *Trends in Ecology & Evolution,* 9**,** 301-304.

ROELFSEMA, C., KOVACS, E. M., SAUNDERS, M. I., PHINN, S., LYONS, M. & MAXWELL, P. 2013. Challenges of remote sensing for quantifying changes in large complex seagrass environments. *Estuarine, Coastal and Shelf Science,* 133**,** 161-171.

ROELFSEMA, C., PHINN, S., UDY, N. & MAXWELL, P. 2009. An integrated field and remote sensing approach for mapping seagrass cover, Moreton Bay, Australia. *Journal of Spatial Science,* 54**,** 45-62.

ROELFSEMA, C. M., LYONS, M., KOVACS, E. M., MAXWELL, P., SAUNDERS, M. I., SAMPER-VILLARREAL, J. & PHINN, S. R. 2014. Multi-temporal mapping of seagrass cover, species and biomass: A semi-automated object based image analysis approach. *Remote Sensing of Environment,* 150**,** 172-187.

ROZAIMI, M., SERRANO, O. & LAVERY, P. 2013. Comparison of carbon stores by two morphologically different seagrasses. *Journal of the Royal Society of Western Australia,* 96**,** 81.

SAMPER-VILLARREAL, J., LOVELOCK, C. E., SAUNDERS, M. I., ROELFSEMA, C. & MUMBY, P. J. 2016. Organic carbon in seagrass sediments is influenced by seagrass canopy complexity, turbidity, wave height, and water depth. *Limnology and Oceanography,* 61**,** 938-952.

SAMPER-VILLARREAL, J., MUMBY, P. J., SAUNDERS, M. I., ROELFSEMA, C. & LOVELOCK, C. E. 2018. Seagrass Organic Carbon Stocks Show Minimal Variation Over Short Time Scales in a Heterogeneous Subtropical Seascape. *Estuaries and Coasts,* 41**,** 1732-1743.

SANDERS, C. J., MAHER, D. T., SMOAK, J. M. & EYRE, B. D. 2019. Large variability in organic carbon and CaCO3 burial in seagrass meadows: a case study from three Australian estuaries. *Marine Ecology Progress Series,* 616**,** 211-218.

SANTAMARíA-GALLEGOS, N. A., SÁNCHEZ-LIZASO, J. L. & FÉLIX-PICO, E. F. 2000. Phenology and growth cycle of annual subtidal eelgrass in a subtropical locality. *Aquatic Botany,* 66**,** 329-339.

SERRANO, O., ALMAHASHEER, H., DUARTE, C. M. & IRIGOIEN, X. 2018. Carbon stocks and accumulation rates in Red Sea seagrass meadows. *Scientific Reports,* 8**,** 1-13.

SERRANO, O., GÓMEZ-LÓPEZ, D. I., SÁNCHEZ-VALENCIA, L., ACOSTA-CHAPARRO, A., NAVAS-CAMACHO, R., GONZÁLEZ-CORREDOR, J., SALINAS, C., MASQUE, P., BERNAL, C. A. & MARBÀ, N. 2021. Seagrass blue carbon stocks and sequestration rates in the Colombian Caribbean. *Scientific Reports,* 11**,** 1-12.

SERRANO, O., LAVERY, P. S., DUARTE, C. M., KENDRICK, G. A., CALAFAT, A., YORK, P. H., STEVEN, A. & MACREADIE, P. I. 2016a. Can mud (silt and clay) concentration be used to predict soil organic carbon content within seagrass ecosystems? *Biogeosciences,* 13**,** 4915-4926.

SERRANO, O., LAVERY, P. S., ROZAIMI, M. & MATEO, M. Á. 2014. Influence of water depth on the carbon sequestration capacity of seagrasses. *Global Biogeochemical Cycles,* 28**,** 950-961.

SERRANO, O., LOVELOCK, C. E., T, B. A., MACREADIE, P. I., CANTO, R., PHINN, S., ARIAS-ORTIZ, A., BAI, L., BALDOCK, J., BEDULLI, C., CARNELL, P., CONNOLLY, R. M., DONALDSON, P., ESTEBAN, A., EWERS LEWIS, C. J., EYRE, B. D., HAYES, M. A., HORWITZ, P., HUTLEY, L. B., KAVAZOS, C. R. J., KELLEWAY, J. J., KENDRICK, G. A., KILMINSTER, K., LAFRATTA, A., LEE, S., LAVERY, P. S., MAHER, D. T., MARBA, N., MASQUE, P., MATEO, M. A., MOUNT, R., RALPH, P. J., ROELFSEMA, C., ROZAIMI, M., RUHON, R., SALINAS, C., SAMPER-VILLARREAL, J., SANDERMAN, J., C, J. S., SANTOS, I., SHARPLES, C., STEVEN, A. D. L., CANNARD, T., TREVATHAN-TACKETT, S. M. & DUARTE, C. M. 2019. Australian vegetated coastal ecosystems as global hotspots for climate change mitigation. *Nat Commun,* 10**,** 4313.

SERRANO, O., RICART, A. M., LAVERY, P. S., MATEO, M. A., ARIAS-ORTIZ, A., MASQUE, P., ROZAIMI, M., STEVEN, A. & DUARTE, C. M. 2016b. Key biogeochemical factors affecting soil carbon storage in Posidonia meadows. *Biogeosciences,* 13**,** 4581-4594.

SERRANO, O., ROZAIMI, M., LAVERY, P. S. & SMERNIK, R. J. 2020. Organic chemistry insights for the exceptional soil carbon storage of the seagrass Posidonia australis. *Estuarine Coastal and Shelf Science,* 237**,** 106662.

SHAPIRO, A. C. & ROHMANN, S. O. 2006. Mapping changes in submerged aquatic vegetation using Landsat imagery and benthic habitat data: coral reef ecosystem monitoring in Vieques Sound between 1985 and 2000. *Bulletin of Marine Science,* 79**,** 375-388.

STANKOVIC, M., HAYASHIZAKI, K.-I., TUNTIPRAPAS, P., RATTANACHOT, E. & PRATHEP, A. 2021. Two decades of seagrass area change: Organic carbon sources and stock. *Marine Pollution Bulletin,* 163**,** 111913.

STANKOVIC, M., PANYAWAI, J., JANSANIT, K., UPANOI, T. & PRATHEP, A. 2017. Carbon content in different seagrass species in Andaman Coast of Thailand. *Sains Malaysiana,* 46**,** 1441-1447.

STANKOVIC, M., TANTIPISANUH, N., RATTANACHOT, E. & PRATHEP, A. 2018. Model-based approach for estimating biomass and organic carbon in tropical seagrass ecosystems. *Marine Ecology Progress Series,* 596**,** 61-70.

THAYER, G. W., KENWORTHY, W. J. & FONSECA, M. S. 1984. *The ecology of eelgrass meadows of the Atlantic coast: a community profile,* Fish and Wildlife Service, US Department of the Interior.

THAYER, G. W., WOLFE, D. A. & WILLIAMS, R. B. 1975. The Impact of Man on Seagrass Systems: Seagrasses must be considered in terms of their interaction with the other sources of primary production that support the estuarine trophic structure before their significance can be fully appreciated. *American Scientist,* 63**,** 288-296.

THORHAUG, A., RICHARDSON, A. & BERLYN, G. 2007. Spectral reflectance of the seagrasses: Thalassia testudinum, Halodule wrightii, Syringodium filiforme and five marine algae. *International Journal of Remote Sensing,* 28**,** 1487-1501.

TOPOUZELIS, K., MAKRI, D., STOUPAS, N., PAPAKONSTANTINOU, A. & KATSANEVAKIS, S. 2018. Seagrass mapping in Greek territorial waters using Landsat-8 satellite images. *International Journal of Applied Earth Observation and Geoinformation,* 67**,** 98-113.

TRAGANOS, D., AGGARWAL, B., POURSANIDIS, D., TOPOUZELIS, K., CHRYSOULAKIS, N. & REINARTZ, P. 2018. Towards Global-Scale Seagrass Mapping and Monitoring Using Sentinel-2 on Google Earth Engine: The Case Study of the Aegean and Ionian Seas. *Remote Sensing,* 10.

TRAGANOS, D. & REINARTZ, P. 2018. Interannual Change Detection of Mediterranean Seagrasses Using RapidEye Image Time Series. *Front Plant Sci,* 9**,** 96.

TREVATHAN-TACKETT, S. M., MACREADIE, P. I., SANDERMAN, J., BALDOCK, J., HOWES, J. M. & RALPH, P. J. 2017. A global assessment of the chemical recalcitrance of seagrass tissues: implications for long-term carbon sequestration. *Frontiers in Plant Science,* 8**,** 925.

UHRIN, A. V. & TOWNSEND, P. A. 2016. Improved seagrass mapping using linear spectral unmixing of aerial photographs. *Estuarine, Coastal and Shelf Science,* 171**,** 11-22.

UHRIN, A. V. & TURNER, M. G. 2018. Physical drivers of seagrass spatial configuration: the role of thresholds. *Landscape Ecology,* 33**,** 2253-2272.

UNEP-WCMC & SHORT, F. T. 2021. Global distribution of seagrasses (version 7.1). Seventh update to the data layer used in Green and Short (2003). *In:* CENTRE, U. E. W. C. M. (ed.). Cambridge.

UNEP 2020. Out of the blue: The value of seagrasses to the environment and to people. Nairobi.

UNSWORTH, R. K., NORDLUND, L. M. & CULLEN‐UNSWORTH, L. C. 2019. Seagrass meadows support global fisheries production. *Conservation Letters,* 12**,** e12566.

URBAŃSKI, J., MAZUR, A. & JANAS, U. 2009. Object-oriented classification of QuickBird data for mapping seagrass spatial structure. *Oceanological and Hydrobiological Studies,* 38**,** 27-43.

VAN KATWIJK, M., BOS, A., HERMUS, D. & SUYKERBUYK, W. 2010. Sediment modification by seagrass beds: Muddification and sandification induced by plant cover and environmental conditions. *Estuarine Coastal and Shelf Science,* 89**,** 175-181.

WABNITZ, C. C., ANDRÉFOUËT, S., TORRES-PULLIZA, D., MÜLLER-KARGER, F. E. & KRAMER, P. A. 2008. Regional-scale seagrass habitat mapping in the Wider Caribbean region using Landsat sensors: Applications to conservation and ecology. *Remote Sensing of Environment,* 112**,** 3455-3467.

WALKER, D. I., OLESEN, B. & PHILLIPS, R. C. 2001. Reproduction and phenology in seagrasses. *In:* SHORT, F. T. & COLES, R. G. (eds.) *Global Seagrass Research Methods.* Elsevier Science.

WICAKSONO, P. & HAFIZT, M. 2013. Mapping seagrass from space: Addressing the complexity of seagrass LAI mapping. *European Journal of Remote Sensing,* 46**,** 18-39.

WIDDOWS, J., POPE, N. D., BRINSLEY, M. D., ASMUS, H. & ASMUS, R. M. 2008. Effects of seagrass beds (Zostera noltii and Z. marina) on near-bed hydrodynamics and sediment resuspension. *Marine Ecology Progress Series,* 358**,** 125-136.

ZOFFOLI, M. L., GERNEZ, P., ROSA, P., LE BRIS, A., BRANDO, V. E., BARILLÉ, A.-L., HARIN, N., PETERS, S., POSER, K., SPAIAS, L., PERALTA, G. & BARILLÉ, L. 2020. Sentinel-2 remote sensing of Zostera noltei-dominated intertidal seagrass meadows. *Remote Sensing of Environment,* 251.

Chapter 4

Mapping fine-scale seagrass disturbance using bi-temporal UAV-acquired images and multivariate alteration detection

This chapter is published as Simpson, J., Davies, K.P., Barber, P. and Bruce, E., 2024. Mapping fine-scale seagrass disturbance using bi-temporal UAV-acquired images and multivariate alteration detection. *Scientific reports, 14*(1), p.19083. https://doi.org/10.1038/s41598-024-69695-8. This text is a reproduction of the published paper. The original version of the paper is available in Appendix A.

This chapter addresses **Aim 2** by developing a method to characterise seagrass that captures spatial heterogeneity. It contributes to **Aim 3** by assessing the relevance of spectral resolution to change identification in seagrass.

4.1 Introduction

Monitoring of seagrass beds to detect changes and disturbances is critical for supporting conservation and restoration efforts of these important ecosystems (Hossain and Hashim, 2019, Griffiths et al., 2020, Unsworth et al., 2022). Drivers of seagrass change include boat propeller scarring, natural hazards such as flood or drought, eutrophication, and climate change-induced increases in sea surface temperatures (Waycott et al., 2009, Lovelock et al., 2017). Disturbances to seagrass beds threaten ecosystem function and interfere with critical ecosystem services such as coastal protection, carbon sequestration, and habitat provision (Brondizio et al., 2019). Direct damage to seagrass which disturbs sediments can lead to remineralisation and emission of stored carbon as CO_2 (Pendleton et al., 2012, O'Brien et al., 2018). Conversely, successful restoration of seagrass beds can rapidly and effectively restore ecosystem function and associated ecosystem services (Orth et al., 2020, Beheshti et al., 2022). Effective monitoring approaches can provide accurate information on rates of disturbance and recovery at ecologically relevant spatio-temporal scales to inform management and implementation of protection and restoration strategies (Barry et al., 2020).

Requirements for seagrass monitoring will vary depending on the character of the ecosystem, and the nature of potential disturbances (Kilminster et al., 2015, O'Brien et al., 2018). Consequently, approaches should consider the site and purpose. Seagrass is commonly monitored through recurrent field observations using permanent transects or quadrats, remote sensing-based methods, or a combination of these. Long-term trends in seagrass abundance or composition across a meadow can be detected using permanent quadrats and transects, which is useful for establishing the effects of large-scale change at representative sites (Kirkman, 1996, Short et al., 2015). Satellite remote sensing has been applied widely for measuring changes in meadow extent, especially at a regional to global scale (Roelfsema et al., 2013, Traganos et al., 2018, Lizcano-Sandoval et al., 2022, Coffer et al., 2023); however, the ability to detect finer-scale seagrass change using satellites is constrained by image spatial resolution.

Airborne-sensors combined with automatic change detection analysis techniques (Fletcher et al., 2009, Uhrin and Townsend, 2016) and manual image interpretation (Orth et al., 2017, Mancini et al., 2023) have been used to detect changes to seagrass at fine spatial scales. Airborne sensors can capture highly localised seagrass disturbances such as boat scars, and patch level heterogeneity in seagrass abundance which might otherwise be obscured in satellite images and permanent transect monitoring (Virnstein, 1999, Kaufman and Bell, 2022). However, airborne data capture is relatively expensive and involves logistical challenges due to the stricter airspace and licensing requirements.

Unoccupied Aerial Vehicles (UAVs) provide an attractive alternative to crewed airborne data capture especially when repeat captures are required for time series monitoring. UAVs are relatively inexpensive, and the increased accessibility of UAV technology has enabled new imaging methods that can capture fine-scale features even in structurally complex meadows (Veettil et al., 2020). UAV-acquired images have been used for mapping seagrass density, ecosystem health, and species composition at fine scales (James et al., 2020, Chen and Sasaki, 2021, Tahara et al., 2022, Price et al., 2022), as well as for identifying disturbances such as boat propeller scars (Karang et al., 2024). UAVs have also supported time series seagrass monitoring with recurrent flights used

to characterise seasonal change (Martin et al., 2020, Krause et al., 2021) and identify long-term impacts of climate change on seagrass (Aoki et al., 2023).

Seagrass change detection with UAV images has used simple bi-temporal comparison of classification outputs (Martin et al., 2020, Krause et al., 2021). This approach generally involves a supervised classification of images acquired on two different dates, and then differencing the classification outputs to determine areas of change. This relatively simple approach can be effective, but supervised classification requires suitable ground truth training and validation data for each classified image (Martin et al., 2020), and is likely to suffer from degraded accuracy associated with post-classification change detection (Singh, 1989). The requirement for extensive training and ground-truth validation data for supervised change detection methods increases time and cost burdens on coastal managers who may need to rapidly detect, investigate, and respond to potential seagrass disturbances. There is a need for a rapid, cost-effective unsupervised change detection approach to reliably map fine-scale disturbances that is not contingent on rigorous ground truth data collection.

The Iteratively Reweighted Multivariate Alteration Detection (IR-MAD)(Nielsen, 2007) method is a relatively simple, unsupervised approach for detecting bi-temporal changes in multispectral images. IR-MAD was originally developed for detecting changes in pairs of multispectral satellite images (Nielsen et al., 1998) and has only had limited application to UAV images for monitoring of the built environment (Liu et al., 2021). IR-MAD has not been applied to fine-scale monitoring of seagrass disturbances using UAV images in the literature to date.

The primary objective of this study is to demonstrate the use of the IR-MAD method for unsupervised seagrass disturbance detection using co-registered UAV images of two seagrass beds in Brisbane Water, New South Wales, Australia. Using the IR-MAD outputs, we identify key change categories and quantitatively determine the separability of change signals.

UAV sensor selection is also an important consideration for coastal managers endeavouring to use a UAV platform for coastal monitoring. There is a wide selection of commercially available sensors ranging from less expensive red-green-blue (RGB)

sensors to more costly multispectral sensors with four or more bands in the visible to near-infrared range of the spectrum. The 10-band multispectral sensor used in this study (Micasense RedEdge-MX Dual) has been shown to enhance seagrass species classification (Román et al., 2021) and the discrimination between seagrass and macroalgae compared to sensors with only three or four bands in the visible range (Davies et al., 2023). However, it is unclear how additional bands provided by more expensive multispectral sensors will affect the results produced by the IR-MAD method.

An additional objective of this research is therefore to assess whether sensor selection will impact on the change detection results produced by the IR-MAD method. We systematically compare IR-MAD results produced from four alternative sensor configurations. Assessing the importance of individual spectral bands for detecting seagrass change will help guide the selection of UAV sensor type when applying this method.

4.2 Methods

4.2.1 Study site

Brisbane Water is a wave-dominated barrier estuary located ~45 km north of Sydney, New South Wales (NSW; Figure 1) with a well-developed marine tidal delta and total area of ~27 km^2 (Roy et al., 2001). The estuary is surrounded by residential development on all sides except Brisbane Water National Park on the western side. The area is used extensively for commercial and recreational activities, including fishing, oyster farming, boating, and swimming.

Approximately 5 km^2 of seagrass beds are present within the Brisbane Water estuary (Roy et al., 2001), including *Zostera capricorni* growth in shallow shoreline areas (West, 2023), and in some areas, more extensive beds of *Z. capricorni* with *Posidonia australis* growing towards the deeper, seaward edge (Jelbart and Ross, 2006). *Halophila ovalis* is present throughout seagrass beds in some parts of the estuary (Jelbart and Ross, 2006).

For this study, two seagrass beds were selected, at St Huberts Island and Empire Bay, hereafter referred to by those names (Figure 1). These beds consist primarily of *Z. capricorni* at varying density as well as *P. australis* which is listed as an endangered

ecological community in this region of NSW (Macreadie et al., 2018). The seagrass beds are in shallow depths less than 1 m at low tide, with some edges extending down to approximately 2.5 m in depth. The study sites overlap with NSW Priority Oyster Aquaculture Areas (NSW Department of Primary Industries, , 2022) and oyster farming infrastructure is present in both seagrass beds.

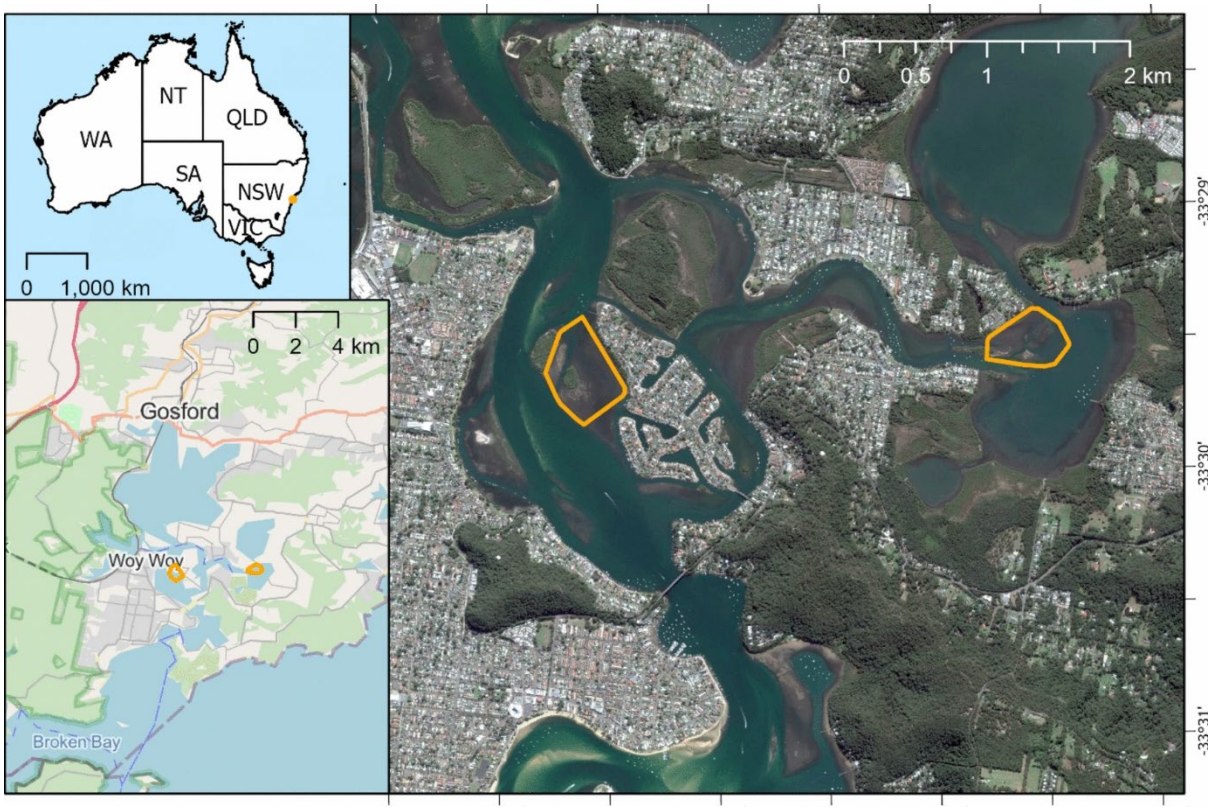

Figure 1. The seagrass study sites (highlighted in red) were located in the Brisbane Water estuary, NSW, Australia. The western and eastern study sites are referred to in the text as St Huberts Island and Empire Bay respectively. Map data: Google, DigitalGlobe, inset map copyright OpenStreetMap contributors and available from https://www.openstreetmap.org

4.2.2 Equipment

Images were captured using a Micasense RedEdge-MX Dual Camera System (referred to as MX-10), which consists of a 5-band RedEdge-MX camera interlinked with a 5-band RedEdge-MX Blue camera providing 10 spectral bands in total (Table 1). Band subsets of each image captured by the MX-10 sensor were used to simulate three sensors with reduced spectral band coverage: the first consisted of the bands captured by the 5-band RedEdge-MX camera referred to as MX-5, and the second and third virtual sensors consisting of six and three bands referred to as VIS-6 and RGB respectively (Table 1). As the images for these three virtual sensors were created using band subsets from the

original images captured by the MX-10 sensor, all images had the same spatial resolution. Compared with the band widths and placements of the Sentinel-2 and Landsat 9 satellite sensors (Figure 2), the MX-10 sensor has a similar coastal band placement with additional bands in the green and red regions. There is also an additional band in the red-edge region compared with Sentinel-2.

Table 1. The sensors used in this study (MX-10) is described by the band centre and band width (FWHM). The band subsets used to represent the three virtual sensors (MX-5, VIS-6 and RGB) are also shown.

Band	**Band centre (nm)**	**FWHM (nm)**	**MX-10**	**MX-5**	**VIS-6 (Virtual)**	**RGB (Virtual)**
Coastal Blue	444	28	✓		✓	
Blue	475	32	✓	✓	✓	✓
Green 1	531	14	✓		✓	
Green 2	560	27	✓	✓	✓	✓
Red 1	650	16	✓		✓	
Red 2	668	14	✓	✓	✓	✓
Red Edge (RE) 1	705	10	✓			
RE 2	717	12	✓	✓		
RE 3	740	18	✓			
Near-Infrared (NIR)	842	57	✓	✓		

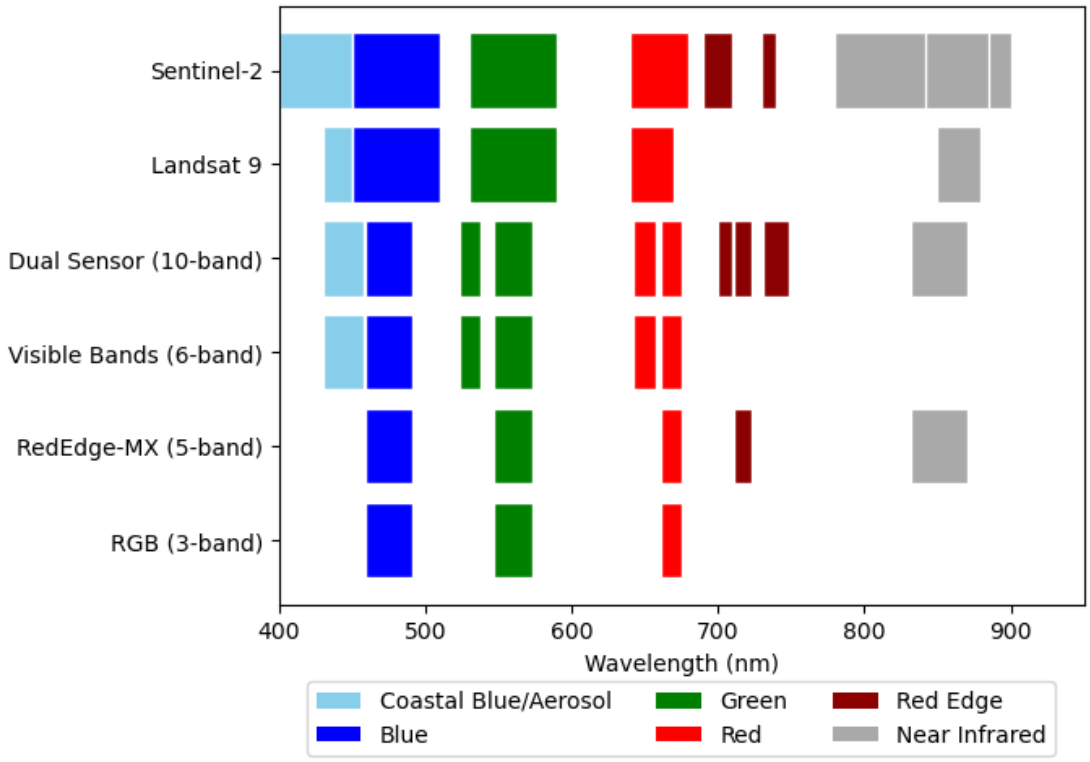

Figure 2. Band placements and widths for the Micasense RedEdge-MX 10 band sensor (MX-10) compared with the Sentinel-2 and Landsat 9 satellite sensors. The three alternative sensors used in this study are also shown.

The camera system was mounted on a DJI Matrice 200 quadcopter UAV (DJI, Nanshan, China) with a standard Micasense RedEdge-MX Dual Camera System mount kit (Figure 3). A downwelling light sensor was connected to the camera system and was used to measure lighting conditions at the time of capture to support radiometric calibration. The GPS contained within the camera system recorded the location of the UAV at each image capture with 3 m accuracy.

Figure 3. The DJI Matrice 200 UAV used in this study. The Micasense RedEdge MX Dual camera system and the downwelling light sensor are labelled. Photo by Jamie Simpson.

4.2.3 Image capture and processing

The UAV was controlled using Measure Ground Control version 4.1.2 (AgEagle Aerial Systems Inc., Wichita, USA) in a planned "lawnmower" pattern with a 100 m flying height to achieve a spatial resolution of ~8 cm. On-board camera software triggered image captures based on distance travelled to achieve 75% overlap and sidelap as is considered ideal for wetland monitoring (Davis et al., 2022). The same flight plan was used to recapture images of the study sites at an interval of 101 days (Table 2). All flights took place during below average tides with calm wind conditions (<10 km/h), clear-sky conditions, and at low sun elevation angles to reduce potential sun glint (Doukari et al., 2021).

Table 2. Metadata for the UAV captures used in this study.

Study Site	Image dates	Start time	End Time	Tide above lowest astronomical tide (m)	Sun elevation (°)	Flight area (ha)	Spatial resolution (cm)
Empire Bay	28/2/23	4:44pm	5:01pm	0.54	34	16.0	8.2
	9/6/23	12:03pm	12:19pm	0.50	34		8.0
St Huberts Island	28/2/23	3:19pm	3:42pm	0.46	50	25.3	7.9
	9/6/23	10:36am	11:14am	0.29	28		7.2

The images were converted to reflectance values using images of the MicaSense Calibrated Reflectance Panel captured immediately before and after each flight, as well as data captured by the downwelling light sensor during each flight. Images were processed into multispectral orthomosaics using Metashape Professional version 2.0.2 (Agisoft LLC, St Petersburg, Russia). The first image captured for each study site was used as the reference image to georeference the second corresponding image capture. Stationary features such as large rocks, poles, and oyster farming infrastructure were used to coregister the images. As this study focused on testing a change detection method, the results were not intended to be used in conjunction with other spatial data so georeferencing to accurate real-world coordinates using real-time kinematic positioning or similar methods. Additionally, as the images vary in spatial resolution, each georeferenced set of images was spatially resampled using nearest neighbour resampling to match the coarsest resolution image for that study site (8.2 cm for Empire Bay and 7.9 cm for St Huberts Island).

4.2.4 Background on IR-MAD

The goal of IR-MAD is to transform a pair of bi-temporal, multispectral images of the same scene into a set of change images with reduced dimensionality, that is, representing change in fewer bands than the original images (Nielsen et al., 1998, Canty and Nielsen, 2006). IR-MAD analysis first involves performing Canonical Correlation Analysis (CCA) (Hotelling, 1936) on a pair of geographically co-registered N-band multispectral images F and G. This identifies two vectors $\mathbf{a}_1$ and $\mathbf{b}_1$ which maximise the positive correlation between $a_1^T F$ and $b_1^T G$, referred to as the first canonical covariate pair U_1 and V_1. Vectors a_2 and b_2 are then identified which maximise the correlation

between $a_2^T F$ and $b_2^T G$, with the additional constraint that the canonical variate pair U_2 and V_2 are uncorrelated with U_1 and V_1 respectively. The end result for an N band image pair will be N canonical variate pairs U_1, V_1 to U_N, V_N.

The canonical variate pairs are then used to produce N difference bands $D_i = U_i - V_i$, referred to as the MAD variates. The MAD variate pixel values are expected to be normally or near-normally distributed, and pixels with more positive or negative values represent greater change. As the canonical variate pairs were ordered by decreasing correlation, the MAD variates will be ordered from least to most change information, referred to as lowest to highest order. Given the canonical variate pairs were uncorrelated with each other, each MAD variate is expected to contain different types of change.

The sum of the MAD variates is chi-squared distributed, and no-change pixels are identified using a pre-determined threshold of the probability density function of this distribution. The MAD process is then repeated with no-change pixels receiving a higher weight during the CCA. This iteration is performed until the correlation between the first canonical variate pair is maximised. The iterative reweighting of no-change pixels results in an improved transformation which better represents change in the final MAD variates (Nielsen, 2007). The three MAD variates containing the most change information can then be displayed in false colour to visualise change that incorporates information from all the original bands but with reduced dimensionality (Canty and Nielsen, 2006).

An important quality of the IR-MAD method for unsupervised change detection is that IR-MAD is insensitive to linear scaling effects between the original image pairs (such as due to differences in atmosphere, illumination, calibration, and sensor response) because the CCA finds linear combinations of the original spectral bands (Canty, 2014).

4.2.5 Application of IR-MAD to the alternative sensors

To assess the relative importance of sensor selection, and the importance of additional spectral bands for detecting change to seagrass, four alternative sensor configurations (Table 1 and Figure 2) were compared in the IR-MAD analysis below. These were the dual MX-10 sensor, the single MX-5 sensor, as well two virtual sensors constructed from

band subsets captured by Micasense sensors. The first virtual sensor represented a conventional RGB camera, and images were constructed from the standard red, green, and blue bands captured by the MX-5 sensor. The second virtual sensor represented a theoretical sensor with additional visible bands to a conventional 3-band RGB sensor. Images for this sensor were constructed from the six shortest-wavelength visible light bands from the MX-10 sensor (referred to as the VIS-6 sensor). The red-edge and near-infrared bands from the MX-10 sensor were not included in the VIS-6 sensor because they are known to have poor water penetration (Kirk, 1994).

The IR-MAD method was applied to the bi-temporal image pair captured by the MX-10 sensor for each study site using the *CRCPython* library (Canty, 2014). The IR-MAD method was then then repeated for the corresponding image pairs for the MX-5, RGB, and VIS-6 sensors for each study site. The result was four IR-MAD outputs for each study site.

4.2.6 Qualitative Identification of Change Categories

To examine the effectiveness of IR-MAD for detecting fine-scale changes to seagrass, the output MAD variates for the MX-10 sensor for each study site were visually assessed to identify and categorise different types of change. MAD variates were first viewed individually to identify the number of variates that contain spatially coherent change features. Notable change signals were then identified and inspected in the original bi-temporal image pairs to qualitatively determine the type of seagrass change.

Six different categories of change were visually identified (Table 3), and their boundaries were manually digitised using the Region of Interest (ROI) Tool in ENVI version 5.6 (NV5 Geospatial Solutions, Broomfield, United States). Separate ROIs were also created for two types of unchanged areas with seagrass present in both images: one without any change signal in the IR-MAD data (Unchanged 1) and one with a false positive change signal (Unchanged 2).

Table 3. Identified change categories and descriptions of change signals identified in IR-MAD outputs, and whether the signal is a false positive indication of change.

Change category	Description of change	Actual change?
Propeller scar	Seagrass changed to bare ground in long, linear features, caused by damage from boat propellers	Yes
Damaged patch	Seagrass changed to bare ground in larger patches, caused by damage from sources other than propellers, such as boat groundings or seagrass die-off	Yes
Regrowth	Bare ground changed to seagrass, possibly caused by seagrass regrowth	Yes
Added oyster cage	Oyster infrastructure added over seagrass bed	Yes
Removed oyster cage	Oyster infrastructure removed from seagrass bed	Yes
Bright sand false positive	Apparent change signals recorded over unchanged sand patches	No
Unchanged 1	Unchanged seagrass or bare ground, submerged in both images	No
Unchanged 2	Unchanged seagrass or bare ground, submerged in one image and above water in the other	No

4.2.7 Comparing effectiveness of disturbance detection between the alternative sensors

In order to quantitatively assess the ability to distinguish the different types of identified change types in the IR-MAD outputs for each of the alternative sensors, the spectral separability between the different change categories was quantitively determined using the Jeffreys-Matusita (JM) distance (Wacker and Landgrebe, 1972). The JM distance is a measure of separability between two sets of probability distributions, commonly used in remote sensing to determine spectral separability of class endmembers to support supervised classifications. The JM distance J between two distributions x and y is defined as (Richards and Richards, 2022):

$$J_{xy} = 2(1 - e^{-B}) \tag{1}$$

Where:

$$B = \frac{1}{8}\left(\mu_x - \mu_y\right)^T \left(\frac{\sum_x + \sum_y}{2}\right)^{-1} \left(\mu_x - \mu_y\right) + \frac{1}{2}\ln\left(\frac{\left|\frac{\sum_x + \sum_y}{2}\right|}{|\sum_x|^{\frac{1}{2}}|\sum_y|^{\frac{1}{2}}}\right) \tag{2}$$

Where μ_x and μ_y are the mean vectors of x and y, and $\sum_x$ and $\sum_y$ are the covariance matrices of x and y.

JM distance values can range from 0 (no separability) to 2 (perfect separability). JM distances can therefore be compared between class pairs in remote sensing images as a measure of statistical separability of different features. For IR-MAD variates, JM distance values can similarly be used as a measure of relative statistical separability of different features (in this case change features) in the image.

The JM distance was used to determine whether the ROIs captured for areas representing actual change were separable from ROIs where no-change occurred, and if ROIs representing different change categories could be distinguished from each other. The JM distance was calculated for each pairwise combination of the eight change ROIs for the MX-10 sensor. This was then repeated for the other three sensors (MX-5, RGB, and VIS-6) to compare the relative strength of detecting change between the four sensors.

4.2.8 Assessing Individual Band Influence on Change Detection using IR-MAD

One of the non-image outputs from the IR-MAD analysis is the set of eigenvector pairs ($a_{1..N}$ and $b_{1..N}$)**.** The eigenvectors contain the final weights applied to the original spectral bands used to produce the canonical variate pairs and the derived MAD variates. The eigenvectors were therefore used to explore which spectral bands in the original bi-temporal image pair had the most influence on the generation of the MAD variate bands. This provides further information to support sensor selection by indicating which bands are most important for change detection.

Vectors a_i and b_i are of length equal to the number of input bands to the IR-MAD process. Therefore, for the bi-temporal image pair captured by the MX-10 sensor at St Huberts Island, the 1st elements of the eigenvectors a_1 and b_1 represents the weights applied to the pair of coastal blue bands used (in part) to produce the first canonical variate pair (CV_1 and CV_2) and subsequent MAD variate. Relatively higher weights in vectors a_i or b_i indicate a greater degree of influence by the corresponding band on the resulting canonical variate pair, and corresponding MAD variate.

The vector weights produced by the IR-MAD method for different image pairs are not directly comparable. To compare the influence of individual bands across different IR-MAD analysis the eigenvector elements were transformed based on their relative contribution to the CCA transformation, and the number of bands present in the image pair. Elements from each eigenvector were selected corresponding to the MAD variates in which spatially coherent change features were present. The absolute values of these elements were averaged and normalised to determine the relative contribution of each band, and each weight scaled to the full number of bands in the original bi-temporal image pair:

$$W_n = n_{max} \times \frac{1}{N} \sum_{i=1}^{N} \frac{|a_i(n)| + |b_i(n)|}{2} \quad (3)$$

Where $a_i(n)$ and $b_i(n)$ are the pair of eigenvector elements for band n, N is the number of IR-MAD bands which contain spatially coherent elements, W_n is the scaled transformed weight for the spectral band n corresponding with the eigenvector element n, and n_{max} is the number of bands in each image in the bi-temporal image pair.

The higher the scaled transformed weights for a band in the eigenvector corresponding with a MAD variate, the more those bands influenced the derivation of that MAD variate.

The normalised and scaled eigenvector weights (W_n) was used to compare the relative contribution of each spectral band for detecting changing using IR-MAD from images captured by the four alternative sensors used in this study.

4.3 Results

4.3.1 IR-MAD analysis for the alternative sensors

For each study site, four sets of MAD variates were produced for the four alternative sensors. Spatially coherent change was visually present in the higher-order MAD variates, while the lower-order variates consisted primarily of noise (Figure 4). Spatially coherent change features were visible in the five highest order variates (6 to 10) derived from the MX-10 sensors, three variates (4 to 6) derived from the VIS-6 sensor, and for all the variates derived from both the MX-5 and RGB sensors.

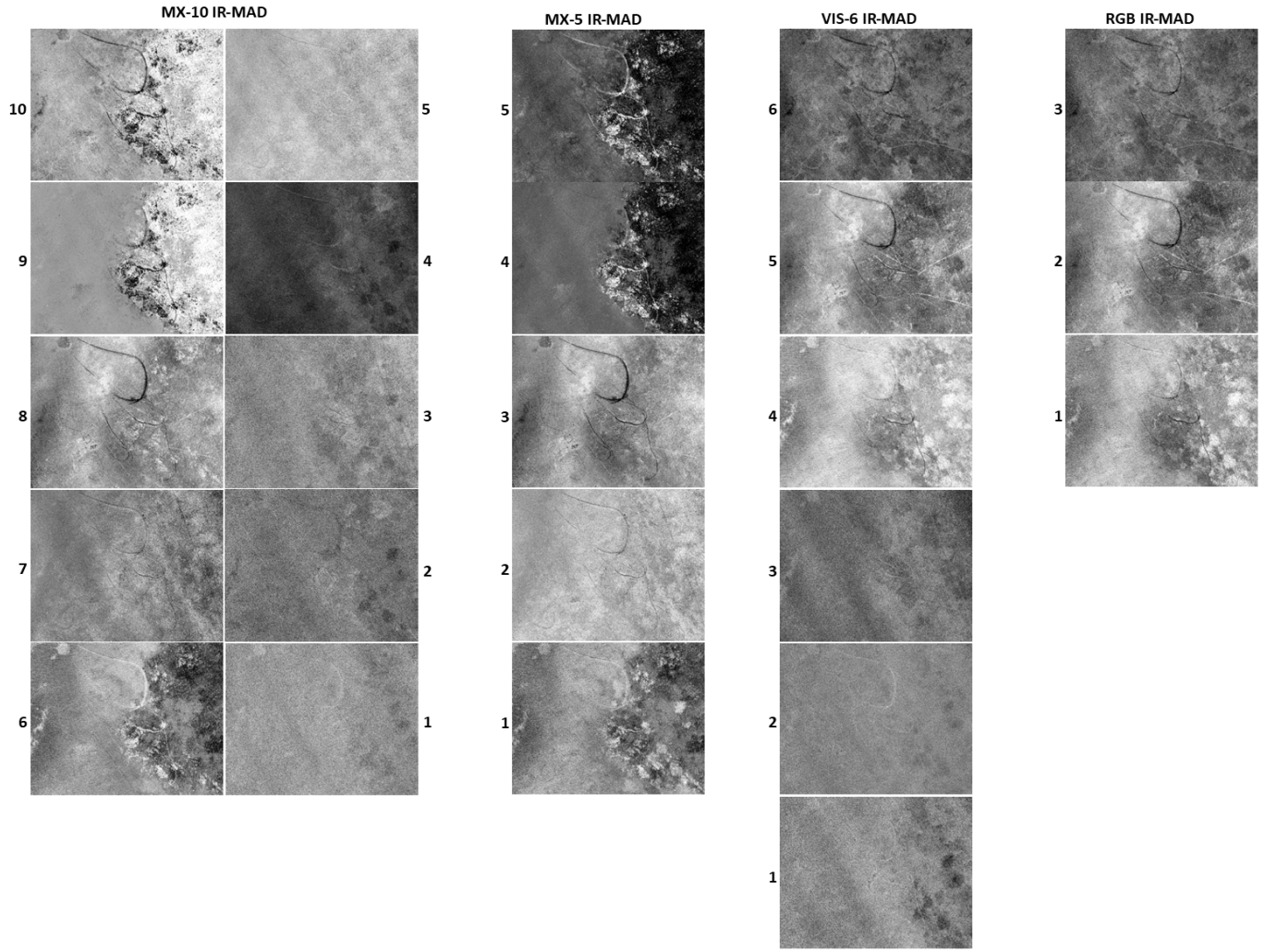

Figure 4. MAD variates for each of the four sensors for a subset of the St Huberts Island study site. Each MAD variate is visualised with a 5% linear greyscale stretch. MAD variates are numbered from 1 representing the lowest order.

4.3.2 Qualitative identification of change categories

Spatially coherent changes were visible in the false colour IR-MAD output images for the MX-10 Sensor (annotated in Figure 5). These changes are visualised with two different sets of variates: the highest order MAD variates in the left column (variates 10, 9, and 8) and variates manually selected to highlight disturbances in the right column (variates 10, 8, and 6 for St Huberts Island; variates 9, 8, and 7 for Empire Bay). These change categories included boat propeller scars, a large area of disturbance, seagrass patches which decreased in density without clear evidence of direct disturbance, apparent regrowth of seagrass, and false positive change signals.

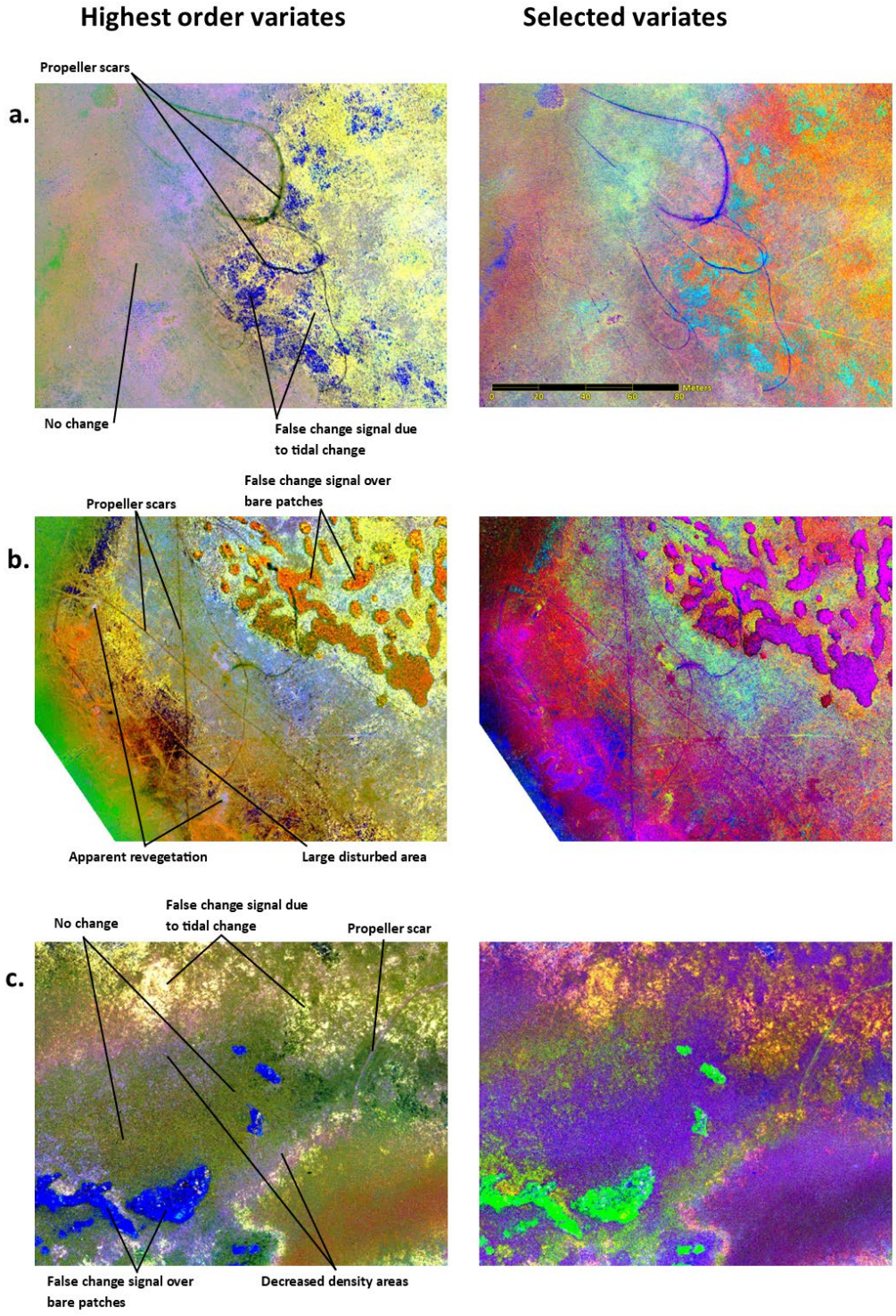

Figure 5. Examples of identified change categories overlayed on false colour change images. Change images were derived using the higher-order MAD variates 10, 9, and 8 (left column), variates 10, 8, and 6 (right column, image a. and b.), and variates 9, 8, and 7 (right column, image c.). Change categories include: a. propeller scars at St Huberts Island, b. a large disturbed area at St Huberts Island , and c. areas of decreased seagrass density at Empire Bay. All variates were derived from bi-temporal images captured by the MX-10 sensor.

Linear propeller scars and non-linear disturbed patches, likely anthropogenic, are visible across the St Huberts Island study site. At the Empire Bay study site, fewer disturbances are visible, including a single propeller scar and decrease in cover density at the edge of the seagrass bed. Existing propeller scars present in both images result in IR-MAD values indicating no change.

New propeller scars and a larger disturbed area are clearly visible in all three locations shown in Figure 5. In the false colour images of St Huberts Island, these features appear black-green when visualised with the highest-order variates (left column) and blue when visualised with selected variates (right column) (Figure 5a. and b.). In the images from Empire Bay, propeller scars are light purple and green in the false colour images created using highest-order variates and selected variates respectively (Figure 5c.). Other parts of Figure 5c. show general decreases in seagrass density across patches, which show a distinct spatial pattern to the boat damage in the St Huberts Island locations. These decreases in seagrass density may be related to disturbance, or to seasonal variation in seagrass density.

Apparent regrowth of seagrass was also identified in the St Huberts Island study site (Figure 6). These areas appear as bare ground in the February image and vegetation in the June image. This pattern may indicate (1) seagrass regrowth over previously bare sediment or propeller scars; (2) seagrass leaves changing in position due to water flow, or (3) spatial inaccuracies in image registration or orthorectification.

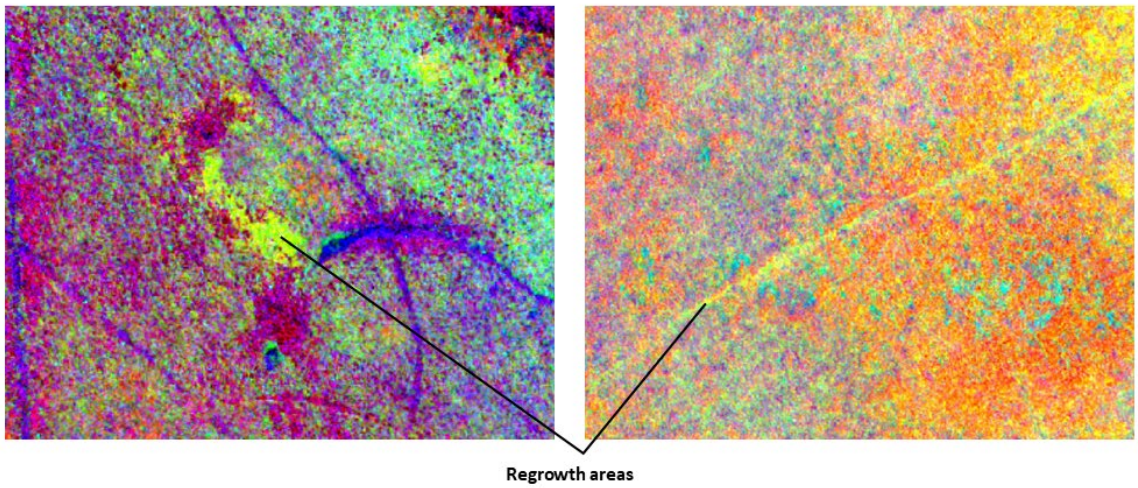

Figure 6. Apparent seagrass regrowth annotated on spatial subsets of false colour images of the IR-MAD outputs (variates 10, 8, and 6) for St Huberts Island (derived from the MX-10 sensor).

The other change categories identified in the qualitative analysis of the St Huberts Island study site included changes related to oyster farms. The oyster farms consist of cages or trays that can be attached to lines as needed and are frequently moved depending on changes to water conditions. These operational practices were identified in the IR-MAD outputs for both study sites (Figure 7).

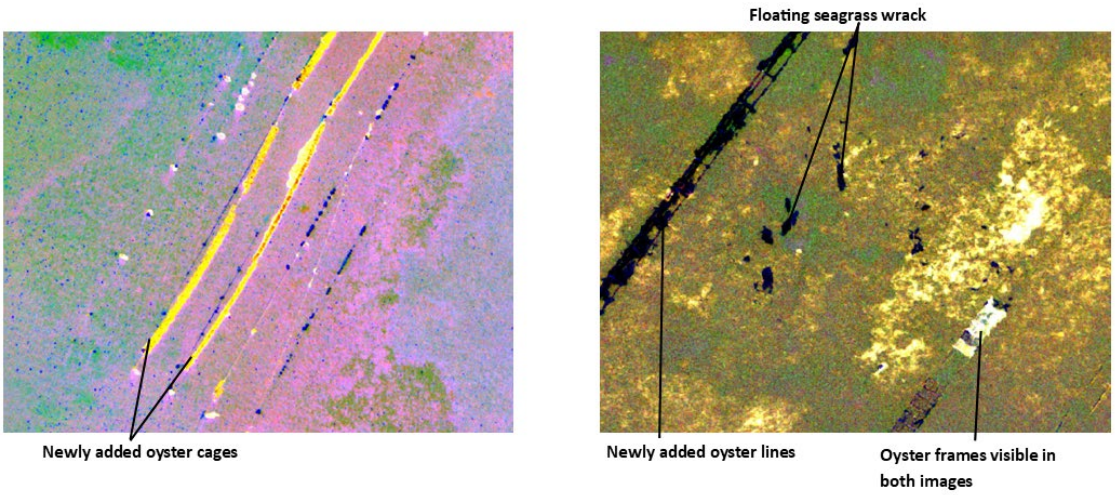

Figure 7. Oyster aquaculture infrastructure changes identified in the IR-MAD outputs for St Huberts Island (left) and Empire Bay (right). Both images were visualised using MAD variates 10, 9, and 8 derived from the bi-temporal image pairs captured by the MX-10 sensor.

4.3.3 Comparing effectiveness of disturbance detection between the alternative sensors

The JM distance values for each class pair are a relative measure of statistical separability, indicating how effectively the change category can be distinguished from others. The JM distance values were calculated across all change category pairs for all four alternative sensors (Table 4). For ease of comparison between sensors in the text, the JM distance results were arbitrarily grouped into three classes – Strong (JM distance >= 1.8), Moderate (1.8 > JM distance >= 1.4), and Weak (1.4 > JM distance) (Table 5).

Table 4. JM distance values between the eight identified change categories for the (a) MX-10 sensor (b) MX-5 sensor, (c) VIS-6 sensor, and (d) RGB sensor. Table cells colour coded from weakest separability (red) to strongest (dark green).

(a)	**Propeller scars**	**Damaged patches**	**Apparent regrowth**	**New oyster infrastructure**	**Removed oyster infrastructure**	**Bright sand false positive**	**Unchanged above water**	**Unchanged below water**
Propeller scars								
Damaged patches	1.40							
Apparent regrowth	1.79	1.99						
New oyster infrastructure	2.00	2.00	1.99					
Removed oyster infrastructure	1.98	2.00	1.99	2.00				
Bright sand false positive	1.69	1.76	1.96	2.00	1.99			
Unchanged above water	1.94	2.00	1.77	1.99	1.99	2.00		
Unchanged below water	1.90	2.00	1.71	2.00	2.00	2.00	1.75	

(b)								
Propeller scars								
Damaged patches	1.30							
Apparent regrowth	1.74	1.98						
New oyster infrastructure	1.98	1.99	1.94					
Removed oyster infrastructure	1.73	1.92	1.79	1.73				
Bright sand false positive	1.43	1.48	1.94	1.97	1.82			
Unchanged above water	1.90	2.00	1.64	1.91	1.92	2.00		
Unchanged below water	1.82	1.99	1.49	1.99	1.96	1.99	1.62	

(c)								
Propeller scars								
Damaged patches	1.21							
Apparent regrowth	1.72	1.95						
New oyster infrastructure	1.79	1.88	1.68					
Removed oyster infrastructure	1.55	1.91	1.40	1.78				
Bright sand false positive	1.57	1.80	1.56	1.19	1.75			
Unchanged above water	1.68	1.97	1.86	1.98	1.81	1.93		
Unchanged below water	1.54	1.96	1.76	1.98	1.76	1.89	0.78	
(d)								
Propeller scars								
Damaged patches	1.13							
Apparent regrowth	1.53	1.93						
New oyster infrastructure	1.55	1.66	1.45					
Removed oyster infrastructure	1.47	1.86	1.10	1.64				
Bright sand false positive	1.20	1.59	1.37	0.46	1.58			
Unchanged above water	1.47	1.95	1.64	1.88	1.67	1.76		
Unchanged below water	1.39	1.96	1.46	1.85	1.61	1.71	0.51	

Table 5. Number of change category pairs with strong (JM distance > 1.8), moderate (1.8 >= JM distance > 1.4), and weak (1.4 >= JM distance) separability for each alternative sensor. Based on JM distance calculated from each alternative sensor's IR-MAD results.

Sensor	Strong	Moderate	Weak
MX-10	21	6	1
MX-5	18	6	4
VIS-6	12	12	4
RGB	6	11	11

The IR-MAD outputs for the MX-10 sensor had the highest JM distance values (Table 4a), with 21 change category pairs showing strong separability (Table 5). Propeller scars and damaged patches had relatively low separability from each other (JM distance 1.40) but moderate to strong separability from all other classes. Apparent regrowth and changes to oyster infrastructure also showed moderate to strong separability from all other classes.

A total of 18 change category pairs had strong separability for the IR-MAD variates derived from the MX-5 sensor (Table 5). Like the MX-10 data, the lowest separability was between the propeller scars and damaged patches (Table 4b). These disturbances

were only moderately separable from the bright sand false positive class in this dataset but were relatively more separable from the others.

JM distances for the VIS-6 sensor (Table 4c) showed 12 strongly separable class pairs (Table 5). Disturbed patches and propeller scars had strong (JM distance >=1.80) and moderate (JM distance >=1.54) separability respectively from all classes except each other (JM distance 1.21). Apparent regrowth showed moderate to strong separability from all other classes except removed oyster infrastructure.

The JM distance results derived from the RGB sensor showed the weakest separability values compared with other sensors. Larger disturbed patches displayed strong or moderate separability from all classes except propeller scars. However, propeller scars showed weak separability (JM distance <1.5) from most other classes, including bright sand false positives and both unchanged classes. Apparent regrowth was separable from both disturbed classes, but showed weaker separability from changes to oyster infrastructure, and the below water unchanged class.

Separability between the two unchanged classes was lower for the two virtual (VIS-6 and RGB) sensors which did not have the red-edge and near-infrared. Submerged unchanged areas and emerged unchanged areas appear more similar in the VIS-6 and RGB sensor IR-MAD outputs data compared to the MX-10 and MX-5 IR-MAD outputs (Figure 8).

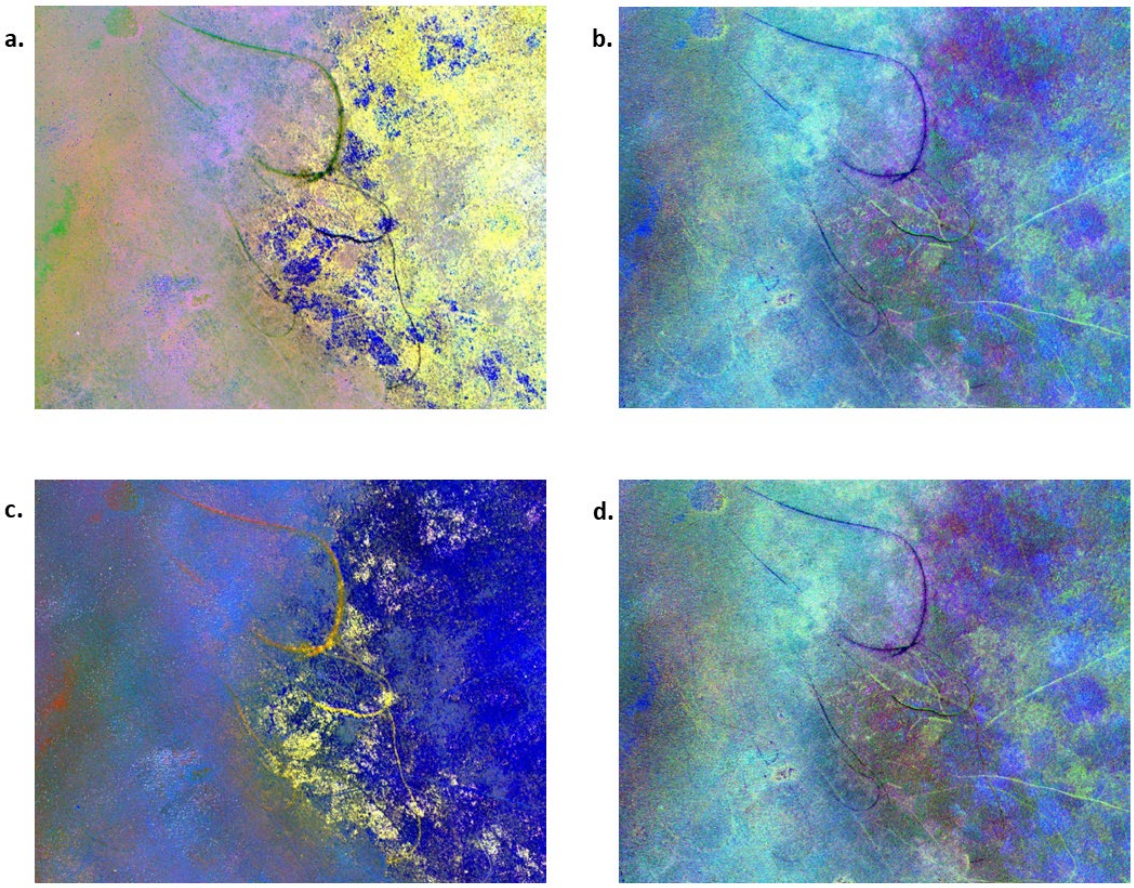

Figure 8. Propeller scars were visibly present at the St Huberts Island in the (a) MX-10 sensor IR-MAD outputs visualised with variates 10, 9, and 8, (b) VIS-6 sensor IR-MAD output visualised with variates 6, 5, and 4, (c) MX-5 sensor IR-MAD output visualised with variates 5, 4, and 3, and (d) the RGB sensor IR-MAD output visualised with variates 3, 2, and 1.

The transformed eigenvector weights were used to assess the contribution of each band to the IR-MAD calculations across both study sites for all four alternative sensors (Table 6).

Table 6. Transformed weights for each eigenvector element, indicating the influence of each corresponding spectral band on MAD outputs.

Band	St Huberts 10-band	Empire Bay 10-band	St Huberts 6-band	Empire Bay 6-band	St Huberts 5-band	Empire Bay 5-band	St Huberts 3-band	Empire Bay 3-band
Coastal Blue	1.24	1.22	1.37	1.1				
Blue	0.73	0.68	0.85	0.73	0.92	1.12	1.16	1.03
Green 1	0.78	0.85	0.69	0.65				
Green 2	1.14	1.28	1.01	0.91	1.04	0.98	0.88	0.94
Red 1	1.29	0.66	0.87	1.02				
Red 2	1.05	1.2	1.2	1.59	1.49	1.15	0.97	1.03
RE 1	0.78	0.97						
RE 2	0.7	0.94			0.80	0.86		
RE 3	1.06	0.86						
NIR	1.23	1.34			0.75	0.90		

Across the data from the MX-10, VIS-6, and MX-5 sensors, the Green 2 and Red 2 bands had a consistently high influence, while the Blue band was consistently less influential on the IR-MAD results. For the RGB sensor data, the blue band had the highest influence. The NIR band in the MX-10 sensor data also had a relatively large statistical influence on the change signals produced by this sensor. The five MX-10 sensor bands that were not available in the MX-5 sensor data had differing influences on change detection results. The Green 1 band had a relatively small influence, the Red 1 band had a variable influence depending on the image pair, and the Coastal Blue band had a consistently high influence.

4.4 Discussion

The IR-MAD method applied to images captured by a UAV was shown to be viable for detecting fine-scale physical disturbances to seagrass beds using the 10-band, 5-band, and 6-band data, and potentially effective for 3-band data. Large areas of disturbed seagrass were visibly identified in IR-MAD results from all sensors and were strongly separable from all other change categories in the 10-band and 5-band data, and from

most other change categories in the 6-band and 3-band data. Propeller scars were visible in all IR-MAD outputs, and JM distance results showed moderate to strong separability for propeller scars in the 10- and 5-band data, moderate separability in the 6-band data, and weak to moderate separability in the 3-band data. This study demonstrates the potential of IR-MAD analysis to support seagrass monitoring and management at relevant finer spatio-temporal resolution, especially when multispectral sensors like the Micasense RedEdge-MX Dual sensor are used.

Substantial changes in seagrass cover were identified at both study sites, but they were noticeably different in the IR-MAD results. At St Huberts Island, many propeller scars and other instances of boat damage were identified, clustered towards the western edge of the meadow and near oyster aquaculture infrastructure, where boat traffic is likely to be highest. At Empire Bay, however, the patterns of change were more spatially consistent potentially indicating seasonal trends or environmental conditions such as water quality.

The full set of 10 bands provided by the MX-10 sensor demonstrated advantages for seagrass change detection. The IR-MAD method using images from the MX-10 sensor detected change features more effectively than the other three sensors, with strongly separable JM distance measurements recorded for all eight change categories tested. Outputs from the theoretical VIS-6 sensor also offered improved change detection over the RGB sensor. Two of the additional visible bands included in IR-MAD analysis for the MX-10 and VIS-6 sensors (Coastal Blue and Red 1), had a relatively high weighting, indicating a strong influence on change detection. This suggests that their addition enhances change detection compared to the MX-5 sensor.

The improvement offered by these additional bands is consistent with past research using satellite-borne sensors for characterising seagrass in coastal ecosystems. For example, the Sentinel-2 coastal blue band was shown to improve seagrass classification (Poursanidis et al., 2019), and analysis of hyperspectral images has shown that the green-red visible range is optimal for predicting seagrass percent cover and related variables (Phinn et al., 2008, Pu et al., 2012, Valle et al., 2015). Multispectral sensors with additional visible light bands compared with a standard RGB sensors has been demonstrated here and elsewhere (Dierssen et al., 2019) to provide improved ability to

characterise seagrass ecosystems without necessitating the use of expensive hyperspectral sensors.

Though the full 10 band MX-10 sensor was the most effective in discriminating change classes, the change class separability results suggest that cheaper and simpler sensors may be sufficient for efficient monitoring of seagrass using IR-MAD. The Micasense RedEdge MX sensor (MX-5) is a commonly available sensor which can be integrated on consumer UAVs at relatively low cost. For visual analysis of IR-MAD outputs, the 5-band images provided by this sensor has been demonstrated here as sufficient for focused management responses to seagrass disturbance.

The red-edge and near-infrared bands can improve accuracy results in seagrass mapping when leaves are on or near the surface of the water due to the absorption of red and scattering of near-infrared light by photosynthetic vegetation (James et al., 2020). However, the high absorbance of red-edge and near-infrared light by water can reduce the effectiveness of bands in these regions when seagrass is fully submerged. The IR-MAD analyses in this study which included red-edge and near-infrared bands detected differences in water level between image captures as a distinct category of change which is separable from disturbance events, and this was reflected in the high level of influence that the NIR band had on the MX-10 change result. However, IR-MAD outputs produced without the red-edge and near-infrared bands are easier to interpret visually as the extensive change signals caused by tidal differences are less apparent, highlighting the change signals representing actual seagrass disturbance. This suggests that excluding the red-edge and near-infrared bands before any IR-MAD analysis may improve results and interpretation if there are significant tidal differences between the bi-temporal image pair.

Spatially coherent patterns by seagrass disturbances were visible in the IR-MAD outputs for the simple 3-band RGB sensor, even though the disturbances were only weakly to moderately separable from other categories. This may provide a more accessible remote sensing option by using consumer-grade UAVs with inbuilt RGB cameras to capture and analyse bi-temporal image pairs for seagrass disturbance. Orthorectified RGB images have been used to map seagrass beds, even radiometrically uncalibrated data (Riniatsih et al., 2021, Hamad et al., 2022, Tahara et al., 2022). However, the poorer separability

values for the RGB data compared to the 6-band VIS-6 sensor demonstrated here highlight the trade-off between achieving improved change detection results using IR-MAD and relative sensor cost and accessibility.

Physical disturbances, especially root-rhizome damage, can lead to further degradation through positive feedback mechanisms as the sediment is destabilised increasing bed exposure to erosion from waves and currents (Larkum, 1976, West, 2012, Swadling et al., 2023). This may lead to the release of stored soil carbon and negative impacts on future carbon sequestration (Bourque et al., 2015, Macreadie et al., 2015). Additionally, physical disturbances to seagrass beds can impact the composition and condition of faunal communities (Reed and Hovel, 2006, Bell et al., 2008, Iacarella et al., 2018). Management interventions, including educating fishers and boaters to reduce propeller damage, restricting activities under certain tidal conditions, or restoring seagrass beds damaged by watercraft can lead to measurable improvements in seagrass condition (Orth et al., 2017, Orth et al., 2010, Rezek et al., 2019). Timely detection of fine-scale physical disturbances such as propeller scars, which are otherwise difficult to detect, is needed to support the implementation of these intervention strategies. Applying IR-MAD to UAV images provides a relatively simple unsupervised method for identifying disturbance.

Effective long-term monitoring is important for the success of seagrass restoration projects (Cunha et al., 2012, Tan et al., 2020) and monitoring cost effectiveness is particularly crucial for projects limited by financial constraints (Macreadie et al., 2022). The effectiveness of blue carbon restoration projects for generating high-quality and verifiable carbon offsetting services requires robust approaches for identifying and tracking change in biomass extent at ecologically relevant spatio-temporal scales. Although IR-MAD cannot provide quantitative measurements of seagrass blue carbon stocks, in detecting fine scale change from baseline conditions, results can complement existing measurement approaches for project reporting.

Change detection using IR-MAD could be further enhanced by adding pre- or post-processing steps. Water column correction, applied to the UAV images, may assist in reducing change signals caused by differences in tidal level between images. Additionally, changes detected in IR-MAD outputs could be automatically extracted

using object-based image analysis methods, image thresholding, or machine learning methods. IR-MAD outputs by themselves, however, offer a valuable resource for coastal managers and scientists due to the unsupervised nature of the process, and the need for no data inputs beyond two coregistered UAV images.

Wider application of IR-MAD for seagrass change detection requires further testing over multi-species seagrass beds and different water optical properties. The study findings are restricted to two temperate water study sites covering predominantly monospecific seagrass beds. Additionally, the band configurations (including band centres and widths) of the two virtual sensors used in this study (VIS-6 and RGB) may not correspond with actual, commercially available sensors. Testing the IR-MAD method using images captured from alternative, commercially available sensors such as a simple RGB sensor commonly integrated on many UAV platforms, may provide further insights into sensor selection considerations for coastal managers.

4.5 Conclusions

Seagrasses perform a range of vital ecosystem functions including sediment stabilisation, carbon sequestration, habitat provision and water purification (Nordlund et al., 2016). There is a need for seagrass monitoring techniques that detect disturbances which interfere with these functions. The application of IR-MAD to co-registered, bi-temporal UAV-acquired images offers a relatively cost-effective, unsupervised method of detecting very fine-scale changes to seagrass beds, at the on-demand temporal resolution UAV imaging provides. IR-MAD applied to UAV-acquired multispectral images can be used to distinguish and map multiple forms of change in seagrass beds, including propeller scars, regrowth, and oyster farming. In detecting key fine-scale change features, this method can inform management interventions designed to prevent seagrass degradation, guide restoration efforts, and contribute to blue carbon accounting. Change detection using IR-MAD is unsupervised, can be implemented in open-source software, with consumer-grade computing power, using images from standard off-the-shelf UAV multispectral sensors.

References

2022. NSW Priority Oyster Aquaculture Areas. NSW Department of Primary Industries.

AOKI, L. R., YANG, B., GRAHAM, O. J., GOMES, C., RAPPAZZO, B., HAWTHORNE, T. L., DUFFY, J. E. & HARVELL, D. 2023. UAV high-resolution imaging and disease surveys combine to quantify climate-related decline in seagrass meadows. *Oceanography,* 36**,** 38.

BARRY, S. C., RASKIN, K. N., HAZELL, J. E., MORERA, M. C. & MONAGHAN, P. F. 2020. Evaluation of interventions focused on reducing propeller scarring by recreational boaters in Florida, USA. *Ocean & Coastal Management,* 186**,** 105089.

BEHESHTI, K. M., WILLIAMS, S. L., BOYER, K. E., ENDRIS, C., CLEMONS, A., GRIMES, T., WASSON, K. & HUGHES, B. B. 2022. Rapid enhancement of multiple ecosystem services following the restoration of a coastal foundation species. *Ecological Applications,* 32.

BELL, S. S., FONSECA, M. S. & KENWORTHY, W. J. 2008. Dynamics of a subtropical seagrass landscape: links between disturbance and mobile seed banks. *Landscape Ecology,* 23**,** 67-74.

BOURQUE, A. S., KENWORTHY, W. J. & FOURQUREAN, J. W. 2015. Impacts of physical disturbance on ecosystem structure in subtropical seagrass meadows. *Marine Ecology Progress Series,* 540**,** 27-41.

BRONDIZIO, E. S., SETTELE, J., DIAZ, S. & NGO, H. T. 2019. Global assessment report on biodiversity and ecosystem services of the Intergovernmental Science-Policy Platform on Biodiversity and Ecosystem Services.

CANTY, M. J. 2014. *Image Analysis, Classification and Change Detection in Remote Sensing, with Algorithms for ENVI/IDL and Python*, Taylor and Francis CRC Press.

CANTY, M. J. & NIELSEN, A. A. 2006. Visualization and unsupervised classification of changes in multispectral satellite imagery. *International Journal of Remote Sensing,* 27**,** 3961-3975.

CHEN, J. & SASAKI, J. 2021. Mapping of subtidal and intertidal seagrass meadows via application of the feature pyramid network to unmanned aerial vehicle orthophotos. *Remote Sensing,* 13**,** 4880.

COFFER, M. M., GRAYBILL, D. D., WHITMAN, P. J., SCHAEFFER, B. A., SALLS, W. B., ZIMMERMAN, R. C., HILL, V., LEBRASSE, M. C., LI, J. & KEITH, D. J. 2023. Providing a framework for seagrass mapping in United States coastal ecosystems using high spatial resolution satellite imagery. *Journal of Environmental Management,* 337**,** 117669.

CUNHA, A. H., MARBÁ, N. N., VAN KATWIJK, M. M., PICKERELL, C., HENRIQUES, M., BERNARD, G., FERREIRA, M. A., GARCIA, S., GARMENDIA, J. M. & MANENT, P. 2012. Changing Paradigms in Seagrass Restoration. *Restoration Ecology,* 20**,** 427-430.

DAVIES, B. F. R., GERNEZ, P., GERAUD, A., OIRY, S., ROSA, P., ZOFFOLI, M. L. & BARILLÉ, L. 2023. Multi- and hyperspectral classification of soft-bottom intertidal vegetation using a spectral library for coastal biodiversity remote sensing. *Remote Sensing of Environment,* 290**,** 113554.

DAVIS, J., GIANNELLI, R., FALVO, C., PUCKETT, B., RIDGE, J. & SMITH, E. 2022. Best practices for incorporating UAS image collection into wetland monitoring efforts: a guide for entry level users.

DIERSSEN, H. M., BOSTROM, K. J., CHLUS, A., HAMMERSTROM, K., THOMPSON, D. R. & LEE, Z. 2019. Pushing the Limits of Seagrass Remote Sensing in the Turbid Waters of Elkhorn Slough, California. *Remote Sensing,* 11.

DOUKARI, M., KATSANEVAKIS, S., SOULAKELLIS, N. & TOPOUZELIS, K. 2021. The effect of environmental conditions on the quality of UAS orthophoto-maps in the coastal environment. *ISPRS international journal of geo-information,* 10**,** 18.

FLETCHER, R. S., PULICH JR, W. & HARDEGREE, B. 2009. A semiautomated approach for monitoring landscape changes in Texas seagrass beds from aerial photography. *Journal of Coastal Research,* 25**,** 500-506.

GRIFFITHS, L. L., CONNOLLY, R. M. & BROWN, C. J. 2020. Critical gaps in seagrass protection reveal the need to address multiple pressures and cumulative impacts. *Ocean & Coastal Management,* 183.

HAMAD, I. Y., STAEHR, P. A., RASMUSSEN, M. B. & SHEIKH, M. 2022. Drone-Based Characterization of Seagrass Habitats in the Tropical Waters of Zanzibar. *Remote Sensing* [Online], 14.

HOSSAIN, M. S. & HASHIM, M. 2019. Potential of Earth Observation (EO) technologies for seagrass ecosystem service assessments. *International Journal of Applied Earth Observation and Geoinformation,* 77**,** 15-29.

HOTELLING, H. 1936. Relations Between Two Sets of Variables. *Biometrika,* 28**,** 321-377.

IACARELLA, J. C., ADAMCZYK, E., BOWEN, D., CHALIFOUR, L., EGER, A., HEATH, W., HELMS, S., HESSING-LEWIS, M., HUNT, B. P. V., MACINNIS, A., O'CONNOR, M. I., ROBINSON, C. L. K., YAKIMISHYN, J. & BAUM, J. K. 2018. Anthropogenic disturbance homogenizes seagrass fish communities. *Global Change Biology,* 24**,** 1904-1918.

JAMES, D., COLLIN, A., HOUET, T., MURY, A., GLORIA, H. & LE POULAIN, N. 2020. Towards Better Mapping of Seagrass Meadows using UAV Multispectral and Topographic Data. *Journal of Coastal Research,* 95.

JELBART, J. E. & ROSS, P. M. 2006. Examination of the Seagrass and Associated Fauna in Gosford Local Government Area (GLGA) including Correa Bay and Patonga Creek. *Report for Gosford City Council.* Central Coast, New South Wales.

KARANG, I. A., PRAVITHA, N. L. P. R., NUARSA, I. W., K., K. B. A. & WICAKSONO, P. 2024. High-Resolution Seagrass Species Mapping and Propeller Scars Detection in Tanjung Benoa, Bali through UAV Imagery. *Journal of Ecological Engineering,* 25.

KAUFMAN, K. A. & BELL, S. S. 2022. The use of imagery and GIS techniques to evaluate and compare seagrass dynamics across multiple spatial and temporal scales. *Estuaries and Coasts,* 45**,** 1028-1044.

KILMINSTER, K., MCMAHON, K., WAYCOTT, M., KENDRICK, G. A., SCANES, P., MCKENZIE, L., O'BRIEN, K. R., LYONS, M., FERGUSON, A., MAXWELL, P., GLASBY, T. & UDY, J. 2015. Unravelling complexity in seagrass systems for management: Australia as a microcosm. *Sci Total Environ,* 534**,** 97-109.

KIRK, J. T. 1994. *Light and photosynthesis in aquatic ecosystems*, Cambridge university press.

KIRKMAN, H. 1996. Baseline and monitoring methods for seagrass meadows. *Journal of Environmental Management,* 47**,** 191-201.

KRAUSE, J. R., HINOJOSA-CORONA, A., GRAY, A. B. & BURKE WATSON, E. 2021. Emerging sensor platforms allow for seagrass extent mapping in a turbid estuary and from the meadow to ecosystem scale. *Remote Sensing,* 13**,** 3681.

LARKUM, A. W. D. 1976. Ecology of Botany Bay. I. Growth of Posidonia australis (Brown) Hook. f. in Botany Bay and other bays of the Sydney basin. *Marine and Freshwater Research,* 27**,** 117-127.

LIU, Y., SUN, Y., TAO, S., WANG, M., SHEN, Q. & HUANG, J. 2021. Discovering potential illegal construction within building roofs from UAV images using semantic segmentation and object-based change detection. *Photogrammetric engineering & Remote sensing,* 87**,** 263-271.

LIZCANO-SANDOVAL, L., ANASTASIOU, C., MONTES, E., RAULERSON, G., SHERWOOD, E. & MULLER-KARGER, F. E. 2022. Seagrass distribution, areal cover, and changes (1990–2021) in coastal waters off West-Central Florida, USA. *Estuarine, Coastal and Shelf Science,* 279**,** 108134.

LOVELOCK, C. E., ATWOOD, T., BALDOCK, J., DUARTE, C. M., HICKEY, S., LAVERY, P. S., MASQUE, P., MACREADIE, P. I., RICART, A. M. & SERRANO, O. 2017. Assessing the risk of carbon dioxide emissions from blue carbon ecosystems. *Frontiers in Ecology and the Environment,* 15**,** 257-265.

MACREADIE, P. I., ROBERTSON, A. I., SPINKS, B., ADAMS, M. P., ATCHISON, J. M., BELL-JAMES, J., BRYAN, B. A., CHU, L., FILBEE-DEXTER, K., DRAKE, L., DUARTE, C. M., FRIESS, D. A., GONZALEZ, F., GRAFTON, R. Q., HELMSTEDT, K. J., KAEBERNICK, M., KELLEWAY, J., KENDRICK, G. A., KENNEDY, H., LOVELOCK, C. E., MEGONIGAL, J. P., MAHER, D. T., PIDGEON, E., ROGERS, A. A., STURGISS, R., TREVATHAN-TACKETT, S. M., WARTMAN, M., WILSON, K. A. & ROGERS, K. 2022. Operationalizing marketable blue carbon. *One Earth,* 5**,** 485-492.

MACREADIE, P. I., SULLIVAN, B., EVANS, S. M. & SMITH, T. M. 2018. Biogeography of Australian Seagrasses: NSW, Victoria, Tasmania, and temperate Queensland. *In:* LARKUM, A. W. D., KENDRICK, G. A. & RALPH, P. J. (eds.) *Seagrasses of Australia: Structure, Ecology, and Conservation.* Springer International Publishing AG.

MACREADIE, P. I., TREVATHAN-TACKETT, S. M., SKILBECK, C. G., SANDERMAN, J., CURLEVSKI, N., JACOBSEN, G. & SEYMOUR, J. R. 2015. Losses and recovery of organic carbon from a seagrass ecosystem following disturbance. *Proceedings of the Royal Society B: Biological Sciences,* 282**,** 20151537.

MANCINI, G., MASTRANTONIO, G., POLLICE, A., LASINIO, G. J., BELLUSCIO, A., CASOLI, E., PACE, D. S., ARDIZZONE, G. & VENTURA, D. 2023. Detecting trends in seagrass cover through aerial imagery interpretation: Historical dynamics of a Posidonia oceanica meadow subjected to anthropogenic disturbance. *Ecological Indicators,* 150**,** 110209.

MARTIN, R., ELLIS, J., BRABYN, L. & CAMPBELL, M. 2020. Change-mapping of estuarine intertidal seagrass (Zostera muelleri) using multispectral imagery flown by remotely piloted aircraft (RPA) at Wharekawa Harbour, New Zealand. *Estuarine, Coastal and Shelf Science,* 246**,** 107046.

NIELSEN, A. A. 2007. The regularized iteratively reweighted MAD method for change detection in multi- and hyperspectral data. *IEEE Transactions on Image processing,* 16**,** 463-478.

NIELSEN, A. A., CONRADSEN, K. & SIMPSON, J. J. 1998. Multivariate alteration detection (MAD) and MAF postprocessing in multispectral, bitemporal image data: New approaches to change detection studies. *Remote Sensing of Environment,* 64**,** 1-19.

NORDLUND, L., KOCH, E. W., BARBIER, E. B. & CREED, J. C. 2016. Seagrass Ecosystem Services and Their Variability across Genera and Geographical Regions. *PLoS One,* 11**,** e0163091.

O'BRIEN, K. R., WAYCOTT, M., MAXWELL, P., KENDRICK, G. A., UDY, J. W., FERGUSON, A. J., KILMINSTER, K., SCANES, P., MCKENZIE, L. J. & MCMAHON, K. 2018. Seagrass ecosystem trajectory depends on the relative timescales of resistance, recovery and disturbance. *Marine Pollution Bulletin,* 134**,** 166-176.

ORTH, R. J., LEFCHECK, J. S., MCGLATHERY, K. S., AOKI, L., LUCKENBACH, M. W., MOORE, K. A., ORESKA, M. P., SNYDER, R., WILCOX, D. J. & LUSK, B. 2020. Restoration of seagrass habitat leads to rapid recovery of coastal ecosystem services. *Science Advances,* 6**,** eabc6434.

ORTH, R. J., LEFCHECK, J. S. & WILCOX, D. J. 2017. Boat propeller scarring of seagrass beds in lower Chesapeake Bay, USA: Patterns, causes, recovery, and management. *Estuaries and Coasts,* 40**,** 1666-1676.

ORTH, R. J., MARION, S. R., MOORE, K. A. & WILCOX, D. J. 2010. Eelgrass (Zostera marina L.) in the Chesapeake Bay region of mid-Atlantic coast of the USA: challenges in conservation and restoration. *Estuaries and Coasts,* 33**,** 139-150.

PENDLETON, L., DONATO, D. C., MURRAY, B. C., CROOKS, S., JENKINS, W. A., SIFLEET, S., CRAFT, C., FOURQUREAN, J. W., KAUFFMAN, J. B. & MARBÀ, N. 2012. Estimating global "blue carbon" emissions from conversion and degradation of vegetated coastal ecosystems.

PHINN, S., ROELFSEMA, C., DEKKER, A., BRANDO, V. & ANSTEE, J. 2008. Mapping seagrass species, cover and biomass in shallow waters: An assessment of satellite multi-spectral and airborne hyper-spectral imaging systems in Moreton Bay (Australia). *Remote Sensing of Environment,* 112**,** 3413-3425.

POURSANIDIS, D., TRAGANOS, D., REINARTZ, P. & CHRYSOULAKIS, N. 2019. On the use of Sentinel-2 for coastal habitat mapping and satellite-derived bathymetry estimation using downscaled coastal aerosol band. *International Journal of Applied Earth Observation and Geoinformation,* 80**,** 58-70.

PRICE, D. M., FELGATE, S. L., HUVENNE, V. A., STRONG, J., CARPENTER, S., BARRY, C., LICHTSCHLAG, A., SANDERS, R., CARRIAS, A. & YOUNG, A. 2022. Quantifying the intra-habitat variation of seagrass beds with unoccupied aerial vehicles (UAVs). *Remote Sensing,* 14**,** 480.

PU, R., BELL, S., MEYER, C., BAGGETT, L. & ZHAO, Y. 2012. Mapping and assessing seagrass along the western coast of Florida using Landsat TM and EO-1 ALI/Hyperion imagery. *Estuarine, Coastal and Shelf Science,* 115**,** 234-245.

REED, B., J. & HOVEL, K., A. 2006. Seagrass habitat disturbance: how loss and fragmentation of eelgrass Zostera marina influences epifaunal abundance and diversity. *Marine Ecology Progress Series,* 326**,** 133-143.

REZEK, R. J., FURMAN, B. T., JUNG, R. P., HALL, M. O. & BELL, S. S. 2019. Long-term performance of seagrass restoration projects in Florida, USA. *Scientific reports,* 9**,** 15514.

RICHARDS, J. A. & RICHARDS, J. A. 2022. *Remote sensing digital image analysis*, Springer.

RINIATSIH, I., AMBARIYANTO, A., YUDIATI, E., REDJEKI, S. & HARTATI, R. 2021. Monitoring the seagrass ecosystem using the unmanned aerial vehicle (UAV) in coastal water of Jepara. *IOP Conference Series: Earth and Environmental Science,* 674**,** 012075.

ROELFSEMA, C., KOVACS, E. M., SAUNDERS, M. I., PHINN, S., LYONS, M. & MAXWELL, P. 2013. Challenges of remote sensing for quantifying changes in large complex seagrass environments. *Estuarine, Coastal and Shelf Science,* 133**,** 161-171.

ROMÁN, A., TOVAR-SÁNCHEZ, A., OLIVÉ, I. & NAVARRO, G. 2021. Using a UAV-Mounted Multispectral Camera for the Monitoring of Marine Macrophytes. *Frontiers in Marine Science,* 8.

ROY, P., WILLIAMS, R., JONES, A., YASSINI, I., GIBBS, P., COATES, B., WEST, R., SCANES, P., HUDSON, J. & NICHOL, S. 2001. Structure and function of south-east Australian estuaries. *Estuarine, coastal and shelf science,* 53**,** 351-384.

SHORT, F. T., COLES, R. G. & SHORT, C. M. 2015. SeagrassNet manual for scientific monitoring of seagrass habitat.

SINGH, A. 1989. Digital change detection techniques using remotely-sensed data. *International journal of remote sensing,* 10**,** 989-1003.

SWADLING, D. S., WEST, G. J., GIBSON, P. T., LAIRD, R. J. & GLASBY, T. M. 2023. Don't go breaking apart: Anthropogenic disturbances predict meadow fragmentation of an endangered seagrass. *Aquatic Conservation: Marine and Freshwater Ecosystems,* 33**,** 56-69.

TAHARA, S., SUDO, K., YAMAKITA, T. & NAKAOKA, M. 2022. Species level mapping of a seagrass bed using an unmanned aerial vehicle and deep learning technique. *PeerJ,* 10**,** e14017.

TAN, Y. M., DALBY, O., KENDRICK, G. A., STATTON, J., SINCLAIR, E. A., FRASER, M. W., MACREADIE, P. I., GILLIES, C. L., COLEMAN, R. A., WAYCOTT, M., VAN DIJK, K.-J., VERGÉS, A., ROSS, J. D., CAMPBELL, M. L., MATHESON, F. E., JACKSON, E. L., IRVING, A. D., GOVERS, L. L., CONNOLLY, R. M., MCLEOD, I. M., RASHEED, M. A., KIRKMAN, H., FLINDT, M. R., LANGE, T., MILLER, A. D. & SHERMAN, C. D. H. 2020. Seagrass Restoration Is Possible: Insights and Lessons From Australia and New Zealand. *Frontiers in Marine Science,* 7.

TRAGANOS, D., AGGARWAL, B., POURSANIDIS, D., TOPOUZELIS, K., CHRYSOULAKIS, N. & REINARTZ, P. 2018. Towards Global-Scale Seagrass Mapping and Monitoring Using Sentinel-2 on Google Earth Engine: The Case Study of the Aegean and Ionian Seas. *Remote Sensing,* 10.

UHRIN, A. V. & TOWNSEND, P. A. 2016. Improved seagrass mapping using linear spectral unmixing of aerial photographs. *Estuarine, Coastal and Shelf Science,* 171**,** 11-22.

UNSWORTH, R. K. F., CULLEN-UNSWORTH, L. C., JONES, B. L. H. & LILLEY, R. J. 2022. The planetary role of seagrass conservation. *Science,* 377**,** 609-613.

VALLE, M., PALÀ, V., LAFON, V., DEHOUCK, A., GARMENDIA, J. M., BORJA, Á. & CHUST, G. 2015. Mapping estuarine habitats using airborne hyperspectral imagery, with special focus on seagrass meadows. *Estuarine, Coastal and Shelf Science,* 164**,** 433-442.

VEETTIL, B. K., WARD, R. D., LIMA, M. D. A. C., STANKOVIC, M., HOAI, P. N. & QUANG, N. X. 2020. Opportunities for seagrass research derived from remote sensing: A review of current methods. *Ecological Indicators,* 117.

VIRNSTEIN, R. W. 1999. Seagrass management in Indian River Lagoon, Florida: Dealing with issues of scale. *Pacific Conservation Biology,* 5**,** 299-305.

WACKER, A. & LANDGREBE, D. 1972. Minimum distance classification in remote sensing. *LARS Technical Reports***,** 25.

WAYCOTT, M., DUARTE, C. M., CARRUTHERS, T. J., ORTH, R. J., DENNISON, W. C., OLYARNIK, S., CALLADINE, A., FOURQUREAN, J. W., HECK JR, K. L. & HUGHES, A. R. 2009. Accelerating loss of seagrasses across the globe threatens coastal ecosystems. *Proceedings of the national academy of sciences,* 106**,** 12377-12381.

WEST, G. J. 2023. Estuarine Macrophytes of NSW. *In:* NSW, I. A. I. (ed.).

WEST, R. J. 2012. Impact of Recreational Boating Activities on the Seagrass Posidonia in SE Australia. *Wetlands (Australia),* 26.

Chapter 5

Estimating vegetation cover in submerged estuarine seagrass meadows using red-edge vegetation indices

This chapter is not published but is written in the format of a paper for future publication.

This chapter addresses **Aim 2** by focusing on mapping seagrass percent cover using UAV images. It also explores spectral vegetation indices using red-edge reflectance, contributing to **Aim 3**.

5.1 Introduction

Estuarine seagrass meadows exhibit fine-scale spatial heterogeneity in cover and biomass, and their ecological function and provision of ecosystem services varies across space accordingly. Seagrass meadows with greater cover sequester carbon more effectively (Samper-Villarreal et al., 2016, Stankovic et al., 2018, Ferretto et al., 2023), enhance biodiversity and faunal habitat provision (McCloskey and Unsworth, 2015, Henderson et al., 2017), and offer greater coastal protection through sediment stabilisation (Van Katwijk et al., 2010, James et al., 2023). Patterns in seagrass cover also shape some ecosystem function, as more fragmented meadows have less capacity for carbon sequestration and wave attenuation (Koch et al., 2009, Ricart et al., 2015, El Allaoui et al., 2016, Ricart et al., 2017). Denser, continuous seagrass meadows are also more resilient to rising sea levels and changing environmental conditions (Unsworth et al., 2015). Spatial heterogeneity in seagrass meadows is closely tied to the ecosystem services the seagrass provides, and mapping and monitoring heterogeneity provides vital information to support ecosystem valuation and management, as well as characterising changes due to disturbance or recovery (Simpson et al., 2022).

Remote sensing provides an effective method for mapping seagrass at a range of spatio-temporal scales (Wabnitz et al., 2008, Traganos et al., 2018, McKenzie et al., 2022). Remote sensing-derived seagrass maps treat seagrass cover either as a continuous variable, usually estimated using regression, or as discrete classes assigned using image classification. Normalised Difference Vegetation Index (NDVI; Rouse Jr et al., 1973), a remote sensing vegetation index developed for mapping terrestrial vegetation, has been

found to correlate with seagrass cover in intertidal areas (Barillé et al., 2010, Zoffoli et al., 2020, Davies et al., 2024). However, mapping of submerged seagrass using NDVI is generally prevented by the high attenuation of near-infrared (NIR) light by water (Kirk, 1994). Remote sensing of submerged seagrass is often limited to the use of visible light wavelengths to map discrete cover classes, which has been criticised for the high potential for misclassification and failing to reliably represent differences within heterogeneous seagrass environments (Lyons et al., 2011).

Developments in UAV-mounted multi-spectral sensors provide an opportunity to derive vegetation indices for characterising seagrass heterogeneity at a fine spatial scale. UAV-captured remote sensing data has been used to successfully classify benthic habitats (James et al., 2020, Elma et al., 2024), and discrete seagrass cover classes (Duffy et al., 2018, Nahirnick et al., 2019, Chand and Bollard, 2021, Román et al., 2021, Hamad et al., 2022, McKenzie et al., 2022, Yang et al., 2023, Sneep et al., 2024), as well as characterise change and disturbance in seagrass meadows (Simpson et al., 2024). Price et al. (2022) used UAV-captured data to estimate seagrass cover as a continuous variable, based on green reflectance. Although this study used only a single green band and limited field data, it demonstrates the detailed picture of seagrass heterogeneity that can be achieved by estimating cover using UAV images. There is a need to investigate optimal vegetation indices for submerged seagrass given the effects of water attenuation in the near-infrared region. This would improve the utility of UAV and satellite-acquired images for capturing the spatiotemporal variability of submerged seagrass.

Chlorophyll, the most abundant pigment in living vegetation, contributes to photosynthesis by absorbing visible light, especially in blue and red wavelengths, while NIR radiation is re-emitted. Generally, the denser and healthier the photosynthesising vegetation, the more red light is absorbed and the more NIR radiation is reflected. Consequently, the normalised difference between red and NIR reflectance, or NDVI, can detect differences in vegetation health and density. Between red and NIR wavelengths, in the red-edge (~680-750 nm), vegetation reflectance increases rapidly with wavelength. Because vegetation reflects in the red-edge more than the red, the normalised difference of red-edge and red bands can be used in a similar manner to

NDVI to predict vegetation percent cover and Leaf Area Index, maintaining sensitivity over a broad range of vegetation densities (Gitelson and Merzlyak, 1994, Delegido et al., 2013, Xie et al., 2018).

Seagrass and bare substrate in the absence of water exhibit reflectance patterns similar to terrestrial equivalents (Anstee et al., 2009) (Figure 1). For *Zostera muelleri* (syn. *Zostera capricorni*), a reflectance peak is present in the green wavelengths (~555 nm), an absorption feature in the red at (~670 nm), and a rapid increase in reflectance is evident through the red edge (~690-750 nm) to the near-infrared (>750 nm) region. Sand has relatively higher reflectance across the entire visible and near-infrared spectrum, but lacks the green and near-infrared peaks, generally increasing in reflectance across the spectrum.

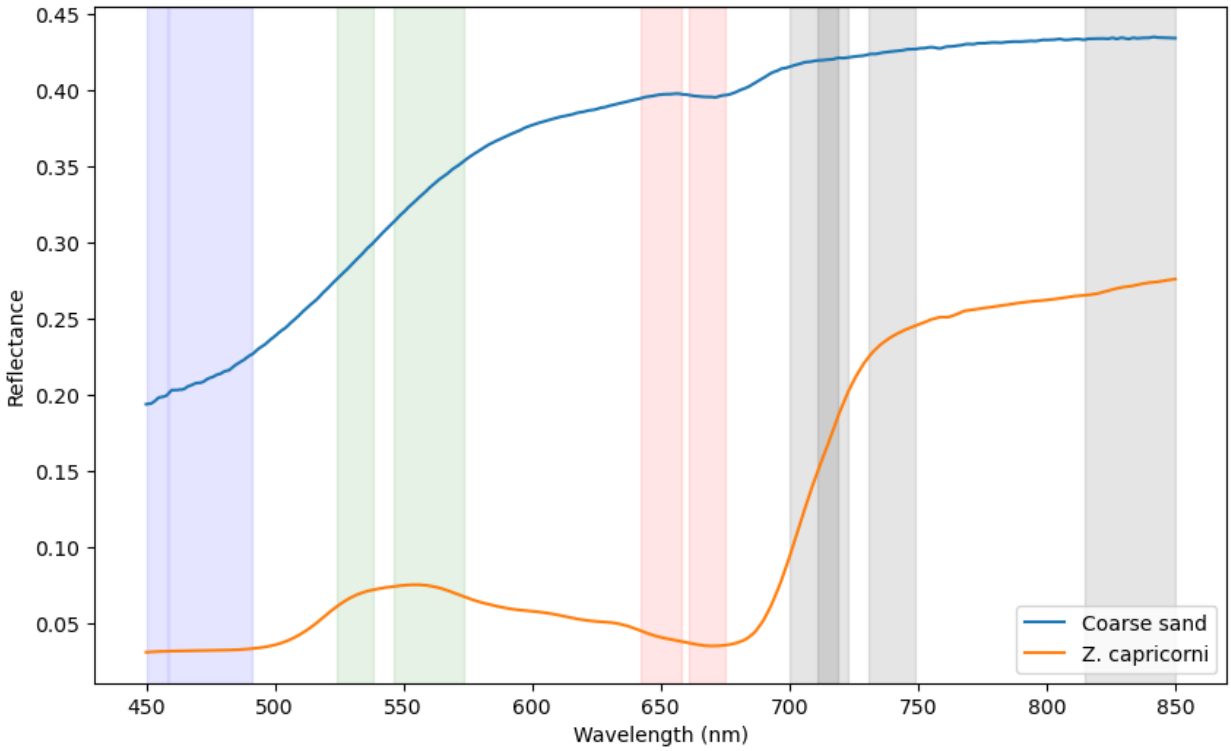

Figure 1. Spectral library reflectances for estuarine sand and *Z. capricorni* from Wallis Lake, NSW. Adapted from Anstee et al. 2008. The 10 Micasense RedEdge-MX Dual Camera system bands are marked as vertical bands.

The water column over submerged seagrass confounds measurement of radiance and derivation of reflectance values due to the absorption and scattering of light by water. Water absorption varies considerably by wavelength across the visible spectrum with a relatively rapid increase in absorption towards near-infrared wavelengths (Buiteveld et al., 1994). In turbid coastal waters typical of temperate estuaries, scattering caused by

the water column, as well as absorption and scattering caused by dissolved and suspended water column constituents, lead to higher attenuation, especially in the near-infrared and lower blue parts of the spectrum (Vahtmäe et al., 2020).

As red-edge light is less rapidly attenuated by water than NIR radiation, it can be used to detect vegetation in shallow water where NIR radiation cannot (Timmer et al., 2022). Red-edge bands therefore offer an alternative to NIR for detecting reflectance signals of submerged shallow water vegetation due to increased penetration depth. The normalised difference of red-edge and red bands captured by Sentinel-2 has been shown to be usable for detecting presence of submerged seagrass (Li et al., 2023), and a similar index using red-edge and green reflectance has been applied to distinguish between seagrass density classes (Chand and Bollard, 2021). Extending this approach further to predict seagrass cover with red-edge based indices requires removal of water column interference, even in shallow water.

The primary objective of this study was to assess the viability of red-edge normalised difference indices (RENDIs) for mapping submerged seagrass percent cover as a continuous variable in a shallow, temperate, estuarine setting, based on red-edge reflectance offering a characteristic vegetation signal that can penetrate shallow water. Four different RENDIs, based on different band combinations, were calculated for UAV-captured image mosaics. An empirical water column correction was applied to estimate benthic reflectance and *in situ* quadrats provided estimates of seagrass percent cover. The specific aims were to determine (1) whether RENDIs are a viable tool for predicting submerged seagrass cover, (2) the most effective available red-edge and red bands for predicting seagrass cover, and (3) the repeatability of the image correction and RENDI calculations at different water levels. It was expected that RENDIs would relate strongly with seagrass percent cover, and that the optimal Sentinel-2 red-edge band would be determined by the highest wavelength red-edge band for which benthic reflectance can be estimated.

5.2 Methods

5.2.1 Study sites

Brisbane Water is a wave-dominated barrier estuary located 45 km north of Sydney, Australia (Roy et al., 2001). The estuary supports fringing seagrass around the shoreline and larger seagrass meadows over intertidal flats and flood tide deltas (Dyall et al., 2018). The seagrass meadows are dominated by *Zostera muelleri*, mixed with *Halophila ovalis,* and some small patches of *Posidonia australis* can be found in deeper areas. The estuary is surrounded by suburban development and is intensively used for fishing and recreational boating. Seagrass meadows and tidal flats throughout the area are used for oyster farming.

Two seagrass meadows in Brisbane Water (hereafter referred to as Empire Bay and St Huberts Island) were selected as case studies for simultaneous ground truth and remote sensing data capture in December 2023 (Figure 2). Both seagrass meadows comprised primarily *Z. muelleri* with seagrass percent cover ranging from 0-100%. Oyster farms are present on both seagrass meadows, and boat traffic is common, especially alongside and across the centrally located St Huberts Island. These sites are shallow (largely <1.5m), and in some areas intertidal.

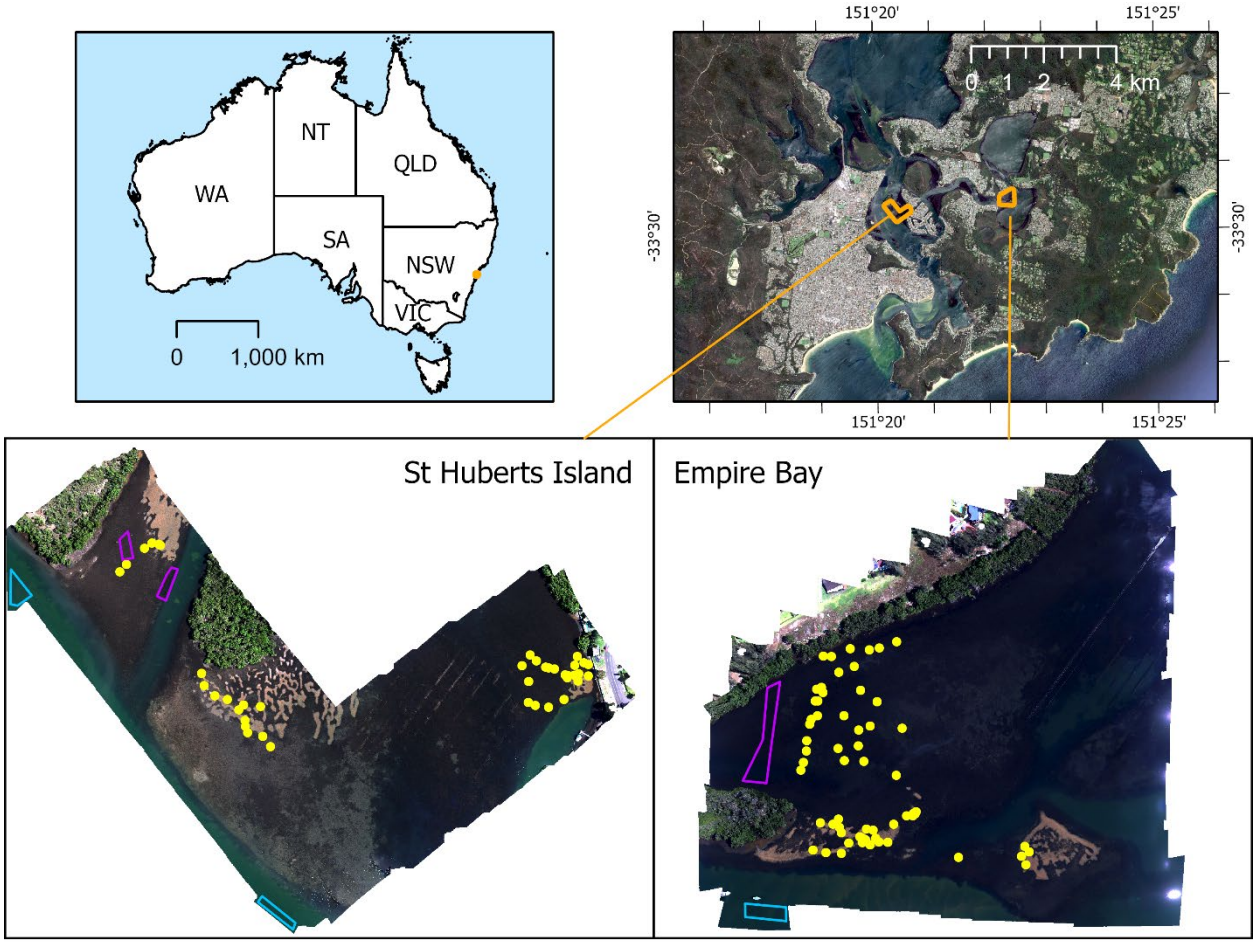

Figure 2. Maps showing site locations within Australia and Brisbane Water, surveyed seagrass meadows including quadrat locations (yellow points), regions sampled for deep water reflectance (blue polygons), and regions sampled for attenuation coefficient derivation (magenta polygons).

5.2.2 Data collection

Ground truth data was gathered using 50 cm x 50 cm (0.25 m^2) quadrats, the quadrat sides marked every 10 cm to assist with cover estimates (Figure 3). One corner of each quadrat was marked with orange tape to correctly orient and align field photographs with UAV surveys. Twenty quadrats were placed across the target area prior to each UAV flight and secured in place with large tent pegs. Nadir-facing photographs were taken of the quadrats after placement using a GoPro HERO11 waterproof camera with the Linear field of view setting (GoPro, San Mateo, USA). Photos were taken above the water's surface to include the entire quadrat in a single frame. Though the photographs were taken in the early morning with a low sun angle, sun glint was present in some images. Multiple photographs were taken of each quadrat to compensate for this. For each quadrat, a field estimate of percent cover was recorded in ArcGIS Field Maps (Esri, Redlands, USA), along with a measurement of depth captured with a depth gauge, time,

and coordinates captured with a Google Pixel 8 smartphone GPS (Google, Mountain View, USA), sufficient to locate the quadrats in the stitched drone image. These quadrats were left *in situ* during the UAV flights for later identification of ground truth sites within the UAV mosaics (Figure 3).

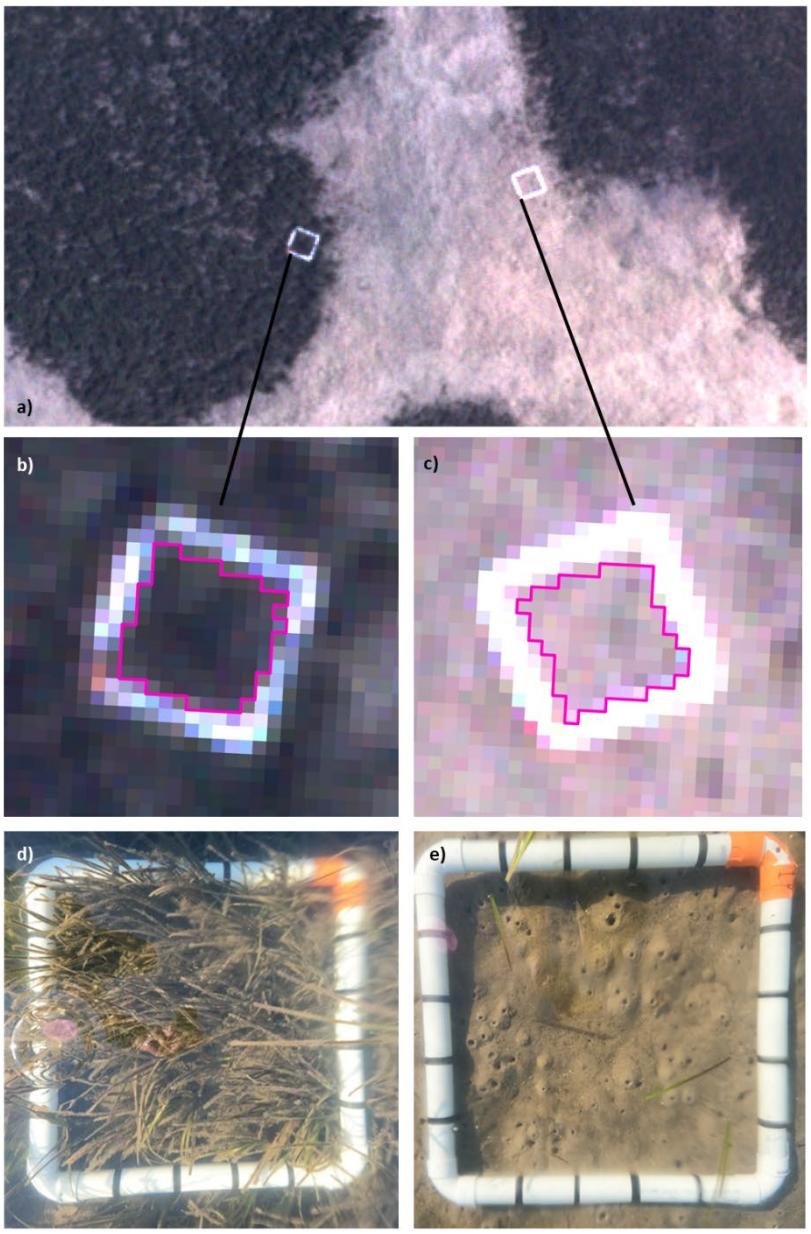

Figure 3. Quadrats used for surveys of seagrass percent cover in Brisbane water. a) In-situ quadrats in UAV images of St Huberts Island site, with two quadrats visible, their corresponding areas of interest b) and c), and corresponding field photos d) in the seagrass meadow, 89% cover, and e) in a bare patch, 0% cover

Remote sensing images were captured using a Micasense RedEdge-MX Dual Camera System (Micasense, Seattle, USA), mounted on a DJI Matrice 200 UAV (DJI, Nanshan, China), operated by Measure Ground Control software (AgEagle Aerial Systems Inc.,

Wichita, USA). The camera system captures data in 10 spectral bands (Figure 1), including two in the red part of the spectrum (at 650 and 668 nm), three in the red edge (at 705, 717, and 740 nm), and one in the near-infrared (at 842 nm). Linked to the camera system and attached to the UAV is a downwelling light sensor which captures lighting conditions at the time of each image capture to allow for radiometric calibration.

All UAV flights were at 60 m above ground level, to achieve a final spatial resolution of approximately 4 cm (Table 1). All images were captured with 75% front and side overlap. A total of three flights were carried out at Empire Bay and two at St Huberts Island. Each flight at a given location followed the same flight plan. Flights were scheduled at approximately the same time each morning to ensure consistent illumination during capture and that sun glint was avoided by maintaining a low sun angle (Joyce et al. 2019). Each flight was carried out during ebb tide, but at a different tidal stage. Throughout the week, the weather was consistently clear and fine, and no notable changes in apparent turbidity were identified. At least one image was captured over deep water for each flight to enable water column correction.

Table 1. Flight data for the seagrass surveys used in this study

Date	Flight start time	Location	Spatial resolution (cm)	Flight area (ha)	Water level (m relative to mean)	Quadrats
4/12/23	10:05 AM	Empire Bay	4.4	15.9	-0.08	20
5/12/23	8:59 AM	St Huberts Island	4.3	21.4	-0.05	20
6/12/23	9:14 AM	Empire Bay	4.4	15.9	0.06	20
7/12/23	9:05 AM	St Huberts Island	4.3	21.4	0.14	20
8/12/23	8:56 AM	Empire Bay	4.3	15.9	0.24	20

5.2.3 Field data processing

Each quadrat photograph was analysed to derive a more accurate percentage cover estimate. Using the 10 cm markings on the edge of the quadrat, the image was divided into 25 segments to assist with cover estimation and to reduce potential for parallax error caused by off-nadir image capture by ensuring cover measurements are equally

weighted across the quadrat. Percentage cover in each segment was estimated to the nearest multiple of 5, then the mean of all segments was taken as a percentage cover estimate for that quadrat. The quadrat data is summarised in Appendix D.

Water level measurements taken in the field were corrected based on water level data from Koolewong station (Manly Hydraulics Laboratory). Using the time of water depth measurement, the time of UAV overpass, and the water level table, corrected water depth measurements were produced representing actual water level at each ground truth site at the time of UAV image capture.

5.2.4 UAV data processing

Images captured by the dual camera system were stitched, radiometrically calibrated, and orthorectified using Metashape Professional (Agisoft LLC, St Petersburg, Russia). The full processing parameters are described in Appendix E. Radiometric calibration was carried out using data from the downwelling light sensor and images of a calibration panel captured before and after each flight. The images for each site were geographically co-registered so they were accurate relative to each other within 2 pixels (~8 cm). The first Empire Bay image (4/12/23) was ultimately discarded due to sun glint caused by it being captured an hour later than the other images, however, the image was still processed and georeferenced so that quadrat boundaries from the day's ground truth data were usable in the analysis. Four UAV mosaics were generated, two each for Empire Bay and St Huberts Island.

The pixels within each quadrat in the UAV image were selected using ENVI (NV5 Geospatial Solutions, Broomfield, USA) with the Region of Interest (ROI) tool to select similar pixels within the quadrat area. Using this method one ROI was selected for each quadrat representing pixels within the quadrat with minimal reflectance contamination from the quadrat frame (Figure 3). Each quadrat ROI was then used to extract reflectance data from all images at that site, resulting in a total of 60 ground truth points for Empire Bay and 40 for St Huberts Island (Figure 2).

The final dataset for assessing indices and relationships contained mean reflectance values for 10 bands, percent cover derived from field photographs, and depth (in cm) at the time of image capture.

5.2.5 Correction of water column effects

To account for the variable influence of the water column on remote sensing signal due to differences in column depth, water column correction was applied based on Maritorena et al. (1994). This analytical model considers reflectance at the water surface as a combination of reflectance from an optically deep water column and bottom reflectance, exponentially attenuated based on depth:

$$R_w = R_\infty + (R_b - R_\infty)e^{-2K_d Z} \quad (1)$$

where R_w represents surface reflectance, R_∞ represents optically deep water reflectance, R_b represents bottom reflectance, $K_d$is an overall attenuation coefficient (in m^{-1}), and Z is depth (in m). All variables except Z are wavelength-dependent. Rearranged, bottom reflectance can be estimated as:

$$R_b = \frac{R_w - R_\infty}{e^{-2K_d Z}} + R_\infty \quad (2)$$

R_∞ was retrieved from each radiometrically calibrated image based on mean reflectance values for manually selected deep water areas.

For water column correction, all images were first resampled bilinearly to 50 cm spatial resolution to reduce noise and match each individual pixel with the resolution of the quadrat dataset. The value of Z was estimated based on the method developed by Stumpf et al. (2003). This approach identifies a ratio of linearised band reflectances which can be related linearly to measured depth values:

$$Z = m\frac{\ln(nR_i)}{\ln(nR_j)} + b \quad (3)$$

where R_i and R_j are reflectances from two bands, n is a factor between 500 and 1500 used to tune the algorithm, and m and b are coefficients derived based on known depth measurements. The depth relationship was derived separately for each site, based on the depth measurements for the quadrats at that site, adjusted based on the tide level at image capture time. Bands used for a given site were selected based on the ratio with the strongest relationship with depth.

Attenuation coefficients for each band were derived from the images and estimated bathymetry using the method developed by Bierwirth et al. (1993) which measures reflectances over an area with varying depth and constant benthic cover. The more common approach of selecting benthic cover with high albedo (e.g. sand) was not available, due to the absence of bare sand across the depth profile of the sites. An area of homogenous dense seagrass coverage across a depth profile for each site was used as an alternative (Figure 2). For each band, the linear relationship between the natural log of reflectance and the estimated depth values was found. The slope of the line of best fit is equal to $-2K_d$. Optically deep water reflectance values were derived by taking the mean reflectance from the bottom quartile of regions of deep water in each image (Figure 2).

Once calculated, the estimated depth images, and the derived optically deep water reflectance and attenuation coefficients were used to produce an estimated bottom reflectance image for each date for the two red bands and two lower wavelength red-edge bands. The same water column correction process was applied to the reflectances derived from the ROIs to compare uncorrected and corrected reflectances to ground truth data.

5.2.6 Comparison of vegetation indices

A series of RENDIs was derived from the images to estimate seagrass cover without relying upon near infrared or upper red-edge wavelengths (Table 2). The third red-edge band (at 740 nm) and the near infrared band (at 842 nm) were deemed too impacted by water column interference to be usable, even with water column correction, as even shallow seagrass could not be detected in these bands.

Table 2. Red-edge normalised difference indices included in this study, with formulae including band centres.

Name	Formula
$NDI_{705\text{-}650}$	$\frac{R_{705} - R_{650}}{R_{705} + R_{650}}$
$NDI_{705\text{-}668}$	$\frac{R_{705} - R_{668}}{R_{705} + R_{668}}$
$NDI_{717\text{-}650}$	$\frac{R_{717} - R_{650}}{R_{717} + R_{650}}$
$NDI_{717\text{-}668}$	$\frac{R_{717} - R_{668}}{R_{717} + R_{668}}$

The strength of the relationship between each of the normalised difference indices and seagrass percent cover was measured using linear regression, once for each image individually. Pearson's correlation coefficient was compared on an individual image basis to identify the best index for each image.

To validate the consistency of RENDI retrievals with water column correction, index values for the ground truth sites were compared across each pair of corrected images using orthogonal regression. This allowed for analysis of the repeatability of the method presented in this article. Similarity of index measurements between each pair of images for the same site was taken to be an indication of consistency of the results under different tidal conditions and therefore the effectiveness of the water column correction.

5.2.7 Prediction of cover using red-edge normalised difference indices

To produce reliable seagrass cover maps, areas outside of the seagrass meadows including land and deep water were manually masked out of all UAV mosaics. Seagrass cover was then predicted by applying the derived index-cover relationship with the highest correlation coefficient for the associated image to the remaining unmasked area. Outputs were bounded to values between 0 and 100 to produce per-pixel maps of predicted percent cover.

Prediction accuracy was tested using leave-one-out cross validation (LOOCV) due to the relatively small number of data points at each site (n = 40-60). LOOCV produced an accuracy assessment by predicting cover for a single quadrat using a model created with all other quadrats, then iterating through the entire dataset until each quadrat has been excluded and predicted once. All model iterations were used to calculate mean absolute error (MAE), root mean square error (RMSE), and coefficient of determination (R^2) for each index and each image.

5.3 Results

5.3.1 Correction of water column effects

Though the original bathymetry estimation method used blue and green bands (Stumpf et al. 2003), green (530 nm) and red (650 nm/665 nm depending upon site) bands were found to relate more strongly to water depth for the Brisbane Water sites. One band ratio-depth relationship was derived for each site, using both images for that site and all relevant field data. The predictive strength of the relationships was good (R^2 = 0.65-0.71; Table 3) with low standard error and were consistent with field observations and known spatial configuration of the site. The depth estimation method of Stumpf et al. (2003) often produces results with stronger relationships than those calculated for the Brisbane Water sites (Traganos and Reinartz, 2018, Vahtmäe et al., 2020), however the limited depth range at the sites and of the ground truth data likely impacts the strength of the relationship in the Brisbane Water data.

Table 3. Band centres used for developing ratio relationship with depth, linear model coefficients, number of samples used, standard error, coefficient of determination, and p-value.

Site	Band centres	*m*	*n*	*b*	N	SE (m)	R^2	p
Empire Bay	530 nm, 665 nm	2.1545	500	-1.8399	80	0.18	0.65	<0.001
St Huberts Island	530 nm, 650 nm	3.4165	500	-3.0495	76	0.26	0.71	<0.001

When attempting to derive attenuation coefficients for bands 9 and 10 (Bierwirth et al., 1993), it was identified that they extinguished too rapidly across the observed depth range, resulting in a non-linear relationship between natural log of reflectance and depth. For this reason, attenuation coefficients were derived only for bands 5, 6, 7, and 8 (650, 668, 705, and 717 nm) to support calculation of red-edge normalised difference indices (Figure 4).

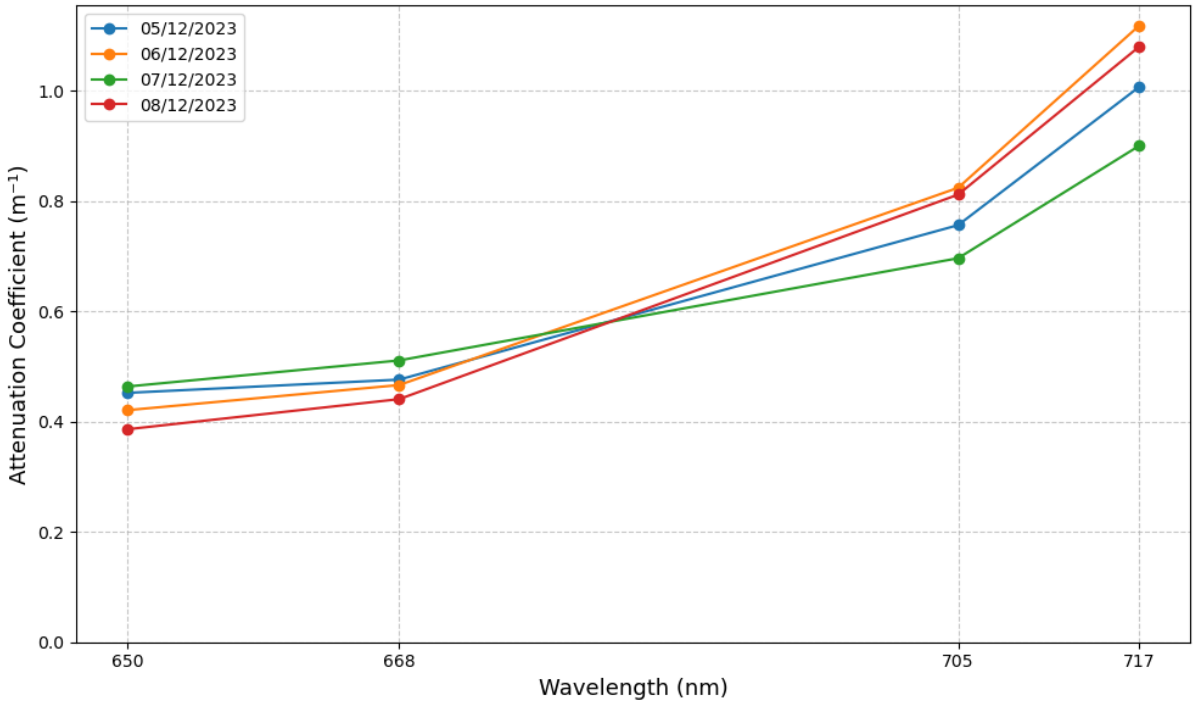

Figure 4. Attenuation coefficients derived using the method described by Bierwirth et al. (1993) for red and red-edge bands across all four images

Derived attenuation coefficient increased with wavelength. The calculated coefficients for Empire Bay were very similar between the two images, as expected given the lack of disruptive events (e.g. rainfall) between the two survey dates, and the capture of data during the same tidal phase, though different tide levels. The coefficients for St Huberts Island diverged more significantly, especially in the red-edge, but still followed the same pattern of increasing attenuation with wavelength.

5.3.2 Correlation between indices and seagrass cover

A strong correlation was found between all red-edge vegetation indices and seagrass percent cover (Figure 5). The predictions were weakest for the second St Huberts Island image (7/12/23) and strongest for the first Empire Bay image (6/12/23). Relationships for both St Huberts Island images were generally weaker. The best performing index on average was $NDI_{717\text{-}668}$, followed by $NDI_{717\text{-}650}$, $NDI_{705\text{-}650}$, and $NDI_{705\text{-}668}$, though the difference between these indices was small. The best performing index for all images was consistently one of the two indices using the 717 nm red-edge band.

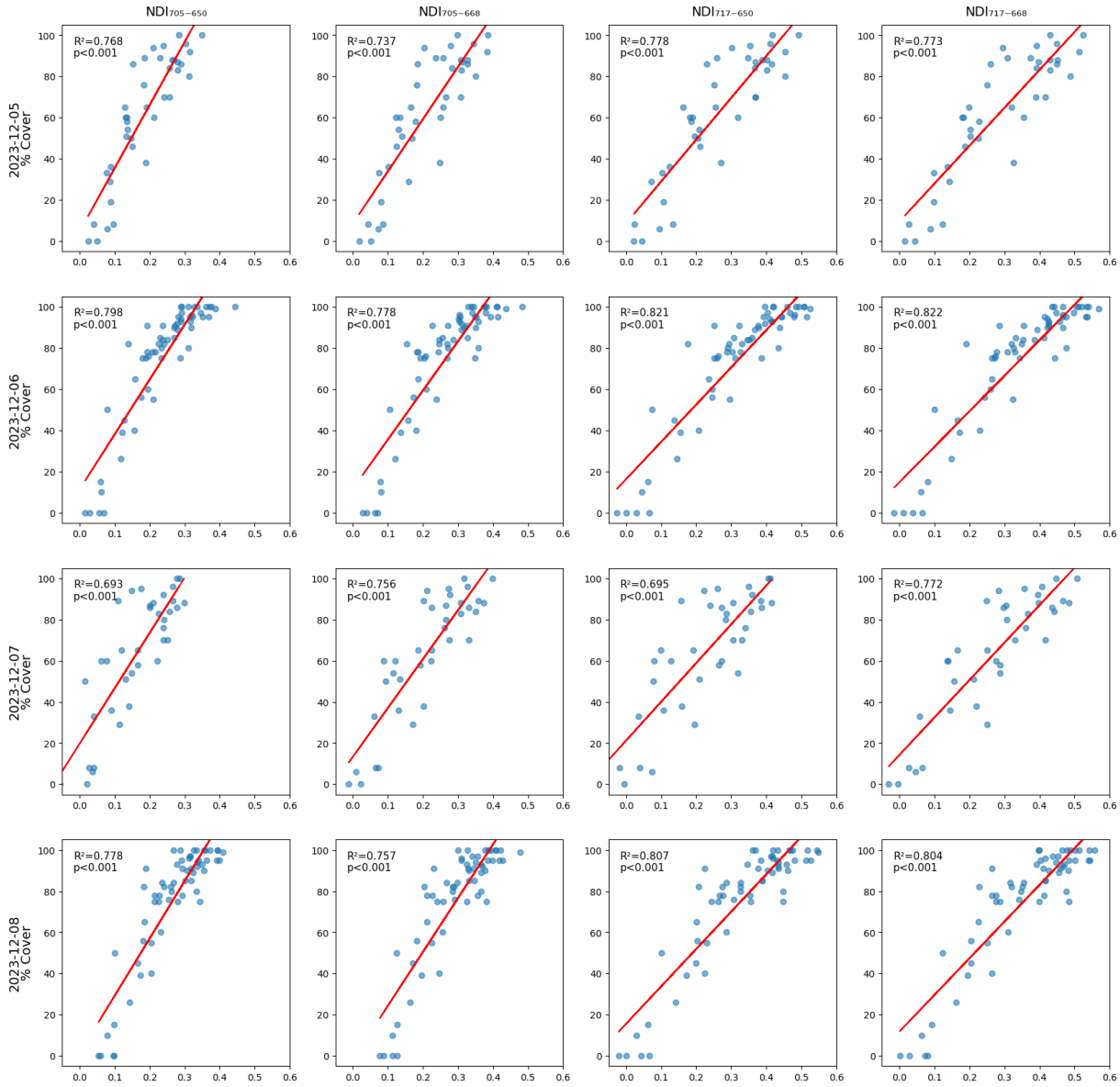

Figure 5. Linear relationship between index and seagrass percent cover for each index and UAV mosaic.

5.3.3 Corrected index measurements between tide levels

Repeated observations were strongly correlated with each other at both Empire Bay (R = 0.94-0.96) and St Huberts Island (R = 0.86-0.92) (Figure 6). The weakest relationships were found in the 7/12/23 St Huberts Island image, for the indices using the 650 nm red band, for which the index values showed lower contrast than those using the 668 nm red band. All other image pairs produced index values with a correlation coefficient greater than 0.90.

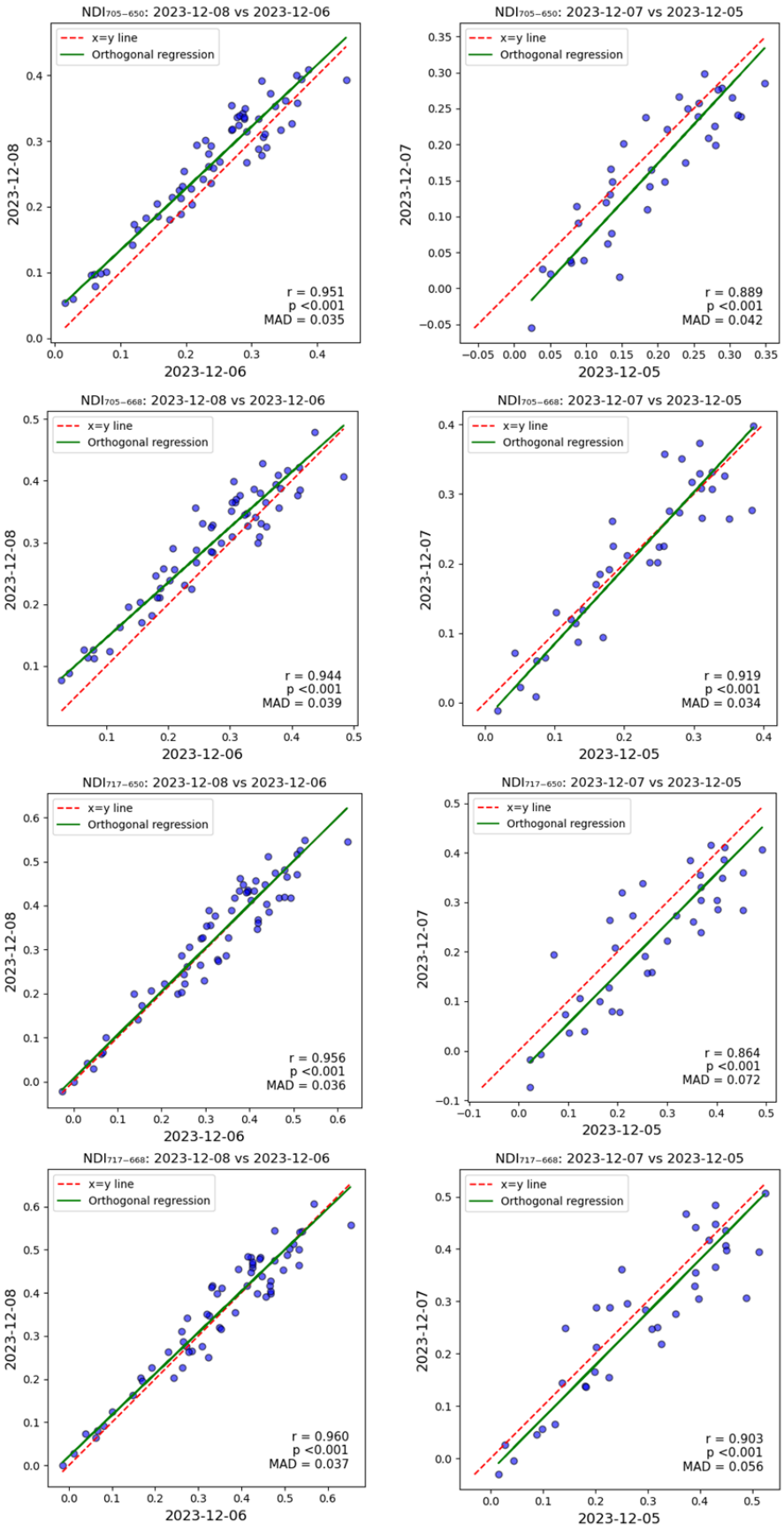

Figure 6. Index values compared using orthogonal regression between repeat observations at the same sites under different water levels.

5.3.4 Predicting seagrass cover at study sites

Seagrass cover was predicted at both sites, using the linear transformation of the index with the highest correlation for each image, applied to the estimated bottom reflectance, followed by bounding the outputs to between 0 and 100. The indices and images used were $NDI_{717-668}$ on the 6/12/23 image at Empire Bay (Figure 7) and $NDI_{717-650}$ on the 5/12/23 image at St Huberts Island (Figure 8). The maps generally agreed with the known extent of seagrass at the sites (West et al. 2023) and provided additional detail about the spatial patterns in seagrass cover at each site.

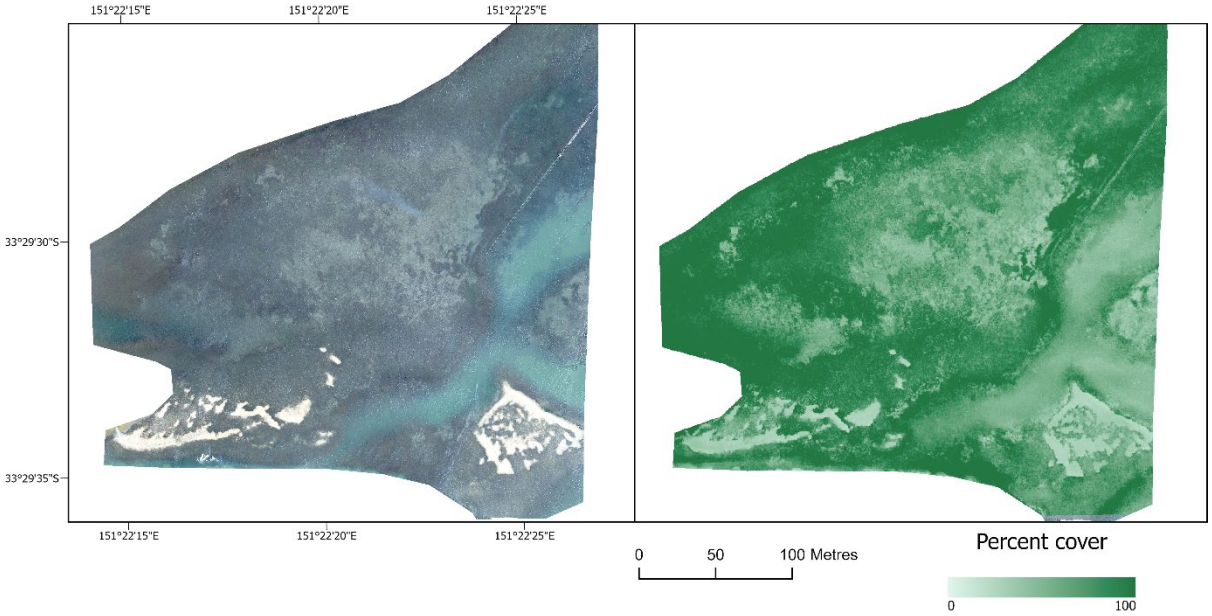

Figure 7. Mapped seagrass percent cover at Empire Bay, based on the image captured on 6/12/23 using the $NDI_{717-668}$ index.

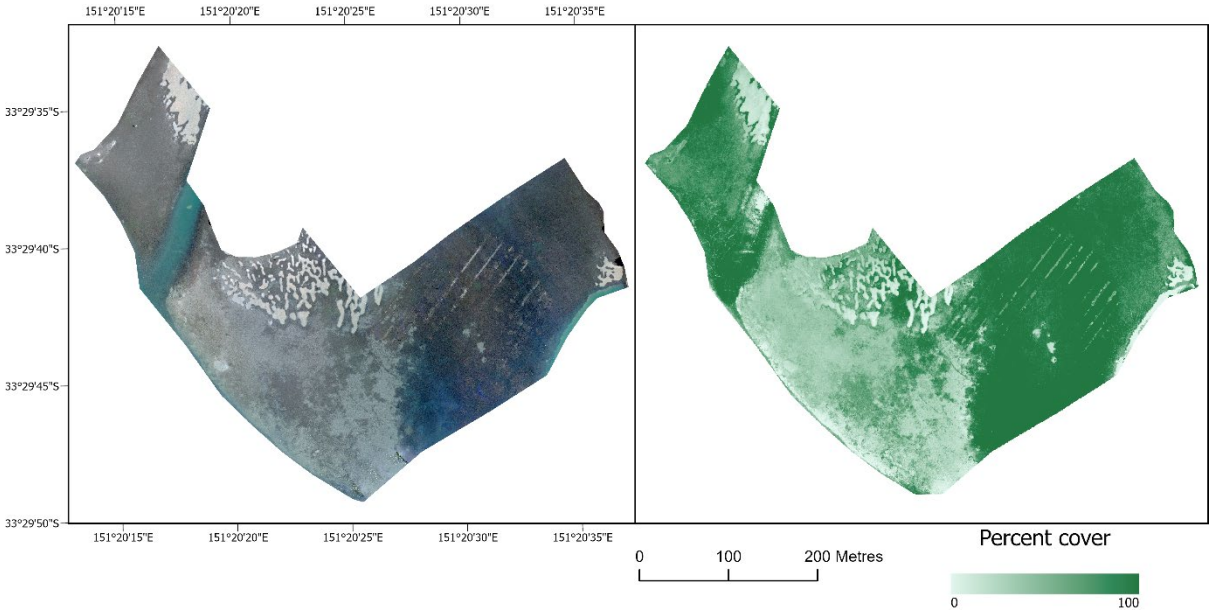

Figure 8. Mapped seagrass percent cover at St Huberts Island, based on the image captured on 5/12/23 using the $NDI_{717-650}$ index.

Empire Bay (Figure 7) was characterised by dense seagrass (80-100% cover) around the edges of the meadow, on the protected western side of the site, and around the oyster farming infrastructure on the eastern side. Throughout the middle of the site, seagrass cover was patchier, with large areas of moderate cover (40-60%) interspersed with denser patches, mostly around 70-80% cover. Shallow patches of bare sand on the southern side of the site were overestimated as having up to ~30% seagrass cover but were still distinct from surrounding dense seagrass. In the deeper channels that run across the site, seagrass meadow edges were visible, but cover appeared underestimated at 50-60%, possibly because of the higher turbidity in these channels compared to other parts of the site.

Seagrass at St Huberts Island was dense close to the shore (70-90%) and across the centre of the mud flat (95-100%) (Figure 8). West of the oyster farming infrastructure, the seagrass density abruptly drops to very low levels (20-35%), with a small number of interspersed denser patches (60-80%). Some patches of bare sand are visible on the southwestern edge of the seagrass meadow, and near the mangrove islands. Seagrass cover in very shallow areas of bare sand was overestimated by up to ~10%. Deeper bare sand areas were correctly recorded as unvegetated. The channel running through the site is lined with dense seagrass (95-100%), while to the north of the channel seagrass cover is moderately dense (60-90%).

Seagrass cover prediction from the Empire Bay image with $NDI_{717-668}$ resulted in an R^2 value of 0.8, seagrass cover MAE of 10.1, and RMSE of 12.9. $NDI_{717-650}$ for predicting cover from the St Huberts Island image resulted in an R^2 of 0.76, MAE of 12.0 and RMSE of 14.9. At both sites, actual and predicted seagrass cover aligned well (Figure 9), though there was a tendency at both sites to overpredict when seagrass cover was at very low levels.

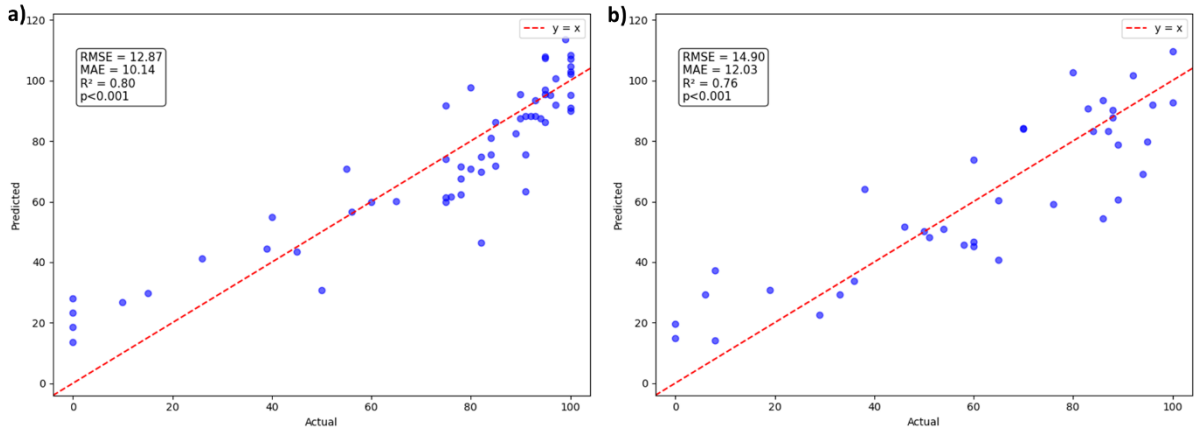

Figure 9. Predicted vs actual values for cover estimation a) based on the 6/12/23 image at Empire Bay using the $NDI_{717-668}$ index, and b) based on the 5/12/23 image at St Huberts Island using the $NDI_{717-650}$ index.

5.4 Discussion

RENDIs were demonstrated to offer a robust method for estimating seagrass cover without using the NIR band, which is impacted in this estuarine study site by water attenuation even at very shallow depths limiting its capacity for submerged vegetation detection. This aligns with other research that found the red-edge based indices have higher depth limits than NIR-based equivalents for detecting kelp (Timmer et al., 2022). Additionally, it contributes to existing literature involving the use of red-edge bands and red-edge based indices for classifying submerged vegetation (Jia et al., 2019, Chand and Bollard, 2021) by using RENDIs to produce estimates of seagrass cover as a continuous variable.

Seagrasses in temperate estuarine environments, including *Zostera spp.* are highly depth limited due to restrictions on light availability (Bulmer et al., 2016), consequently meadow stability and density decreases with depth (Greve and Krause-Jensen, 2005b). As a result, the extent of temperate estuarine seagrass is often limited to 3-4 m depth (Greve and Krause-Jensen, 2005a, Duarte, 1991), and a substantial proportion of

estuarine seagrass meadows grows in much shallower water. This contrasts with other seagrass habitats, such as those in the tropics and the Mediterranean Sea, where water is clearer, and seagrass grows over a wider range of depths (Duarte, 1991, Serrano et al., 2014). In such locations, remote sensing data in red-edge wavelengths would have less utility as it would be mostly attenuated before benthic reflectance leaves the water's surface. The need for different remote sensing image processing in tropical, Mediterranean and temperate estuarine locations highlights the importance of remote sensing approaches that are tailored to specific environmental conditions, rather than generalised across diverse and physically distinct coastal settings.

While non-linear relationships between remote sensing reflectance and submerged seagrass cover have been demonstrated (Price et al., 2022), this study presents a robust predictive model based on the physical properties of the characteristic reflectance spectrum of submerged photosynthesising vegetation. Using the relationship between an RENDI value and seagrass percent cover as demonstrated here, this method provides wide applicability in shallow areas, producing a linear predictive relationship comparable to NDVI for terrestrial vegetation, though with reduced contrast. The consistency of measurements at different water depths allows for easier repeat measurements without needing to align capture times with specific tide levels allowing greater flexibility in data acquisition. Additionally, correcting for water column influence, the RENDI approach is more suited to standard satellite image data, where overpass image capture times are determined by the satellite's orbital parameters and not user defined.

Corrected for water column interference, RENDIs extend the geographical area of synoptic remote sensing-based monitoring to temperate estuarine mud flats and tidal deltas, where NDVI is frequently not suitable. Consistent monitoring of changes in seagrass over time provides valuable information to support ecosystem service assessments. Assessing and monitoring the blue carbon storage potential of seagrass meadows in estuarine environments is challenging due to the physical limitations to remote sensing of submerged targets at variable depths and turbidity levels (Malerba et al., 2023). The RENDI method presented in this study allows for repeatable monitoring of submerged seagrass meadows in a shallow setting that would otherwise require field-

based monitoring. Given that seagrass is vulnerable to fine-scale and localised disturbances (Simpson et al., 2024, Karang et al., 2024), the synoptic view provided by remote sensing is an important tool for understanding temporal trends in seagrass monitoring, except in areas physically limited by depth or high turbidity.

Translating the RENDI method, developed here using 10-band UAV camera that approximates the Sentinel-2 sensor, to satellite data would enable ongoing estuarine seagrass monitoring over large spatial scales. Additionally, the image-based derivation of variables for water column correction naturally lends itself to satellite monitoring, as ongoing water attenuation coefficient data is rarely available. The results of this study highlight the importance of appropriate sensor selection for mapping submerged estuarine vegetation. The Micasense RedEdge-MX dual sensor used in this study includes three red-edge bands for agricultural applications, but this is uncommon for satellite sensors. Sentinel-2, Planet SuperDove, and Worldview-3 data include red-edge bands at 704, 705 and 725 nm respectively (Mansaray et al., 2021). Future sensors, such as Landsat Next, due for launch in 2030, will offer more options for estuarine seagrass mapping with two red-edge bands (US Geological Survey, 2023). This study has demonstrated that mapping shallow submerged vegetation is a viable additional application for red-edge bands, increasing their usefulness from a sensor design perspective.

We present an application of the Maritorena et al. (1994) method for correcting water column interference UAV-captured images, requiring only depth measurements as field data. The attenuation coefficients, estimated from the images, were not validated, but they follow the expected increasing pattern of attenuation coefficients at this wavelength range and are generally aligned with other attenuation coefficients, both derived and measured, for coastal and marine waters (Kirk, 1977, Buiteveld et al., 1994, Turpie, 2013, Traganos and Reinartz, 2018). Further validation of this approach should involve in-situ measurements of light attenuation. Small errors in red-edge attenuation coefficient are a possible explanation for the lower agreement between corrected images at St Huberts Island, where the estimated attenuation coefficients deviated from each other. Additionally, we applied this method over a narrower depth range than it was originally intended, so factors such as differences in seagrass canopy height likely

impact on the model more significantly than in sites with a greater range of applicable depths. However, the method for deriving attenuation coefficients remains theoretically applicable over small depth ranges (Bierwirth et al., 1993), the predictive strength of the bathymetry estimation was strong, and the attenuation coefficients derived agree with other published attenuation values, so the corrections performed were considered accurate.

Several aspects of the RENDI approach require further exploration. Identifying practical depth limits of the red-edge bands will provide insight into the range of shallow water estuarine settings in which RENDIs are applicable for seagrass mapping, and the inherent physical limitations on the RENDI method. Improvement of the water column correction approach may also strengthen the application of RENDIs, for instance, deriving bathymetry with green LiDAR or using in situ measurements for derivation of attenuation coefficients would retrieve benthic reflectance more accurately than image-based derivations of these variables. In situ approaches to deriving attenuation coefficients will also provide information about how small differences in water column composition may impact index measurements. However, limits will remain in certain areas with consistently high turbidity, such as the estuaries that were excluded from this study for that reason. Other methods such as relating indices with biomass rather than cover and utilising non-linear predictive models or machine learning for estimating biophysical attributes could further improve the use of RENDI data in shallow estuarine waters. Even with improved processing methods, the RENDI approach will remain limited. The red-edge bands used in this study are attenuated to below 10% of reflectance by ~2 m of water, meaning that RENDI for prediction of seagrass cover is not applicable in environments dominated by deeper seagrass, such as many tropical areas or coral reefs.

5.5 Conclusions

RENDIs, the normalised difference of red-edge and red reflectance, offer a robust option for estimating submerged seagrass cover as a continuous variable. In the shallow estuarine environment of Brisbane Water, water column correction requiring only *in situ* depth gauge measurements was successfully performed on the red and red-edge

bands, and seagrass percent cover estimated with low error (MAE 10.1-12.0, RMSE 12.9-14.9). This relationship is expected to be applicable across similar temperate estuaries featuring seagrass meadows. These findings concur with others that have used red-edge bands and red-edge based indices to detect seagrass and extend this work by identifying a linear relationship for predicting seagrass percent cover. For UAV remote sensing of seagrass meadows, RENDIs can be considered a viable approach to mapping cover. Translating RENDI to satellite remote sensing data could allow for effective large-scale monitoring of submerged estuarine seagrass cover that captures the natural heterogeneity and complexity found in many seagrass meadows.

References

ANSTEE, J. M., BOTHA, E. J. & DEKKER, A. G. 2009. Study on the remote sensing of estuarine macrophytes and saltmarsh vegetation in Wallis Lake; . *CSIRO Water for a Healthy Country Flagship.* Canberra, Australia.

BARILLÉ, L., ROBIN, M., HARIN, N., BARGAIN, A. & LAUNEAU, P. 2010. Increase in seagrass distribution at Bourgneuf Bay (France) detected by spatial remote sensing. *Aquatic Botany,* 92**,** 185-194.

BIERWIRTH, P., LEE, T. & BURNE, R. 1993. Shallow sea-floor reflectance and water depth derived by unmixing multispectral imagery. *Photogrammetric Engineering and Remote Sensing,* 59.

BUITEVELD, H., HAKVOORT, J. & DONZE, M. Optical properties of pure water. Ocean Optics XII, 1994. SPIE, 174-183.

BULMER, R., KELLY, S. & JEFFS, A. 2016. Light requirements of the seagrass, Zostera muelleri, determined by observations at the maximum depth limit in a temperate estuary, New Zealand. *New Zealand Journal of Marine and Freshwater Research,* 50**,** 183-194.

CHAND, S. & BOLLARD, B. 2021. Low altitude spatial assessment and monitoring of intertidal seagrass meadows beyond the visible spectrum using a remotely piloted aircraft system. *Estuarine, Coastal and Shelf Science,* 255**,** 107299.

DAVIES, B. F. R., OIRY, S., ROSA, P., ZOFFOLI, M. L., SOUSA, A. I., THOMAS, O. R., SMALE, D. A., AUSTEN, M. C., BIERMANN, L. & ATTRILL, M. J. 2024. Intertidal seagrass extent from Sentinel-2 time-series show distinct trajectories in Western Europe. *Remote Sensing of Environment,* 312**,** 114340.

DELEGIDO, J., VERRELST, J., MEZA, C., RIVERA, J., ALONSO, L. & MORENO, J. 2013. A red-edge spectral index for remote sensing estimation of green LAI over agroecosystems. *European Journal of Agronomy,* 46**,** 42-52.

DUARTE, C. M. 1991. Seagrass depth limits. *Aquatic botany,* 40**,** 363-377.

DUFFY, J. P., PRATT, L., ANDERSON, K., LAND, P. E. & SHUTLER, J. D. 2018. Spatial assessment of intertidal seagrass meadows using optical imaging systems and a lightweight drone. *Estuarine, Coastal and Shelf Science,* 200**,** 169-180.

DYALL, A., TOBIN, G., GALINEC, V., CREASEY, J., GALLAGHER, J., RYAN, D. A., HEAP, A. D. & MURRAY, E. 2018. New South Wales Coastal Waterways Geomorphic Habitat Mapping, Version 2 (1:100 000 scale digital data).

EL ALLAOUI, N., SERRA, T., COLOMER, J., SOLER, M., CASAMITJANA, X. & OLDHAM, C. 2016. Interactions between fragmented seagrass canopies and the local hydrodynamics. *PLoS One,* 11**,** e0156264.

ELMA, E., GAULTON, R., CHUDLEY, T. R., SCOTT, C. L., EAST, H. K., WESTOBY, H. & FITZSIMMONS, C. 2024. Evaluating UAV-based multispectral imagery for mapping an intertidal seagrass environment. *Aquatic Conservation: Marine and Freshwater Ecosystems,* 34**,** e4230.

FERRETTO, G., VERGÉS, A., POORE, A. G., GLASBY, T. M. & GRIFFIN, K. J. 2023. Habitat provision and erosion are influenced by seagrass meadow complexity: a seascape perspective. *Diversity,* 15**,** 125.

GITELSON, A. & MERZLYAK, M. N. 1994. Spectral reflectance changes associated with autumn senescence of Aesculus hippocastanum L. and Acer platanoides L. leaves. Spectral features and relation to chlorophyll estimation. *Journal of plant physiology,* 143**,** 286-292.

GREVE, T. & KRAUSE-JENSEN, D. 2005a. Predictive modelling of eelgrass (Zostera marina) depth limits. *Marine Biology,* 146**,** 849-858.

GREVE, T. M. & KRAUSE-JENSEN, D. 2005b. Stability of eelgrass (Zostera marina L.) depth limits: influence of habitat type. *Marine Biology,* 147**,** 803-812.

HAMAD, I. Y., STAEHR, P. A., RASMUSSEN, M. B. & SHEIKH, M. 2022. Drone-Based Characterization of Seagrass Habitats in the Tropical Waters of Zanzibar. *Remote Sensing* [Online], 14.

HENDERSON, C. J., GILBY, B. L., LEE, S. Y. & STEVENS, T. 2017. Contrasting effects of habitat complexity and connectivity on biodiversity in seagrass meadows. *Marine Biology,* 164**,** 117.

JAMES, D., COLLIN, A., HOUET, T., MURY, A., GLORIA, H. & LE POULAIN, N. 2020. Towards Better Mapping of Seagrass Meadows using UAV Multispectral and Topographic Data. *Journal of Coastal Research,* 95.

JAMES, R., KEYZER, L., VAN DE VELDE, S., HERMAN, P. M., VAN KATWIJK, M. & BOUMA, T. 2023. Climate change mitigation by coral reefs and seagrass beds at risk: How global change compromises coastal ecosystem services. *Science of the Total Environment,* 857**,** 159576.

JIA, M., WANG, Z., WANG, C., MAO, D. & ZHANG, Y. 2019. A new vegetation index to detect periodically submerged mangrove forest using single-tide Sentinel-2 imagery. *Remote Sensing,* 11**,** 2043.

JOYCE, K., DUCE, S., LEAHY, S., LEON, J. X. & MAIER, S. 2019. Principles and practice of acquiring drone based image data in marine environments. *Marine and Freshwater Research,* 70, 952-963

KARANG, I., PRAVITHA, N. L. P. R., NUARSA, I. W., BASHEER AHAMMED, K. & WICAKSONO, P. 2024. High-resolution seagrass species mapping and propeller scars detection in Tanjung Benoa, Bali through UAV imagery. *Journal of Ecological Engineering,* 25.

KIRK, J. 1977. Attenuation of light in natural waters. *Marine and Freshwater Research,* 28**,** 497-508.

KIRK, J. T. 1994. *Light and photosynthesis in aquatic ecosystems*, Cambridge university press.

KOCH, E. W., BARBIER, E. B., SILLIMAN, B. R., REED, D. J., PERILLO, G. M., HACKER, S. D., GRANEK, E. F., PRIMAVERA, J. H., MUTHIGA, N. & POLASKY, S. 2009. Non-linearity in ecosystem services: temporal and spatial variability in coastal protection. *Frontiers in Ecology and the Environment,* 7**,** 29-37.

LI, Y., BAI, J., CHEN, S., CHEN, B. & ZHANG, L. 2023. Mapping seagrasses on the basis of Sentinel-2 images under tidal change. *Marine Environmental Research,* 185**,** 105880.

LYONS, M., PHINN, S. & ROELFSEMA, C. 2011. Integrating Quickbird Multi-Spectral Satellite and Field Data: Mapping Bathymetry, Seagrass Cover, Seagrass Species and Change in Moreton Bay, Australia in 2004 and 2007. *Remote Sensing,* 3**,** 42-64.

MALERBA, M. E., DE PAULA COSTA, M. D., FRIESS, D. A., SCHUSTER, L., YOUNG, M. A., LAGOMASINO, D., SERRANO, O., HICKEY, S. M., YORK, P. H. & RASHEED, M. 2023. Remote sensing for cost-effective blue carbon accounting. *Earth-Science Reviews,* 238**,** 104337.

MANSARAY, A. S., DZIALOWSKI, A. R., MARTIN, M. E., WAGNER, K. L., GHOLIZADEH, H. & STOODLEY, S. H. 2021. Comparing PlanetScope to Landsat-8 and Sentinel-2 for sensing water quality in reservoirs in agricultural watersheds. *Remote Sensing,* 13**,** 1847.

MARITORENA, S., MOREL, A. & GENTILI, B. 1994. Diffuse reflectance of oceanic shallow waters: Influence of water depth and bottom albedo. *Limnology and Oceanography,* 39**,** 1689-1703.

MCCLOSKEY, R. & UNSWORTH, R. 2015. Decreasing seagrass density negatively influences associated fauna. PeerJ 3: e1053.

MCKENZIE, L. J., LANGLOIS, L. A. & ROELFSEMA, C. M. 2022. Improving approaches to mapping seagrass within the Great Barrier Reef: From field to spaceborne earth observation. *Remote Sensing,* 14**,** 2604.

NAHIRNICK, N. K., RESHITNYK, L., CAMPBELL, M., HESSING-LEWIS, M., COSTA, M., YAKIMISHYN, J. & LEE, L. 2019. Mapping with confidence; delineating seagrass habitats using Unoccupied Aerial Systems (UAS). *Remote Sensing in Ecology and Conservation,* 5**,** 121-135.

PRICE, D. M., FELGATE, S. L., HUVENNE, V. A., STRONG, J., CARPENTER, S., BARRY, C., LICHTSCHLAG, A., SANDERS, R., CARRIAS, A. & YOUNG, A. 2022. Quantifying the intra-habitat variation of seagrass beds with unoccupied aerial vehicles (UAVs). *Remote Sensing,* 14**,** 480.

RICART, A. M., PÉREZ, M. & ROMERO, J. 2017. Landscape configuration modulates carbon storage in seagrass sediments. *Estuarine, Coastal and Shelf Science,* 185**,** 69-76.

RICART, A. M., YORK, P. H., RASHEED, M. A., PÉREZ, M., ROMERO, J., BRYANT, C. V. & MACREADIE, P. I. 2015. Variability of sedimentary organic carbon in patchy seagrass landscapes. *Marine Pollution Bulletin,* 100**,** 476-482.

ROMÁN, A., TOVAR-SÁNCHEZ, A., OLIVÉ, I. & NAVARRO, G. 2021. Using a UAV-Mounted Multispectral Camera for the Monitoring of Marine Macrophytes. *Frontiers in Marine Science,* 8.

ROUSE JR, J., HAAS, R., SCHELL, J. & DEERING, D. Monitoring vegetation systems in the Great Plains with ERTS. Third ERTS-1 symposium: The Proceedings of a Symposium Held by Goddard Space Flight center, 1973 Washington, DC. 309.

ROY, P., WILLIAMS, R., JONES, A., YASSINI, I., GIBBS, P., COATES, B., WEST, R., SCANES, P., HUDSON, J. & NICHOL, S. 2001. Structure and function of south-east Australian estuaries. *Estuarine, coastal and shelf science,* 53**,** 351-384.

SAMPER-VILLARREAL, J., LOVELOCK, C. E., SAUNDERS, M. I., ROELFSEMA, C. & MUMBY, P. J. 2016. Organic carbon in seagrass sediments is influenced by seagrass canopy complexity, turbidity, wave height, and water depth. *Limnology and Oceanography,* 61**,** 938-952.

SERRANO, O., LAVERY, P. S., ROZAIMI, M. & MATEO, M. Á. 2014. Influence of water depth on the carbon sequestration capacity of seagrasses. *Global Biogeochemical Cycles,* 28**,** 950-961.

SIMPSON, J., BRUCE, E., DAVIES, K. P. & BARBER, P. 2022. A blueprint for the estimation of seagrass carbon stock using remote sensing-enabled proxies. *Remote Sensing,* 14**,** 3572.

SIMPSON, J., DAVIES, K. P., BARBER, P. & BRUCE, E. 2024. Mapping fine-scale seagrass disturbance using bi-temporal UAV-acquired images and multivariate alteration detection. *Scientific reports,* 14, 19083.

SNEEP, A., DEVILLERS, R., ROBERT, K., LE BRIS, A. & EDINGER, E. 2024. Mapping and Characterizing Eelgrass Meadows Using UAV Imagery in Placentia Bay and Trinity Bay, Newfoundland and Labrador, Canada. *Sustainability,* 16, 3471.

STANKOVIC, M., TANTIPISANUH, N., RATTANACHOT, E. & PRATHEP, A. 2018. Model-based approach for estimating biomass and organic carbon in tropical seagrass ecosystems. *Marine Ecology Progress Series,* 596, 61-70.

STUMPF, R. P., HOLDERIED, K. & SINCLAIR, M. 2003. Determination of water depth with high-resolution satellite imagery over variable bottom types. *Limnology and Oceanography,* 48, 547-556.

TIMMER, B., RESHITNYK, L. Y., HESSING-LEWIS, M., JUANES, F. & COSTA, M. 2022. Comparing the use of red-edge and near-infrared wavelength ranges for detecting submerged kelp canopy. *Remote Sensing,* 14, 2241.

TRAGANOS, D., AGGARWAL, B., POURSANIDIS, D., TOPOUZELIS, K., CHRYSOULAKIS, N. & REINARTZ, P. 2018. Towards Global-Scale Seagrass Mapping and Monitoring Using Sentinel-2 on Google Earth Engine: The Case Study of the Aegean and Ionian Seas. *Remote Sensing,* 10.

TRAGANOS, D. & REINARTZ, P. 2018. Machine learning-based retrieval of benthic reflectance and Posidonia oceanica seagrass extent using a semi-analytical inversion of Sentinel-2 satellite data. *International Journal of Remote Sensing,* 39, 9428-9452.

TURPIE, K. R. 2013. Explaining the spectral red-edge features of inundated marsh vegetation. *Journal of Coastal Research,* 29, 1111-1117.

U.S. GEOLOGICAL SURVEY 2023. *Landsat Next* [Online]. Available: https://www.usgs.gov/landsat-missions/landsat-next [Accessed 14/9/2024].

UNSWORTH, R. K., COLLIER, C. J., WAYCOTT, M., MCKENZIE, L. J. & CULLEN-UNSWORTH, L. C. 2015. A framework for the resilience of seagrass ecosystems. *Marine pollution bulletin,* 100, 34-46.

VAHTMÄE, E., KUTSER, T. & PAAVEL, B. 2020. Performance and Applicability of Water Column Correction Models in Optically Complex Coastal Waters. *Remote Sensing,* 12.

VAN KATWIJK, M., BOS, A., HERMUS, D. & SUYKERBUYK, W. 2010. Sediment modification by seagrass beds: Muddification and sandification induced by plant cover and environmental conditions. *Estuarine Coastal and Shelf Science,* 89, 175-181.

WABNITZ, C. C., ANDRÉFOUËT, S., TORRES-PULLIZA, D., MÜLLER-KARGER, F. E. & KRAMER, P. A. 2008. Regional-scale seagrass habitat mapping in the Wider Caribbean region using Landsat sensors: Applications to conservation and ecology. *Remote Sensing of Environment,* 112, 3455-3467.

XIE, Q., DASH, J., HUANG, W., PENG, D., QIN, Q., MORTIMER, H., CASA, R., PIGNATTI, S., LANEVE, G. & PASCUCCI, S. 2018. Vegetation indices combining the red and red-edge spectral information for leaf area index retrieval. *IEEE Journal of selected topics in applied earth observations and remote sensing,* 11, 1482-1493.

YANG, B., HAWTHORNE, T. L., AOKI, L., BEATTY, D. S., COPELAND, T., DOMKE, L. K., ECKERT, G. L., GOMES, C. P., GRAHAM, O. J. & HARVELL, C. D. 2023. Low-Altitude UAV Imaging Accurately Quantifies Eelgrass Wasting Disease From Alaska to California. *Geophysical Research Letters,* 50, e2022GL101985.

ZOFFOLI, M. L., GERNEZ, P., ROSA, P., LE BRIS, A., BRANDO, V. E., BARILLÉ, A.-L., HARIN, N., PETERS, S., POSER, K., SPAIAS, L., PERALTA, G. & BARILLÉ, L. 2020. Sentinel-2 remote sensing of Zostera noltei-dominated intertidal seagrass meadows. *Remote Sensing of Environment,* 251.

Chapter 6

Characterising variability in estuarine seagrass cover using a Sentinel-2 time series

This chapter is not published but is written in the format of a paper for future publication.

This chapter addresses **Aim 4** by scaling up the approaches developed in earlier chapters to a larger geographical area using satellite remote sensing data.

6.1 Introduction

Seagrass is recognized as an important blue carbon ecosystem contributing to climate change mitigation through organic carbon (C_{org}) sequestration and storage (Fourqurean et al., 2012). However, carbon stocks within seagrass meadows can be highly heterogenous and variable over time (Ricart et al., 2020, Simpson et al., 2022; Chapter 3) and neglecting this potential for spatio-temporal variability may undermine the robustness of remote sensing based carbon accounting estimates. Variation in seagrass biomass over time has the potential to influence seagrass C_{org} sequestration, with previous studies indicating that more stable meadows are associated with higher stocks (Mazarrasa et al., 2018, Stankovic et al., 2021, Bijak et al., 2023). The dynamic nature of seagrass meadows is frequently not captured in carbon inventory maps, which are generally limited to extent, species composition, or horizontally projected cover classes (Chapter 2). Developing methods to characterise and map seagrass habitat variability using time series analysis would enhance the reliability of carbon monitoring required for supporting the monitoring and reporting of a growing number of international blue carbon projects (Duarte et al., 2025).

Seagrass biomass is controlled by the complex interaction of factors including nutrient availability, temperature, salinity, light availability, wave energy, herbivory, water conditions, and geomorphic setting (Short, 1987, Lirman and Cropper, 2003, Clausen et al., 2014, Suykerbuyk et al., 2016, Tecchiato et al., 2019, James et al. 2020). Seasonal patterns in seagrass biomass may vary considerably between locations and years (Kirkman et al., 1982, Kerr and Strother, 1990, Turner and Schwarz, 2006, Matheson

and Schwarz, 2007, Turner, 2007). The factors that control seagrass biomass can also vary over short periods and local geographical scales in response to episodic natural events such as storms, or anthropogenic disturbances such as pollution (Cabaço et al., 2007). Human activities also directly impact seagrass biomass including through destruction by boat propellers and moorings (Walker et al., 1989, Unsworth et al., 2017, Simpson et al., 2024; Chapter 4). Disturbances at a very fine scale may have a negligible impact on overall carbon stocks (Macreadie et al., 2014), but larger or longer-term disturbances impact carbon stocks significantly and can lead to remineralisation of stored C_{org} into atmospheric CO_2 (Macreadie et al., 2015). Seagrass can also undergo autocatalytic collapse in response to disturbance events as rhizomes are damaged and sediments destabilized, leading to meadow fragmentation with unknown consequences for carbon stock (Larkum, 1976, Swadling et al., 2023). Seagrass above-ground biomass is therefore potentially highly variable. Understanding spatiotemporal variability at a landscape scale provides valuable information for site selection and management of seagrass blue carbon projects, can provide insight into the geographical drivers of variability and improve carbon estimates.

Recurrent data captured by satellite remote sensing platforms are well-placed to monitor seagrass meadows and characterise their spatial dynamics over time (Phinn et al., 2018). Many remote sensing techniques applied to terrestrial vegetation are not applicable to submerged seagrass, as near-infrared reflectance required for derivation of variables such as NDVI is rapidly extinguished by water (Kirk, 1994). Recent seagrass remote sensing studies have found that estuarine seagrass, often growing under relatively shallow water, can be reliably detected using techniques which utilise reflectance of solar irradiance in the red-edge region of the spectrum (about 680-750 nm) (Chapter 5; also Li et al., 2023). The normalised difference between the red-edge and red reflectances, or red-edge normalised difference index (RENDI) of seagrass correlates linearly with seagrass percent cover (Chapter 5), as long as the water is shallow enough for red-edge light to penetrate. Therefore, variability in the RENDI is expected to correspond with variability in seagrass cover, provided that confounding factors affecting spectral response, most importantly water level and water optical properties, can be accounted for.

Due to the high complexity of estuarine environments, numerous approaches have been developed to support management by categorising parts of estuaries based on their environmental characteristics (Dye, 2006). Multiple typologies of geomorphic zonation, which characterise the hydrological, ecological, and sedimentary conditions in different parts of the estuary, have been developed to provide a simplified model of conditions as they vary within estuaries (Rochford, 1959, Whitfield, 1992, Roy et al., 2001, Dyall et al., 2018). Many of the environmental characteristics summarised in geomorphic zonations are related to seagrass biomass, including sediment nutrients, salinity, and overall hydrodynamic energy, and as a result, seagrass extent and biomass can be partly predicted by geomorphic zonation (Tecchiato et al., 2015, Mazarrasa et al., 2021), though the complexity of the drivers of seagrass biomass make these relationships weak under some circumstances, especially in areas where seagrass cover is highly dynamic (Grech and Coles, 2010). With reliable maps of seagrass cover variability, it may be possible to capture this dynamism by identifying relationships between relative variability and environmental conditions using geomorphic zonation as a proxy for environmental conditions.Following on from the identification of the relationship between degree of variability and carbon sequestration (Simpson et al., 2022; Chapter 3), high rate of small-scale disturbances in estuarine seagrass (Simpson et al., 2024; Chapter 4), and new cover mapping techniques (Chapter 5), this chapter investigates the potential to generate maps of relative temporal variability in seagrass cover using Sentinel-2 image derived RENDI. The relationship between seagrass cover variability and geomorphic zonation is then tested to advance the understanding of the relationship between geomorphic conditions and seagrass extent by considering the stability of seagrass habitats across geomorphic zones. This chapter focuses on three aims:

1. Determine whether the red-edge normalized difference index previously demonstrated using high spatial resolution UAV-acquired images (Chapter 5) can be applied to medium spatial scale satellite data;
2. Establish whether there are seasonal trends in seagrass biomass in NSW estuarine environments;

3. Determine the relationship between spatial patterns in seagrass variability and estuarine geomorphic zonation.

6.2 Methods

6.2.1 Study sites

A total of 13 estuaries in the state of New South Wales, Australia, were initially selected based on the geologically-based conceptual framework for comparing Australian estuaries developed by Roy et al. (2001). Estuaries with less than 2 km^2 of seagrass were excluded from the study (Roy et al. 2001). The red-edge based seagrass detection method from Chapter 5 was developed and validated for a shallow barrier estuary, therefore embayments and tide-dominated estuaries (where seagrass generally grows in deeper water) were also excluded from the study. Clarence River and Smiths Lake were omitted due to reduction in seagrass area to almost zero since Roy et al. (2001) was published (NSW Department of Primary Industries, 2023). A further two, Myall River and Camden Haven, were omitted due to consistent high turbidity levels, visually assessed using Sentinel-2 images, throughout the entire study period preventing detection of seagrass. Nine estuaries remained for inclusion in this study. The nine estuaries, with varying physical characteristics (Figure 1), represented 58% of the total seagrass area in NSW (NSW Department of Primary Industries, 2023)

Site	Entrance type	Evolutionary maturity	Estuary type	Water level/tide station name
Clarence River*	Open, trained	Mature	Wave-dominated barrier estuary	Oyster Channel
Camden Haven River*	Open, trained	Intermediate	Wave-dominated barrier estuary	Lakewood
Wallis Lake	Open, trained	Youthful	Wave-dominated barrier estuary	Forster
Smiths Lake*	Intermittent	Intermediate	Saline coastal lagoon	Tarbuck Bay
Myall River*	Open	Semi-mature	Wave-dominated interbarrier estuary	Tea Gardens
Lake Macquarie	Open, trained	Youthful	Wave-dominated barrier estuary	Swansea Channel
Tuggerah Lakes	Intermittent	Intermediate	Wave-dominated barrier estuary	Long Jetty
Brisbane Water	Open	Youthful	Wave-dominated barrier estuary	Koolewong
Lake Illawarra	Open, trained	Intermediate	Wave-dominated barrier estuary	Cudgeree Bay 2
St Georges Basin	Open	Intermediate	Wave-dominated barrier estuary	Sussex Inlet
Coila Lake	Intermittent	Youthful	Saline coastal lagoon	Coila Lake
Wagonga Inlet	Open, trained	Intermediate	Wave-dominated barrier estuary	Barlows Bay
Merimbula Lake	Open	Intermediate	Wave-dominated barrier estuary	Merimbula Wharf

Figure 1. Estuaries considered for inclusion in this study based on characteristics defined in Roy et al. (2001). 'Trained' entrances refer to those with a breakwater or seawall constructed to keep the estuary open. *Estuary excluded from this study due to significant loss of seagrass since publication of Roy et al. (2001), or consistently high water turbidity over the study period determined from Sentinel-2 images.

6.2.2 Satellite data selection and validation

6.2.2.1 Satellite data

Sentinel-2 is a satellite mission operated by the European Space Agency to capture data using two earth observation satellites, Sentinel-2A and Sentinel-2B, launched in June 2015 and March 2017 respectively. It captures data in visible, red-edge, and near-infrared wavelengths at spatial resolutions of 10, 20, or 60 metres. Visible (10 m resolution), red-edge, and near-infrared (both 20 m resolution) bands were used in this analysis, with 10 m bands resampled to 20 m resolution. Sentinel-2 was preferred over alternative options due to the red-edge band, not included in Landsat data, and the longer period of available observations compared to Planet SuperDove. Google Earth Engine (GEE; Gorelick et al., 2017) was used for the analysis to allow for easy creation of seasonal composite images.

6.2.2.2 Validating Sentinel-2 red-edge normalised difference index for mapping seagrass cover

A linear relationship between RENDI and seagrass cover was established using images from a UAV-mounted Micasense RedEdge-MX Dual Camera System (Chapter 5). Seagrass cover maps of two sites in Brisbane Water (Chapter 5) were used to confirm that the relationship between RENDI and seagrass is applicable to Sentinel-2 images. A Sentinel-2 image captured over Brisbane Water on 7 December 2023 was compared to cover maps, produced from UAV surveys on 5 December 2023 (St Huberts Island) and 6 December 2023 (Empire Bay). Cover maps were resampled using bilinear resampling to 20 m to match the Sentinel-2 resolution. Across all pixels in the seagrass meadows, the correlation between resampled percent cover and the RENDI value for the same pixel was measured.

6.2.3 Satellite data filtering and masking

The Sentinel-2 data captures variations caused by environmental conditions separate from changes in seagrass cover, including clouds, variable water level, and turbidity, as well as capturing entire scenes that include land and deep water. This section describes the process of masking land and optically deep water areas, removing cloud from the images, and filtering images based on water level and turbidity at the time of image capture.

6.2.3.1 Masking cloud in Sentinel-2 time series

GEE provides Sentinel-2 images calibrated to surface reflectance (L2A) but are only consistently available from 2019 onwards. Calibration to L2A surface reflectance of earlier Sentinel-2 images acquired over the study areas in 2017 and 2018 was attempted. However significant inconsistencies in calibrated surface reflectance values were found between the manually corrected 2017-2018 images, and the L2A images provided by GEE, therefore the earlier 2017-2018 images were excluded. The time period for this study was 6 years from 1 January 2019 to 31 December 2024.

All images captured over the study sites were filtered based on cloud cover using image metadata, with any images greater than 50% cloud omitted from analysis (Figure 2). The Sentinel Hub S2cloudless method (Zupanc, 2017) was then used to mask cloudy and cloud shadow pixels with a probability greater than 50%.

Figure 2. Flow diagram of full processing workflow applied to filter and mask Sentinel-2 image collection to remove cloud and select low tide and turbidity images, calculate the maximum seagrass area, and generate seasonal composites and seasonally averaged time series.

6.2.3.2 Determining water level at time of image capture

The water level at the time of image capture was required for multiple steps in the image processing workflow (Figure 2). Each image was therefore assigned a water level metadata value based on data from the nearest available water level or tide gauge

(Figure 1). Water level readings were available every 15 minutes, and images were assigned the water level value at the reading time nearest to image capture time. If no readings were available within one hour of satellite image capture, the image was excluded from further analysis.

6.2.3.3 Masking land areas

A median composite image was created for each estuary using only images captured when water level was recorded within the top 10% of all water level measurements at the relevant water level station from 2019-2024 (Figure 2). Modified Normalised Difference Water Index (MNDWI) (Xu, 2006) was calculated for each composite as the normalised difference of green and short-wave infrared reflectance to mask land areas. MNDWI was used due to the effectiveness of this index in distinguishing between water and land while minimising interference from built-up land areas (Xu, 2006). The adaptive thresholding method developed by Donchyts et al. (2016) was applied, which uses edge detection (Canny, 1986) to constrain the calculation of the Otsu threshold (Otsu, 1975), allowing for reliable delineation of boundaries between land and water (Donchyts et al., 2016). This approach uses a buffered area around edges detected based on an initial threshold to ensure that approximately even numbers of water and land pixels are included in the analysis, then calculates the Otsu threshold for the buffered area. Through iterative testing, an initial MNDWI threshold value of –0.2 was identified as appropriate for all estuaries.

6.2.3.4 Masking optically deep waters

A second median composite image was created using the bottom 10% of all observations from the relevant water level station (Figure 2). A binary supervised classification was performed on the median image using a Support Vector Machines classifier (Li et al., 2023), with training data selected based on visual inspection of higher resolution aerial images and SPOT 6 satellite images provided by NSW Department of Primary Industries. The results were visually inspected to confirm that only optically deep areas were masked out.

6.2.3.5 Filtering the time series based on tide and turbidity

It was necessary that all images were captured at low water level with low turbidity and that this was relatively consistent between images. For each estuary, the bottom 30% of all water level observations were selected to ensure sufficient images for analysis whilst maintaining low and consistent water levels between images (Figure 2). The tidal filtering largely constrained images to those captured within a range of ~0.3 m or less, with an interquartile range of ~0.15m or less (Table 1). The exception was Coila Lake where intermittent closure and opening of the estuary mouth led to a large range (0.52 m) and interquartile range (0.20 m) of water level observations.

Table 1. Ranges of water level observations, relative to mean sea level, seen in satellite images for each estuary, after tide and turbidity filtering.

Estuary	Range (m)	75th percentile (m)	25th percentile (m)	Interquartile range (m)
Wallis Lake	0.28	-0.24	-0.39	0.14
Lake Macquarie	0.28	-0.14	-0.23	0.09
Tuggerah Lakes	0.15	0.26	0.22	0.04
Brisbane Water	0.32	-0.04	-0.15	0.11
Lake Illawarra	0.27	0.04	-0.09	0.14
St Georges Basin	0.20	0.09	0.03	0.06
Coila Lake	0.52	0.32	0.13	0.20
Wagonga Inlet	0.31	-0.12	-0.25	0.12
Merimbula Lake	0.19	-0.09	-0.14	0.04

Initial visual inspection found that approximately 20-30% of images at each estuary were impacted by turbidity. To exclude turbidity-impacted images, the Normalised Difference Turbidity Index (NDTI), which correlates with turbidity, was used (Lacaux et al., 2007). For each derived NDTI image, 300 randomly located sample points were generated over deep water areas defined based on the deep water mask. Deep water areas were used so that the sample points would represent general turbidity across the estuary and not be impacted by benthic reflectance. The mean NDTI value was found for the 300 sample points for each image. Though turbidity may be localised in parts of

the estuary in some cases, this method identifies images where overall turbidity is relatively high and low. Based on iterative inspection of outputs, again finding a balance between consistent image results and maintaining enough images in the time series, images within the top 30% of mean NDTI values were eliminated from the analysis (Figure 2). Removing turbid images also eliminated images impacted by sun glint or residual cloud which results in pixels with high NDTI values. Samples of estuary images at different turbidity levels are provided in Appendix G. The final number of available images for time series analysis for each estuary ranged from 37 to 161 images (Table 2).

Table 2. Stages of image filtering for each study site. Each stage of filtering removed images so the final time series consisted only of cloud-free, low-tide, low-turbidity conditions.

Estuary	Total available images	Cloud masked	Tide filtered	All filters
Wallis Lake	449	254	55	37
Lake Macquarie	866	506	106	74
Tuggerah Lakes	876	511	162	106
Brisbane Water	1766	1015	247	161
Lake Illawarra	1725	964	149	106
St Georges Basin	536	313	74	43
Coila Lake	862	498	182	136
Wagonga Inlet	864	498	125	100
Merimbula Lake	866	501	135	102

The remaining images were not temporally consistent throughout the study period. Extended periods of wet and cloudy weather, low tide coinciding with cloud interference, and seasonal biases in turbidity, cloud cover, and water level at time of image capture contributed to gaps in the time series. Images in summer were least common, while those in winter were most common, coinciding with patterns of cloud cover and rainfall in NSW. No case study estuary had cloud-free, low-tide and low-turbidity images available for every season (Table 3). Measuring seasonal variation between estuaries required images representing each season during the study period. This criterion was not met for Wagonga Inlet, with no summer images available for the entire study period (Table 3). Image counts were low in 2022 and in all summers across all sites. Coila Lake and Lake Illawarra also had periods of greater than one year where no images were available. Despite the gaps in the filtered time series, there were sufficient available seasons to produce maps of seagrass variability for each estuary.

Table 3. Images remaining after filtering for each estuary by season. The rightmost column provides a count of seasons with at least one image remaining after cloud masking, tide, and turbidity filters were applied.

Estuary	Summer 2019	Summer 2020	Summer 2021	Summer 2022	Summer 2023	Summer 2024	Autumn 2019	Autumn 2020	Autumn 2021	Autumn 2022	Autumn 2023	Autumn 2024	Winter 2019	Winter 2020	Winter 2021	Winter 2022	Winter 2023	Winter 2024	Spring 2019	Spring 2020	Spring 2021	Spring 2022	Spring 2023	Spring 2024	Available seasons
Wallis Lake	1	0	0	1	1	0	1	1	0	0	2	2	5	4	5	2	5	1	2	2	2	0	0	0	16
Lake Macquarie	4	0	1	1	2	0	5	5	1	0	2	2	10	5	9	5	8	0	2	3	3	1	4	1	20
Tuggerah Lake	3	3	1	0	6	0	0	5	5	0	0	2	0	11	10	4	0	7	1	12	13	7	7	9	17
Brisbane Water	2	2	2	0	4	0	4	9	6	0	5	9	24	10	20	8	18	8	8	7	7	0	8	0	19
Lake Illawarra	0	0	2	4	0	4	0	0	4	0	4	12	0	4	7	4	17	10	0	7	5	3	3	2	16
St Georges Basin	1	0	1	0	0	1	3	3	1	0	0	1	3	6	3	1	3	2	2	3	2	0	2	0	17
Coila Lake	4	0	0	0	0	0	22	19	0	0	0	2	22	16	4	0	4	0	8	0	0	0	12	0	10
Wagonga Inlet	0	0	0	0	0	0	4	8	4	4	3	4	9	6	8	11	6	6	5	2	2	2	2	0	17
Merimbula Lake	0	0	0	0	0	2	2	6	0	0	4	4	10	6	8	7	6	10	4	2	4	6	4	4	17

6.2.4 Index and index time series calculation

Converting the masked and filtered Sentinel-2 time series to estimates of seagrass variability required derivation of RENDI and masking of non-seagrass areas. The 10 m red band from each of the time series images was resampled to 20 m to match the resolution of the red-edge band. The normalised difference of the two 20 m bands was calculated for each image (Chapter 5):

$$\frac{(R_{705} - R_{665})}{(R_{705} + R_{665})}$$

where R_{705} and R_{665} are reflectance values for the first red-edge band (B5) and the red band (B4) respectively.

6.2.4.1 Deriving maximum seagrass extent

Maximum seagrass extent over the study period was derived for each estuary to create a baseline area for calculating seagrass variability (Figure 2). This allowed the variability analysis to include areas which were only vegetated for part of the study period. The maximum possible seagrass extent across the entire study period for each estuary was derived by taking the 90th percentile of all RENDI values, with possible seagrass identified where the index was greater than 0 (the equivalent of the ratio of bands being greater than 1, see Li et al. 2023). The 90th percentile was used rather than the maximum to reduce noise. In some cases, shoreline infrastructure and boats moored in a single location for an extended period resulted in false positive seagrass pixels due to their high reflectance in all bands. Using the 90th percentile layer and high-resolution satellite images, these areas were manually selected and masked out.

6.2.5 Producing composites to assess estuary-scale seasonal patterns

The remaining images, consisting of only those captured in low tide and turbidity conditions with non-seagrass areas masked were used for analysis of seagrass cover variability. Seasonal factors have previously been identified as the primary driver of seagrass variability (Duarte, 1989). To identify comparative differences in seagrass seasonality between estuaries, four seasonal composites were created for each estuary, calculated across the entire study period (i.e. the summer composite was calculated

using all summer images from 2019-2024, etc.). Each of these seasonal composites was derived by calculating the mean RENDI value from all available images for the estuary and corresponding season. Four seasonal composite images were generated for each estuary, aside from Wagonga Inlet where no summer images were available. The distribution of index values present in the seasonal composites was calculated for each estuary, including median index value, low and high percentiles. These data were used to assess whether estuary-scale seasonal patterns were present, and how these patterns differed by study site.

6.2.6 Creating a seasonally averaged time series

6.2.6.1 Producing the time series

A seasonally averaged time series was created for each estuary to analyse seagrass cover variability by taking the mean RENDI for all images with each annual season. Mean values were considered representative, as outliers were removed through the extensive masking process. Seasonal compositing could have produced a possible 24 composites for each estuary, however, some estuaries did not have available images for all seasons and therefore the actual number of composites by estuary ranged from 10 to 20 (Table 4).

6.2.6.2 Calculating mean index and index variability values

Non-seagrass areas were masked out from each composite using the maximum seagrass extent image derived above for each estuary. The masked seasonally averaged time series were used for comparing variability within estuaries over the study period. Mean and standard deviation of the red-edge normalised difference index over the seasonally averaged time series were calculated on a per-pixel basis. This produced two output layers per estuary, representing mean RENDI response and variability in RENDI response. These data layers represent seagrass cover and cover variability respectively, though the former is confounded by differences in index response over depth gradients.

6.2.6.3 Assessing geomorphological patterns in seagrass cover variability

To consider the influence of local geomorphology and sedimentological environment, zonal statistics were calculated for the seagrass variability within estuarine geomorphic

facies (Dyall et al., 2018). Five geomorphic facies in the studied estuaries overlaid with mapped seagrass area: channel, central basin, fluvial (bay-head) delta, ebb- and flood-tide delta, and intertidal flats. Based on the geomorphic typology (Dyall et al. 2018), this method was used to examine the relationship between environmental conditions associated with each geomorphic facies and variability in seagrass growth.

6.2.6.4 Case studies

The output maps and zonal statistics were analysed to identify geographic patterns in variability within estuaries. These datasets were used in a series of three case studies to assess the benefit of considering variability in seagrass cover over time in addition to extent and cover captured in static mapping. The case studies represented three different examples of patterns of seagrass variability drawn from the data, at Tuggerah Lakes, Brisbane Water, and Lake Illawarra. Tuggerah Lakes was selected for case study due to distinct geographical patterns in the seagrass cover and cover variability datasets. Brisbane Water was selected as it was already established that different parts of the estuary underwent different degrees of change in 2023 (Chapter 4). Lake Illawarra was selected because of known significant change in seagrass cover which occurred during the study period.

6.3 Results

6.3.1 Index validation

RENDI values calculated from the Sentinel-2 image captured on 7 December 2023 showed a significant positive relationship with the UAV-derived seagrass cover maps for both sites (Figure 3).

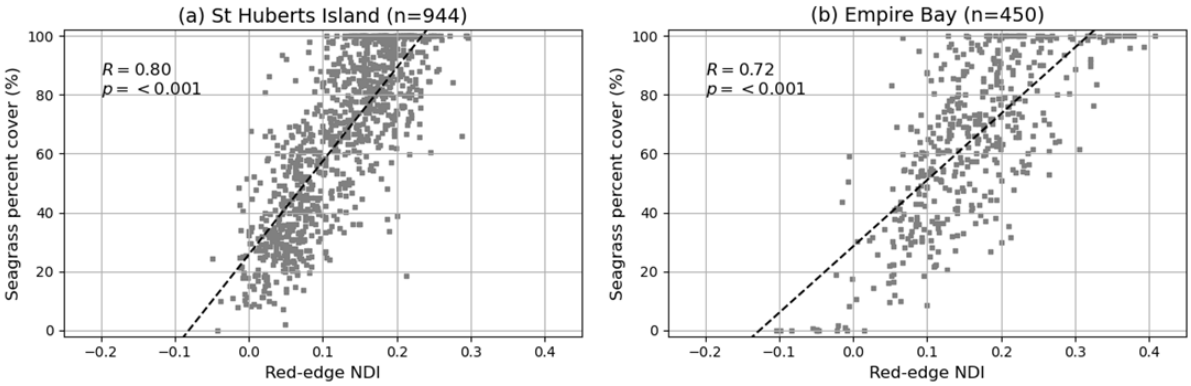

Figure 3. Relationship between Sentinel-2 derived red-edge normalised difference index and percent cover for (a) St Huberts Island and (b) Empire Bay, Brisbane Water NSW.

The relationship was slightly stronger for St Huberts Island (R = 0.80, p<0.001) than for Empire Bay (R = 0.72, p<0.001). RENDI values vary somewhat for a given cover level but are more widely spread in the Empire Bay results, especially at high cover levels. The correlation of the Sentinel-2 derived RENDI with seagrass cover is comparable to UAV-captured images without application of water column correction (see appendix F) and demonstrates that seagrass cover can be predicted from Sentinel-2 images.

6.3.2 Comparing seasonal variation between estuaries

The distribution of RENDI values was summarised by season, for each estuary, (Figure 4) to determine potential differences in RENDI values at an estuary scale, as well as the full range and distribution of RENDI values at each estuary.

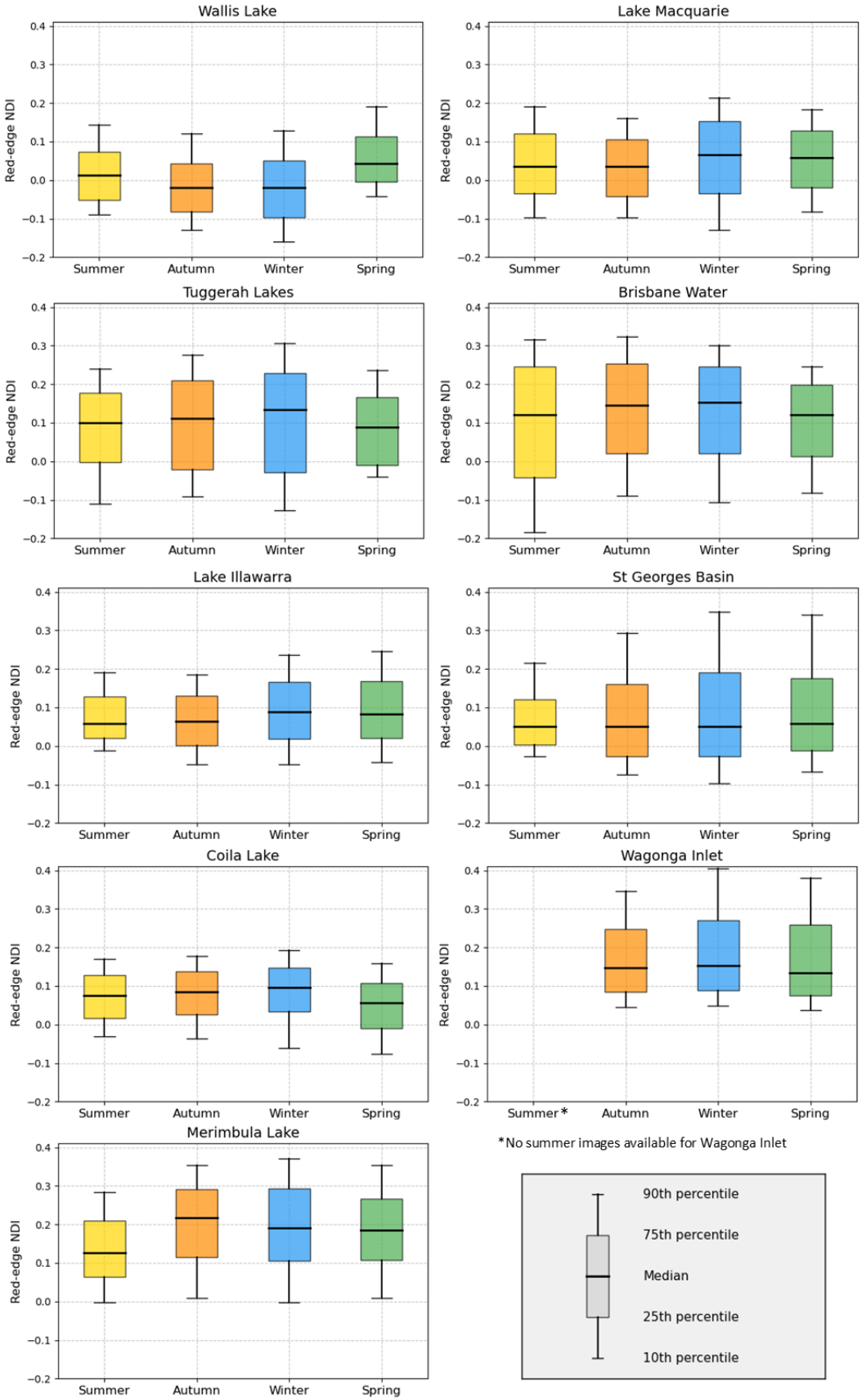

Figure 4. Estuary scale seasonality of seagrass derived from red-edge normalised difference index seasonal composites. A summer seasonal composite for Wagonga Inlet was not available.

Most estuaries did not exhibit an obvious seasonal pattern. The results for Wallis Lake and Merimbula Lake indicate slight seasonal patterns, though the difference in RENDI values between highest and lowest season is only 0.05 for Wallis Lake and 0.1 for Merimbula Lake. For Wallis Lake (the northernmost site), the RENDI was highest in spring, followed by summer, autumn, then winter. RENDI values were highest in winter at Lake Macquarie, Tuggerah Lakes, Brisbane Water, Lake Illawarra, Coila Lake, and Wagonga Inlet, though in all cases the spread of values overlapped considerably with other seasons, and winter was not considered to be a seasonal peak. At St Georges Basin, RENDI values were highest in spring by a very small margin over winter. Merimbula Lake, the southernmost site, saw a peak in RENDI values in autumn, with summer values being substantially lower.

6.3.3 Comparing variability across geomorphic zones

Seagrass cover variability differed across geomorphic zones, with intertidal flats and fluvial deltas tending to show the lowest variability (Figure 5). Both of these geomorphic zones were the least variable zone at all estuaries except Lake Macquarie. The channel and central basin geomorphic zones showed the highest variability at all sites except Tuggerah Lakes. Overall, variability was lowest for intertidal flats, followed by fluvial deltas, ebb- and flood-tide deltas, channels, and basins.

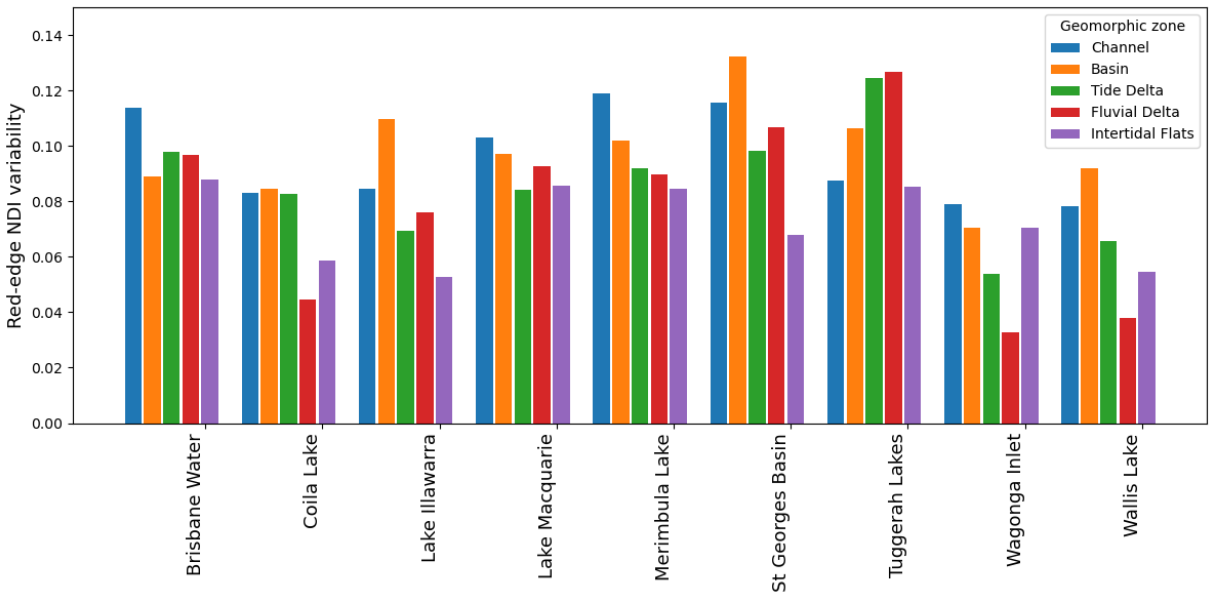

Figure 5. Average seagrass percent cover variability calculated for each geomorphic zone in each NSW estuary.

6.3.4 Seagrass variability across key estuaries

Three case studies were used to provide insight into the potential advantage of mapping spatiotemporal variability in seagrass over static maps of extent or seagrass cover. These case studies highlight different patterns of seagrass spatiotemporal variability that can be determined from the dataset produced in this chapter. RENDI and variability maps for the other six estuaries are provided in Appendix H.

6.3.4.1 Tuggerah Lakes

Tuggerah Lakes, located approximately 90 km north of Sydney, is a series of connected lagoons intermittently open to the ocean in the southern, largest lagoon, which is in turn connected to two northern lagoons. Large *Z. capricorni* meadows are present on the delta and intertidal flats surrounding the entrance, the fluvial deltas on the western side of the estuary, and a large, sheltered area in the central lagoon, which is largely exposed at low tide but classified as central basin the geomorphological facies dataset. Much of the shoreline is also fringed by narrow seagrass meadows. Figure 6 shows the mean RENDI and variability maps for Tuggerah Lakes.

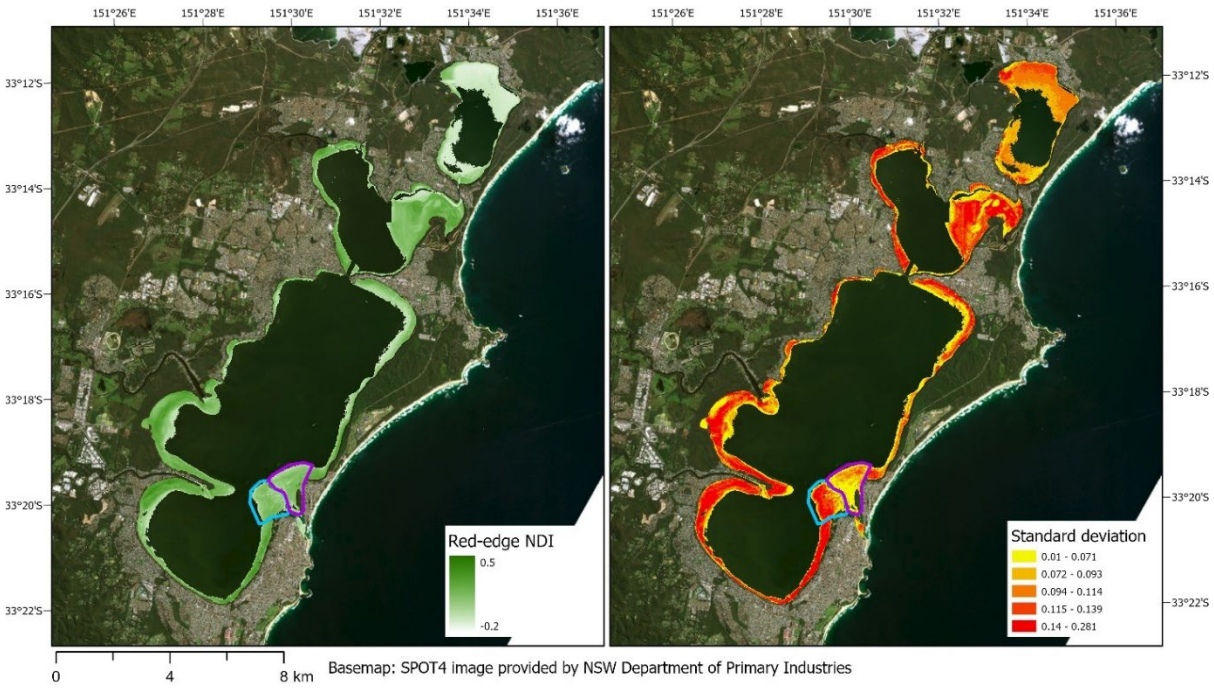

Figure 6. Maps of mean red-edge normalised difference index (RENDI) and standard deviation over the time series for Tuggerah Lakes. RENDI is visualised as a continuous scale between -0.2 and 0.5. Standard deviation is

visualised in quintiles. The northern area of interest is outlined by a magenta polygon and the southern area of interest is outlined by a blue polygon.

Distinct spatial patterns were evident in the maps (Figure 6) and the geomorphic zonation data (Figure 5). The entrance supports seagrass meadows of similar average density on either side in close proximity to each other, but in different geomorphic zones. The southern side of the entrance, a tidal delta, shows higher variability than the northern side, comprising intertidal flats that are more sheltered from tidal current on the leeward side of Terilbah Island. The seasonally averaged time series shows similar trajectories for these two parts of the site, but the magnitude of variation is greater for the southern side of the entrance than for the northern side (Figure 7).

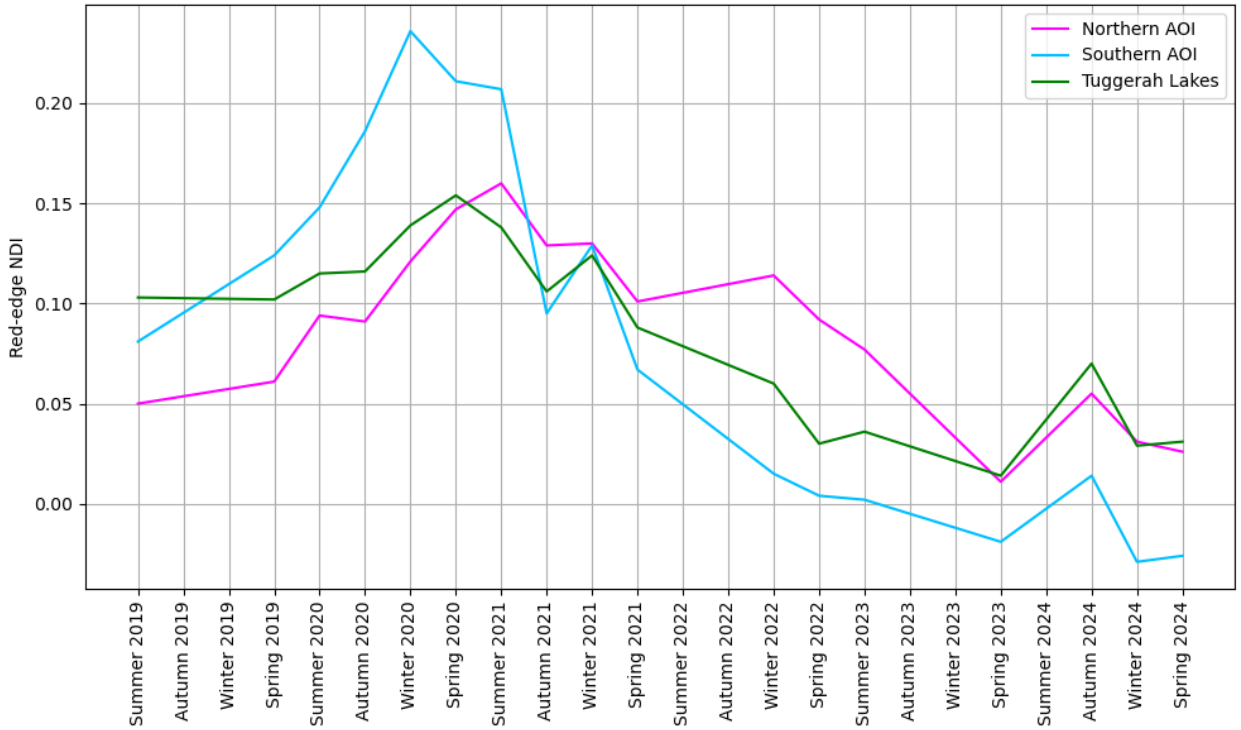

Figure 7. Red-edge normalised difference index time series for selected areas of interest at Tuggerah Lakes. Lines represent time series for the northern AOI, the southern AOI, and the entire estuary. See Figure 6 for area of interest boundaries.

The fluvial deltas on the western side of the estuary support small seagrass areas that demonstrate high variability in percent cover, where patches of seagrass have died off and regrown during the study period. The highest variability in seagrass growth occurs around the shoreline in the south of the estuary, generally decreasing northwards away from the entrance. In the large seagrass meadow within the central lagoon, has

undergone significant change, aside from some small patches which have maintained consistently low seagrass cover across the entire 6-year study period.

6.3.4.2 Brisbane Water

Brisbane Water is an open, wave-dominated estuary about 40 km north of Sydney. The estuary consists of a relatively narrow channel, featuring large intertidal and subtidal seagrass meadows, which opens into a large basin. To the east of the channel is Empire Bay and Kincumber Broadwater, connected to the rest of the estuary by a secondary, narrow channel behind two islands, Rileys and St Huberts Island. Like Tuggerah Lakes, much of the shoreline is fringed by seagrass. Although RENDI values are reasonably consistent across the estuary, variability differs considerably between the central and eastern arms of the estuary (Figure 8).

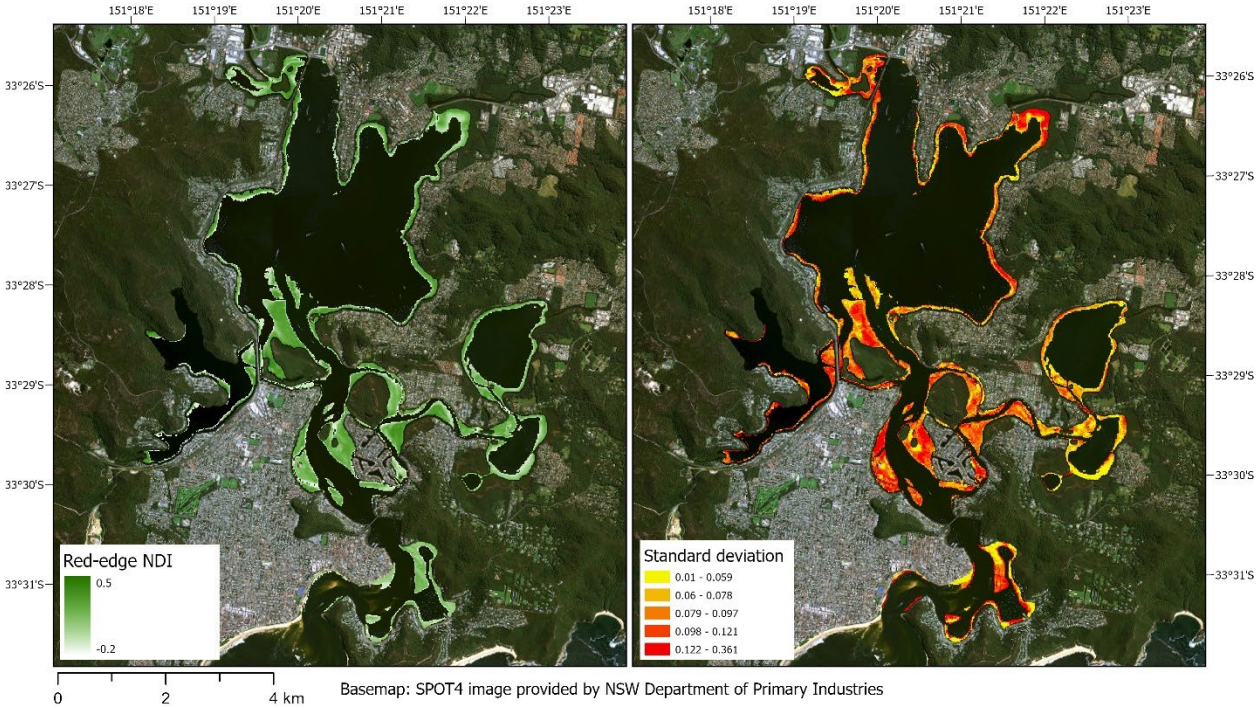

Figure 8. Maps of mean red-edge normalised difference index (RENDI) and standard deviation over the time series for Brisbane Water. RENDI is visualised as a continuous scale between -0.2 and 0.5. Standard deviation is visualised in quintiles.

Though there is little difference in variability between geomorphic facies at Brisbane Water (Figure 5), the map of seagrass variability shows a clear geographical pattern in seagrass variability. Average RENDI values are largely consistent across most seagrass meadows, but the meadows along the main channel and in the large basin exhibit higher variability than those to the east of Rileys and St Huberts Islands. Though no detailed

model of energy within the estuary is available, the eastern arm of the estuary is more sheltered and likely less exposed.

6.3.4.3 Lake Illawarra

Lake Illawarra is a wave-dominated barrier estuary about 100 km south of Sydney. Three large areas of seagrass are present across the tide delta, two small bays in the southwest of the estuary, and the mud flat on the landward side of the barrier (Figure 9). The mud flat on the eastern side of the estuary is classified in the geomorphic zonation mapping data as part of the central basin.

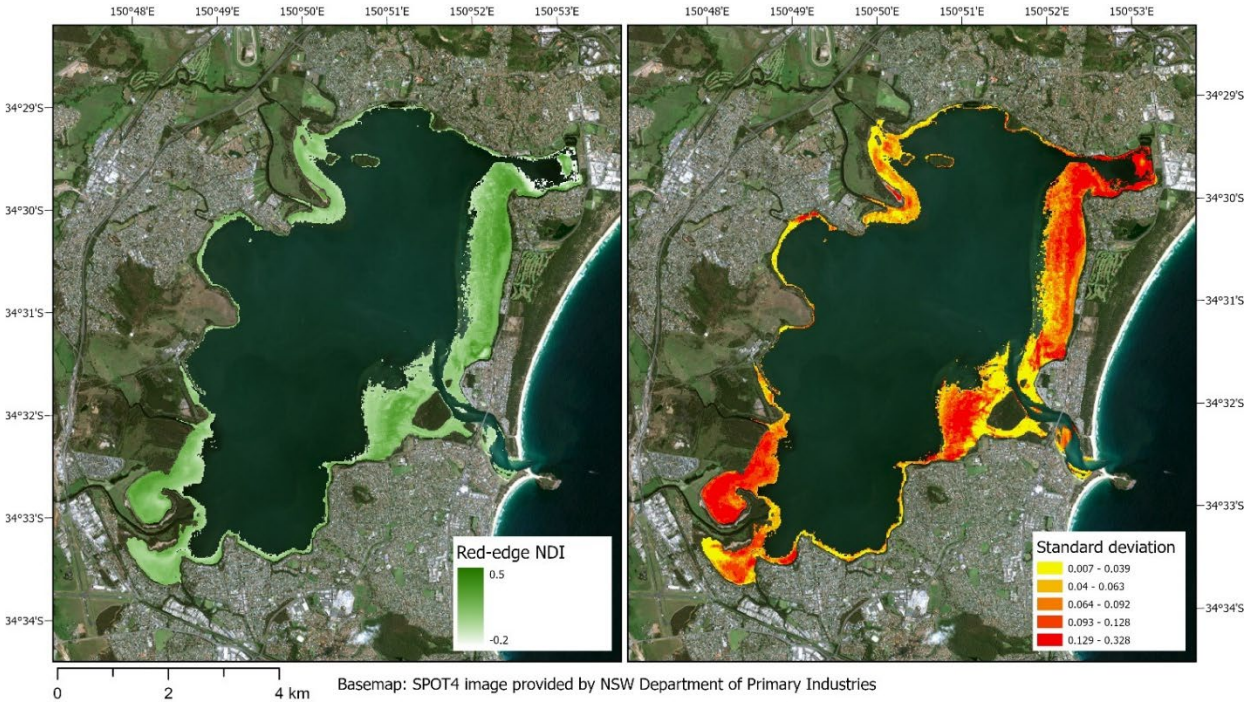

Figure 9. Maps of mean red-edge normalised difference index (RENDI) and standard deviation over the time series for Lake Illawarra. RENDI is visualised as a continuous scale between -0.2 and 0.5. Standard deviation is visualised in quintiles.

This site is notable for the significant weather events over the 6-year study period. A series of rainfall events in 2024 led to high volumes of sediment deposition over the seagrass in Lake Illawarra (Costa, pers. comm. 6/11/2024). This is reflected in the seasonally averaged time series, as RENDI values decreased significantly over the entire estuary through 2023 and 2024 (Figure 10).

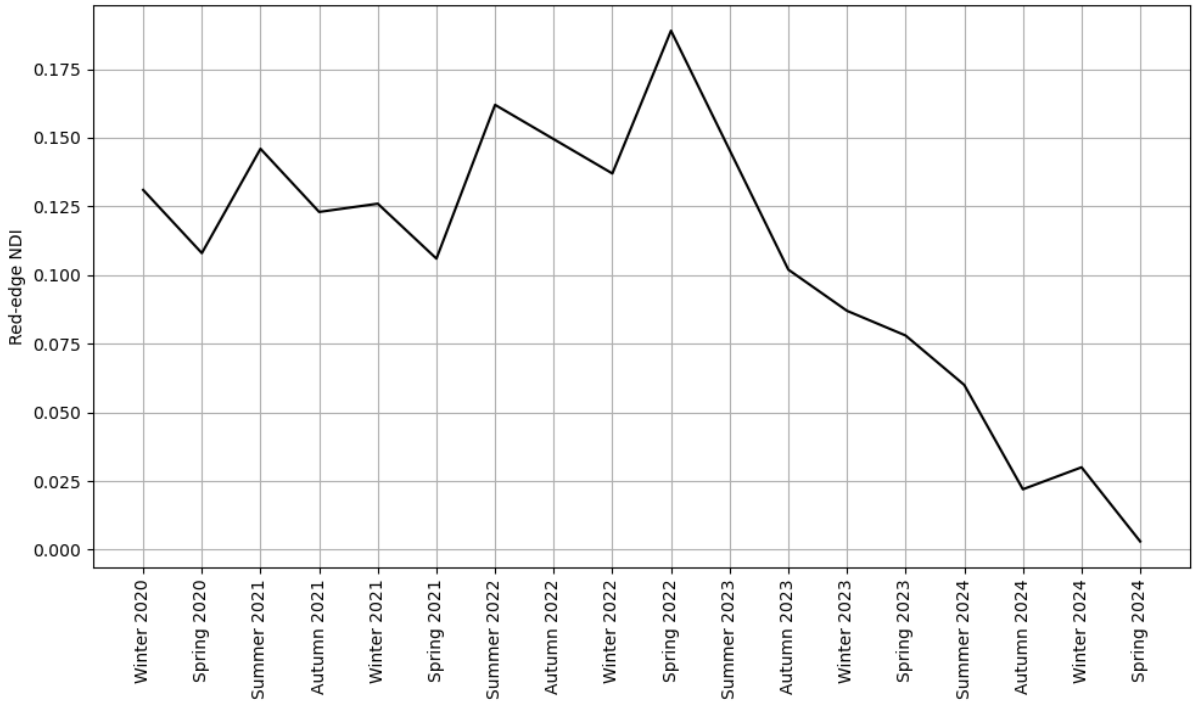

Figure 10. Average seagrass red-edge normalised difference index over the time series for Lake Illawarra, showing a substantial decline through 2023 and 2024.

The seagrass variability map appears to capture this, with high variability across much of the eastern seagrass meadow, highest towards the north of this meadow. High variability can also be seen in parts of the southwestern corner and the tidal delta. Only small areas of seagrass exhibit low variability, in the northwestern fluvial delta, the southwestern corner, and around the entrance.

6.4 Discussion

Seagrass mapping based on RENDI derived from Sentinel-2 data can be used to measure spatio-temporal variability in seagrass growth across estuarine environments. This method enabled comparison of the variability of seagrass cover within estuaries, across different geomorphic zones and parts of the estuary. Understanding seagrass cover variability is valuable for blue carbon assessments because more stable seagrass meadows tend to host higher carbon stocks (Mazarassa et al. 2018). Estuary-scale seasonal patterns were not detected at most sites in NSW over the six-year time series. Higher seagrass variability may therefore be attributed to other factors, such as greater wave energy or exposure to disturbance. Though spatial data showing overall wave energy and human activity were not available, differences in variability across the

estuaries may be able to be explained by these factors, and geographical differences in seagrass cover variability suggest this. Geomorphic zonation data, which broadly represent different hydrological and sedimentary environments across the estuaries, partly supports this by demonstrating that seagrass variability relates to hydrological regime in some circumstances. This may suggest a relationship between geomorphic zonation and expected carbon stock.

Maps of seagrass variability provide valuable information for blue carbon projects, as they highlight areas where carbon stocks may be expected to be higher due to lower variability (Mazarrasa et al., 2018, Stankovic et al., 2021, Bijak et al., 2023). Additionally, they provide information for estuary managers by highlighting areas which may be more prone to disturbance and therefore require interventions such as localised prevention of boat damage or strategic restoration (Cullen-Unsworth et al., 2016).

The RENDI, even without water column correction, was shown to correlate with estimates of seagrass percent cover derived from UAV images (R = 0.72-0.80). Large-scale prediction of seagrass cover using RENDI calculated without water column correction is not viable due to the confounding effect of differing water depths between pixels. However, with water depth and optical properties controlled by filtering for turbidity and tide, variability of RENDI values in a single pixel, which does not vary in depth otherwise than with tide, can be related to seagrass cover variability. A possible limitation is the saturation of the index, leading to a large spread of RENDI values representing 100% cover, especially in the Empire Bay validation data. This is a likely explanation for the tendency for variability to be higher in high cover areas, as seen in the case study maps. Performing water column correction on seasonal mean images is challenging as there is no single set of coefficients which describe the depth and optical properties of the water. However, the limited range of water levels and selection of low-turbidity images maximises the capacity to attribute variability in the RENDI to seagrass cover variability. Ideally, this index would be tested in different locations, and in the same locations at different times during the study period to confirm that temporal variations in RENDI correspond to temporal variations in seagrass cover, however this was not possible due to a lack of required field data.

Previous field studies of above-ground biomass in *Zostera capricorni*, the dominant species in all studied estuaries except Merimbula Lake, show inconsistent seasonal patterns, this is partly attributed to latitude. In Port Hacking, NSW, two years of surveys showed multiple biomass peaks, in January, May and September (Kirkman et al., 1982). Field studies in subtropical Moreton Bay, Queensland by Boon (1986) reported a maximum biomass in May (Austral late autumn), while in tropical environments *Zostera* meadows have been found to have a peak biomass more consistently in October-November and reach a minimum in June-July (McKenzie, 1994). In temperate New Zealand *Z. capricorni* meadows, significant biomass peaks have been identified in summer (Turner, 2007), though this is not consistent across New Zealand estuaries, and meadows can show larger differences in biomass between years than between seasons (Turner and Schwarz, 2006). Geographical and interannual differences in peak *Z. capricorni* biomass highlight the importance of techniques, such as that demonstrated here, which can detect spatiotemporal differences in biomass variability.

The northernmost estuary, Wallis Lake, appears to show higher seagrass cover in Spring than other seasons. Wallis Lake is further north than the other studied estuaries (32.2° S, compared to 33.1-36.9° S), and this may be attributable to subtropical conditions. However, findings for the other eight estuaries do not suggest consistent seasonal patterns in seagrass cover between 2019 and 2024. There are numerous possible explanations for this. The seagrass in these areas may not exhibit seasonal patterns or inconsistent conditions over the six-year time series may mean trends are not apparent in this dataset. There may also be seasonal variations too minor to be detected, or natural variations in biomass that are not restricted to seasons. Given the wide variety of seasonal patterns observed in field studies of *Z. capricorni* meadows, and the lack of consistent seasonal patterns identified in this study, consideration should be given to other factors that shape seagrass biomass variability.

Variability in seagrass biomass can be tied to environmental factors and anthropogenic disturbance. There is a complex relationship between light availability, mediated by tidal exposure and turbidity, and seagrass biomass. While turbid or deep water limits photosynthesis and can reduce seagrass biomass (Giesen et al., 1990), seagrass can situationally be adapted to high turbidity conditions (McKenzie, 1994), and extended

periods of tidal exposure can also lead to loss of seagrass biomass through desiccation (McKenzie, 1994, Unsworth et al., 2012). Further, the impacts of turbidity fluctuations on seagrass cover may be delayed by several months (Neverauskas, 1988) and depends on the season in which high turbidity events occur (Wong et al., 2020). The complexity of this relationship may explain the lack of consistent seasonal patterns, especially in temperate areas where temperature and sunlight are more variable and rainfall is distributed more evenly throughout the year. Estuary-wide patterns of seagrass variability, like those seen at Lake Illawarra, are best explained by turbidity events that limit light availability. In this case, the lowest variability was seen in the shallow western parts of the estuary, where turbidity may have a less significant effect and dense stands of seagrass can reduce desiccation by retaining water (McKenzie, 1994).

Higher wave energy has been shown to be related to higher variability in seagrass biomass in some locations (Erftemeijer and Herman, 1994), though other work has found that both sheltered and highly exposed meadows show lower variability than intermediate energy meadows (El-Hacen et al., 2019). Changes in wave energy can cause transitions between stable states, forming dense meadows in low energy environments and fragmented patches in high energy environments (Uhrin and Turner, 2018). In NSW barrier estuaries, which are generally low energy overall (Kench, 1999), this may be expressed as a gradient of increasing stability towards more sheltered areas. In Brisbane Water, an apparent gradient of lower seagrass variability was seen towards the more sheltered eastern parts of the estuary, while at Tuggerah Lakes the southernmost lagoon, connected directly to the ocean and therefore exposed to be higher energy conditions, showed the highest variability. In the absence of hydrodynamic modelling, the relationship between energy and seagrass variability cannot be confirmed, but the geographical patterns in seagrass variability shown in these findings suggest that a potential relationship warrants further investigation.

Disturbances can also lead to variation in seagrass cover, especially when a disturbance is large enough to lead to autocatalytic collapse (Swadling et al., 2023). Episodic natural disturbances such as storms cause sudden increases in energy even in low-energy estuarine environments, leading to rapid rearrangement of sediment (Vila-Concejo et al., 2010), and potentially, burying of seagrass, leading to the general estuary-wide

decrease in seagrass cover seen in Lake Illawarra. Repeated anthropogenic disturbance could partly explain the higher variability seen in the central part of Brisbane Water, where higher boat traffic leads to more direct damage to the seagrass meadow than the sheltered Empire Bay seagrass bed (Simpson et al., 2024; Chapter 4). However, without more detailed analysis of individual events, it is not possible to draw conclusions about the relationship between disturbances, both natural and anthropogenic, and seagrass variability.

Geomorphic zonation potentially explains differences in seagrass variability. In most estuaries, intertidal flats showed the lowest variability, followed by fluvial deltas. Intertidal flats represent relatively low energy environments, as shallow water dissipates waves, and tidal variation leads to waves being distributed across the tidal range (Harris and Heap, 2003). As energy varies along estuaries and fluvial deltas are generally located at the landward side of the estuary, fluvial deltas would be expected to experience lower wave energy (Skilbeck et al., 2017). The apparent relationship between geomorphic zonation and seagrass variability is clearly shown in Tuggerah Lakes, where the seagrass on the northern side of the entrance, sheltered by Terilbah Island and classified as intertidal flats, shows considerably lower variability than the unsheltered tidal delta immediately to the south. Intertidal flats and fluvial deltas represent muddier and more stable sedimentary environments than other geomorphic zones (Roy et al., 2001). Geomorphic zonation also shapes sediment nutrient content (Kench, 1999, Bruce et al., 2011), which strongly influences seagrass growth (Short, 1987). Given the importance of sedimentation for seagrass C_{org} stocks (Oreska et al., 2018), the significant differences in seagrass carbon stocks within estuaries (Ricart et al., 2020), and the observed differences in seagrass habitat stability across geomorphic zones, geomorphic zonation may be a useful proxy for identifying seagrass meadows with higher carbon stock and sequestration potential.

Though this work provides valuable insight into differences in seagrass variability across NSW estuaries, untangling the processes that shape this is challenging. These patterns are reflected somewhat in the geomorphic facies data and the geography of Brisbane Waters and Tuggerah Lakes, however, geomorphology alone is insufficient to explain these differences. There may be other, finer scale factors affecting seagrass cover

variability, or the geomorphic zonation data may lack the resolution to capture features (Grech and Coles, 2010). A more detailed analysis of the drivers of seagrass variability within a local context is required to understand the role of geomorphic setting. Further relating this to carbon stores presents an additional challenge, though the depositional environment may influence carbon storage, it is not a reliable predictor (Mazarrasa et al., 2021).

The presence of seagrass has been presumed in many areas based on the measured RENDI values and previous seagrass mapping work (Li et al., 2023). This approach may have excluded areas of seagrass which are too sparse or deep for the RENDI value to exceed 0. Future work to correct the effects of water column interference directly may allow for detection of sparse or deeper seagrass. Difficulty of detecting deeper seagrass is an inherent physical limitation on the use of RENDIs, though this is a relatively minor issue in NSW, where most seagrass grows in shallow water. The methods described in this chapter could not be applied in many areas, such as deep-water tropical seagrass beds. The presence of macroalgae may be an additional confounding factor for the approach demonstrated here, absent ground truth data. It has been established that submerged macroalgae would produce RENDI values similar to those produced by seagrass, due to their similar reflectance properties (Timmer et al., 2022). However, based on the author's knowledge of the field site and the existing extent data on estuarine macrophytes, it is not believed that macroalgae had a significant impact on the results of this study.

Remote sensing provides an overview of geographical differences in seagrass variability within estuaries. However, the approach shown here only quantifies variability, and cannot distinguish between different types of variability. Analysis of trends in seagrass cover change could provide further insight into what may be driving variability, such as identifying periodic variation as opposed to shifts in seagrass habitat state. As this approach relies upon red-edge reflectance data, the analysis is limited to the period since satellite data with red-edge bands became available. Sensors with long archives of data, most notably Landsat ETM+ and OLI, are not applicable for the RENDI approach, preventing characterisation of longer-term variability. Extending the period of this

analysis as the Sentinel-2 image archive expands would enable further exploration of the link between seagrass variability and the processes discussed.

6.5 Conclusions

Seagrass is an ecologically important species in estuarine environments and can exhibit high variability under certain conditions which vary at a local scale. Capturing patterns and differences in seagrass variability is challenging. This pilot study has demonstrated the viability of using satellite remote sensing data and cloud geoprocessing to detect variability in seagrass cover. The RENDI has been demonstrated to correlate with seagrass cover, though it may be impacted by water depth or water column constituents. Accounting for water level and turbidity at the time of image capture, even with relatively simple methods, assures that differences in RENDI variability can be attributed to differences in seagrass variability. Understanding local differences in seagrass variability may improve modelling of carbon storage and sequestration, as well as supporting site selection for blue carbon projects, providing information which is not captured in single-date seagrass extent or cover mapping.

References

BIJAK, A. L., REYNOLDS, L. K. & SMYTH, A. R. 2023. Seagrass meadow stability and composition influence carbon storage. *Landscape Ecology,* 38**,** 4419-4437.

BOON, P. 1986. Nitrogen pools in seagrass beds of Cymodocea serrulata and Zostera capricorni of Moreton Bay, Australia. *Aquatic Botany,* 25**,** 1-19.

BRUCE, E., BRUCE, L. & COWELL, P. Incorporating geomorphic zonation in nutrient models for coastal-estuarine environments: coupling GIS and aquatic ecosystem modeling. 19th International Congress on Modelling and Simulation: Sustaining our future: understanding and living with uncertainty, 2011. 1867-1873.

CABAÇO, S., MACHÁS, R. & SANTOS, R. 2007. Biomass–density relationships of the seagrass Zostera noltii: a tool for monitoring anthropogenic nutrient disturbance. *Estuarine, Coastal and Shelf Science,* 74**,** 557-564.

CANNY, J. 1986. A computational approach to edge detection. *IEEE Transactions on pattern analysis and machine intelligence***,** 679-698.

CLAUSEN, K. K., KRAUSE-JENSEN, D., OLESEN, B. & MARBÀ, N. 2014. Seasonality of eelgrass biomass across gradients in temperature and latitude. *Marine Ecology Progress Series,* 506**,** 71-85.

CULLEN-UNSWORTH, L. C., UNSWORTH, R. K. & FRID, C. 2016. Strategies to enhance the resilience of the world's seagrass meadows. *Journal of Applied Ecology,* 53**,** 967-972.

DONCHYTS, G., SCHELLEKENS, J., WINSEMIUS, H., EISEMANN, E. & VAN DE GIESEN, N. 2016. A 30 m resolution surface water mask including estimation of positional and thematic differences using landsat 8, srtm and openstreetmap: a case study in the Murray-Darling Basin, Australia. *Remote Sensing,* 8**,** 386.

DUARTE, C. M. 1989. Temporal biomass variability and production/biomass relationships of seagrass communities. *Marine ecology progress series. Oldendorf,* 51**,** 269-276.

DUARTE, C. M., APOSTOLAKI, E. T., SERRANO, O., STECKBAUER, A. & UNSWORTH, R. K. 2025. Conserving seagrass ecosystems to meet global biodiversity and climate goals. *Nature Reviews Biodiversity***,** 1-16.

DYALL, A., TOBIN, G., GALINEC, V., CREASEY, J., GALLAGHER, J., RYAN, D. A., HEAP, A. D. & MURRAY, E. 2018. New South Wales Coastal Waterways Geomorphic Habitat Mapping, Version 2 (1:100 000 scale digital data).

DYE, A. 2006. Is geomorphic zonation a useful predictor of patterns of benthic infauna in intermittent estuaries in New South Wales, Australia? *Estuaries and Coasts,* 29**,** 455-464.

EL-HACEN, E.-H. M., BOUMA, T. J., GOVERS, L. L., PIERSMA, T. & OLFF, H. 2019. Seagrass Sensitivity to Collapse Along a Hydrodynamic Gradient: Evidence from a Pristine Subtropical Intertidal Ecosystem. *Ecosystems,* 22**,** 1007-1023.

ERFTEMEIJER, P. L. & HERMAN, P. M. 1994. Seasonal changes in environmental variables, biomass, production and nutrient contents in two contrasting tropical intertidal seagrass beds in South Sulawesi, Indonesia. *Oecologia,* 99**,** 45-59.

FOURQUREAN, J. W., DUARTE, C. M., KENNEDY, H., MARBÀ, N., HOLMER, M., MATEO, M. A., APOSTOLAKI, E. T., KENDRICK, G. A., KRAUSE-JENSEN, D. & MCGLATHERY, K. J. 2012. Seagrass ecosystems as a globally significant carbon stock. *Nature geoscience,* 5**,** 505-509.

GIESEN, W., VAN KATWIJK, M. & DEN HARTOG, C. 1990. Eelgrass condition and turbidity in the Dutch Wadden Sea. *Aquatic Botany,* 37**,** 71-85.

GORELICK, N., HANCHER, M., DIXON, M., ILYUSHCHENKO, S., THAU, D. & MOORE, R. 2017. Google Earth Engine: Planetary-scale geospatial analysis for everyone. *Remote sensing of Environment,* 202**,** 18-27.

GRECH, A. & COLES, R. 2010. An ecosystem-scale predictive model of coastal seagrass distribution. *Aquatic Conservation: marine and freshwater ecosystems,* 20**,** 437-444.

HARRIS, P. T. & HEAP, A. D. 2003. Environmental management of clastic coastal depositional environments: inferences from an Australian geomorphic database. *Ocean & Coastal Management,* 46**,** 457-478.

JAMES, R. K., CHRISTIANEN, M. J. A, VAN KATWIJK, M. M., DE SMIT, J. C., BAKKER, E. S., HERMAN, P. M. J. & BOUMA, T. J. 2020. Seagrass coastal protection services reduced by invasive species expansion and megaherbivore grazing. *Journal of Ecology,* 108, 2025-2037

KENCH, P. S. 1999. Geomorphology of Australian estuaries: review and prospect. *Australian Journal of Ecology,* 24**,** 367-380.

KERR, E. & STROTHER, S. 1990. Seasonal changes in standing crop of Zostera muelleri in south-eastern Australia. *Aquatic Botany,* 38**,** 369-376.

KIRK, J. T. 1994. *Light and photosynthesis in aquatic ecosystems*, Cambridge university press.

KIRKMAN, H., COOK, I. & REID, D. 1982. Biomass and growth of Zostera capricorni aschers. in port hacking, NSW, Australia. *Aquatic Botany,* 12**,** 57-67.

LACAUX, J., TOURRE, Y., VIGNOLLES, C., NDIONE, J. & LAFAYE, M. 2007. Classification of ponds from high-spatial resolution remote sensing: Application to Rift Valley Fever epidemics in Senegal. *Remote sensing of environment,* 106**,** 66-74.

LARKUM, A. 1976. Ecology of Botany Bay. I. Growth of Posidonia australis (Brown) Hook. f. in Botany Bay and other bays of the Sydney basin. *Marine and Freshwater Research,* 27**,** 117-127.

LI, Y., BAI, J., CHEN, S., CHEN, B. & ZHANG, L. 2023. Mapping seagrasses on the basis of Sentinel-2 images under tidal change. *Marine Environmental Research,* 185**,** 105880.

LIRMAN, D. & CROPPER, W. P. 2003. The influence of salinity on seagrass growth, survivorship, and distribution within Biscayne Bay, Florida: field, experimental, and modeling studies. *Estuaries,* 26**,** 131-141.

MACREADIE, P. I., TREVATHAN-TACKETT, S. M., SKILBECK, C. G., SANDERMAN, J., CURLEVSKI, N., JACOBSEN, G. & SEYMOUR, J. R. 2015. Losses and recovery of organic carbon from a seagrass ecosystem following disturbance. *Proceedings of the Royal Society B: Biological Sciences,* 282**,** 20151537.

MACREADIE, P. I., YORK, P. H., SHERMAN, C. D. H., KEOUGH, M. J., ROSS, D. J., RICART, A. M. & SMITH, T. M. 2014. No detectable impact of small-scale disturbances on 'blue carbon' within seagrass beds. *Marine Biology,* 161**,** 2939-2944.

MATHESON, F. & SCHWARZ, A.-M. 2007. Growth responses of Zostera capricorni to estuarine sediment conditions. *Aquatic Botany,* 87**,** 299-306.

MAZARRASA, I., LAVERY, P., DUARTE, C. M., LAFRATTA, A., LOVELOCK, C. E., MACREADIE, P. I., SAMPER-VILLARREAL, J., SALINAS, C., SANDERS, C. J. & TREVATHAN-TACKETT, S. 2021. Factors determining seagrass blue carbon across bioregions and geomorphologies. *Global Biogeochemical Cycles,* 35**,** e2021GB006935.

MAZARRASA, I., SAMPER-VILLARREAL, J., SERRANO, O., LAVERY, P. S., LOVELOCK, C. E., MARBÀ, N., DUARTE, C. M. & CORTÉS, J. 2018. Habitat characteristics provide insights of carbon storage in seagrass meadows. *Marine pollution bulletin,* 134**,** 106-117.

MCKENZIE, L. J. 1994. Seasonal changes in biomass and shoot characteristics of a Zostera capricorni Aschers. dominant meadow in Cairns Harbour, northern Queensland. *Marine and Freshwater Research,* 45**,** 1337-1352.

NEVERAUSKAS, V. 1988. Response of a Posidonia community to prolonged reduction in light. *Aquatic Botany,* 31**,** 361-366.

NSW DEPARTMENT OF PRIMARY INDUSTRIES. 2023. NSW Estuarine Macrophytes 2023.

ORESKA, M. P., WILKINSON, G. M., MCGLATHERY, K. J., BOST, M. & MCKEE, B. A. 2018. Non-seagrass carbon contributions to seagrass sediment blue carbon. *Limnology and Oceanography,* 63**,** S3-S18.

OTSU, N. 1975. A threshold selection method from gray-level histograms. *Automatica,* 11**,** 23-27.

PHINN, S., ROELFSEMA, C., KOVACS, E., CANTO, R., LYONS, M., SAUNDERS, M. & MAXWELL, P. 2018. Mapping, monitoring and modelling seagrass using remote sensing techniques. *Seagrasses of Australia: Structure, ecology and conservation***,** 445-487.

RICART, A. M., YORK, P. H., BRYANT, C. V., RASHEED, M. A., IERODIACONOU, D. & MACREADIE, P. I. 2020. High variability of Blue Carbon storage in seagrass meadows at the estuary scale. *Scientific reports,* 10**,** 5865.

ROCHFORD, D. 1959. Classification of Australian estuarine systems. *Archives of Oceanography and Limnology,* 11**,** 171-177.

ROY, P., WILLIAMS, R., JONES, A., YASSINI, I., GIBBS, P., COATES, B., WEST, R., SCANES, P., HUDSON, J. & NICHOL, S. 2001. Structure and function of south-east Australian estuaries. *Estuarine, coastal and shelf science,* 53**,** 351-384.

SHORT, F. T. 1987. Effects of sediment nutrients on seagrasses: literature review and mesocosm experiment. *Aquatic botany,* 27**,** 41-57.

SIMPSON, J., BRUCE, E., DAVIES, K. P. & BARBER, P. 2022. A blueprint for the estimation of seagrass carbon stock using remote sensing-enabled proxies. *Remote Sensing,* 14**,** 3572.

SIMPSON, J., DAVIES, K. P., BARBER, P. & BRUCE, E. 2024. Mapping fine-scale seagrass disturbance using bi-temporal UAV-acquired images and multivariate alteration detection. *Scientific reports,* 14, 19083.

SKILBECK, C. G., HEAP, A. D. & WOODROFFE, C. D. 2017. Geology and sedimentary history of modern estuaries. *Applications of paleoenvironmental techniques in estuarine studies*, 45-74.

STANKOVIC, M., HAYASHIZAKI, K.-I., TUNTIPRAPAS, P., RATTANACHOT, E. & PRATHEP, A. 2021. Two decades of seagrass area change: Organic carbon sources and stock. *Marine Pollution Bulletin,* 163, 111913.

SUYKERBUYK, W., BOUMA, T. J., GOVERS, L. L., GIESEN, K., DE JONG, D. J., HERMAN, P., HENDRIKS, J. & VAN KATWIJK, M. M. 2016. Surviving in Changing Seascapes: Sediment Dynamics as Bottleneck for Long-Term Seagrass Presence. *Ecosystems,* 19, 296-310.

SWADLING, D. S., WEST, G. J., GIBSON, P. T., LAIRD, R. J. & GLASBY, T. M. 2023. Don't go breaking apart: Anthropogenic disturbances predict meadow fragmentation of an endangered seagrass. *Aquatic Conservation: Marine and Freshwater Ecosystems,* 33, 56-69.

TECCHIATO, S., BUOSI, C., IBBA, A., DEL DEO, C., PARNUM, I., O'LEARY, M. & DE MURO, S. 2019. Geomorphological and sedimentological surrogates for the understanding of seagrass distribution within a temperate nearshore setting (Esperance Western Australia). *Geo-Marine Letters,* 39, 249-264.

TECCHIATO, S., COLLINS, L., PARNUM, I. & STEVENS, A. 2015. The influence of geomorphology and sedimentary processes on benthic habitat distribution and littoral sediment dynamics: Geraldton, Western Australia. *Marine Geology,* 359, 148-162.

TIMMER, B., RESHITNYK, L. Y., HESSING-LEWIS, M., JUANES, F. & COSTA, M. 2022. Comparing the use of red-edge and near-infrared wavelength ranges for detecting submerged kelp canopy. *Remote Sensing,* 14, 2241.

TURNER, S. 2007. Growth and productivity of intertidal Zostera capricorni in New Zealand estuaries. *New Zealand Journal of Marine and Freshwater Research,* 41, 77-90.

TURNER, S. J. & SCHWARZ, A. M. 2006. Biomass development and photosynthetic potential of intertidal Zostera capricorni in New Zealand estuaries. *Aquatic Botany,* 85, 53-64.

UHRIN, A. V. & TURNER, M. G. 2018. Physical drivers of seagrass spatial configuration: the role of thresholds. *Landscape Ecology,* 33, 2253-2272.

UNSWORTH, R. K., RASHEED, M. A., CHARTRAND, K. M. & ROELOFS, A. J. 2012. Solar radiation and tidal exposure as environmental drivers of Enhalus acoroides dominated seagrass meadows. *PLoS One,* 7, e34133.

UNSWORTH, R. K., WILLIAMS, B., JONES, B. L. & CULLEN-UNSWORTH, L. C. 2017. Rocking the boat: damage to eelgrass by swinging boat moorings. *Frontiers in Plant Science,* 8, 262774.

VILA-CONCEJO, A., HUGHES, M. G., SHORT, A. D. & RANASINGHE, R. 2010. Estuarine shoreline processes in a dynamic low-energy system. *Ocean Dynamics,* 60, 285-298.

WALKER, D., LUKATELICH, R., BASTYAN, G. & MCCOMB, A. 1989. Effect of boat moorings on seagrass beds near Perth, Western Australia. *Aquatic Botany,* 36, 69-77.

WHITFIELD, A. 1992. A characterization of southern African estuarine systems. *Southern African Journal of Aquatic Science,* 18, 89-103.

WONG, M. C., GRIFFITHS, G. & VERCAEMER, B. 2020. Seasonal Response and Recovery of Eelgrass (Zostera marina) to Short-Term Reductions in Light Availability. *Estuaries and Coasts,* 43, 120-134.

XU, H. 2006. Modification of normalised difference water index (NDWI) to enhance open water features in remotely sensed imagery. *International journal of remote sensing,* 27, 3025-3033.

ZUPANC, A. 2017. Improving cloud detection with machine learning. *Accessed: Oct,* 10, 2019.

Chapter 7

Discussion and Conclusions

7.1 General discussion

Seagrasses, flowering plants adapted for marine conditions, are ecologically important species that influence local hydrological, nearshore sediment dynamics, and biological systems (Duarte and Chiscano, 1999, Hemminga and Duarte, 2000). Based on these functions, their role in providing critical ecosystem services including coastal stabilisation, habitat provision, water quality improvement, and sequestration of carbon is well established (Nordlund et al., 2016). The potential of carbon financing mechanisms to support protection, restoration, and development of seagrass habitats, has contributed to the emergence of a growing field of research into the carbon sequestration potential of seagrass (McLeod et al., 2011, Greiner et al., 2013, Duarte et al., 2025). A key concept that has guided this research is that seagrass carbon stocks, though disproportionately high in comparison to other terrestrial ecosystems (Fourqurean et al., 2012), are variable between seagrass meadows and heterogeneous within seagrass meadows, shaped by the species, environmental conditions, density, spatial arrangement, and life cycle of seagrass species (Lavery et al., 2013, Serrano et al., 2014, Ricart et al., 2017, Serrano et al., 2018, Ricart et al., 2020, Kennedy et al., 2022, Bijak et al., 2023, Krause et al., 2025). These sources of variability and heterogeneity are summarised in Simpson et al. (2022; Chapter 3).

Despite growing interest in seagrass for blue carbon-based climate mitigation and the proliferation of seagrass mapping and monitoring research, remote sensing methods that capture the variability and heterogeneity of seagrass remain understudied relative to that of other coastal habitats (Orth and Heck Jr, 2023, Nguyen and Winters, 2025). Remote sensing facilitates large-scale mapping and monitoring of earth surface features and processes, and identifying seagrass areas using remote sensing has been recognised as both feasible and valuable since data from early generation satellite sensors such as Landsat MSS became available (Harwood et al., 1977). Now a mature field, coastal remote sensing continues to evolve rapidly with ongoing advancements in techniques

and technologies. Spaceborne sensors have undergone significant advancements in spatial, spectral and temporal resolution. Sentinel-2 images have been freely accessible at up to 10 m spatial resolution with coastal blue and red-edge bands since 2015 (European Space Agency, n.d.). Planet has provided 8-band data at up to daily temporal resolution since 2020 (Planet Labs 2025). Relatively new cloud platforms for remote sensing data analysis, such as Google Earth Engine (GEE) and the Open Data Cube (ODC), make available new geoprocessing options which would have previously been time-consuming, computationally intensive, or impossible (Gorelick et al., 2017, Ross et al., 2017). Meanwhile, miniaturised sensors and affordable Unoccupied Aerial Vehicles (UAVs) have proven to be cost-effective and accessible options for mapping coastal habitats (Joyce et al., 2023, Simpson et al., 2024, Chapter 4). These developing remote sensing technologies unlock new opportunities for enhancing seagrass mapping and monitoring.

This chapter integrates the findings presented in the preceding chapters in relation to the overarching aims of this thesis and the broader research context. The research outcomes are examined in alignment with each aim, and key themes that have emerged across this research are identified and discussed. The implications of these findings are then evaluated in the context of seagrass carbon stock estimation and broader seagrass management. The chapter concludes with a discussion of potential directions for future research directions and a final summary of the thesis.

In addressing research Aim 1, potential biophysical characteristics of seagrass that relate to carbon stock and sequestration rates were identified and possibilities for their remote sensing-based measurement were examined drawing on the literature. Four remote sensing proxies, species, density or cover, spatial configuration and temporal variation, were identified for enhancing more detailed assessments of seagrass blue carbon potential and general understanding of seagrass habitats (Simpson et al., 2022, Chapter 3). These proxies informed the design of the research in the remaining chapters. Remote sensing based mapping of seagrass percent cover commonly involves the classification of discrete classes (Chapter 2), which often produces lower data accuracy and may mask heterogeneity in seagrass cover (Lyons et al., 2013), while continuous mapping of percent cover was relatively uncommon until recently, especially in submerged

environments (Chapter 2). Spatial arrangement and temporal variability are rarely or never directly mapped as distinct parameters using remote sensing methods (Chapter 2). Although these characteristics may be implicitly captured in very fine-scale seagrass mapping (Price et al., 2022, Hamad et al., 2022) and time series analysis of seagrass cover (Lyons et al., 2013) respectively, methods that explicitly measure spatio-temporal variability have been understudied until recently (Wicaksono et al., 2025a, Wicaksono et al., 2025b). Robust techniques for distinguishing seagrass species using remote sensing are well established (Phinn et al., 2008, Roelfsema et al., 2014, Koedsin et al., 2016, Wicaksono et al., 2022). For this reason, as well as the low number (1-3) of seagrass species present within the temperate estuarine study sites, the methods developed to address the remaining three research aims focused on density, spatial configuration and temporal variability proxies.

The application of fine-scale UAV remote sensing for quantifying change in seagrass meadow configuration was demonstrated in Chapters 4 and 5, addressing Aim 2. UAV image spatial resolution allowed detection of features including boat propeller scars at St Huberts Island and Empire Bay. It also allowed characterisation of fine-scale differences in seagrass percent cover across seagrass beds, providing insight into seagrass configuration in Brisbane Water. Continuous, less fragmented meadows tend to baffle sediments more effectively and accumulate more organic material (Ricart et al., 2017, Ricart et al., 2015, Oreska et al., 2017), highlighting the importance of methods for monitoring bed configuration. The unsupervised change detection method IR-MAD was shown to provide a simple approach for mapping changes in seagrass spatial configuration due to meadow-scale change or localised disturbance (Simpson et al., 2024; Chapter 4). Repeated surveys with this method would support an understanding of recovery trajectories, important for characterising soil carbon stocks (Macreadie et al., 2014, Macreadie et al., 2015). Using a high resolution, repeatable approach is of particular relevance to estuarine seagrass beds, which tend to be shallow and located in heavily trafficked areas, therefore more prone to anthropogenic disturbances (Bourque et al., 2015). Unsupervised change detection using IR-MAD provided detailed representation of spatial configuration and scale of disturbances in seagrass beds that

has only previously been reported using manual delineation of disturbance features (Orth et al., 2017).

UAV remote sensing was also demonstrated to be effective for quantifying seagrass cover, using simple water column correction and red-edge normalised difference indices (RENDIs). The maps of seagrass cover at Brisbane Water reported in Chapter 5 provided seagrass biophysical data at a high spatial resolution and with comprehensive coverage (Aim 2). Previous UAV seagrass mapping work (Price et al., 2022) was extended by developing a vegetation index which correlates linearly with seagrass cover. In using additional field data with recurrent coregistered images captured with *in situ* quadrats placed in different positions this study involved more ground truth data and enabled comparison of the same ground truth points across different tide levels. Mapping seagrass cover as a continuous variable may provide a more robust proxy of overall carbon potential. Previous research has established a relationship between above-ground and below-ground biomass (Collier et al., 2021), and overall biomass plays an important, though complex, role in shaping soil carbon (Fourqurean et al., 2023, Fourqurean et al., 2025). Additionally, seagrass often exhibits high heterogeneity within habitats which is not captured if differences in cover are not considered (Pu and Bell, 2017, Price et al., 2022, Chapter 5). For intertidal seagrass, where water column interference is minimal, continuous mapping of cover is easily achievable (Barillé et al., 2010, Davies et al., 2024). Estimating cover in subtidal seagrass meadows from images captured above the water's surface is more difficult but can be achieved using green reflectance (Fauzan et al., 2017, Carpenter et al., 2022). Building on studies which have identified the value of red-edge reflectance for detecting submerged vegetation (e.g. Pu et al., 2012), the red-edge based indices explored in Chapter 5 provide an effective approach which, for shallow sites such as temperate estuaries, may be more robust than single band methods such as using green reflectance only.

The use of a UAV-mounted sensor with additional spectral bands, a total of six visible and four red-edge and NIR, allowed the contribution of these bands to seagrass mapping to be tested (Aim 3). Additional visible bands in the blue and red were shown to be effective at improving the ability of IR-MAD to detect change in seagrass spatial arrangement (Chapter 4). Vegetation reflectance in the red-edge was also used to map

seagrass cover (Chapter 5). The blue and red-edge have previously been identified as potentially useful in the context of hyperspectral vegetation indices for seagrass mapping (Pu et al., 2012, Borfecchia et al., 2013, Pu et al., 2015). The results from Chapters 4 and 5 suggest that additional spectral bands beyond those commonly available in commercial multispectral sensors, but not hyperspectral bands, improve detection of seagrass and seagrass change in temperate estuarine environments. This finding has important implications in the context of future remote sensing platforms such as Landsat Next, due for launch in 2030, which will include three additional visible bands and two red-edge bands (US Geological Survey, 2023). Extending application of the red-edge index developed in Chapter 5 to Sentinel-2 time series data (Chapter 6), the viability of dynamic measurement of variability in seagrass cover was demonstrated (Aim 4). Seagrass exhibits high variability in biomass over time due to variation in environmental conditions and disturbance (Kilminster et al., 2015), and this variability relates to its ecosystem function, including sequestration of carbon (Mazarrasa et al., 2018, Stankovic et al., 2021). This approach produced maps of relative stability in seagrass cover which display spatially explicit patterns of seagrass variability and are resistant to cumulative error found in approaches involving classification of time series images (Lyons et al., 2013). The three case studies in Chapter 6 demonstrate how these variability maps can be interpreted in terms of geographic setting to better understand local differences in temporal patterns of seagrass cover change. Given the relevance of seagrass biomass variability to carbon stock assessment (Mazarrasa et al., 2018, Stankovic et al., 2021), and the influences of environmental conditions and disturbances on change in biomass (Carr et al., 2012), seagrass cover variability should be considered in carbon stock mapping. This study demonstrated a spatially dynamic approach for mapping this variable from time series data using repeated measurements of RENDI (Chapter 6).

Three unifying themes emerged from this research that connect each study.

1. Remote sensing can play a multifaceted role in seagrass mapping and monitoring, beyond detection of extent, species composition, or discrete percent cover classes, by measuring percent cover as a continuous variable and detecting relative temporal stability. Seagrass beds can have complex spatial configuration

which change over short time scales in response to disturbances (Bell et al., 2006). Remote sensing, especially with very high-resolution UAV images, captures spatial configuration, and repeat UAV captures can easily identify fine-scale changes. Field surveys cannot capture the arrangement of meadows with the ease and accuracy of UAV images, nor can they detect fine-scale disturbance, unless disturbed sites coincide with field survey sampling locations (transects or quadrats). UAV remote sensing in this case can feed back into field surveying by providing information about the precise locations of disturbances or other features of interest. UAV and satellite remote sensing can similarly complement field methods for measuring seagrass variability. Recurrent field surveys of seagrass sites can be applied to characterise seagrass temporal variability at a very high level of detail (e.g. shoot counts, leaf area measurements). Cloud geoprocessing of spatio-temporally dense satellite data cannot achieve the same level of detail but can instead map variability over large areas with relatively minimal resources compared to extensive field campaigns. This can complement field surveying, highlighting different levels of variability, growth cycles, and exposure to disturbance.

2. Emerging remote sensing technologies enable new, ecologically informed approaches to seagrass habitat assessment. Water column attenuation restricts options for optical remote sensing for seagrass mapping in temperate waters and its impact changes over time according to turbidity and water level (Phinn et al., 2018). Though field surveys provide more detailed data on seagrass characteristics, and other approaches (such as acoustic remote sensing) can successfully map seagrass habitats, optical remote sensing remains the best option for mapping and monitoring seagrass over large areas (Veettil et al., 2020). Emergent techniques and technologies to collect and process remote sensing data will continue to facilitate improvements in mapping and the reliability of carbon stock estimates. Using UAV-captured data at a very fine spatial resolution and an improved spectral resolution compared to standard multispectral images can not only improve accuracy but develop novel ways to map and monitor seagrass that characterise ecologically relevant variables not

previously characterised with remote sensing data. With increasing accessibility of these technologies, remote sensing will play a greater role in the management, conservation, and restoration of seagrass habitats globally.

3. Seagrass mapping and monitoring approaches must be geographically tailored and contextually relevant. This studied focused on estuarine seagrass beds in subtropical to temperate Australia. The techniques used, including quadrat field surveys, UAV flights and estimates of cover based on red-edge reflectance, are well suited to mid-sized *Zostera* growing in the shallow, sheltered waters of protected estuaries. In other environmental settings, seagrass can grow on unprotected coasts, in water over 100 m deep, and can range from cryptic and sparse *Halophila decipiens* to dense *Posidonia oceanica*. Methods used in the estuarine sites studied here may not be applicable in these other seagrass environments, just as approaches for deep-water seagrass mapping are not applicable in estuarine settings prone to varying turbidity levels. Further, as demonstrated in Chapters 4 and 6, seagrass varies in patterns of disturbance and change between, and even within, estuaries. This demonstrates the importance of selecting approaches to remote sensing data analysis based on the physical characteristics of the site, including overall water depth, tides, turbidity, and seagrass species present.

7.2 Implications of research outcomes

7.2.1 Implications for monitoring and mapping seagrass as a blue carbon ecosystem

Estimates of seagrass carbon stock are produced by applying global or regional averages to measurements of seagrass area, referred to by IPCC as Tier 1 and 2 methods respectively (IPCC, 2006). The use of averages masks the heterogeneous nature of seagrass carbon stocks, even within habitats, and spatially explicit estimates of seagrass carbon stock (Tier 3) are not widely used for greenhouse emission reporting or related activities (UNEP, 2020). Other terrestrial habitats, such as forests, have well-developed methods to estimate spatially heterogeneous and temporally variable carbon stock using remote sensing-derived variables such as vegetation indices and species classifications, disturbance detection methods, and other environmental factors

including elevation and topography (Bhardwaj et al., 2016, Chinembiri et al., 2023, Vangi et al., 2023). This research has contributed to the growing body of literature that may enable similarly rigorous approaches for seagrass.

Seagrass cover relates directly to overall biomass and indirectly to soil carbon, but cover is spatially heterogeneous and varies over environmental gradients (Bach et al., 1998, Collier et al., 2007). Enabled by a consumer grade UAV and an affordable sensor with red-edge bands, a method for mapping continuous seagrass cover at very high resolution to capture heterogeneity has been demonstrated (Chapter 5). This approach was scaled up using Sentinel-2 data, with potential for application to other satellite sensors that detect red-edge reflectance. The satellite-based approach provides spatially explicit information with full site coverage not feasible with field survey methods alone. Additionally, the cover estimates provided are continuous, not discrete, which better represents the inherent heterogeneity in patterns of seagrass growth (Lyons et al., 2011).

Seagrass cover often varies inter- or intra-annually and the seasonal timing of peaks in seagrass cover can differ considerably with geographical location. Forest carbon mapping in terrestrial environments often relies on estimates of peak biomass (Xu et al. 2025) but achieving similar estimates for seagrass is challenging due to potential differences in seasonal seagrass cover patterns (Chapter 6). The method explored in Chapters 5 and 6 based on water column correction and red-edge normalised difference provides a robust approach for addressing this challenge by enabling consistency in repeated estimates of seagrass cover over time.

Temporal variability in seagrass cover has potential to influence carbon stock estimation in seagrass habitats. Sediment carbon is the greatest contributor to overall carbon in seagrass beds. Seagrass beds with stable growth patterns and minimal temporal variability have been linked to higher soil carbon stores (Mazarrasa et al., 2018, Stankovic et al., 2021, Bijak et al., 2023). Further research is required to establish this relationship but accounting for variability in growth could improve the reliability of stock estimates. Repeated satellite-derived cover estimates could provide a valuable secondary dataset for carbon stock modelling.

Disturbance events are a key input into many terrestrial models of spatially explicit carbon stock estimates (Williams et al., 2012). Understanding the scale and recovery trajectory of seagrass disturbance is important to seagrass carbon stock modelling, especially as impacts on carbon stock can vary in complex ways depending on the scale of disturbance events (Macreadie et al., 2014, Trevathan-Tackett et al., 2018). The unsupervised change detection method (IR-MAD) demonstrated in Chapter 4 offers a relatively simple method of mapping fine-scale disturbance events, while the satellite-based method in Chapter 6 implicitly captures disturbance and recovery. In applying UAV IR-MAD change detection and extending satellite-based variability measurement methods to incorporate detection of changes in seagrass cover, the methods presented in Chapters 4 and 6 provide approaches for characterising disturbance events.

Spatial configuration of seagrass meadows was not quantitatively measured as part of this thesis, but its relationship to seagrass carbon stocks is established in the literature (Oreska et al., 2017, Ricart et al., 2017). The fine-scale maps of seagrass cover and change (Chapters 4 and 5) demonstrate the patchiness of the meadows studied. Quantifying seagrass cover with landscape ecology metrics (Pittman, 2018) from UAV-derived seagrass cover maps may provide a way to capture the differences in carbon stock between fragmented and continuous meadows.

7.2.2 Informing estuarine management, conservation, and restoration

The health of seagrass meadows has been identified as an indicator of overall estuary health (Trevathan-Tackett et al., 2013, Wainger et al., 2017, Purvaja et al., 2018) and is therefore relevant to estuarine management, and conservation and restoration programs. The techniques developed in this thesis also contribute to monitoring seagrass ecosystem health.

Changes detected at the Brisbane Water site (Simpson et al., 2024; Chapter 4) are clearly caused by boating activities. Dynamic change maps allow coastal managers to understand where human impacts occur and prioritise conservation efforts, such as further field monitoring, restricting boat traffic, and seagrass restoration (Cullen-Unsworth et al., 2016). Cover estimates from UAV-captured images (Chapter 5) have relevance for monitoring natural unmodified seagrass sites as well as tracking regrowth

in restored sites. As UAV platforms and UAV-mounted sensors are now relatively affordable and accessible, they are a viable and promising tool for management of seagrass in estuarine settings.

Deriving longer term variability of seagrass from remote sensing data (Chapter 6) provides quantitative information about estuary-scale differences in the conditions that govern seagrass life cycle and susceptibility to disturbance. This provides valuable information for prioritising management efforts, as well as informing site selection for conservation and restoration (Van Katwijk et al., 2009, Fonseca, 2011, Hotaling-Hagan et al., 2017). Further, repeated captures of satellite images allow detection over extended time periods of estuary-wide changes that may indicate overall decline in water quality or estuary health. Publicly available satellite image sources like Sentinel-2 and cloud-based open access processing platforms such as GEE can allow estuary managers to leverage time series analysis for estuarine monitoring. A monitoring program using UAV images with RENDI cover estimation and unsupervised change detection using IR-MAD would provide a comprehensive view of restoration progress, with affordable equipment and minimal fieldwork requirements.

7.3 Future research directions

This research extends current approaches for understanding geographical variability in seagrass environments, however, several limitations highlight opportunities for further research.

Although research findings discussed in Chapters 5 and 6 demonstrated a relationship between the red-edge normalised indices and seagrass cover, this initial work should be replicated across seagrass beds of varying species and environmental conditions. The red-edge normalised difference indices are based on physical characteristics of seagrass leaves, expected to be universal across species. Red-edge based index mapping of seagrass has only been demonstrated in the literature for two other settings: *Z. muelleri* beds in New Zealand (Chand and Bollard, 2021), and beds dominated by *Enhalus acoroides* and *Thalassia hemprichii* in Hainan, China (Li et al., 2023). Only monospecific beds of *Z. muelleri* were mapped in the current research. Further work to apply the red-edge normalised difference approach to other species is needed.

The methods developed in this thesis were applied to subtropical and temperate estuarine environments, as these environmental settings are understudied in the seagrass remote sensing literature. However, the approaches may be applicable to other shallow-water environments in which a red-edge reflectance signal can be detected from seagrass. Assessing the transferability of RENDIs to other coastal environments would require further work on the depth and turbidity limits of the method. Timmer et al. (2022) identified macroalgae deeper than 1 m were detectable with red-edge indices but did not consider deeper features. Understanding depth thresholds for the red-edge indices is an important step in determining how a site's environmental conditions inform the most appropriate seagrass mapping workflow.

Red-edge index based seagrass mapping may further be improved by incorporating water column correction approaches that use measured attenuation values (Lee et al., 1999) to produce more robust estimates of benthic reflectance (Pu et al., 2014). Research in this area may provide information about how estuarine water conditions impact depth limits for seagrass detection. The relationship between water depth, water column constituents and reflectance could be further explored with hyperspectral imaging of submerged seagrass beds.

Though the depth limits of the RENDI approach have not been identified as part of this thesis, it is expected it would be limited in many seagrass environments. In deeper water seagrass beds, such as those common in tropical areas, light in red-edge wavelengths would be unusable due to attenuation by water. Seagrass habitats are highly diverse globally, differing in morphology, geomorphic and sedimentological setting, water depth, and water optical properties. RENDIs offer a valuable improvement for shallow, estuarine settings, such as those in NSW, by characterising heterogeneity and variability, providing insight into spatio-temporal dynamics. The approaches explored in this thesis will not offer improvement in other environments. This highlights the importance of tailoring remote sensing methods to the target being studied, and the potential of a suite of different approaches to more reliably characterise seagrass globally.

Chapter 6 demonstrates a method for analysing seagrass dynamics using a dense time stack of Sentinel-2 images. This approach could be extended to other sensors that have

red-edge bands, such as Planet's SuperDove, already demonstrated as an effective platform for seagrass mapping in tropical coastal environments (Wicaksono et al., 2022). Planet sensors provide near-daily temporal resolution, resulting in a higher number of available images, increasing the probability of images captured at low tide and reduced turbidity.

Seasonally averaged Sentinel-2 composites did not produce sufficient information over the nine NSW estuary sites to allow trend analysis or detection of disturbance events. This may be possible if the approach is applied to other estuarine sites and data from alternative satellite sensors, such as Planet SuperDoves. Refined tide and turbidity filtering methods may also enable trend analysis, as will a longer Sentinel-2 archive into the future. Further analysis of the relationship between the stability of seagrass growth patterns and estuarine geomorphic zonation would enable variables such as depositional environment to be used as potential proxies for seagrass carbon estimates.

The contribution towards remote sensing based methods for quantifying seagrass carbon presented in this thesis is focused on variables measurable using remote sensing, not direct modelling of carbon stock. Further understanding of the relationships between model inputs and field measurements of above ground and overall carbon stock is necessary, especially for poorly studied variables such as temporal variability. Other variables, such as allochthonous input of organic carbon, that are not measurable with remote sensing data must also be considered. In estuarine settings, where input of organic material from rivers and nearby habitats, such as mangroves influences soil carbon stocks (Chen et al., 2017, Ricart et al., 2020, Asplund et al., 2021), it is critical to account for these other variables in total carbon estimates. Remote sensing provides a powerful method for characterising heterogeneity in estuarine environments, but other data inputs are required to model overall seagrass carbon stocks.

7.4 Conclusions

This thesis set out to develop methods for characterising estuarine seagrass using remote sensing data, with a focus on capturing spatial heterogeneity and temporal variability. The purpose of developing new methods was to enhance carbon stock estimates, addressing the high level of geographical difference in carbon stock between

and within seagrass beds. Accounting for heterogeneity and variability will contribute towards building spatially explicit models of seagrass carbon stock, bringing estimation methods for seagrass in line with terrestrial standards.

Multiple factors contribute to the high carbon stock levels in seagrass beds, this underscores the need for accurate and detailed seagrass maps and monitoring data. This research has demonstrated how remote sensing can capture changes in spatial configuration, fine-scale heterogeneity of seagrass, and longer-term variability of seagrass cover. More nuanced maps of seagrass habitats that provide more detail than bed extent is a priority for supporting blue carbon research (Duarte et al., 2025). By detecting fine-scale changes in seagrass beds, mapping heterogeneous seagrass cover, and characterising relative long-term variability, multiple new dimensions of seagrass mapping have been demonstrated here. These remote sensing methods offer opportunities to produce more accurate estimates of seagrass ecosystem services as they vary geographically (Nordlund et al., 2016).

Utilising consumer-grade equipment and data and processing platforms freely available to researchers, the methods demonstrated in this thesis are widely applicable. They have impacts across geographical scales, from guiding management decisions for mitigating damage to individual seagrass beds (Cullen-Unsworth et al., 2016) to supporting spatially explicit carbon stock modelling for Nationally Determined Contributions of parties to the Paris Agreement (UNEP, 2020). Widespread access to emerging remote sensing technologies, including UAVs, higher spectral resolution sensors, and cloud geoprocessing, enables more advanced mapping of seagrass biophysical characteristics. As these tools become more widely used among blue carbon researchers and estuary managers, it will become possible to further untangle the spatio-temporal complexity of seagrass carbon sequestration. Future development of remote sensing technologies will further support this by offering more capable UAV platforms, bands in new spectral regions, and improved processing pipelines.

Monitoring changes in spatial configuration, mapping percent cover as a continuous variable, and characterising relative variability of seagrass at the estuary scale provides novel insights into estuarine seagrass habitat dynamics in the context of carbon stock. They demonstrate the multifaceted role that remote sensing can play in mapping

seagrass, and the importance of emerging remote sensing technologies. The insights gained from this research contribute to advancement of spatially explicit modelling of seagrass carbon stores, and valuable information for seagrass conservation, restoration efforts and broader estuarine management.

References

ASPLUND, M. E., DAHL, M., ISMAIL, R. O., ARIAS-ORTIZ, A., DEYANOVA, D., FRANCO, J. N., HAMMAR, L., HOAMBY, A. I., LINDERHOLM, H. W. & LYIMO, L. D. 2021. Dynamics and fate of blue carbon in a mangrove–seagrass seascape: influence of landscape configuration and land-use change. *Landscape Ecology,* 36**,** 1489-1509.

BACH, S. S., BORUM, J., FORTES, M. D. & DUARTE, C. M. J. M. E. P. S. 1998. Species composition and plant performance of mixed seagrass beds along a siltation gradient at Cape Bolinao, The Philippines. 174**,** 247-256.

BARILLÉ, L., ROBIN, M., HARIN, N., BARGAIN, A. & LAUNEAU, P. 2010. Increase in seagrass distribution at Bourgneuf Bay (France) detected by spatial remote sensing. *Aquatic Botany,* 92**,** 185-194.

BELL, S. S., FONSECA, M. S. & STAFFORD, N. B. 2006. 'Seagrass ecology: new contributions from a landscape perspective' in LARKUM, A. W. D., ORTH, R. J. & DUARTE, C. M. (eds.). *Seagrasses: Biology, Ecology and Conservation*. The Netherlands: Springer, pp. 625-645

BHARDWAJ, D., BANDAY, M., PALA, N. A. & RAJPUT, B. S. 2016. Variation of biomass and carbon pool with NDVI and altitude in sub-tropical forests of northwestern Himalaya. *Environmental monitoring and assessment,* 188**,** 1-13.

BIJAK, A. L., REYNOLDS, L. K. & SMYTH, A. R. 2023. Seagrass meadow stability and composition influence carbon storage. *Landscape Ecology,* 38**,** 4419-4437.

BORFECCHIA, F., DE CECCO, L., MARTINI, S., CERIOLA, G., BOLLANOS, S., VLACHOPOULOS, G., VALIANTE, L. M., BELMONTE, A. & MICHELI, C. 2013. Posidonia oceanica genetic and biometry mapping through high-resolution satellite spectral vegetation indices and sea-truth calibration. *International Journal of Remote Sensing,* 34**,** 4680-4701.

BOURQUE, A. S., KENWORTHY, W. J. & FOURQUREAN, J. W. 2015. Impacts of physical disturbance on ecosystem structure in subtropical seagrass meadows. *Marine Ecology Progress Series,* 540**,** 27-41.

CARPENTER, S., BYFIELD, V., FELGATE, S. L., PRICE, D. M., ANDRADE, V., COBB, E., STRONG, J., LICHTSCHLAG, A., BRITTAIN, H. & BARRY, C. 2022. Using unoccupied aerial vehicles (UAVs) to map seagrass cover from Sentinel-2 imagery. *Remote Sensing,* 14**,** 477.

CARR, J. A., D'ODORICO, P., MCGLATHERY, K. J. & WIBERG, P. L. 2012. Stability and resilience of seagrass meadows to seasonal and interannual dynamics and environmental stress. *Journal of Geophysical Research: Biogeosciences,* 117.

CHAND, S. & BOLLARD, B. 2021. Low altitude spatial assessment and monitoring of intertidal seagrass meadows beyond the visible spectrum using a remotely piloted aircraft system. *Estuarine, Coastal and Shelf Science,* 255**,** 107299.

CHEN, G., AZKAB, M. H., CHMURA, G. L., CHEN, S., SASTROSUWONDO, P., MA, Z., DHARMAWAN, I. W. E., YIN, X. & CHEN, B. 2017. Mangroves as a major source of soil carbon storage in adjacent seagrass meadows. *Scientific Reports,* 7**,** 1-10.

CHINEMBIRI, T. S., MUTANGA, O. & DUBE, T. 2023. Carbon Stock Prediction in Managed Forest Ecosystems Using Bayesian and Frequentist Geostatistical Techniques and New Generation Remote Sensing Metrics. *Remote Sensing,* 15**,** 1649.

COLLIER, C., LANGLOIS, L., MCMAHON, K. M., UDY, J., RASHEED, M., LAWRENCE, E., CARTER, A., FRASER, M. & MCKENZIE, L. 2021. What lies beneath: predicting seagrass below-ground biomass from above-ground biomass, environmental conditions and seagrass community composition. *Ecological indicators,* 121**,** 107156.

COLLIER, C. J., LAVERY, P. S., MASINI, R. J. & RALPH, P. J. J. M. E. P. S. 2007. Morphological, growth and meadow characteristics of the seagrass Posidonia sinuosa along a depth-related gradient of light availability. 337**,** 103-115.

CULLEN-UNSWORTH, L. C., UNSWORTH, R. K. & FRID, C. 2016. Strategies to enhance the resilience of the world's seagrass meadows. *Journal of Applied Ecology,* 53**,** 967-972.

DAVIES, B. F. R., OIRY, S., ROSA, P., ZOFFOLI, M. L., SOUSA, A. I., THOMAS, O. R., SMALE, D. A., AUSTEN, M. C., BIERMANN, L. & ATTRILL, M. J. 2024. Intertidal seagrass extent from Sentinel-2 time-series show distinct trajectories in Western Europe. *Remote Sensing of Environment,* 312**,** 114340.

DUARTE, C. M., APOSTOLAKI, E. T., SERRANO, O., STECKBAUER, A. & UNSWORTH, R. K. 2025. Conserving seagrass ecosystems to meet global biodiversity and climate goals. *Nature Reviews Biodiversity*, 1-16.

DUARTE, C. M. & CHISCANO, C. L. 1999. Seagrass biomass and production: a reassessment. *Aquatic Botany,* 65**,** 159-174.

EUROPEAN SPACE AGENCY. n.d. *Sentinel-2: Facts and Figures*. Available at: https://www.esa.int/Applications/Observing_the_Earth/Copernicus/Sentinel-2/Facts_and_figures (Accessed 21/4/2025)

FAUZAN, M. A., KUMARA, I. S., YOGYANTORO, R., SUWARDANA, S., FADHILAH, N., NURMALASARI, I., APRIYANI, S. & WICAKSONO, P. 2017. Assessing the capability of Sentinel-2A data for mapping seagrass percent cover in Jerowaru, East Lombok. *Indonesian Journal of Geography,* 49**,** 195-203.

FONSECA, M. S. 2011. Addy revisited: what has changed with seagrass restoration in 64 years? *Ecological Restoration,* 29**,** 73-81.

FOURQUREAN, J. W., CAMPBELL, J. E., RHOADES, O. K., MUNSON, C. J., KRAUSE, J. R., ALTIERI, A. H., DOUGLASS, J. G., HECK JR, K. L., PAUL, V. J. & ARMITAGE, A. R. 2023. Seagrass abundance predicts surficial soil organic carbon stocks across the range of Thalassia testudinum in the Western North Atlantic. *Estuaries and coasts,* 46**,** 1280-1301.

FOURQUREAN, J. W., DUARTE, C. M., KENNEDY, H., MARBÀ, N., HOLMER, M., MATEO, M. A., APOSTOLAKI, E. T., KENDRICK, G. A., KRAUSE-JENSEN, D. & MCGLATHERY, K. J. 2012. Seagrass ecosystems as a globally significant carbon stock. *Nature geoscience,* 5**,** 505-509.

FOURQUREAN, J. W., KRAUSE, J. R., MANUEL, S. A., COATES, K. A., WORBOYS, P. E., GONZÁLES-CORREDOR, J. D., ZUILL, T. D., RODEN, A. & CAMPBELL, J. E. 2025. Seagrass organic carbon stocks are not correlated with seagrass abundance at local scale, but loss of seagrasses does lead to decrease in surficial sediment organic carbon at the seascape scale in Bermuda. *Estuaries and Coasts,* 48**,** 1-15.

GORELICK, N., HANCHER, M., DIXON, M., ILYUSHCHENKO, S., THAU, D. & MOORE, R. 2017. Google Earth Engine: Planetary-scale geospatial analysis for everyone. *Remote sensing of Environment,* 202**,** 18-27.

GREINER, J. T., MCGLATHERY, K. J., GUNNELL, J. & MCKEE, B. A. 2013. Seagrass restoration enhances "blue carbon" sequestration in coastal waters. *PLoS One,* 8**,** e72469.

HAMAD, I. Y., STAEHR, P. A. U., RASMUSSEN, M. B. & SHEIKH, M. 2022. Drone-based characterization of seagrass habitats in the tropical waters of Zanzibar. *Remote Sensing, 14*(3), 680

HARWOOD, P., FINLEY, R., MCCULLOCH, S., MALIN, P. & SCHELL, J. 1977. Development and application of operational techniques for the inventory and monitoring of resources and uses for the Texas coastal zone. Volume 1: Text.

HEMMINGA, M. A. & DUARTE, C. M. 2000. *Seagrass ecology*, Cambridge University Press.

HOTALING-HAGAN, A., SWETT, R., ELLIS, L. R. & FRAZER, T. K. 2017. A spatial model to improve site selection for seagrass restoration in shallow boating environments. *Journal of environmental management,* 186**,** 42-54.

IPCC 2006. *2006 IPCC Guidelines for National Greenhouse Gas Inventories, Prepared by the National Greenhouse Gas Inventories Programme,* Japan, IGES.

JOYCE, K. E., FICKAS, K. C. & KALAMANDEEN, M. 2023. The unique value proposition for using drones to map coastal ecosystems. *Cambridge prisms: coastal futures,* 1**,** e6.

KENNEDY, H., PAGÈS, J., LAGOMASINO, D., ARIAS-ORTIZ, A., COLARUSSO, P., FOURQUREAN, J., GITHAIGA, M., HOWARD, J., KRAUSE-JENSEN, D. & KUWAE, T. 2022. Species traits and geomorphic setting as drivers of global soil carbon stocks in seagrass meadows. *Global Biogeochemical Cycles,* 36**,** e2022GB007481.

KILMINSTER, K., MCMAHON, K., WAYCOTT, M., KENDRICK, G. A., SCANES, P., MCKENZIE, L., O'BRIEN, K. R., LYONS, M., FERGUSON, A., MAXWELL, P., GLASBY, T. & UDY, J. 2015. Unravelling complexity in seagrass systems for management: Australia as a microcosm. *Sci Total Environ,* 534**,** 97-109.

KOEDSIN, W., INTARARUANG, W., RITCHIE, R. & HUETE, A. 2016. An Integrated Field and Remote Sensing Method for Mapping Seagrass Species, Cover, and Biomass in Southern Thailand. *Remote Sensing,* 8.

KRAUSE, J. R., CAMERON, C., ARIAS-ORTIZ, A., CIFUENTES-JARA, M., CROOKS, S., DAHL, M., FRIESS, D. A., KENNEDY, H., LIM, K. E. & LOVELOCK, C. E. 2025. Global seagrass carbon stock variability and emissions from seagrass loss. *Nature Communications,* 16**,** 1-9.

LAVERY, P. S., MATEO, M.-Á., SERRANO, O. & ROZAIMI, M. 2013. Variability in the carbon storage of seagrass habitats and its implications for global estimates of blue carbon ecosystem service. *PloS one,* 8**,** e73748.

LEE, Z., CARDER, K. L., MOBLEY, C. D., STEWARD, R. G. & PATCH, J. S. 1999. Hyperspectral remote sensing for shallow waters: 2. Deriving bottom depths and water properties by optimization. *Applied Optics,* 38**,** 3831-3843.

LI, Y., BAI, J., CHEN, S., CHEN, B. & ZHANG, L. 2023. Mapping seagrasses on the basis of Sentinel-2 images under tidal change. *Marine Environmental Research,* 185**,** 105880.

LYONS, M., PHINN, S. & ROELFSEMA, C. 2011. Integrating Quickbird Multi-Spectral Satellite and Field Data: Mapping Bathymetry, Seagrass Cover, Seagrass Species and Change in Moreton Bay, Australia in 2004 and 2007. *Remote Sensing,* 3**,** 42-64.

LYONS, M. B., ROELFSEMA, C. M. & PHINN, S. R. 2013. Towards understanding temporal and spatial dynamics of seagrass landscapes using time-series remote sensing. *Estuarine, Coastal and Shelf Science,* 120**,** 42-53.

MACREADIE, P. I., TREVATHAN-TACKETT, S. M., SKILBECK, C. G., SANDERMAN, J., CURLEVSKI, N., JACOBSEN, G. & SEYMOUR, J. R. 2015. Losses and recovery of organic carbon from a seagrass ecosystem following disturbance. *Proceedings of the Royal Society B: Biological Sciences,* 282**,** 20151537.

MACREADIE, P. I., YORK, P. H., SHERMAN, C. D. H., KEOUGH, M. J., ROSS, D. J., RICART, A. M. & SMITH, T. M. 2014. No detectable impact of small-scale disturbances on 'blue carbon' within seagrass beds. *Marine Biology,* 161**,** 2939-2944.

MAZARRASA, I., SAMPER-VILLARREAL, J., SERRANO, O., LAVERY, P. S., LOVELOCK, C. E., MARBA, N., DUARTE, C. M. & CORTES, J. 2018. Habitat characteristics provide insights of carbon storage in seagrass meadows. *Mar Pollut Bull,* 134**,** 106-117.

MCLEOD, E., CHMURA, G. L., BOUILLON, S., SALM, R., BJÖRK, M., DUARTE, C. M., LOVELOCK, C. E., SCHLESINGER, W. H. & SILLIMAN, B. R. 2011. A blueprint for blue carbon: toward an improved understanding of the role of vegetated coastal habitats in sequestering CO2. *Frontiers in Ecology and the Environment,* 9**,** 552-560.

NGUYEN, H. M. & WINTERS, G. 2025. Trends in seagrass research in the 21st century–are we there yet? *Marine Environmental Research***,** 107198.

NORDLUND, L., KOCH, E. W., BARBIER, E. B. & CREED, J. C. 2016. Seagrass Ecosystem Services and Their Variability across Genera and Geographical Regions. *PLoS One,* 11**,** e0163091.

ORESKA, M. P. J., MCGLATHERY, K. J. & PORTER, J. H. 2017. Seagrass blue carbon spatial patterns at the meadow-scale. *PLoS One,* 12**,** e0176630.

ORTH, R. J. & HECK JR, K. L. 2023. The dynamics of seagrass ecosystems: History, past accomplishments, and future prospects. *Estuaries and Coasts,* 46**,** 1653-1676.

ORTH, R. J., LEFCHECK, J. S. & WILCOX, D. J. 2017. Boat propeller scarring of seagrass beds in lower Chesapeake Bay, USA: Patterns, causes, recovery, and management. *Estuaries and Coasts,* 40**,** 1666-1676.

PHINN, S., ROELFSEMA, C., DEKKER, A., BRANDO, V. & ANSTEE, J. 2008. Mapping seagrass species, cover and biomass in shallow waters: An assessment of satellite multi-spectral and airborne hyper-spectral imaging systems in Moreton Bay (Australia). *Remote Sensing of Environment,* 112**,** 3413-3425.

PHINN, S., ROELFSEMA, C., KOVACS, E., CANTO, R., LYONS, M., SAUNDERS, M. & MAXWELL, P. 2018. Mapping, monitoring and modelling seagrass using remote sensing techniques. In: LARKUM, A. W. D., KENDRICK, G. A. & RALPH, P. J. *Seagrasses of Australia: Structure, ecology and conservation***,** The Netherlands: Springer, pp. 445-487.

PITTMAN, S. J. 2018. Introducing Seascape Ecology. *In:* PITTMAN, S. J. (ed.) *Seascape Ecology.* Oxford: Wiley Blackwell.

PLANET LABS. 2025. *PlanetScope*. Available at: https://docs.planet.com/data/imagery/planetscope/ (Accessed 20/5/2025)

PRICE, D. M., FELGATE, S. L., HUVENNE, V. A., STRONG, J., CARPENTER, S., BARRY, C., LICHTSCHLAG, A., SANDERS, R., CARRIAS, A. & YOUNG, A. 2022. Quantifying the intra-habitat variation of seagrass beds with unoccupied aerial vehicles (UAVs). *Remote Sensing,* 14**,** 480.

PU, R. & BELL, S. 2017. Mapping seagrass coverage and spatial patterns with high spatial resolution IKONOS imagery. *International Journal of Applied Earth Observation and Geoinformation,* 54**,** 145-158.

PU, R., BELL, S. & ENGLISH, D. 2015. Developing Hyperspectral Vegetation Indices for Identifying Seagrass Species and Cover Classes. *Journal of Coastal Research,* 313**,** 595-615.

PU, R., BELL, S. & MEYER, C. 2014. Mapping and assessing seagrass bed changes in Central Florida's west coast using multitemporal Landsat TM imagery. *Estuarine, Coastal and Shelf Science,* 149**,** 68-79.

PU, R., BELL, S., MEYER, C., BAGGETT, L. & ZHAO, Y. 2012. Mapping and assessing seagrass along the western coast of Florida using Landsat TM and EO-1 ALI/Hyperion imagery. *Estuarine, Coastal and Shelf Science,* 115**,** 234-245.

PURVAJA, R., ROBIN, R., GANGULY, D., HARIHARAN, G., SINGH, G., RAGHURAMAN, R. & RAMESH, R. 2018. Seagrass meadows as proxy for assessment of ecosystem health. *Ocean & coastal management,* 159**,** 34-45.

RICART, A. M., PÉREZ, M. & ROMERO, J. 2017. Landscape configuration modulates carbon storage in seagrass sediments. *Estuarine, Coastal and Shelf Science,* 185**,** 69-76.

RICART, A. M., YORK, P. H., BRYANT, C. V., RASHEED, M. A., IERODIACONOU, D. & MACREADIE, P. I. 2020. High variability of Blue Carbon storage in seagrass meadows at the estuary scale. *Scientific reports,* 10**,** 5865.

RICART, A. M., YORK, P. H., RASHEED, M. A., PÉREZ, M., ROMERO, J., BRYANT, C. V. & MACREADIE, P. I. 2015. Variability of sedimentary organic carbon in patchy seagrass landscapes. *Marine Pollution Bulletin,* 100**,** 476-482.

ROELFSEMA, C. M., LYONS, M., KOVACS, E. M., MAXWELL, P., SAUNDERS, M. I., SAMPER-VILLARREAL, J. & PHINN, S. R. 2014. Multi-temporal mapping of seagrass cover, species and biomass: A semi-automated object based image analysis approach. *Remote Sensing of Environment,* 150**,** 172-187.

ROSS, J., KILLOUGH, B., DHU, T. & PAGET, M. 2017. Open Data Cube and the committee on earth observation satellites data cube initiative. *IAC*.

SERRANO, O., ALMAHASHEER, H., DUARTE, C. M. & IRIGOIEN, X. 2018. Carbon stocks and accumulation rates in Red Sea seagrass meadows. *Scientific reports,* 8**,** 15037.

SERRANO, O., LAVERY, P. S., ROZAIMI, M. & MATEO, M. Á. 2014. Influence of water depth on the carbon sequestration capacity of seagrasses. *Global Biogeochemical Cycles,* 28**,** 950-961.

SIMPSON, J., BRUCE, E., DAVIES, K. P. & BARBER, P. 2022. A blueprint for the estimation of seagrass carbon stock using remote sensing-enabled proxies. *Remote Sensing,* 14**,** 3572.

SIMPSON, J., DAVIES, K. P., BARBER, P. & BRUCE, E. 2024. Mapping fine-scale seagrass disturbance using bi-temporal UAV-acquired images and multivariate alteration detection. *Scientific reports,* 14**,** 19083.

STANKOVIC, M., HAYASHIZAKI, K.-I., TUNTIPRAPAS, P., RATTANACHOT, E. & PRATHEP, A. 2021. Two decades of seagrass area change: Organic carbon sources and stock. *Marine Pollution Bulletin,* 163**,** 111913.

SURVEY, U. G. 2023. *Landsat Next* [Online]. Available: https://www.usgs.gov/landsat-missions/landsat-next [Accessed 14/9/2024].

TIMMER, B., RESHITNYK, L. Y., HESSING-LEWIS, M., JUANES, F. & COSTA, M. 2022. Comparing the use of red-edge and near-infrared wavelength ranges for detecting submerged kelp canopy. *Remote Sensing,* 14**,** 2241.

TREVATHAN-TACKETT, S. M., LAUER, N., LOUCKS, K., ROSSI, A. M. & ROSS, C. 2013. Assessing the relationship between seagrass health and habitat quality with wasting disease prevalence in the Florida Keys. *Journal of Experimental Marine Biology and Ecology,* 449**,** 221-229.

TREVATHAN-TACKETT, S. M., WESSEL, C., CEBRIÁN, J., RALPH, P. J., MASQUÉ, P. & MACREADIE, P. I. 2018. Effects of small-scale, shading-induced seagrass loss on blue carbon storage: Implications for management of degraded seagrass ecosystems. *Journal of Applied Ecology,* 55**,** 1351-1359.

UNEP 2020. Out of the blue: The value of seagrasses to the environment and to people. Nairobi.

VAN KATWIJK, M., BOS, A., DE JONGE, V., HANSSEN, L., HERMUS, D. & DE JONG, D. 2009. Guidelines for seagrass restoration: importance of habitat selection and donor population, spreading of risks, and ecosystem engineering effects. *Marine pollution bulletin,* 58**,** 179-188.

VANGI, E., D'AMICO, G., FRANCINI, S., BORGHI, C., GIANNETTI, F., CORONA, P., MARCHETTI, M., TRAVAGLINI, D., PELLIS, G. & VITULLO, M. 2023. Large-scale high-resolution yearly modeling of forest growing stock volume and above-ground carbon pool. *Environmental Modelling & Software,* 159**,** 105580.

VEETTIL, B. K., WARD, R. D., LIMA, M. D. A. C., STANKOVIC, M., HOAI, P. N. & QUANG, N. X. 2020. Opportunities for seagrass research derived from remote sensing: A review of current methods. *Ecological Indicators,* 117, 106560

WAINGER, L. A., SECOR, D. H., GURBISZ, C., KEMP, W., GLIBERT, P. M., HOUDE, E. D., RICHKUS, J. & BARBER, M. C. 2017. Resilience indicators support valuation of estuarine ecosystem restoration under climate change. *Ecosystem Health and Sustainability,* 3**,** e01268.

WICAKSONO, P., MAISHELLA, A., LAZUARDI, W. & MUHAMMAD, F. H. 2022. Consistency assessment of multi-date PlanetScope imagery for seagrass percent cover mapping in different seagrass meadows. *Geocarto International,* 37**,** 15161-15186.

WICAKSONO, P., MAISHELLA, A. & RAMADHAN. 2025a. Capturing the dynamics of aboveground carbon stock in intertidal seagrass meadows using Sentinel-2 time-series imagery. *Remote Sensing Applications: Society and Environment,* 38

WICAKSONO, P., RAMADHAN, HARAHAP, S. D., KARTIKA, C. S. D. & KAMAL, M. 2025b. Mapping the dynamics of seagrass aboveground carbon stock in a developing coastal area: case study of Kuta Mandalika, Lombok Island, Indonesia. *Environmental Monitoring and Assessment,* 197, 1093

WILLIAMS, C. A., COLLATZ, G. J., MASEK, J. & GOWARD, S. N. 2012. Carbon consequences of forest disturbance and recovery across the conterminous United States. *Global Biogeochemical Cycles,* 26.

Appendix A. Papers published during candidature

remote sensing

MDPI

Review

A Blueprint for the Estimation of Seagrass Carbon Stock Using Remote Sensing-Enabled Proxies

Jamie Simpson [1,2,*], Eleanor Bruce [1,2], Kevin P. Davies [1,2] and Paul Barber [2,3,4]

1 School of Geosciences, University of Sydney, Madsen Building, Eastern Avenue, Sydney, NSW 2006, Australia; eleanor.bruce@sydney.edu.au (E.B.); kevin.davies@sydney.edu.au (K.P.D.)
2 Centre for CubeSats, UAVs and Their Applications (CUAVA), University of Sydney, Sydney, NSW 2006, Australia; p.barber@arborcarbon.com.au
3 ArborCarbon Pty Ltd., Murdoch University, Rota Trans 1, Murdoch, WA 6150, Australia
4 Centre for Terrestrial Ecosystem Science & Sustainability, Harry Butler Institute, Murdoch University, Murdoch, WA 6150, Australia
* Correspondence: james.simpson@sydney.edu.au

Abstract: Seagrass ecosystems sequester carbon at disproportionately high rates compared to terrestrial ecosystems and represent a powerful potential contributor to climate change mitigation and adaptation projects. However, at a local scale, rich heterogeneity in seagrass ecosystems may lead to variability in carbon sequestration. Differences in carbon sequestration rates, both within and between seagrass meadows, are related to a wide range of interrelated biophysical and environmental variables that are difficult to measure holistically using traditional field surveys. Improved methods for producing robust, spatially explicit estimates of seagrass carbon storage across large areas would be highly valuable, but must capture complex biophysical heterogeneity and variability to be accurate and useful. Here, we review the current and emerging literature on biophysical processes which shape carbon storage in seagrass beds, alongside studies that map seagrass characteristics using satellite remote sensing data, to create a blueprint for the development of remote sensing-enabled proxies for seagrass carbon stock and sequestration. Applications of satellite remote sensing included measuring seagrass meadow extent, estimating above-ground biomass, mapping species composition, quantifying patchiness and patch connectivity, determining broader landscape environmental contexts, and characterising seagrass life cycles. All of these characteristics may contribute to variability in seagrass carbon storage. As such, remote sensing methods are uniquely placed to enable proxy-based estimates of seagrass carbon stock by capturing their biophysical characteristics, in addition to the spatiotemporal heterogeneity and variability of these characteristics. Though the outlined approach is complex, it is suitable for accurately and efficiently producing a full picture of seagrass carbon stock. This review has drawn links between the processes of seagrass carbon sequestration and the capabilities of remote sensing to detect and characterise these processes. These links will facilitate the development of remote sensing-enabled proxies and support spatially explicit estimates of carbon stock, ensuring climate change mitigation and adaptation projects involving seagrass are accounted for with increased accuracy and reliability.

Keywords: blue carbon; seagrass; carbon stock; proxy

Citation: Simpson, J.; Bruce, E.; Davies, K.P.; Barber, P. A Blueprint for the Estimation of Seagrass Carbon Stock Using Remote Sensing-Enabled Proxies. *Remote Sens.* **2022**, *14*, 3572. https://doi.org/10.3390/rs14153572

Academic Editor: Mingming Jia

Received: 26 May 2022
Accepted: 22 July 2022
Published: 25 July 2022

1. Introduction

The potential role of blue carbon as a natural climate mitigation strategy has prompted increased research focus on methods for monitoring coastal ecosystems [1]. Although the ecological value of seagrass meadows is long established [2], recognition of their value as important sinks in the global carbon cycle [3] highlights the need for robust monitoring and reporting on greenhouse gas (GHG) offset projects [4]. Seagrasses contribute disproportionately to organic carbon (C_{org}) burial, sequestering 10% of oceanic buried C_{org} despite occupying less than 0.2% of ocean area [5]. Despite their relatively small global area

compared to tropical, temperate and boreal forests, they sequester carbon at a comparable rate [6]. Seagrasses also influence water flows, cycle nutrients, form the base of food webs, and offer shelter for a range of marine species [7], positioning them as providers of multiple ecosystem services beyond carbon sequestration [8,9]. Development of methods to accurately map seagrass and produce robust estimates of seagrass carbon storage across large geographical areas is needed to improve global carbon monitoring schemes and support protection and restoration efforts crucial for maintaining ecosystem services.

The carbon sequestration capacity of seagrass is of critical interest in climate change mitigation and adaptation including emissions reporting, GHG abatement schemes and offset projects [1,3]. Protocols for accurate quantification of seagrass carbon stock in the field have been developed [10], and incorporated into some national GHG inventories [11]. However, high inter- and intra-habitat variability in seagrass carbon stock and burial rates [12–15] suggests that regional-scale reporting would be strengthened by measurements which accurately capture this variability.

Satellite remote sensing has been used for continuous broad-scale monitoring of seagrass biomass and condition [16,17]. Synoptic monitoring of coastal ecosystems by satellite remote sensing can provide vital spatial information about the ecological characteristics of seagrasses as they change over time, supporting coastal management and conservation [18–20]. To incorporate seagrass in quantitative climate change mitigation and adaptation strategies, robust methods are required to translate these satellite-derived ecological characteristics into metrics relevant to estimates of carbon stock and sequestration rates. This involves consideration of the ecological characteristics of seagrass meadows as they relate to carbon sequestration and the capabilities of current and future remote sensing platforms.

Although optical satellite remote sensing has been used to characterise the ecological characteristics of seagrass, direct measurement of seagrass carbon stock or sequestration rates using only remote sensing data is still not possible. Therefore, determining estimates of seagrass carbon stocks from remote sensing-based measurements requires an understanding of biophysical processes that underlie seagrass carbon sequestration, and the spatial, temporal and spectral scales relevant to those processes. Developing this understanding is important for identifying biophysical variables usable in carbon stock assessments which are measurable from remote observation platforms. Addressing this challenge requires developing and refining biophysical proxies for total carbon stock that can be derived from remote sensing data and understanding the limitations of current and next-generation remote sensing platforms in sensing these proxies. Here, we present a new perspective on the role of current and emerging remote sensing technologies for broad scale assessment of seagrass carbon stocks through the development of suitable proxy measures.

This review will establish a framework for developing methods for satellite remote sensing-enabled estimation of seagrass carbon stock. In Section 2, we provide background on the key challenges for carbon accounting in seagrass environments. In Section 3, we outline the biophysical processes operating within seagrass environments that drive carbon sequestration rates. In Sections 4 and 5, we carry out a literature review in order to identify viable methods for satellite remote sensing of seagrass biophysical characteristics. Based on this review, we consider a set of remote sensing proxies for carbon storage in seagrass which account for spatial heterogeneity and change over time. Finally, in Section 6, we relate these remote sensing proxies to current seagrass carbon accounting requirements, creating a blueprint for applying Tier 3 spatially explicit methods to seagrass carbon stock mapping and monitoring.

2. Background

Activities within the Land-Use, Land-Use Change and Forestry (LULUCF) sector, such as afforestation and habitat restoration, can provide cost-effective mechanisms for offsetting emissions, which play a key role in current and planned global climate change mitigation policy. Previous mitigation efforts of the LULUCF sector were generally focused on terrestrial forests and grasslands and omitted seagrass and other coastal ecosystems

from national GHG inventories [21]. The Intergovernmental Panel on Climate Change (IPCC) addressed this omission with the release of the Coastal Wetlands supplement to their guidelines on GHG inventories [22]. However, seagrass contributions to carbon emissions have remained underreported and were yet to be fully integrated into national inventories [11,23]. National-level plans for climate change mitigation and adaptation, such as the Nationally Determined Contributions (NDCs) of parties to the Paris Agreement, continue to largely omit seagrass reporting. Of the 185 NDCs submitted by countries as of 2020, 64 included coastal wetlands, while only ten provided explicit reference to seagrasses [11].

Accurate carbon accounting intersects with issues of seagrass conservation. Seagrass meadows are degrading globally, with a rate of loss possibly as high as 7% per year [24]. Degradation of seagrass ecosystems represents a two-fold climate risk: reducing the capacity of blue carbon ecosystems to sequester carbon and provide co-benefits [25], and increased emissions caused by stored C_{org} partially remineralising to become atmospheric CO_2 [26]. Conversely, seagrass meadow restoration substantially increases carbon storage in the soil [3,27]. A recent study estimated the combined possible mitigation benefit from avoided seagrass degradation and seagrass restoration to be 341 $TgCO_2$ equivalent y^{-1} [28], based on a conservative global extent estimate [29]. Given the disproportionate carbon storage and high rate of change, incorporating seagrass conservation and restoration into national emissions reporting, GHG abatement schemes, and offset projects is critical to global climate mitigation efforts.

Accurate inclusion of seagrass ecosystems in carbon accounting estimates is currently limited by existing methodologies. Seagrass reporting in GHG inventories under the IPCC guidelines often employs Tier 1 or Tier 2 methods which rely on global and regional estimates of carbon stock, respectively [30]. Tier 3 methods model carbon stocks using spatially explicit methods. Unlike terrestrial LULUCF inventory contributions, methods for Tier 3 reporting have not been established for seagrass ecosystems. Tier 3 approaches are intended to provide greater accuracy than Tier 1 or 2, and require a robust understanding of underlying processes, and identification of appropriate inputs for models of carbon stock over time [31]. The ability to accurately model carbon stocks in seagrass meadows is contingent upon capture of reliable, high resolution remote sensing data that can be used to represent biophysical characteristics of seagrass ecosystems relevant to carbon sequestration at ecologically appropriate spatiotemporal scales. Improving remote sensing methods for characterising seagrass ecosystems therefore forms a critical agenda for improving coastal carbon accounting mechanisms [32].

A key challenge for developing accurate Tier 3 representations of seagrass is the heterogeneous biophysical characteristics of these ecosystems. The contribution of seagrasses toward carbon sequestration and co-benefits can vary geographically, and are influenced by biophysical characteristics and environmental conditions in ways that are still poorly understood [33–36]. Spatial heterogeneity introduces uncertainty in quantifying ecosystem services in other contexts [37,38], and measurements of carbon stock across different seagrass environments frequently vary by a factor > 20 [12,39]. Spatially explicit Tier 3 models would need to capture spatio-temporal heterogeneity inherent in seagrass meadows to enable accurate emissions reporting.

Carbon stocks in seagrass, as in other environments, can be divided into pools, primarily above-ground biomass (AGB), below-ground biomass (BGB), and soil carbon. In seagrass ecosystems, the soil pool comprises as much as 98% of the total ecosystem carbon stock [40]. Studies have shown that carbon storage potential can be extremely high even in areas with low AGB, primary productivity and areal extent [41,42]. This is a barrier for optical remote sensing as only the above-ground components of the plant and soil background contribute to the optical signal, making estimation of total carbon stock from the optical signal challenging. Despite these challenges, the absorption of electromagnetic radiation by water limits the use of other remote sensing methods, such as microwave remote sensing, to targets above the surface of water. As many seagrass meadows are

fully submerged, satellite-borne optical remote sensing is most promising for producing synoptic seagrass biophysical data; however, microwave remote sensing may contribute complementary information for seagrasses present in the intertidal zone.

Accurate and broad-scale seagrass mapping for carbon reporting requires the repeatable, synoptic coverage provided by satellite remote sensing, rigorously calibrated and validated through field-based verification [43]. However, the heterogeneity within seagrass meadows and the challenges associated with optical remote sensing of seagrass carbon stock limits the use of direct measurement of total carbon from space, necessitating the use of measurable biophysical "proxies" that can capture seagrass ecosystem heterogeneity and contribute to GHG inventories and carbon stock mapping. Appropriate proxies must reliably characterise overall carbon stock and the associated spatial heterogeneity and be measurable with optical remote sensing by satellite. It is also critical that the limitations of remotely sensed proxies for mapping overall carbon stock in seagrass meadows are clearly understood and described to provide accurate estimates of seagrass carbon stock and account for bias.

3. Processes and Drivers of Carbon Sequestration in Seagrass Meadows

Understanding the biophysical processes which drive seagrass carbon sequestration is key to identifying suitable remote sensing proxies to ensure that approaches to development of total carbon stock estimation methods have ecological relevance. Mazarrasa et al. [44] identified three processes which contribute to carbon stock in the soil pool: biomass accumulation (especially below-ground), allochthonous C_{org} sedimentation, and efficient burial of C_{org} (Figure 1).

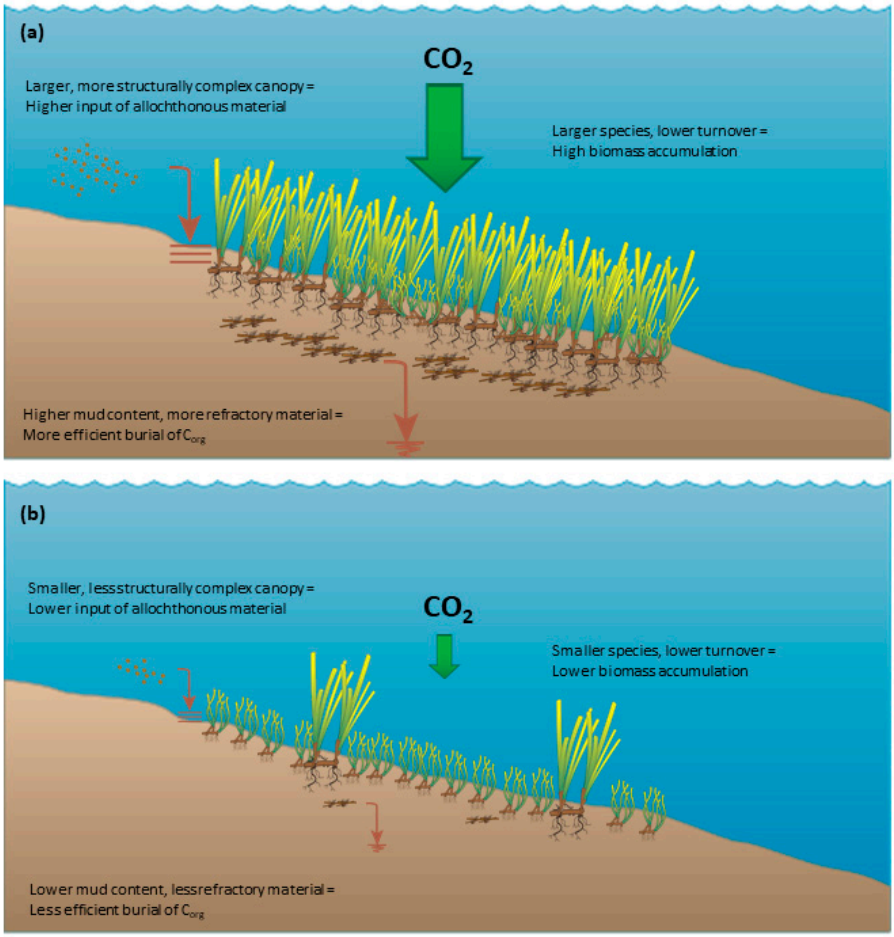

Figure 1. Three key processes in accumulation of seagrass carbon stock: biomass accumulation, input of allochthonous material, and efficient burial of C_{org}, and examples of the biophysical characteristics which drive higher (**a**) and lower (**b**) carbon stocks.

3.1. Biomass Accumulation and Autochthonous Contributions to C_{org} Stocks

Biomass accumulation is closely linked to the species composition of seagrass meadows, as seagrasses display large interspecific differences in biomass. For example, AGB can vary from 2.3 g m^{-2} (*Halophila stipulacea*) to 1005 g m^{-2} (*Amphibolis antarctica*) [45], due to significant differences in shoot and leaf morphology. BGB varies similarly between species, with larger species tending to show both higher biomass and higher BGB to AGB ratios [45]. Certain species, most notably *Posidonia oceanica*, produce particularly large mattes of root and rhizome material [46]. Intraspecies variations in biomass have also been identified, occurring across environmental gradients, including nutrient availability, light availability, salinity and temperature [47–50]. The higher BGB to AGB ratio of morphologically larger seagrasses is important for carbon sequestration as roots and rhizomes are composed of more refractory material than shoots, are less prone to export via herbivory or physical disturbance, and are already located within the anoxic soils which facilitate long term C_{org} storage [51–55]. Morphologically larger seagrasses trend towards higher carbon storage [12,56–58], and have higher relative contribution of autochthonous compared to allochthonous inputs into the carbon stock [59,60].

The life cycles of seagrasses also show considerable interspecies variations. Smaller, colonizing species may exhibit full life cycles on the scale of months, while larger persistent species can take many years [61]. This is an important factor influencing carbon sequestration, as the lower turnover rates of persistent species lead to high biomass accumulation [44]. However, seagrass life cycles can also vary intraspecifically depending on environmental conditions [62,63]. The variation is significant enough that the same species can form both enduring and transitory meadows under different conditions [61,64]. These changing environmental conditions can follow annual cycles, or be related to shorter or longer-term changes caused by fluctuations in dynamic environments or major disturbance events such as storms [61]. Though the relationship between persistence and carbon storage is established [44], there has been limited investigation of intraspecific variation in seagrass life cycle or meadow form and its relationship to carbon sequestration.

3.2. Input of Allochthonous C_{org} into the Ecosystem

Input of allochthonous C_{org} is controlled both by biophysical characteristics of seagrass meadows and environmental conditions. Seagrass canopies influence the local hydrodynamic environment, increasing sedimentation and decreasing resuspension [54,65–67]. Morphologically larger species and mixed species meadows form canopies with higher complexity, which more effectively encourage sedimentation as they reduce water velocity and baffle sediments [44,68]. Higher density meadows also have a larger impact on local flow rates and sedimentation [69,70]. Input of allochthonous C_{org} is therefore influenced by the same set of biotic factors as biomass accumulation [44]. However, unlike biomass accumulation, which is indirectly shaped by abiotic factors that determine seagrass growth patterns, the input of allochthonous C_{org} is more heavily influenced by abiotic factors, especially those relating to sediment. The capture of allochthonous C_{org} by seagrass meadows first requires a sediment source, therefore source sediment characteristics including density, grain size, and C_{org} content influence carbon stocks [34,71–73]. Geomorphic setting also influences input of allochthonous C_{org} into the seagrass ecosystem. Small species in high-energy coastal settings have less capacity to capture sediment, while low-energy estuarine settings are associated with higher amounts of sedimentary C_{org} accumulation [60,74]. Although relationships between canopy complexity and supply of allochthonous C_{org} appear to exist [75], this relationship is complicated by the abiotic factors which influence sedimentation rate and sediment C_{org} content.

The spatial arrangement of the seagrass landscape is an additional dimension that influences input of allochthonous C_{org} into seagrass carbon stocks. Continuous meadows capture sediment more effectively than meadows fragmented into patches [76,77]. Carbon stocks within a patch tend to increase with distance from the patch edge [78]. The arrangement of gaps in seagrass meadows relative to the direction of water flow may

also impact sedimentation, as flow attenuation will differ with variations in gap shape and arrangement [79,80]. The broader coastal landscape is also important, as proximal ecosystems that are highly productive such as mangroves can contribute C_{org} to seagrass sediments [81,82]. Similarly, the presence of nearby barrier reefs can drive the input of allochthonous C_{org} by reducing local wave energy [83]. The input of allochthonous C_{org} is therefore driven by the complex interactions of biotic and abiotic characteristics acting across varying spatial scales.

3.3. Efficient Burial of C_{org}

The burial efficiency of C_{org} determines the amount of organic material that will remain in the soil in the long term after being introduced through the processes of biomass accumulation and allochthonous sedimentation. This is influenced by conditions which lead to relatively high levels of recalcitrance, therefore lower levels of degradation into atmospheric CO_2, in organic material in the soil. An anoxic soil environment, high mud content, and a large proportion of more refractory material such as roots and rhizomes are conducive to higher burial efficiency [44]. Seagrasses increase mud concentration in the soil by capturing fine sediments, in turn encouraging anoxic conditions and seagrass tissue recalcitrance [84]. The proportion of refractory material is linked to its origin, as autochthonous material tends to be more refractory than allochthonous. The efficient burial of C_{org} is therefore in part driven by the same conditions which lead to high biomass accumulation (morphologically larger, persistent species) and high input of allochthonous C_{org} (high rates of sedimentation and C_{org}-rich sediments).

3.4. Summary: Processes and Drivers of Seagrass Carbon Stocks

The drivers of seagrass carbon sequestration are complex. Larger, more persistent species lead to higher carbon stocks, especially when meadows are dense and less fragmented. This applies to both autochthonous and allochthonous components of total carbon stock, though the latter is more influenced by geomorphic setting and source sediment properties. Estimation of carbon stocks therefore requires an understanding of the species composition and morphology, the spatial arrangement of seagrass meadows, patterns of spatiotemporal change, and the broader coastal landscape context in which the meadow is situated.

Although larger seagrass species have consistently higher C_{org} stocks, other drivers of carbon sequestration can act in highly variable ways depending upon context [60]. The complexity of the relationships between drivers and carbon stocks highlights the need to account for key biophysical characteristics, their variability and heterogeneity, as well as environmental setting in the mapping of seagrass carbon stocks.

4. Review Method

A literature review was carried out to generate a library of established remote sensing methods to ascertain what biophysical characteristics have been measured in the past, how they were measured, and any technical limitations on their measurement. Studies to include in this library were identified through a systematic literature search.

Many remote sensing studies characterise seagrass without explicit reference to carbon stock or sequestration. For this reason, the search terms did not include reference to carbon, instead focusing on the subject (seagrass) and the method (satellite remote sensing). The following search terms were entered into Web of Science and Scopus: ("Seagrass" OR "submerged aquatic vegetation") AND ("remote sensing" OR "remotely sensed" OR "satellite" OR "earth observation" OR "Landsat" OR "WorldView" OR "PlanetScope" OR "QuickBird" OR "IKONOS" OR "Sentinel-2"). The search was limited to academic journal articles published in English and studies published on or before 30 April 2022.

After deduplication, 1119 records were identified. The abstracts of these studies were examined and irrelevant records excluded. The full texts of the remaining studies were reviewed to ensure they:

1. Contained a clearly described and repeatable method;
2. Used optical satellite remote sensing data to attempt to measure at least one biophysical characteristic of seagrass;
3. Did not exclusively use manual image interpretation techniques.

A total of 204 studies fulfilled these criteria and were used to create the database of seagrass remote sensing methods, including a record of different methodological techniques and contextual information such as study site location.

5. Identifying Remote Sensing Proxies for Seagrass Carbon Stock: Possibilities and Challenges

Levels of carbon stock within seagrass meadows are influenced by biomass accumulation, the input of allochthonous C_{org}, the efficient burial of C_{org} [44], and the biophysical and environmental drivers of those processes. In this section, we examine potential remote sensing proxies for improving the measurement of seagrass carbon stocks and evaluate direct monitoring of blue carbon potential from space. Although recent modelling has highlighted the complexity of the relationships between potential remote proxies and seagrass carbon stock [36,60,85], the identification of proxies that can be measured from space, and an assessment of the limitations of such an approach is an important first step in conceiving a holistic remote sensing-enabled methodology for spatially explicit mapping of seagrass carbon stock.

5.1. Meadow Characteristics and Dynamics as Proxy Indicators of Carbon Stock

5.1.1. Aboveground Biomass (AGB)

Direct estimates of AGB, as well as the related biophysical metrics of percent cover and Leaf Area Index (LAI), have been widely used in studies characterising seagrass using satellite remote sensing [86–91] Approaches applied include discrete mapping of percent cover classes (e.g., [88,92]) and regression-based estimates of AGB on a per-pixel basis (e.g., [91,93]). Although AGB contributes as little as 2% of total carbon stock in seagrass ecosystems [40], AGB is closely related to both BGB and soil carbon [75,94]. The importance of seagrass productivity and canopy complexity in carbon sequestration and the viability of remote sensing-based measurements of AGB and related characteristics highlight the potential of seagrass AGB as a remote sensing-based proxy for carbon stock.

The challenge in identifying the ideal approach for deriving estimates of seagrass AGB as a proxy for carbon stock is the selection of remote sensing methods that are both ecologically appropriate and capable of producing accurate results. From the three interrelated metrics described above, percent cover is more easily derived from remote sensing data compared to LAI and AGB, as it contributes more directly to the remote sensing signal. In comparison, LAI and AGB estimates are more limited, especially in dense seagrass meadows, due to saturation of the remote sensing signal [90,95,96]. As AGB incorporates information about the three-dimensional volume of plants it is the most abstracted of these three metrics from the remote sensing signal [97]. However, percent cover is less directly related to the accumulation of biomass and capture of allochthonous C_{org} than AGB and therefore a less direct proxy for overall carbon stock.

In the case of intertidal seagrass beds, the periodic absence of the water column provides additional remote sensing options for characterising seagrass AGB. Access to wavelengths of light which are highly attenuated by water makes common vegetation indices which rely upon near infrared reflectance, including the Normalised Difference Vegetation Index (NDVI), viable in intertidal environments [95,98]. Additionally, recent research has suggested that Synthetic Aperture Radar (SAR) data improve the accuracy of seagrass mapping, including AGB estimates, by providing information on surface structure which complements optical remote sensing data [99,100]. These approaches may also be applicable for seagrass beds which are emergent but not fully intertidal. These studies suggest that AGB estimates could be approached differently for intertidal and subtidal seagrass.

An important additional methodological consideration is whether to map AGB in discrete classes or as continuous values. As seagrass density can vary over light availability gradients [101,102], a continuous measurement would be more ecologically appropriate [103]. Remote sensing-derived estimates of AGB are likely to be an important proxy for total carbon stock, but their effective use requires a deeper understanding of methodological complexities to identify sensor properties data analysis techniques which can most accurately and reliably produce AGB estimates.

5.1.2. Meadow Species Composition

Species composition is an important consideration for the effective use of AGB-based carbon stock proxies. Significant differences in morphology and AGB to BGB ratio among seagrass species [45] suggest that classification of seagrasses by species could enhance the accuracy of satellite derived prediction of overall carbon stock. Although species composition is not a reliable direct proxy for carbon stock, it can complement AGB data and improve remote sensing-enabled carbon stock estimates.

Many species of seagrass are spectrally separable [87,104], and are therefore distinguishable using optical satellite remote sensing. However, spectral differences between seagrass species are often subtle [105], and epiphytic growth can interfere with spectral separability [106]. Beyond the spectral properties of individual leaves, the morphology of shoots can also impact their detection. Traganos and Reinartz [107,108] mapped two morphologically distinct species (*Posidonia oceanica* and *Cymodocea nodosa*) using Sentinel-2 [107] and RapidEye [108] satellite images. Sentinel-2 has a broader spectral range compared to RapidEye with data captured in a shorter wavelength coastal blue band. In both cases *P. oceanica* was classified more accurately than *C. nodosa.* When the narrower spectral range RapidEye images were used, the difference was considerable with an accuracy of 89–92% for *P. oceanica* and 50–61% for *C. nodosa*. These results suggest that although smaller species are more difficult to map accurately, a broader spectral range has the potential to improve detection. Methods that incorporate non-spectral data such as secondary textural characteristics or object-based approaches are effective in classifying species, even in relatively species-rich tropical areas [109–111]. These approaches may offer a useful alternative for overcoming spectral similarity and other species classification challenges such as turbidity which can impact on the spectral information.

5.1.3. Intra-Annual Variation in Seagrass Growth

Seagrass meadows exhibit intra-annual, seasonal variation in AGB [64,112] and at the extremes of habitat suitability, shoots can be completely absent for months of the year when water temperatures are outside the habitable range [113]. This is particularly relevant when using AGB as a proxy for carbon stock, because despite seasonal variability in seagrass growth, soil carbon and total carbon stock are more temporally stable [114]. Traditionally, biomass assessments were recommended during the peak growing season [115]. However, significant intraspecific differences in seagrass phenology can exist even with minor differences in environmental conditions. This is further complicated in mixed meadows, where interspecific differences in phenology lead to biomass peaks at different times [116]. Given the complex factors dictating peak biomass and the apparent variability in the ratio of AGB to overall carbon stock, assessments at intra-annual timescales should be considered to ensure robustness when measuring AGB as a proxy for overall carbon stock. In addition, importance of regular monitoring will increase in the future as the environmental conditions which dictate seagrass phenology shift under changing climate conditions [117].

5.2. Landscape Ecology Metrics and Spatial Characteristics as Proxies for Carbon Stock

5.2.1. Landscape Ecology Metrics Applied to Seagrass Meadows

The spatial structure and arrangement of seagrass meadows have been linked to rates of carbon burial, with studies showing that continuous seagrass meadows capture allochthonous C_{org} more effectively than fragmented meadows, leading to greater input

of C_{org} into the sediments [76–78]. Landscape ecology metrics, which offer methods of quantifying the spatial arrangement of landscapes, may therefore provide a suitable remote sensing-based proxy for carbon stock across the seagrass landscape. Recognition of the system properties present in heterogeneous seascapes has prompted growing application of landscape ecology concepts and techniques to coastal and marine environments, including consideration of spatial context, configuration, connectivity, and the effects of scale [118].

Seagrass patches vary widely in size, often from 1–100 m in diameter [119]; however, the spatial scales at which spatial configuration and fragmentation significantly affect carbon sequestration are not well established. Although seascape metrics could provide an effective indicator of potential carbon stock, there is a need to determine the appropriate spatio-temporal scale for adequately capturing the biophysical processes influencing the relationship between the spatial configuration of seagrass meadows and carbon sequestration [120].

The spatial, spectral and temporal resolution of remote sensing data products will determine the seascape metrics that can realistically be measured [121]. Seascape metrics such as patch shape, area and edge length have been measured using aerial platforms [122–124] and patch complexity, connectivity and diversity have been quantified using high spatial resolution platforms, including GeoEye-1, IKONOS and SPOT 7 [125–127]. Studies have demonstrated the importance of ultra-high spatial resolution imagery for mapping patch level fragmentation [128,129], which may otherwise be masked in measures of overall seagrass density based on coarser spatial resolution imagery (Figure 2). Although there has been limited research linking landscape metrics and carbon stock using remote sensing data, modelling has shown that metrics related to heterogeneity and patch fragmentation are strong predictors of overall carbon stocks [36,72].

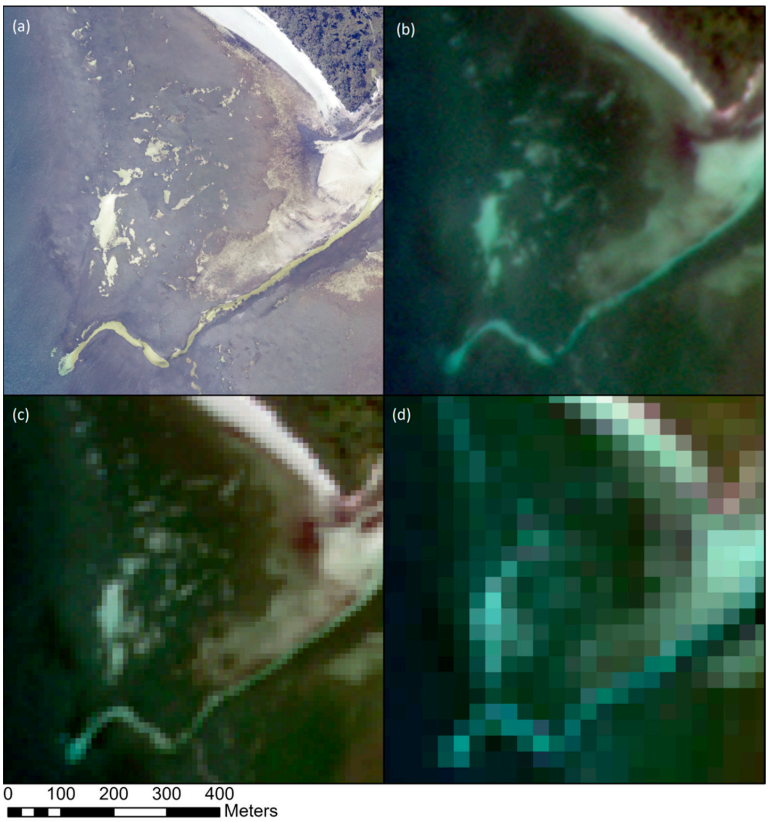

Figure 2. A patchy seagrass meadow in Jervis Bay NSW, Australia, displayed at four different spatial resolutions. This demonstrates the effect of image spatial resolution on the representation of spatial arrangement in seagrass ecosystems. Images sourced from (**a**) ArborCam aerial imagery (0.05 m spatial resolution, captured 15 October 2020), (**b**) PlanetScope (3 m spatial resolution, captured 14 October 2020), (**c**) Sentinel-2A (10 m spatial resolution, captured 12 October 2020), and (**d**) Landsat 8 OLI (30 m spatial resolution, captured 22 September 2020).

5.2.2. Landscape Context

Local landscape context influences the quantity and carbon content of sediment deposits [14,72]. In estuarine environments, seagrass meadows further inland and in areas less exposed to wave energy have higher sediment accretion rates, with studies showing carbon stocks decreasing along an oceanward gradient [14,85]. Additionally, proximity to ecosystems with high productivity and outflow of organic material, such as mangroves, is associated with increased carbon storage in seagrass meadows [36,81].

Broad characterisations of geomorphic setting have been found to be insufficient for predicting seagrass total carbon stocks, suggesting that the influence of landscape context varies locally depending on factors such as sediment deposition rates and surrounding geology [60,130]. This is relevant for remote sensing-based estimates of carbon stock as it suggests that measuring seagrass characteristics alone, without landscape context, risks missing key variables. Further, Asplund et al. [36] found that the predictive power of patch fragmentation metrics for estimating sedimentary C_{org} stock varied considerably between seagrass species. This work suggests that the effective use of landscape ecology-based proxies for seagrass carbon stock requires site specific understanding, including local landscape context and nearshore sedimentary environment.

5.3. Seagrass Life History and Phenological Time Series Analysis

Carbon storage potential is also influenced by the temporal dynamics of seagrass meadows, a characteristic that can be detected using remote sensing-based change detection analysis. Enduring seagrass meadows have higher carbon stores than transitory meadows [44,131], highlighting the importance of seasonal and multi-decadal monitoring of vegetation cover. Change detection can support carbon stock assessments in two ways. First, through classification of life history (e.g., persistent/opportunistic/colonising, enduring/transitory; [61]) which would enable differentiation between areas which show significant intraspecies differences in life cycle (not measurable using single date or annual image capture, see Figure 3). Second, using temporal analysis to derive phenological metrics can assist in differentiating species where spectral separability is poor, an approach successfully applied in terrestrial contexts [132]. Measures of intra-annual change and phenology have the potential to contribute directly as carbon storage proxies, or indirectly by supporting more accurate species classification.

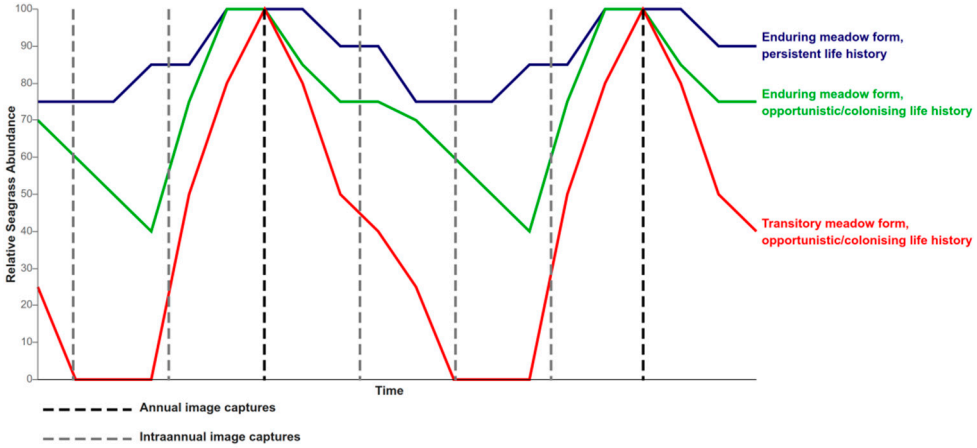

Figure 3. Conceptual comparison of different seagrass life cycles, highlighting the differences in representation between annual and intra-annual capture of remote sensing images. Indicative seagrass life cycles adapted from [61].

Multi-temporal remote sensing analysis of seagrass introduces challenges. Differences in water column properties (e.g., tidal level, turbidity) between image dates or poor georegistration of mutitemporal images can introduce errors when they are confused for changes in seagrass extent or biophysical properties [133,134].

Despite the dynamic nature of seagrass meadows, there has been limited research on the use of remote sensing for characterising intra-annual variability, with most time series studies focused on longer-term change [108,135–137]. A relatively small number of studies have examined shorter term variation in seagrass using satellite remote sensing, often showing complex intra-annual dynamics [133,138,139]. Given the potential significance of seagrass life cycle for carbon storage, further research is needed on the application of remote sensing for continuous capture of phenological patterns across seagrass meadows.

6. Enabling Carbon Stock Estimates from Space

Remote sensing-based proxies of seagrass carbon stocks should be informed by an understanding of the underlying biophysical processes and drivers of carbon sequestration. Satellite remote sensing is well placed to:

1. Estimate AGB and its heterogeneity across space;
2. Classify seagrass ecosystems by species composition or dominant species;
3. Characterise the spatial configuration and landscape context of seagrass ecosystems, and quantify these characteristics using landscape ecology metrics;
4. Capture intra-annual variability of seagrass species composition and AGB to monitor seagrass life cycles and temporal change (Figure 4).

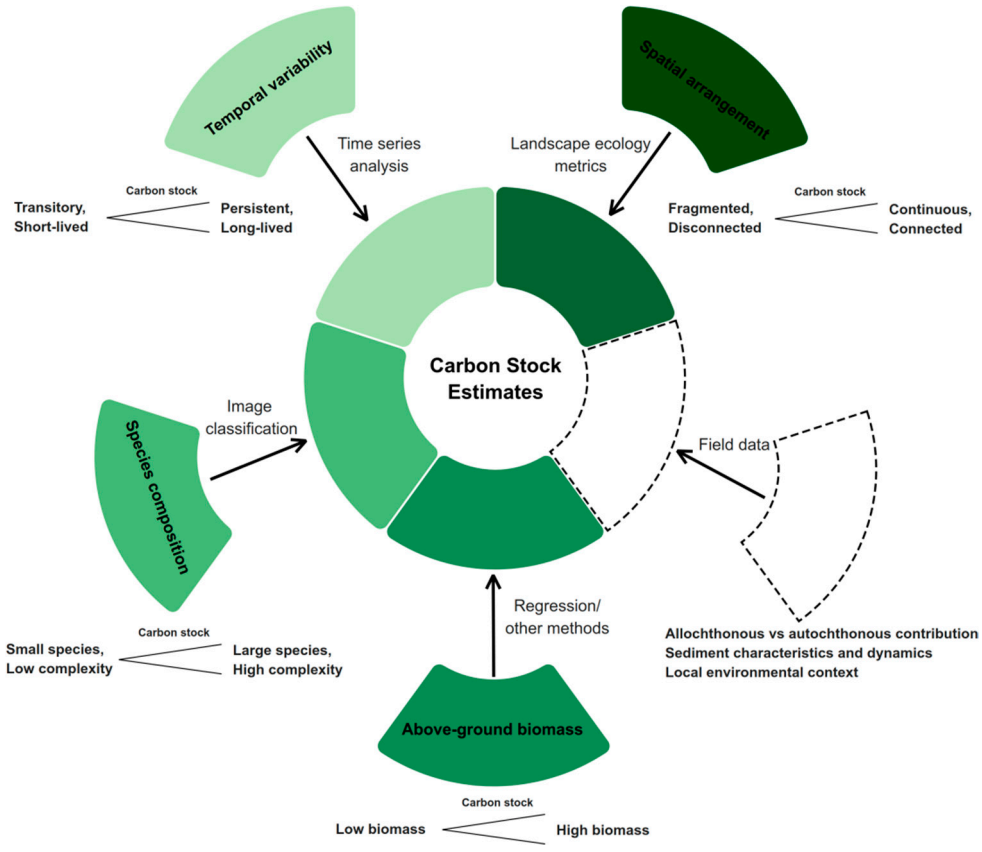

Figure 4. Potential proxies for estimating seagrass carbon stock. Filled in segments represent individual proxies measurable with remote sensing methods, while the dashed outline segment represents complementary field data for important variables not currently measurable using remote sensing.

However, the processes underlying seagrass carbon sequestration are complex, often non-linear in nature and abstracted from remote sensing signals. For example, while measurement of seagrass AGB can be detected via remote sensing, critical carbon accounting variables such as sediment properties, including grain size, sedimentation rate and C_{org} content, cannot be directly measured from space. In many coastal settings, these sediment properties are the primary driver of carbon burial [14], while in other environments

seagrass properties, such as species composition, play an important role [36]. Accurate estimates must be verified, not only through in situ field validation of satellite data, but through incorporating knowledge of seascape context, sediment dynamics and the relative contributions of different biophysical processes. Characterising the relative contributions of allochthonous and autochthonous C_{org} to the seagrass carbon pool, the variation in these processes over space and time, and the sediment properties determining the efficiency of C_{org} burial is critical for deriving effective spatially explicit estimates of carbon stock to support carbon accounting (Figure 4).

7. Conclusions

The globally significant contribution of seagrass ecosystems to carbon sequestration highlights the importance of rigorous methods to quantify carbon stock and stock change for incorporation into emissions reporting, GHG abatement schemes and offset projects. The processes involved in seagrass carbon sequestration are complex and require accurate characterisation of key biophysical characteristics of the seagrass.

Future work to develop spatially explicit models of seagrass carbon stock should focus on determining reliable proxies of carbon stock which can be measured in a synoptic manner. Seagrass carbon stocks have been estimated using predictive modelling [36,60,72], and the inclusion of ecologically relevant remote sensing-based data can ensure that these models accurately capture the complexity and heterogeneity of seagrass ecosystems. This will support the effective use of remote sensing data by helping to identify the roles of local environmental processes in shaping carbon sequestration. Additionally, seagrass carbon stock estimation may be improved through optimising remote sensing data collection (e.g., sensor spatial, temporal and spectral properties) and data analysis (e.g., accuracy and thematic resolution of outputs). Addressing these priorities will improve spatially explicit carbon stock estimations in critical seagrass ecosystems.

Author Contributions: Conceptualization, J.S., E.B., and K.P.D.; investigation, J.S.; resources, E.B., P.B. and K.P.D.; writing—original draft preparation, J.S.; writing—review and editing, J.S., E.B., P.B. and K.P.D.; visualization, J.S., E.B. and P.B.; supervision, E.B., P.B. and K.P.D.; project administration, E.B. and K.P.D.; funding acquisition, E.B. All authors have read and agreed to the published version of the manuscript.

Funding: This research was funded by the Australian Research Council, grant number IC170100023.

Data Availability Statement: Not applicable.

Acknowledgments: ArborCam images provided by ArborCarbon Pty Ltd., Murdoch, Australia.

Conflicts of Interest: The funders had no role in the design of the study; in the collection, analyses, or interpretation of data; in the writing of the manuscript; or in the decision to publish the results. P.B. is an employee of ArborCarbon.

References

1. Macreadie, P.I.; Costa, M.D.; Atwood, T.B.; Friess, D.A.; Kelleway, J.J.; Kennedy, H.; Lovelock, C.E.; Serrano, O.; Duarte, C.M. Blue carbon as a natural climate solution. *Nat. Rev. Earth Environ.* **2021**, *2*, 826–839. [CrossRef]
2. Thayer, G.W.; Wolfe, D.A.; Williams, R.B. The Impact of Man on Seagrass Systems: Seagrasses must be considered in terms of their interaction with the other sources of primary production that support the estuarine trophic structure before their significance can be fully appreciated. *Am. Sci.* **1975**, *63*, 288–296.
3. Oreska, M.P.; McGlathery, K.J.; Aoki, L.R.; Berger, A.C.; Berg, P.; Mullins, L. The greenhouse gas offset potential from seagrass restoration. *Sci. Rep.* **2020**, *10*, 7325. [CrossRef] [PubMed]
4. Campbell, A.D.; Fatoyinbo, T.; Charles, S.P.; Bourgeau-Chavez, L.L.; Goes, J.; Gomes, H.; Halabisky, M.; Holmquist, J.; Lohrenz, S.; Mitchell, C.; et al. A review of carbon monitoring in wet carbon systems using remote sensing. *Environ. Res. Lett.* **2022**, *17*, 025009. [CrossRef]
5. Fourqurean, J.W.; Duarte, C.M.; Kennedy, H.; Marbà, N.; Holmer, M.; Mateo, M.A.; Apostolaki, E.T.; Kendrick, G.A.; Krause-Jensen, D.; McGlathery, K.J. Seagrass ecosystems as a globally significant carbon stock. *Nat. Geosci.* **2012**, *5*, 505–509. [CrossRef]

6. McLeod, E.; Chmura, G.L.; Bouillon, S.; Salm, R.; Björk, M.; Duarte, C.M.; Lovelock, C.E.; Schlesinger, W.H.; Silliman, B.R. A blueprint for blue carbon: Toward an improved understanding of the role of vegetated coastal habitats in sequestering CO_2. *Front. Ecol. Environ.* **2011**, *9*, 552–560. [CrossRef]
7. Hemminga, M.A.; Duarte, C.M. *Seagrass Ecology*; Cambridge University Press: Cambridge, UK, 2000.
8. Nordlund, L.; Koch, E.W.; Barbier, E.B.; Creed, J.C. Seagrass Ecosystem Services and Their Variability across Genera and Geographical Regions. *PLoS ONE* **2016**, *11*, e0163091. [CrossRef] [PubMed]
9. Unsworth, R.K.; Nordlund, L.M.; Cullen-Unsworth, L.C. Seagrass meadows support global fisheries production. *Conserv. Lett.* **2019**, *12*, e12566. [CrossRef]
10. Howard, J.; Hoyt, S.; Isensee, K.; Telszewski, M.; Pidgeon, E. *Coastal Blue Carbon: Methods for Assessing Carbon Stocks and Emissions Factors in Mangroves, Tidal Salt Marshes, and Seagrasses*; Conservation International: Arlington, VA, USA, 2014.
11. United Nations Environment Programme. *Out of the Blue: The Value of Seagrasses to the Environment and to People*; UNEP: Nairobi, Kenya, 2020.
12. Lavery, P.S.; Mateo, M.A.; Serrano, O.; Rozaimi, M. Variability in the carbon storage of seagrass habitats and its implications for global estimates of blue carbon ecosystem service. *PLoS ONE* **2013**, *8*, e73748. [CrossRef] [PubMed]
13. Sanders, C.J.; Maher, D.T.; Smoak, J.M.; Eyre, B.D. Large variability in organic carbon and $CaCO_3$ burial in seagrass meadows: A case study from three Australian estuaries. *Mar. Ecol. Prog. Ser.* **2019**, *616*, 211–218. [CrossRef]
14. Ricart, A.M.; York, P.H.; Bryant, C.V.; Rasheed, M.A.; Ierodiaconou, D.; Macreadie, P.I. High variability of Blue Carbon storage in seagrass meadows at the estuary scale. *Sci. Rep.* **2020**, *10*, 5865. [CrossRef] [PubMed]
15. Kim, S.H.; Suonan, Z.; Qin, L.-Z.; Kim, H.; Park, J.-I.; Kim, Y.K.; Lee, S.; Kim, S.-G.; Kang, C.-K.; Lee, K.-S. Variability in blue carbon storage related to biogeochemical factors in seagrass meadows off the coast of the Korean peninsula. *Sci. Total Environ.* **2022**, *813*, 152680. [CrossRef]
16. Bramante, J.F.; Ali, S.M.; Ziegler, A.D.; Sin, T.M. Decadal biomass and area changes in a multi-species meadow in Singapore: Application of multi-resolution satellite imagery. *Bot. Mar.* **2018**, *61*, 289–304. [CrossRef]
17. Poursanidis, D.; Traganos, D.; Teixeira, L.; Shapiro, A.; Muaves, L. Cloud-native seascape mapping of Mozambique's Quirimbas National Park with Sentinel-2. *Remote Sens. Ecol. Conserv.* **2021**, *7*, 275–291. [CrossRef]
18. Topouzelis, K.; Makri, D.; Stoupas, N.; Papakonstantinou, A.; Katsanevakis, S. Seagrass mapping in Greek territorial waters using Landsat-8 satellite images. *Int. J. Appl. Earth Obs. Geoinf.* **2018**, *67*, 98–113. [CrossRef]
19. Randazzo, G.; Italiano, F.; Micallef, A.; Tomasello, A.; Cassetti, F.P.; Zammit, A.; D'Amico, S.; Saliba, O.; Cascio, M.; Cavallaro, F. WebGIS Implementation for Dynamic Mapping and Visualization of Coastal Geospatial Data: A Case Study of BESS Project. *Appl. Sci.* **2021**, *11*, 8233. [CrossRef]
20. McKenzie, L.J.; Langlois, L.A.; Roelfsema, C.M. Improving Approaches to Mapping Seagrass within the Great Barrier Reef: From Field to Spaceborne Earth Observation. *Remote Sens.* **2022**, *14*, 2604. [CrossRef]
21. Herr, D.; Pidgeon, E.; Laffoley, D.d.A. *Blue Carbon Policy Framework 2.0: Based on the Discussion of the International Blue Carbon Policy Working Group*; IUCN: Gland, Switzerland, 2012.
22. Intergovernmental Panel on Climate Change. *2013 Supplement to the 2006 IPCC Guidelines for National Greenhouse Gas Inventories: Wetlands*; Hiraishi, T., Krug, T., Tanabe, K., Srivastava, N., Baasunsuren, J., Fukuda, M., Troxler, T.G., Eds.; IPCC: Geneva, Switzerland, 2014.
23. Ralph, P.J.; Crosswell, J.; Cannard, T.; Steven, A.D. Estimating seagrass blue carbon and policy implications: The Australian perspective. In *Seagrasses of Australia*; Springer: Berlin/Heidelberg, Germany, 2018; pp. 743–758.
24. Orth, R.J.; Carruthers, T.J.; Dennison, W.C.; Duarte, C.M.; Fourqurean, J.W.; Heck, K.L.; Hughes, A.R.; Kendrick, G.A.; Kenworthy, W.J.; Olyarnik, S. A global crisis for seagrass ecosystems. *Bioscience* **2006**, *56*, 987–996. [CrossRef]
25. Hopkinson, C.S.; Cai, W.-J.; Hu, X. Carbon sequestration in wetland dominated coastal systems—A global sink of rapidly diminishing magnitude. *Curr. Opin. Environ. Sustain.* **2012**, *4*, 186–194. [CrossRef]
26. Lovelock, C.E.; Atwood, T.; Baldock, J.; Duarte, C.M.; Hickey, S.; Lavery, P.S.; Masque, P.; Macreadie, P.I.; Ricart, A.M.; Serrano, O. Assessing the risk of carbon dioxide emissions from blue carbon ecosystems. *Front. Ecol. Environ.* **2017**, *15*, 257–265. [CrossRef]
27. Greiner, J.T.; McGlathery, K.J.; Gunnell, J.; McKee, B.A. Seagrass restoration enhances "blue carbon" sequestration in coastal waters. *PLoS ONE* **2013**, *8*, e72469.
28. Griscom, B.W.; Adams, J.; Ellis, P.W.; Houghton, R.A.; Lomax, G.; Miteva, D.A.; Schlesinger, W.H.; Shoch, D.; Siikamäki, J.V.; Smith, P.J. Natural climate solutions. *Proc. Natl. Acad. Sci. USA* **2017**, *114*, 11645–11650. [CrossRef] [PubMed]
29. UNEP-WCMC; Short, F.T. *Global Distribution of Seagrasses (Version 7.1). Seventh Update to the Data Layer Used in Green and Short (2003)*; UN Environment Programme World Conservation Monitoring Centre: Cambridge, UK, 2021.
30. Intergovernmental Panel on Climate Change. *2006 IPCC Guidelines for National Greenhouse Gas Inventories, Prepared by the National Greenhouse Gas Inventories Programme*; Eggleston, H.S., Buendia, L., Miwa, K., Ngara, T., Tanabe, K., Eds.; IGES: Hayama, Japan, 2006.
31. Intergovernmental Panel on Climate Change. *2019 Refinement to the 2006 IPCC Guidelines for National Greenhouse Gas Inventories*; Calvo Buendia, E., Tanabe, K., Kranjc, A., Baasunsuren, J., Fukuda, M., Ngarize, S., Osako, A., Pyrozhenko, Y., Shermanau, P., Federici, S., Eds.; IPCC: Geneva, Switzerland, 2019.
32. Macreadie, P.I.; Baird, M.E.; Trevathan-Tackett, S.M.; Larkum, A.W.; Ralph, P.J. Quantifying and modelling the carbon sequestration capacity of seagrass meadows—A critical assessment. *Mar. Pollut. Bull.* **2014**, *83*, 430–439. [CrossRef] [PubMed]

33. Miyajima, T.; Hori, M.; Hamaguchi, M.; Shimabukuro, H.; Adachi, H.; Yamano, H.; Nakaoka, M. Geographic variability in organic carbon stock and accumulation rate in sediments of East and Southeast Asian seagrass meadows. *Glob. Biogeochem. Cycles* **2015**, *29*, 397–415. [CrossRef]
34. Dahl, M.; Deyanova, D.; Gutschow, S.; Asplund, M.E.; Lyimo, L.D.; Karamfilov, V.; Santos, R.; Bjork, M.; Gullstrom, M. Sediment Properties as Important Predictors of Carbon Storage in Zostera marina Meadows: A Comparison of Four European Areas. *PLoS ONE* **2016**, *11*, e0167493. [CrossRef]
35. Mazarrasa, I.; Marbà, N.; Garcia-Orellana, J.; Masqué, P.; Arias-Ortiz, A.; Duarte, C.M. Effect of environmental factors (wave exposure and depth) and anthropogenic pressure in the C sink capacity of Posidonia oceanica meadows. *Limnol. Oceanogr.* **2017**, *62*, 1436–1450. [CrossRef]
36. Asplund, M.E.; Dahl, M.; Ismail, R.O.; Arias-Ortiz, A.; Deyanova, D.; Franco, J.N.; Hammar, L.; Hoamby, A.I.; Linderholm, H.W.; Lyimo, L.D. Dynamics and fate of blue carbon in a mangrove–seagrass seascape: Influence of landscape configuration and land-use change. *Landsc. Ecol.* **2021**, *36*, 1489–1509. [CrossRef]
37. Dong, M.; Bryan, B.A.; Connor, J.D.; Nolan, M.; Gao, L. Land use mapping error introduces strongly-localised, scale-dependent uncertainty into land use and ecosystem services modelling. *Ecosyst. Serv.* **2015**, *15*, 63–74. [CrossRef]
38. Mattsson, E.; Ostwald, M.; Wallin, G.; Nissanka, S. Heterogeneity and assessment uncertainties in forest characteristics and biomass carbon stocks: Important considerations for climate mitigation policies. *Land Use Policy* **2016**, *59*, 84–94. [CrossRef]
39. Ewers Lewis, C.J.; Carnell, P.E.; Sanderman, J.; Baldock, J.A.; Macreadie, P.I. Variability and Vulnerability of Coastal 'Blue Carbon' Stocks: A Case Study from Southeast Australia. *Ecosystems* **2017**, *21*, 263–279. [CrossRef]
40. Serrano, O.; Lovelock, C.E.; Atwood, T.B.; Macreadie, P.I.; Canto, R.; Phinn, S.; Arias-Ortiz, A.; Bai, L.; Baldock, J.; Bedulli, C.; et al. Australian vegetated coastal ecosystems as global hotspots for climate change mitigation. *Nat. Commun.* **2019**, *10*, 4313. [CrossRef]
41. Armitage, A.R.; Fourqurean, J.W. Carbon storage in seagrass soils: Long-term nutrient history exceeds the effects of near-term nutrient enrichment. *Biogeosciences* **2016**, *13*, 313–321. [CrossRef]
42. Serrano, O.; Gómez-López, D.I.; Sánchez-Valencia, L.; Acosta-Chaparro, A.; Navas-Camacho, R.; González-Corredor, J.; Salinas, C.; Masque, P.; Bernal, C.A.; Marbà, N. Seagrass blue carbon stocks and sequestration rates in the Colombian Caribbean. *Sci. Rep.* **2021**, *11*, 11067. [CrossRef] [PubMed]
43. Duffy, J.E.; Benedetti-Cecchi, L.; Trinanes, J.; Muller-Karger, F.E.; Ambo-Rappe, R.; Boström, C.; Buschmann, A.H.; Byrnes, J.; Coles, R.G.; Creed, J.; et al. Toward a Coordinated Global Observing System for Seagrasses and Marine Macroalgae. *Front. Mar. Sci.* **2019**, *6*, 317. [CrossRef]
44. Mazarrasa, I.; Samper-Villarreal, J.; Serrano, O.; Lavery, P.S.; Lovelock, C.E.; Marba, N.; Duarte, C.M.; Cortes, J. Habitat characteristics provide insights of carbon storage in seagrass meadows. *Mar. Pollut. Bull.* **2018**, *134*, 106–117. [CrossRef] [PubMed]
45. Duarte, C.M.; Chiscano, C.L. Seagrass biomass and production: A reassessment. *Aquat. Bot.* **1999**, *65*, 159–174. [CrossRef]
46. Pergent, G.; Romero, J.; Pergent-Martini, C.; Mateo, M.-A.; Boudouresque, C.-F. Primary production, stocks and fluxes in the Mediterranean seagrass Posidonia oceanica. *Mar. Ecol. Prog. Ser.* **1994**, 139–146. [CrossRef]
47. Lirman, D.; Cropper, W.P. The influence of salinity on seagrass growth, survivorship, and distribution within Biscayne Bay, Florida: Field, experimental, and modeling studies. *Estuaries* **2003**, *26*, 131–141. [CrossRef]
48. Ferdie, M.; Fourqurean, J.W. Responses of seagrass communities to fertilization along a gradient of relative availability of nitrogen and phosphorus in a carbonate environment. *Limnol. Oceanogr.* **2004**, *49*, 2082–2094. [CrossRef]
49. Collier, C.J.; Lavery, P.S.; Ralph, P.J.; Masini, R.J. Physiological characteristics of the seagrass Posidonia sinuosa along a depth-related gradient of light availability. *Mar. Ecol. Progr. Ser.* **2008**, *353*, 65–79. [CrossRef]
50. Serrano, O.; Lavery, P.S.; Rozaimi, M.; Mateo, M.Á. Influence of water depth on the carbon sequestration capacity of seagrasses. *Glob. Biogeochem. Cycles* **2014**, *28*, 950–961. [CrossRef]
51. Harrison, P.G. Detrital processing in seagrass systems: A review of factors affecting decay rates, remineralization and detritivory. *Aquat. Bot.* **1989**, *35*, 263–288. [CrossRef]
52. Hemminga, M.; Harrison, P.; Van Lent, F. The balance of nutrient losses and gains in seagrass meadows. *Mar. Ecol. Prog. Ser.* **1991**, *71*, 85–96. [CrossRef]
53. Fourqurean, J.W.; Schrlau, J.E. Changes in nutrient content and stable isotope ratios of C and N during decomposition of seagrasses and mangrove leaves along a nutrient availability gradient in Florida Bay, USA. *Chem. Ecol.* **2003**, *19*, 373–390. [CrossRef]
54. Mateo, M.A.; Cebrian, J.; Dunton, K.; Mutchler, T. Carbon Flux in Seagrass Ecosystems. In *Seagrasses: Biology, Ecology and Conservation*; Larkum, A.W.D., Orth, R.J., Duarte, C.M., Eds.; Springer: Dordrecht, The Netherlands, 2006; pp. 159–192.
55. Trevathan-Tackett, S.M.; Macreadie, P.I.; Sanderman, J.; Baldock, J.; Howes, J.M.; Ralph, P.J. A global assessment of the chemical recalcitrance of seagrass tissues: Implications for long-term carbon sequestration. *Front. Plant Sci.* **2017**, *8*, 925. [CrossRef]
56. Rozaimi, M.; Serrano, O.; Lavery, P. Comparison of carbon stores by two morphologically different seagrasses. *J. Royal Soc. West. Aust.* **2013**, *96*, 81.
57. Stankovic, M.; Panyawai, J.; Jansanit, K.; Upanoi, T.; Prathep, A. Carbon content in different seagrass species in Andaman Coast of Thailand. *Sains Malays.* **2017**, *46*, 1441–1447. [CrossRef]
58. Serrano, O.; Almahasheer, H.; Duarte, C.M.; Irigoien, X. Carbon stocks and accumulation rates in Red Sea seagrass meadows. *Sci. Rep.* **2018**, *8*, 15037. [CrossRef]

59. Bañolas, G.; Fernández, S.; Espino, F.; Haroun, R.; Tuya, F. Evaluation of carbon sinks by the seagrass Cymodocea nodosa at an oceanic island: Spatial variation and economic valuation. *Ocean Coast. Manag.* **2020**, *187*, 105112. [CrossRef]
60. Mazarrasa, I.; Lavery, P.; Duarte, C.M.; Lafratta, A.; Lovelock, C.E.; Macreadie, P.I.; Samper-Villarreal, J.; Salinas, C.; Sanders, C.; Trevathan-Tackett, S. Factors determining seagrass Blue Carbon across bioregions and geomorphologies. *Glob. Biogeochem. Cycles* **2021**, e2021GB006935. [CrossRef]
61. Kilminster, K.; McMahon, K.; Waycott, M.; Kendrick, G.A.; Scanes, P.; McKenzie, L.; O'Brien, K.R.; Lyons, M.; Ferguson, A.; Maxwell, P.; et al. Unravelling complexity in seagrass systems for management: Australia as a microcosm. *Sci. Total Environ.* **2015**, *534*, 97–109. [CrossRef] [PubMed]
62. Thayer, G.W.; Kenworthy, W.J.; Fonseca, M.S. *The Ecology of Eelgrass Meadows of the Atlantic Coast: A Community Profile*; Fish and Wildlife Service; US Department of the Interior: Washington, DC, USA, 1984.
63. Walker, D.I.; Olesen, B.; Phillips, R.C. Reproduction and phenology in seagrasses. In *Global Seagrass Research Methods*; Short, F.T., Coles, R.G., Eds.; Elsevier: Amsterdam, The Netherlands, 2001; pp. 59–74.
64. Duarte, C.M. Temporal biomass variability and production/biomass relationships of seagrass communities. *Mar. Ecol. Prog. Ser.* **1989**, *51*, 269–276. [CrossRef]
65. Fonseca, M.S.; Fisher, J.S. A comparison of canopy friction and sediment movement between four species of seagrass with reference to their ecology and restoration. *Mar. Ecol. Prog. Ser.* **1986**, *29*, 5–22. [CrossRef]
66. Gambi, M.C.; Nowell, A.R.; Jumars, P.A. Flume observations on flow dynamics in *Zostera marina* (eelgrass) beds. *Mar. Ecol. Prog. Ser.* **1990**, *61*, 159–169. [CrossRef]
67. France, R.L.; Holmquist, J.G. Delta13C variability of macroalgae: Effects of water motion via baffling by seagrasses and mangroves. *Mar. Ecol. Prog. Ser.* **1997**, *149*, 305–308. [CrossRef]
68. Potouroglou, M.; Bull, J.C.; Krauss, K.W.; Kennedy, H.A.; Fusi, M.; Daffonchio, D.; Mangora, M.M.; Githaiga, M.N.; Diele, K.; Huxham, M. Measuring the role of seagrasses in regulating sediment surface elevation. *Sci. Rep.* **2017**, *7*, 11917. [CrossRef]
69. Van Katwijk, M.; Bos, A.; Hermus, D.; Suykerbuyk, W. Sediment modification by seagrass beds: Muddification and sandification induced by plant cover and environmental conditions. *Estuar. Coast. Shelf Sci.* **2010**, *89*, 175–181. [CrossRef]
70. Widdows, J.; Pope, N.D.; Brinsley, M.D.; Asmus, H.; Asmus, R.M. Effects of seagrass beds (*Zostera noltii* and *Z. marina*) on near-bed hydrodynamics and sediment resuspension. *Mar. Ecol. Prog. Ser.* **2008**, *358*, 125–136. [CrossRef]
71. Serrano, O.; Ricart, A.M.; Lavery, P.S.; Mateo, M.A.; Arias-Ortiz, A.; Masque, P.; Rozaimi, M.; Steven, A.; Duarte, C.M. Key biogeochemical factors affecting soil carbon storage in Posidonia meadows. *Biogeosciences* **2016**, *13*, 4581–4594. [CrossRef]
72. Gullström, M.; Lyimo, L.D.; Dahl, M.; Samuelsson, G.S.; Eggertsen, M.; Anderberg, E.; Rasmusson, L.M.; Linderholm, H.W.; Knudby, A.; Bandeira, S.; et al. Blue Carbon Storage in Tropical Seagrass Meadows Relates to Carbonate Stock Dynamics, Plant–Sediment Processes, and Landscape Context: Insights from the Western Indian Ocean. *Ecosystems* **2017**, *21*, 551–566. [CrossRef]
73. Lima, M.d.A.C.; Ward, R.D.; Joyce, C.B. Environmental drivers of sediment carbon storage in temperate seagrass meadows. *Hydrobiologia* **2020**, *847*, 1773–1792. [CrossRef]
74. Serrano, O.; Lavery, P.S.; Duarte, C.M.; Kendrick, G.A.; Calafat, A.; York, P.H.; Steven, A.; Macreadie, P.I. Can mud (silt and clay) concentration be used to predict soil organic carbon content within seagrass ecosystems? *Biogeosciences* **2016**, *13*, 4915–4926. [CrossRef]
75. Samper-Villarreal, J.; Lovelock, C.E.; Saunders, M.I.; Roelfsema, C.; Mumby, P.J. Organic carbon in seagrass sediments is influenced by seagrass canopy complexity, turbidity, wave height, and water depth. *Limnol. Oceanogr.* **2016**, *61*, 938–952. [CrossRef]
76. Oreska, M.P.J.; McGlathery, K.J.; Porter, J.H. Seagrass blue carbon spatial patterns at the meadow-scale. *PLoS ONE* **2017**, *12*, e0176630. [CrossRef] [PubMed]
77. Ricart, A.M.; Pérez, M.; Romero, J. Landscape configuration modulates carbon storage in seagrass sediments. *Estuar. Coast. Shelf Sci.* **2017**, *185*, 69–76. [CrossRef]
78. Ricart, A.M.; York, P.H.; Rasheed, M.A.; Pérez, M.; Romero, J.; Bryant, C.V.; Macreadie, P.I. Variability of sedimentary organic carbon in patchy seagrass landscapes. *Mar. Pollut. Bull.* **2015**, *100*, 476–482. [CrossRef]
79. Adhitya, A.; Bouma, T.; Folkard, A.; Van Katwijk, M.; Callaghan, D.; De Iongh, H.; Herman, P. Comparison of the influence of patch-scale and meadow-scale characteristics on flow within seagrass meadows: A flume study. *Mar. Ecol. Prog. Ser.* **2014**, *516*, 49–59. [CrossRef]
80. El Allaoui, N.; Serra, T.; Colomer, J.; Soler, M.; Casamitjana, X.; Oldham, C. Interactions between fragmented seagrass canopies and the local hydrodynamics. *PLoS ONE* **2016**, *11*, e0156264. [CrossRef]
81. Chen, G.; Azkab, M.H.; Chmura, G.L.; Chen, S.; Sastrosuwondo, P.; Ma, Z.; Dharmawan, I.W.E.; Yin, X.; Chen, B. Mangroves as a major source of soil carbon storage in adjacent seagrass meadows. *Sci. Rep.* **2017**, *7*, 42406. [CrossRef]
82. Hemminga, M.; Slim, F.; Kazungu, J.; Ganssen, G.; Nieuwenhuize, J.; Kruyt, N. Carbon outwelling from a mangrove forest with adjacent seagrass beds and coral reefs (Gazi Bay, Kenya). *Mar. Ecol. Prog. Ser.* **1994**, *106*, 291–301. [CrossRef]
83. Guerra-Vargas, L.A.; Gillis, L.G.; Mancera-Pineda, J.E. Stronger Together: Do Coral Reefs Enhance Seagrass Meadows "Blue Carbon" Potential? *Front. Mar. Sci.* **2020**, *7*, 628. [CrossRef]
84. Serrano, O.; Rozaimi, M.; Lavery, P.S.; Smernik, R.J. Organic chemistry insights for the exceptional soil carbon storage of the seagrass Posidonia australis. *Estuar. Coast. Shelf Sci.* **2020**, *237*, 106662. [CrossRef]

85. Alemu, J.B.; Yaakub, S.M.; Yando, E.S.; San Lau, R.Y.; Lim, C.C.; Puah, J.Y.; Friess, D.A. Geomorphic gradients in shallow seagrass carbon stocks. *Estuar. Coast. Shelf Sci.* **2022**, *265*, 107681. [CrossRef]
86. Ackleson, S.; Klemas, V. Remote sensing of submerged aquatic vegetation in lower Chesapeake Bay: A comparison of Landsat MSS to TM imagery. *Remote Sens. Environ.* **1987**, *22*, 235–248. [CrossRef]
87. Phinn, S.; Roelfsema, C.; Dekker, A.; Brando, V.; Anstee, J. Mapping seagrass species, cover and biomass in shallow waters: An assessment of satellite multi-spectral and airborne hyper-spectral imaging systems in Moreton Bay (Australia). *Remote Sens. Environ.* **2008**, *112*, 3413–3425. [CrossRef]
88. Roelfsema, C.; Phinn, S.; Udy, N.; Maxwell, P. An integrated field and remote sensing approach for mapping seagrass cover, Moreton Bay, Australia. *J. Spat. Sci.* **2009**, *54*, 45–62. [CrossRef]
89. Lyons, M.B.; Phinn, S.R.; Roelfsema, C.M. Long term land cover and seagrass mapping using Landsat and object-based image analysis from 1972 to 2010 in the coastal environment of South East Queensland, Australia. *ISPRS J. Photogramm. Remote Sens.* **2012**, *71*, 34–46. [CrossRef]
90. Pu, R.; Bell, S.; Meyer, C.; Baggett, L.; Zhao, Y. Mapping and assessing seagrass along the western coast of Florida using Landsat TM and EO-1 ALI/Hyperion imagery. *Estuar. Coast. Shelf Sci.* **2012**, *115*, 234–245. [CrossRef]
91. Wicaksono, P.; Hafizt, M. Mapping seagrass from space: Addressing the complexity of seagrass LAI mapping. *Eur. J. Remote Sens.* **2013**, *46*, 18–39. [CrossRef]
92. Wabnitz, C.C.; Andréfouët, S.; Torres-Pulliza, D.; Müller-Karger, F.E.; Kramer, P.A. Regional-scale seagrass habitat mapping in the Wider Caribbean region using Landsat sensors: Applications to conservation and ecology. *Remote Sens. Environ.* **2008**, *112*, 3455–3467. [CrossRef]
93. Lyons, M.; Roelfsema, C.; Kovacs, E.; Samper-Villarreal, J.; Saunders, M.; Maxwell, P.; Phinn, S. Rapid monitoring of seagrass biomass using a simple linear modelling approach, in the field and from space. *Mar. Ecol. Prog. Ser.* **2015**, *530*, 1–14. [CrossRef]
94. Stankovic, M.; Tantipisanuh, N.; Rattanachot, E.; Prathep, A. Model-based approach for estimating biomass and organic carbon in tropical seagrass ecosystems. *Mar. Ecol. Prog. Ser.* **2018**, *596*, 61–70. [CrossRef]
95. Zoffoli, M.L.; Gernez, P.; Rosa, P.; Le Bris, A.; Brando, V.E.; Barillé, A.-L.; Harin, N.; Peters, S.; Poser, K.; Spaias, L.; et al. Sentinel-2 remote sensing of Zostera noltei-dominated intertidal seagrass meadows. *Remote Sens. Environ.* **2020**, *251*, 112020. [CrossRef]
96. Borfecchia, F.; De Cecco, L.; Martini, S.; Ceriola, G.; Bollanos, S.; Vlachopoulos, G.; Valiante, L.M.; Belmonte, A.; Micheli, C. Posidonia oceanica genetic and biometry mapping through high-resolution satellite spectral vegetation indices and sea-truth calibration. *Int. J. Remote Sens.* **2013**, *34*, 4680–4701. [CrossRef]
97. Pu, R.; Bell, S. A protocol for improving mapping and assessing of seagrass abundance along the West Central Coast of Florida using Landsat TM and EO-1 ALI/Hyperion images. *J. Photogramm. Remote Sens.* **2013**, *83*, 116–129. [CrossRef]
98. Barillé, L.; Robin, M.; Harin, N.; Bargain, A.; Launeau, P. Increase in seagrass distribution at Bourgneuf Bay (France) detected by spatial remote sensing. *Aquat. Bot.* **2010**, *92*, 185–194. [CrossRef]
99. Müller, G.; Stelzer, K.; Smollich, S.; Gade, M.; Adolph, W.; Melchionna, S.; Kemme, L.; Geißler, J.; Millat, G.; Reimers, H.-C.; et al. Remotely sensing the German Wadden Sea—A new approach to address national and international environmental legislation. *Environ. Monit. Assess.* **2016**, *188*, 1–17. [CrossRef]
100. Ha, N.T.; Manley-Harris, M.; Pham, T.D.; Hawes, I. The use of radar and optical satellite imagery combined with advanced machine learning and metaheuristic optimization techniques to detect and quantify above ground biomass of intertidal seagrass in a New Zealand estuary. *Int. J. Remote Sens.* **2021**, *42*, 4712–4738. [CrossRef]
101. Bach, S.S.; Borum, J.; Fortes, M.D.; Duarte, C. Species composition and plant performance of mixed seagrass beds along a siltation gradient at Cape Bolinao, The Philippines. *Mar. Ecol. Prog. Ser.* **1998**, *174*, 247–256. [CrossRef]
102. Collier, C.J.; Lavery, P.S.; Masini, R.J.; Ralph, P.J. Morphological, growth and meadow characteristics of the seagrass Posidonia sinuosa along a depth-related gradient of light availability. *Mar. Ecol. Prog. Ser.* **2007**, *337*, 103–115. [CrossRef]
103. Lyons, M.; Phinn, S.; Roelfsema, C. Integrating Quickbird Multi-Spectral Satellite and Field Data: Mapping Bathymetry, Seagrass Cover, Seagrass Species and Change in Moreton Bay, Australia in 2004 and 2007. *Remote Sens.* **2011**, *3*, 42–64. [CrossRef]
104. Fyfe, S. Spatial and temporal variation in spectral reflectance: Are seagrass species spectrally distinct? *J. Limnol. Oceanogr.* **2003**, *48*, 464–479. [CrossRef]
105. Thorhaug, A.; Richardson, A.; Berlyn, G. Spectral reflectance of the seagrasses: Thalassia testudinum, Halodule wrightii, Syringodium filiforme and five marine algae. *Int. J. Remote Sens.* **2007**, *28*, 1487–1501. [CrossRef]
106. Dekker, A.G.; Brando, V.E.; Anstee, J.M. Retrospective seagrass change detection in a shallow coastal tidal Australian lake. *Remote Sens. Environ.* **2005**, *97*, 415–433. [CrossRef]
107. Traganos, D.; Aggarwal, B.; Poursanidis, D.; Topouzelis, K.; Chrysoulakis, N.; Reinartz, P. Towards Global-Scale Seagrass Mapping and Monitoring Using Sentinel-2 on Google Earth Engine: The Case Study of the Aegean and Ionian Seas. *Remote Sens.* **2018**, *10*, 1227. [CrossRef]
108. Traganos, D.; Reinartz, P. Interannual Change Detection of Mediterranean Seagrasses Using RapidEye Image Time Series. *Front. Plant Sci.* **2018**, *9*, 96. [CrossRef]
109. Mumby, P.J.; Edwards, A.J. Mapping marine environments with IKONOS imagery: Enhanced spatial resolution can deliver greater thematic accuracy. *Remote Sens. Environ.* **2002**, *82*, 248–257. [CrossRef]

110. Roelfsema, C.M.; Lyons, M.; Kovacs, E.M.; Maxwell, P.; Saunders, M.I.; Samper-Villarreal, J.; Phinn, S.R. Multi-temporal mapping of seagrass cover, species and biomass: A semi-automated object based image analysis approach. *Remote Sens. Environ.* **2014**, *150*, 172–187. [CrossRef]
111. Kovacs, E.; Roelfsema, C.; Lyons, M.; Zhao, S.; Phinn, S. Seagrass habitat mapping: How do Landsat 8 OLI, Sentinel-2, ZY-3A, and Worldview-3 perform? *Remote Sens. Lett.* **2018**, *9*, 686–695. [CrossRef]
112. Gilbert, S.; Clark, K.B. Seasonal variation in standing crop of the seagrass Syringodium filiforme and associated macrophytes in the northern Indian River, Florida. *Estuaries* **1981**, *4*, 223–225. [CrossRef]
113. Santamaría-Gallegos, N.A.; Sánchez-Lizaso, J.L.; Félix-Pico, E.F. Phenology and growth cycle of annual subtidal eelgrass in a subtropical locality. *Aquat. Bot.* **2000**, *66*, 329–339. [CrossRef]
114. Samper-Villarreal, J.; Mumby, P.J.; Saunders, M.I.; Roelfsema, C.; Lovelock, C.E. Seagrass Organic Carbon Stocks Show Minimal Variation Over Short Time Scales in a Heterogeneous Subtropical Seascape. *Estuaries Coasts* **2018**, *41*, 1732–1743. [CrossRef]
115. McComb, A.; Cambridge, M.; Kirkman, H.; Kuo, J. *The Biology of Australian Seagrasses*; University of Western Australia Press: Crawley, WA, Australia, 1981.
116. de Boer, W.F. Biomass dynamics of seagrasses and the role of mangrove and seagrass vegetation as different nutrient sources for an intertidal ecosystem. *Aquat. Bot.* **2000**, *66*, 225–239. [CrossRef]
117. Olsen, Y.S.; Collier, C.; Ow, Y.X.; Kendrick, G.A. Global Warming and Ocean Acidification: Effects on Australian Seagrass Ecosystems. In *Seagrasses of Australia: Structure, Ecology and Conservation*; Larkum, A.W., Kendrick, G.A., Ralph, P.J., Eds.; Springer: Cham, Switzerland, 2018; pp. 705–742.
118. Pittman, S.; Yates, K.; Bouchet, P.; Alvarez-Berastegui, D.; Andréfouët, S.; Bell, S.; Berkström, C.; Boström, C.; Brown, C.; Connolly, R. Seascape ecology: Identifying research priorities for an emerging ocean sustainability science. *Mar. Ecol. Prog. Ser.* **2021**, *663*, 1–29. [CrossRef]
119. Robbins, B.D.; Bell, S.S. Seagrass landscapes: A terrestrial approach to the marine subtidal environment. *Trends Ecol. Evol.* **1994**, *9*, 301–304. [CrossRef]
120. Costa, B.; Walker, B.K.; Dijkstra, J.A. Mapping and Quantifying Seascape Patterns. In *Seascape Ecology*; Pittman, S.J., Ed.; Wiley Blackwell: Oxford, UK, 2018; pp. 27–56.
121. Bell, S.S.; Fonseca, M.S.; Stafford, N.B. Seagrass ecology: New contributions from a landscape perspective. In *Seagrasses: Biology, Ecology and Conservation*; Springer: Berlin/Heidelberg, Germany, 2007; pp. 625–645.
122. Hamylton, S.; Spencer, T. Geomorphological modelling of tropical marine landscapes: Optical remote sensing, patches and spatial statistics. *Cont. Shelf Res.* **2011**, *31*, S151–S161. [CrossRef]
123. Uhrin, A.V.; Townsend, P.A. Improved seagrass mapping using linear spectral unmixing of aerial photographs. *Estuar. Coast. Shelf Sci.* **2016**, *171*, 11–22. [CrossRef]
124. Uhrin, A.V.; Turner, M.G. Physical drivers of seagrass spatial configuration: The role of thresholds. *Landsc. Ecol.* **2018**, *33*, 2253–2272. [CrossRef]
125. Rioja-Nieto, R.; Barrera-Falcón, E.; Hinojosa-Arango, G.; Riosmena-Rodríguez, R. Benthic habitat β-diversity modeling and landscape metrics for the selection of priority conservation areas using a systematic approach: Magdalena Bay, Mexico, as a case study. *Ocean Coast. Manag.* **2013**, *82*, 95–103. [CrossRef]
126. Helmi, M.; Purwanto, W.A.; Subardjo, P.; Aysira, A. Benthic Diversity Mapping and Analysis Base on Remote Sensing and Seascape Ecology Approach at Parang Islands, Karimunjawa National Park, Indonesia. *Int. J. Civ. Eng. Technol.* **2018**, *9*, 227–235.
127. Cajica, A.K.O.; Hinojosa-Arango, G.; Garza-Pérez, J.R.; Rioja-Nieto, R. Seascape metrics, spatio-temporal change, and intensity of use for the spatial conservation prioritization of a Caribbean marine protected area. *Ocean Coast. Manag.* **2020**, *194*, 105265. [CrossRef]
128. Urbański, J.; Mazur, A.; Janas, U. Object-oriented classification of QuickBird data for mapping seagrass spatial structure. *Oceanol. Hydrobiol. Stud.* **2009**, *38*, 27–43. [CrossRef]
129. Pu, R.; Bell, S. Mapping seagrass coverage and spatial patterns with high spatial resolution IKONOS imagery. *Int. J. Appl. Earth Obs. Geoinf.* **2017**, *54*, 145–158. [CrossRef]
130. Ewers Lewis, C.J.; Young, M.A.; Ierodiaconou, D.; Baldock, J.A.; Hawke, B.; Sanderman, J.; Carnell, P.E.; Macreadie, P.I. Drivers and modelling of blue carbon stock variability in sediments of southeastern Australia. *Biogeosciences* **2020**, *17*, 2041–2059. [CrossRef]
131. Stankovic, M.; Hayashizaki, K.-I.; Tuntiprapas, P.; Rattanachot, E.; Prathep, A. Two decades of seagrass area change: Organic carbon sources and stock. *Mar. Pollut. Bull.* **2021**, *163*, 111913. [CrossRef] [PubMed]
132. Madonsela, S.; Cho, M.A.; Mathieu, R.; Mutanga, O.; Ramoelo, A.; Kaszta, Ż.; Van De Kerchove, R.; Wolff, E. Multi-phenology WorldView-2 imagery improves remote sensing of savannah tree species. *Int. J. Appl. Earth Obs. Geoinf.* **2017**, *58*, 65–73. [CrossRef]
133. Lyons, M.B.; Roelfsema, C.M.; Phinn, S.R. Towards understanding temporal and spatial dynamics of seagrass landscapes using time-series remote sensing. *Estuar. Coast. Shelf Sci.* **2013**, *120*, 42–53. [CrossRef]
134. Roelfsema, C.; Kovacs, E.M.; Saunders, M.I.; Phinn, S.; Lyons, M.; Maxwell, P. Challenges of remote sensing for quantifying changes in large complex seagrass environments. *Estuar. Coast. Shelf Sci.* **2013**, *133*, 161–171. [CrossRef]
135. Michalek, J.L.; Wagner, T.W.; Luczkovich, J.J.; Stoffle, R.W. Multispectral change vector analysis for monitoring coastal marine environments. *Photogramm. Eng. Remote Sens.* **1993**, *59*, 381–384.

136. Shapiro, A.C.; Rohmann, S.O. Mapping changes in submerged aquatic vegetation using Landsat imagery and benthic habitat data: Coral reef ecosystem monitoring in Vieques Sound between 1985 and 2000. *Bull. Mar. Sci.* **2006**, *79*, 375–388.
137. Blakey, T.; Melesse, A.; Hall, M.O. Supervised classification of benthic reflectance in shallow subtropical waters using a generalized pixel-based classifier across a time series. *Remote Sens.* **2015**, *7*, 5098–5116. [CrossRef]
138. Fauzan, M.A.; Wicaksono, P. Characterizing Derawan seagrass cover change with time-series Sentinel-2 images. *Reg. Stud. Mar. Sci.* **2021**, *48*, 102048. [CrossRef]
139. Krause, J.R.; Hinojosa-Corona, A.; Gray, A.B.; Burke Watson, E. Emerging Sensor Platforms Allow for Seagrass Extent Mapping in a Turbid Estuary and from the Meadow to Ecosystem Scale. *Remote Sens.* **2021**, *13*, 3681. [CrossRef]

www.nature.com/scientificreports

scientific reports

Check for updates

OPEN

Mapping fine-scale seagrass disturbance using bi-temporal UAV-acquired images and multivariate alteration detection

Jamie Simpson[1,2✉], Kevin P. Davies[1,2], Paul Barber[2,3,4] & Eleanor Bruce[1,2]

Seagrasses provide critical ecosystem services but cumulative human pressure on coastal environments has seen a global decline in their health and extent. Key processes of anthropogenic disturbance can operate at local spatio-temporal scales that are not captured by conventional satellite imaging. Seagrass management strategies to prevent longer-term loss and ensure successful restoration require effective methods for monitoring these fine-scale changes. Current seagrass monitoring methods involve resource-intensive fieldwork or recurrent image classification. This study presents an alternative method using iteratively reweighted multivariate alteration detection (IR-MAD), an unsupervised change detection technique originally developed for satellite images. We investigate the application of IR-MAD to image data acquired using an unoccupied aerial vehicle (UAV). UAV images were captured at a 14-week interval over two seagrass beds in Brisbane Water, NSW, Australia using a 10-band Micasense RedEdge-MX Dual camera system. To guide sensor selection, a further three band subsets representing simpler sensor configurations (6, 5 and 3 bands) were also analysed using eight categories of seagrass change. The ability of the IR-MAD method, and for the four different sensor configurations, to distinguish the categories of change were compared using the Jeffreys-Matusita (JM) distance measure of spectral separability. IR-MAD based on the full 10-band sensor images produced the highest separability values indicating that human disturbances (propeller scars and other seagrass damage) were distinguishable from all other change categories. IR-MAD results for the 6-band and 5-band sensors also distinguished key seagrass change features. The IR-MAD results for the simplest 3-band sensor (an RGB camera) detected change features, but change categories were not strongly separable from each other. Analysis of IR-MAD weights indicated that additional visible bands, including a coastal blue band and a second red band, improve change detection. IR-MAD is an effective method for seagrass monitoring, and this study demonstrates the potential for multispectral sensors with additional visible bands to improve seagrass change detection.

Monitoring of seagrass beds to detect changes and disturbances is critical for supporting conservation and restoration efforts of these important ecosystems[1–3]. Drivers of seagrass change include boat propeller scarring, natural hazards such as flood or drought, eutrophication, and climate change-induced increases in sea surface temperatures[4,5]. Disturbances to seagrass beds threaten ecosystem function and interfere with critical ecosystem services such as coastal protection, carbon sequestration, and habitat provision[6]. Direct damage to seagrass which disturbs sediments can lead to remineralisation and emission of stored carbon as CO_2[7,8]. Conversely, successful restoration of seagrass beds can rapidly and effectively restore ecosystem function and associated ecosystem services[9,10]. Effective monitoring approaches can provide accurate information on rates of disturbance

[1]School of Geosciences, Faculty of Science, University of Sydney, Sydney, NSW 2006, Australia. [2]Centre for CubeSats, UAVs and Their Applications (CUAVA), University of Sydney, Sydney, NSW 2006, Australia. [3]ArborCarbon Pty Ltd., Murdoch University, Rota Trans 1, Murdoch, WA 6150, Australia. [4]Centre for Terrestrial Ecosystem Science & Sustainability, Harry Butler Institute, Murdoch University, Murdoch, WA 6150, Australia. ✉email: james.simpson@sydney.edu.au

and recovery at ecologically relevant spatio-temporal scales to inform management and implementation of protection and restoration strategies[11].

Requirements for seagrass monitoring will vary depending on the character of the ecosystem, and the nature of potential disturbances[8,12]. Consequently, approaches should consider the site and purpose. Seagrass is commonly monitored through recurrent field observations using permanent transects or quadrats, remote sensing-based methods, or a combination of these. Long-term trends in seagrass abundance or composition across a meadow can be detected using permanent quadrats and transects, which is useful for establishing the effects of large-scale change at representative sites[13,14]. Satellite remote sensing has been applied widely for measuring changes in meadow extent, especially at a regional to global scale[15–18]; however, the ability to detect finer-scale seagrass change using satellites is constrained by image spatial resolution.

Airborne-sensors combined with automatic change detection analysis techniques[19,20] and manual image interpretation[21,22] have been used to detect changes to seagrass at fine spatial scales. Airborne sensors can capture highly localised seagrass disturbances such as boat scars, and patch level heterogeneity in seagrass abundance which might otherwise be obscured in satellite images and permanent transect monitoring[23,24]. However, airborne data capture is relatively expensive and involves logistical challenges due to the stricter airspace and licensing requirements.

Unoccupied aerial vehicles (UAVs) provide an attractive alternative to crewed airborne data capture especially when repeat captures are required for time series monitoring. UAVs are relatively inexpensive, and the increased accessibility of UAV technology has enabled new imaging methods that can capture fine-scale features even in structurally complex meadows[25]. UAV-acquired images have been used for mapping seagrass density, ecosystem health, and species composition at fine scales[26–29], as well as for identifying disturbances such as boat propeller scars[30]. UAVs have also supported time series seagrass monitoring with recurrent flights used to characterise seasonal change[31,32] and identify long-term impacts of climate change on seagrass[33].

Seagrass change detection with UAV images has used simple bi-temporal comparison of classification outputs[31,32]. This approach generally involves a supervised classification of images acquired on two different dates, and then differencing the classification outputs to determine areas of change. This relatively simple approach can be effective, but supervised classification requires suitable ground truth training and validation data for each classified image[31], and is likely to suffer from degraded accuracy associated with post-classification change detection[34]. The requirement for extensive training and ground-truth validation data for supervised change detection methods increases time and cost burdens on coastal managers who may need to rapidly detect, investigate, and respond to potential seagrass disturbances. There is a need for a rapid, cost-effective unsupervised change detection approach to reliably map fine-scale disturbances that is not contingent on rigorous ground truth data collection.

The iteratively reweighted multivariate alteration detection (IR-MAD)[35] method is a relatively simple, unsupervised approach for detecting bi-temporal changes in multispectral images. IR-MAD was originally developed for detecting changes in pairs of multispectral satellite images[36] and has only had limited application to UAV images for monitoring of the built environment[37]. IR-MAD has not been applied to fine-scale monitoring of seagrass disturbances using UAV images in the literature to date.

The primary objective of this study is to demonstrate the use of the IR-MAD method for unsupervised seagrass disturbance detection using co-registered UAV images of two seagrass beds in Brisbane Water, New South Wales, Australia. Using the IR-MAD outputs, we identify key change categories and quantitatively determine the separability of change signals.

UAV sensor selection is also an important consideration for coastal managers endeavouring to use a UAV platform for coastal monitoring. There is a wide selection of commercially available sensors ranging from less expensive red–green–blue (RGB) sensors to more costly multispectral sensors with four or more bands in the visible to near-infrared range of the spectrum. The 10-band multispectral sensor used in this study (Micasense RedEdge-MX Dual) has been shown to enhance seagrass species classification[38] and the discrimination between seagrass and macroalgae compared to sensors with only three or four bands in the visible range[39]. However, it is unclear how additional bands provided by more expensive multispectral sensors will affect the results produced by the IR-MAD method.

An additional objective of this research is therefore to assess whether sensor selection will impact on the change detection results produced by the IR-MAD method. We systematically compare IR-MAD results produced from four alternative sensor configurations. Assessing the importance of individual spectral bands for detecting seagrass change will help guide the selection of UAV sensor type when applying this method.

Methods

Study site

Brisbane Water is a wave-dominated barrier estuary located ~ 45 km north of Sydney, New South Wales (NSW; Fig. 1) with a well-developed marine tidal delta and total area of ~ 27 km^2[40]. The estuary is surrounded by residential development on all sides except Brisbane Water National Park on the western side. The area is used extensively for commercial and recreational activities, including fishing, oyster farming, boating, and swimming.

Approximately 5 km^2 of seagrass beds are present within the Brisbane Water estuary[40], including *Zostera capricorni* growth in shallow shoreline areas[41], and in some areas, more extensive beds of *Z. capricorni* with *Posidonia australis* growing towards the deeper, seaward edge[42]. *Halophila ovalis* is present throughout seagrass beds in some parts of the estuary[42].

For this study, two seagrass beds were selected, at St Huberts Island and Empire Bay, hereafter referred to by those names (Fig. 1). These beds consist primarily of *Z. capricorni* at varying density as well as *P. australis* which is listed as an endangered ecological community in this region of NSW[43]. The seagrass beds are in shallow

Figure 1. The seagrass study sites (highlighted in red) were located in the Brisbane Water estuary, NSW, Australia. The western and eastern study sites are referred to in the text as St Huberts Island and Empire Bay respectively. Map data: Google, DigitalGlobe, inset map copyright OpenStreetMap contributors and available from https://www.openstreetmap.org. Map created using ArcGIS Pro (version 3.1.0, https://www.esri.com/en-us/arcgis/products/arcgis-pro/overview).

depths less than 1 m at low tide, with some edges extending down to approximately 2.5 m in depth. The study sites overlap with NSW Priority Oyster Aquaculture Areas[44] and oyster farming infrastructure is present in both seagrass beds.

Equipment

Images were captured using a Micasense RedEdge-MX dual camera system (referred to as MX-10), which consists of a 5-band RedEdge-MX camera interlinked with a 5-band RedEdge-MX Blue camera providing 10 spectral bands in total (Table 1). Band subsets of each image captured by the MX-10 sensor were used to simulate three sensors with reduced spectral band coverage: the first consisted of the bands captured by the 5-band RedEdge-MX camera referred to as MX-5, and the second and third virtual sensors consisting of six and three bands referred to as VIS-6 and RGB respectively (Table 1). As the images for these three virtual sensors were created using band subsets from the original images captured by the MX-10 sensor, all images had the same spatial resolution. Compared with the band widths and placements of the Sentinel-2 and Landsat 9 satellite sensors (Fig. 2), the

Band	Band centre (nm)	FWHM (nm)	MX-10	MX-5	VIS-6 (virtual)	RGB (virtual)
Coastal blue	444	28	✓		✓	
Blue	475	32	✓	✓	✓	✓
Green 1	531	14	✓		✓	
Green 2	560	27	✓	✓	✓	✓
Red 1	650	16	✓		✓	
Red 2	668	14	✓	✓	✓	✓
Red Edge (RE) 1	705	10	✓			
RE 2	717	12	✓	✓		
RE 3	740	18	✓			
Near-infrared (NIR)	842	57	✓	✓		

Table 1. The sensors used in this study (MX-10) is described by the band centre and band width (FWHM).

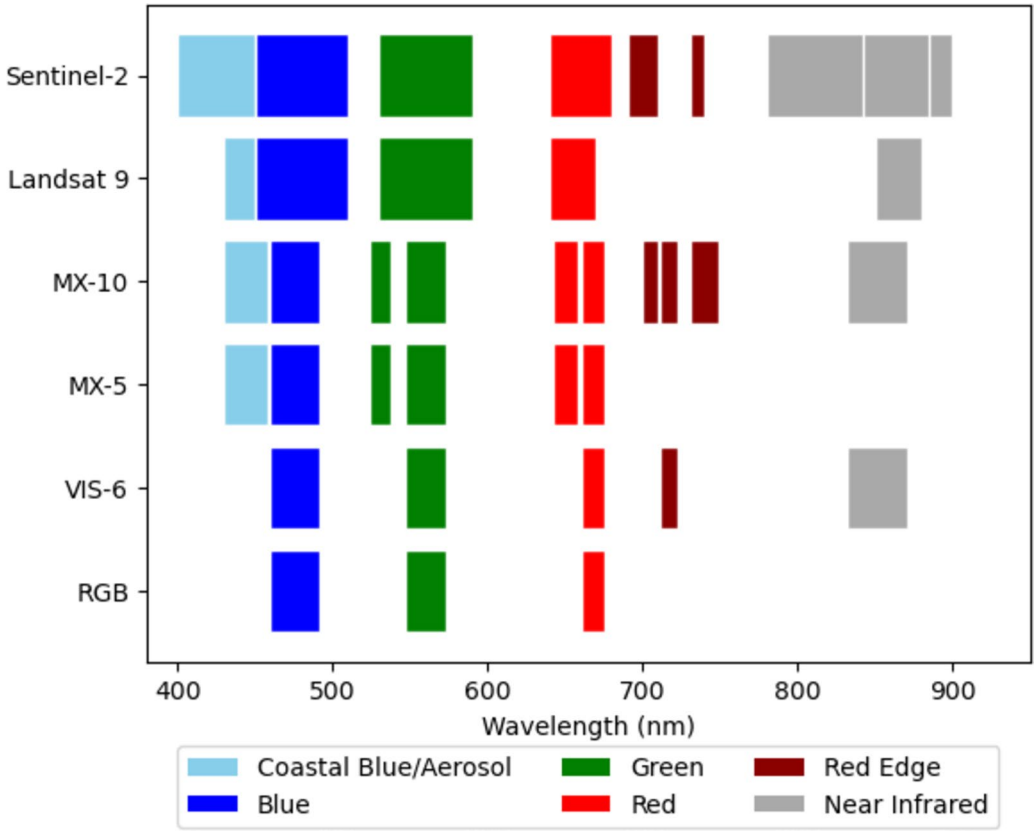

Figure 2. Band placements and widths for the Micasense RedEdge-MX 10 band sensor (MX-10) compared with the Sentinel-2 and Landsat 9 satellite sensors. The three alternative sensors used in this study are also shown.

MX-10 sensor has a similar coastal band placement with additional bands in the green and red regions. There is also an additional band in the red-edge region compared with Sentinel-2.

The band subsets used to represent the three virtual sensors (MX-5, VIS-6 and RGB) are also shown.

The camera system was mounted on a DJI Matrice 200 quadcopter UAV (DJI, Nanshan, China) with a standard Micasense RedEdge-MX Dual Camera System mount kit (Fig. 3). A downwelling light sensor was connected to the camera system and was used to measure lighting conditions at the time of capture to support radiometric calibration. The GPS contained within the camera system recorded the location of the UAV at each image capture with 3 m accuracy.

Image capture and processing

The UAV was controlled using Measure Ground Control version 4.1.2 (AgEagle Aerial Systems Inc., Wichita, USA) in a planned "lawnmower" pattern with a 100 m flying height to achieve a spatial resolution of ~ 8 cm. On-board camera software triggered image captures based on distance travelled to achieve 75% overlap and sidelap as is considered ideal for wetland monitoring[45]. The same flight plan was used to recapture images of the study sites at an interval of 101 days (Table 2). All flights took place during below average tides with calm wind conditions (< 10 km/h), clear-sky conditions, and at low sun elevation angles to reduce potential sun glint[46].

The images were converted to reflectance values using images of the MicaSense Calibrated Reflectance Panel captured immediately before and after each flight, as well as data captured by the downwelling light sensor during each flight. Images were processed into multispectral orthomosaics using Metashape Professional version 2.0.2 (Agisoft LLC, St Petersburg, Russia). The first image captured for each study site was used as the reference image to georeference the second corresponding image capture. Stationary features such as large rocks, poles, and oyster farming infrastructure were used to coregister the images. As this study focused on testing a change detection method, the results were not intended to be used in conjunction with other spatial data so georeferencing to accurate real-world coordinates using real-time kinematic positioning or similar methods. Additionally, as the images vary in spatial resolution, each georeferenced set of images was spatially resampled using nearest neighbour resampling to match the coarsest resolution image for that study site (8.2 cm for Empire Bay and 7.9 cm for St Huberts Island).

Background on IR-MAD

The goal of IR-MAD is to transform a pair of bi-temporal, multispectral images of the same scene into a set of change images with reduced dimensionality, that is, representing change in fewer bands than the original

Figure 3. The DJI Matrice 200 UAV used in this study. The Micasense RedEdge MX Dual camera system and the downwelling light sensor are labelled. Photo by Jamie Simpson.

Study site	Image dates	Start time	End time	Tide above lowest astronomical tide	Sun elevation	Flight area	Spatial resolution
Empire bay	28/2/23	4:44pm	5:01pm	0.54m	34°	16.0 ha	8.2 cm
	9/6/23	12:03pm	12:19pm	0.50m	34°		8.0 cm
St Huberts island	28/2/23	3:19pm	3:42pm	0.46m	50°	25.3 ha	7.9 cm
	9/6/23	10:36am	11:14am	0.29m	28°		7.2 cm

Table 2. Metadata for the UAV captures used in this study.

images[36,47]. IR-MAD analysis first involves performing Canonical Correlation Analysis (CCA)[48] on a pair of geographically co-registered *N*-band multispectral images **F** and **G**. This identifies two vectors $\mathbf{a_1}$ and $\mathbf{b_1}$ which maximise the positive correlation between $\mathbf{a_1}^T\mathbf{F}$ and $\mathbf{b_1}^T\mathbf{G}$, referred to as the first canonical covariate pair $\mathbf{U_1}$ and $\mathbf{V_1}$. Vectors $\mathbf{a_2}$ and $\mathbf{b_2}$ are then identified which maximise the correlation between $\mathbf{a_2}^T\mathbf{F}$ and $\mathbf{b_2}^T\mathbf{G}$, with the additional constraint that the canonical variate pair $\mathbf{U_2}$ and $\mathbf{V_2}$ are uncorrelated with $\mathbf{U_1}$ and $\mathbf{V_1}$ respectively. The end result for an *N* band image pair will be N canonical variate pairs $\mathbf{U_1}$,$\mathbf{V_1}$ to $\mathbf{U_N}$,$\mathbf{V_N}$.

The canonical variate pairs are then used to produce ***N*** difference bands $\boldsymbol{D_i = U_i - V_i}$, referred to as the MAD variates. The MAD variate pixel values are expected to be normally or near-normally distributed, and pixels with more positive or negative values represent greater change. As the canonical variate pairs were ordered by decreasing correlation, the MAD variates will be ordered from least to most change information, referred to as lowest to highest order. Given the canonical variate pairs were uncorrelated with each other, each MAD variate is expected to contain different types of change.

The sum of the MAD variates is chi-squared distributed, and no-change pixels are identified using a pre-determined threshold of the probability density function of this distribution. The MAD process is then repeated with no-change pixels receiving a higher weight during the CCA. This iteration is performed until the correlation between the first canonical variate pair is maximised. The iterative reweighting of no-change pixels results in an improved transformation which better represents change in the final MAD variates[35]. The three MAD variates containing the most change information can then be displayed in false colour to visualise change that incorporates information from all the original bands but with reduced dimensionality[47].

An important quality of the IR-MAD method for unsupervised change detection is that IR-MAD is insensitive to linear scaling effects between the original image pairs (such as due to differences in atmosphere, illumination, calibration, and sensor response) because the CCA finds linear combinations of the original spectral bands[49].

Application of IR-MAD to the alternative sensors

To assess the relative importance of sensor selection, and the importance of additional spectral bands for detecting change to seagrass, four alternative sensor configurations (Table 1 and Fig. 2) were compared in the IR-MAD analysis below. These were the dual MX-10 sensor, the single MX-5 sensor, as well two virtual sensors constructed from band subsets captured by Micasense sensors. The first virtual sensor represented a conventional RGB camera, and images were constructed from the standard red, green, and blue bands captured by the MX-5 sensor. The second virtual sensor represented a theoretical sensor with additional visible bands to a conventional 3-band RGB sensor. Images for this sensor were constructed from the six shortest-wavelength visible light bands from the MX-10 sensor (referred to as the VIS-6 sensor). The red-edge and near-infrared bands from the MX-10 sensor were not included in the VIS-6 sensor because they are known to have poor water penetration[50].

The IR-MAD method was applied to the bi-temporal image pair captured by the MX-10 sensor for each study site using the The *CRCPython* library[49]. The IR-MAD method was then then repeated for the corresponding image pairs for the MX-5, RGB, and VIS-6 sensors for each study site. The result was four IR-MAD outputs for each study site.

Qualitative identification of change categories

To examine the effectiveness of IR-MAD for detecting fine-scale changes to seagrass, the output MAD variates for the MX-10 sensor for each study site were visually assessed to identify and categorise different types of change. MAD variates were first viewed individually to identify the number of variates that contain spatially coherent change features. Notable change signals were then identified and inspected in the original bi-temporal image pairs to qualitatively determine the type of seagrass change.

Six different categories of change were visually identified (Table 3), and their boundaries were manually digitised using the Region of Interest (ROI) Tool in ENVI version 5.6 (NV5 Geospatial Solutions, Broomfield, United States). Separate ROIs were also created for two types of unchanged areas with seagrass present in both images: one without any change signal in the IR-MAD data (Unchanged 1) and one with a false positive change signal (Unchanged 2).

Comparing effectiveness of disturbance detection between the alternative sensors

In order to quantitatively assess the ability to distinguish the different types of identified change types in the IR-MAD outputs for each of the alternative sensors, the spectral separability between the different change categories was quantitively determined using the Jeffreys-Matusita (JM) distance[51]. The JM distance is a measure of separability between two sets of probability distributions, commonly used in remote sensing to determine spectral separability of class endmembers to support supervised classifications. The JM distance J between two distributions x and y is defined as[52]:

$$J_{xy} = 2\left(1 - e^{-B}\right), \tag{1}$$

where

$$B = \frac{1}{8}\left(\mu_x - \mu_y\right)^T \left(\frac{\sum_x + \sum_y}{2}\right)^{-1} \left(\mu_x - \mu_y\right) + \frac{1}{2}\ln\left(\frac{\left|\frac{\sum_x + \sum_y}{2}\right|}{\left|\sum_x\right|^{\frac{1}{2}}\left|\sum_y\right|^{\frac{1}{2}}}\right), \tag{2}$$

where μ_x and μ_y are the mean vectors of x and y, and $\sum_x$ and $\sum_y$ are the covariance matrices of x and y.

JM distance values can range from 0 (no separability) to 2 (perfect separability). JM distances can therefore be compared between class pairs in remote sensing images as a measure of statistical separability of different features. For IR-MAD variates, JM distance values can similarly be used as a measure of relative statistical separability of different features (in this case change features) in the image.

The JM distance was used to determine whether the ROIs captured for areas representing actual change were separable from ROIs where no-change occurred, and if ROIs representing different change categories could be distinguished from each other. The JM distance was calculated for each pairwise combination of the eight

Change category	Description of change	Actual change?
Propeller scar	Seagrass changed to bare ground in long, linear features, caused by damage from boat propellers	Yes
Damaged patch	Seagrass changed to bare ground in larger patches, caused by damage from sources other than propellers, such as boat groundings or seagrass die-off	Yes
Regrowth	Bare ground changed to seagrass, possibly caused by seagrass regrowth	Yes
Added oyster cage	Oyster infrastructure added over seagrass bed	Yes
Removed oyster cage	Oyster infrastructure removed from seagrass bed	Yes
Bright sand false positive	Apparent change signals recorded over unchanged sand patches	No
Unchanged 1	Unchanged seagrass or bare ground, submerged in both images	No
Unchanged 2	Unchanged seagrass or bare ground, submerged in one image and above water in the other	No

Table 3. Identified change categories and descriptions of change signals identified in IR-MAD outputs, and whether the signal is a false positive indication of change.

change ROIs for the MX-10 sensor. This was then repeated for the other three sensors (MX-5, RGB, and VIS-6) to compare the relative strength of detecting change between the four sensors.

Assessing individual band influence on change detection using IR-MAD

One of the non-image outputs from the IR-MAD analysis is the set of eigenvector pairs ($\mathbf{a_{1..N}}$ and $\mathbf{b_{1..N}}$). The eigenvectors contain the final weights applied to the original spectral bands used to produce the canonical variate pairs and the derived MAD variates. The eigenvectors were therefore used to explore which spectral bands in the original bi-temporal image pair had the most influence on the generation of the MAD variate bands. This provides further information to support sensor selection by indicating which bands are most important for change detection.

Vectors $\mathbf{a_i}$ and $\mathbf{b_i}$ are of length equal to the number of input bands to the IR-MAD process. Therefore, for the bi-temporal image pair captured by the MX-10 sensor at St Huberts Island, the 1st elements of the eigenvectors $\mathbf{a_1}$ and $\mathbf{b_1}$ represents the weights applied to the pair of coastal blue bands used (in part) to produce the first canonical variate pair ($\mathbf{CV_1}$ and $\mathbf{CV_2}$) and subsequent MAD variate. Relatively higher weights in vectors $\mathbf{a_i}$ or $\mathbf{b_i}$ indicate a greater degree of influence by the corresponding band on the resulting canonical variate pair, and corresponding MAD variate.

The vector weights produced by the IR-MAD method for different image pairs are not directly comparable. To compare the influence of individual bands across different IR-MAD analysis the eigenvector elements were transformed based on their relative contribution to the CCA transformation, and the number of bands present in the image pair. Elements from each eigenvector were selected corresponding to the MAD variates in which spatially coherent change features were present. The absolute values of these elements were averaged and normalised to determine the relative contribution of each band, and each weight scaled to the full number of bands in the original bi-temporal image pair:

$$W_n = n_{max} \times \frac{1}{N}\sum_{i=1}^{N} \frac{|a_i(n)|+|b_i(n)|}{2}, \tag{3}$$

where $a_i(n)$ and $b_i(n)$ are the pair of eigenvector elements for band n, N is the number of IR-MAD bands which contain spatially coherent elements, W_n is the scaled transformed weight for the spectral band n corresponding with the eigenvector element n, and n_{max} is the number of bands in each image in the bi-temporal image pair.

The higher the scaled transformed weights for a band in the eigenvector corresponding with a MAD variate, the more those bands influenced the derivation of that MAD variate.

The normalised and scaled eigenvector weights (W_n) was used to compare the relative contribution of each spectral band for detecting changing using IR-MAD from images captured by the four alternative sensors used in this study.

Results

IR-MAD analysis for the alternative sensors

For each study site, four sets of MAD variates were produced for the four alternative sensors. Spatially coherent change was visually present in the higher-order MAD variates, while the lower-order variates consisted primarily of noise (Fig. 4). Spatially coherent change features were visible in the five highest order variates (6 to 10) derived from the MX-10 sensors, three variates (4 to 6) derived from the VIS-6 sensor, and for all the variates derived from both the MX-5 and RGB sensors.

Qualitative identification of change categories

Spatially coherent changes were visible in the false colour IR-MAD output images for the MX-10 Sensor (annotated in Fig. 5). These changes are visualised with two different sets of variates: the highest order MAD variates in the left column (variates 10, 9, and 8) and variates manually selected to highlight disturbances in the right column (variates 10, 8, and 6 for St Huberts Island; variates 9, 8, and 7 for Empire Bay). These change categories included boat propeller scars, a large area of disturbance, seagrass patches which decreased in density without clear evidence of direct disturbance, apparent regrowth of seagrass, and false positive change signals.

Linear propeller scars and non-linear disturbed patches, likely anthropogenic, are visible across the St Huberts Island study site. At the Empire Bay study site, fewer disturbances are visible, including a single propeller scar and decrease in cover density at the edge of the seagrass bed. Existing propeller scars present in both images result in IR-MAD values indicating no change.

New propeller scars and a larger disturbed area are clearly visible in all three locations shown in Fig. 5. In the false colour images of St Huberts Island, these features appear black-green when visualised with the highest-order variates (left column) and blue when visualised with selected variates (right column) (Fig. 5). In the images from Empire Bay, propeller scars are light purple and green in the false colour images created using highest-order variates and selected variates respectively (Fig. 5). Other parts of Fig. 5 show general decreases in seagrass density across patches, which show a distinct spatial pattern to the boat damage in the St Huberts Island locations. These decreases in seagrass density may be related to disturbance, or to seasonal variation in seagrass density.

Apparent regrowth of seagrass was also identified in the St Huberts Island study site (Fig. 6). These areas appear as bare ground in the February image and vegetation in the June image. This pattern may indicate (1) seagrass regrowth over previously bare sediment or propeller scars; (2) seagrass leaves changing in position due to water flow, or (3) spatial inaccuracies in image registration or orthorectification.

The other change categories identified in the qualitative analysis of the St Huberts Island study site included changes related to oyster farms. The oyster farms consist of cages or trays that can be attached to lines as needed

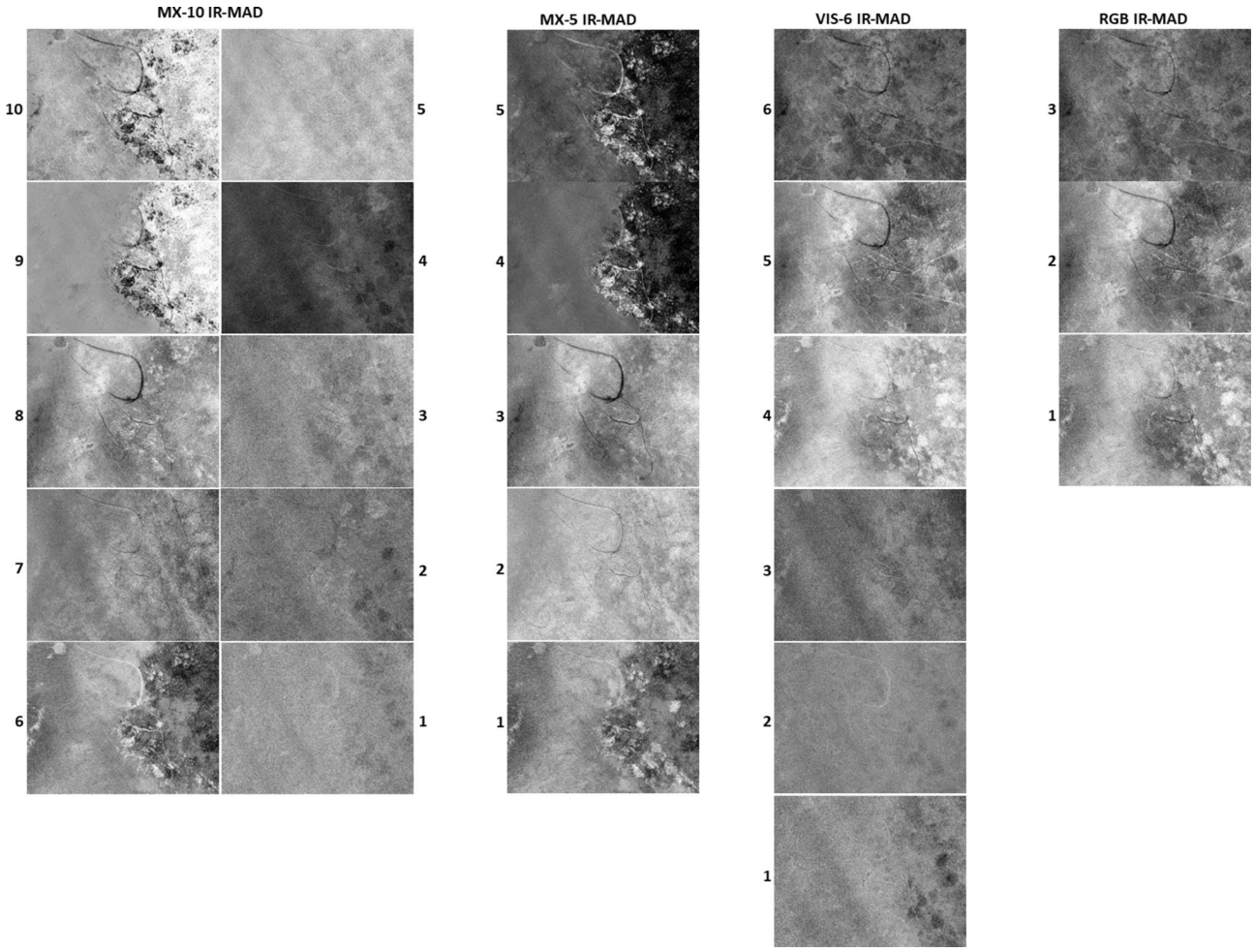

Figure 4. MAD variates for each of the four sensors for a subset of the St Huberts Island study site. Each MAD variate is visualised with a 5% linear greyscale stretch. MAD variates are numbered from 1 representing the lowest order.

and are frequently moved depending on changes to water conditions. These operational practices were identified in the IR-MAD outputs for both study sites (Fig. 7).

Comparing effectiveness of disturbance detection between the alternative sensors

The JM distance values for each class pair are a relative measure of statistical separability, indicating how effectively the change category can be distinguished from others. The JM distance values were calculated across all change category pairs for all four alternative sensors (Table 4). For ease of comparison between sensors in the text, the JM distance results were arbitrarily grouped into three classes–Strong (JM distance ≥ 1.8), Moderate (1.8 > JM distance ≥ 1.4), and Weak (1.4 > JM distance) (Table 5).

The IR-MAD outputs for the MX-10 sensor had the highest JM distance values (Table 4), with 21 change category pairs showing strong separability (Table 5). Propeller scars and damaged patches had relatively low separability from each other (JM distance 1.40) but moderate to strong separability from all other classes. Apparent regrowth and changes to oyster infrastructure also showed moderate to strong separability from all other classes.

A total of 18 change category pairs had strong separability for the IR-MAD variates derived from the MX-5 sensor (Table 5). Like the MX-10 data, the lowest separability was between the propeller scars and damaged patches (Table 4). These disturbances were only moderately separable from the bright sand false positive class in this dataset but were relatively more separable from the others.

JM distances for the VIS-6 sensor (Table 4) showed 12 strongly separable class pairs (Table 5). Disturbed patches and propeller scars had strong (JM distance ≥ 1.80) and moderate (JM distance ≥ 1.54) separability respectively from all classes except each other (JM distance 1.21). Apparent regrowth showed moderate to strong separability from all other classes except removed oyster infrastructure.

The JM distance results derived from the RGB sensor (Table 4) showed the weakest separability values compared with other sensors. Larger disturbed patches displayed strong or moderate separability from all classes except propeller scars. However, propeller scars showed weak separability (JM distance < 1.5) from most other classes, including bright sand false positives and both unchanged classes. Apparent regrowth was separable from

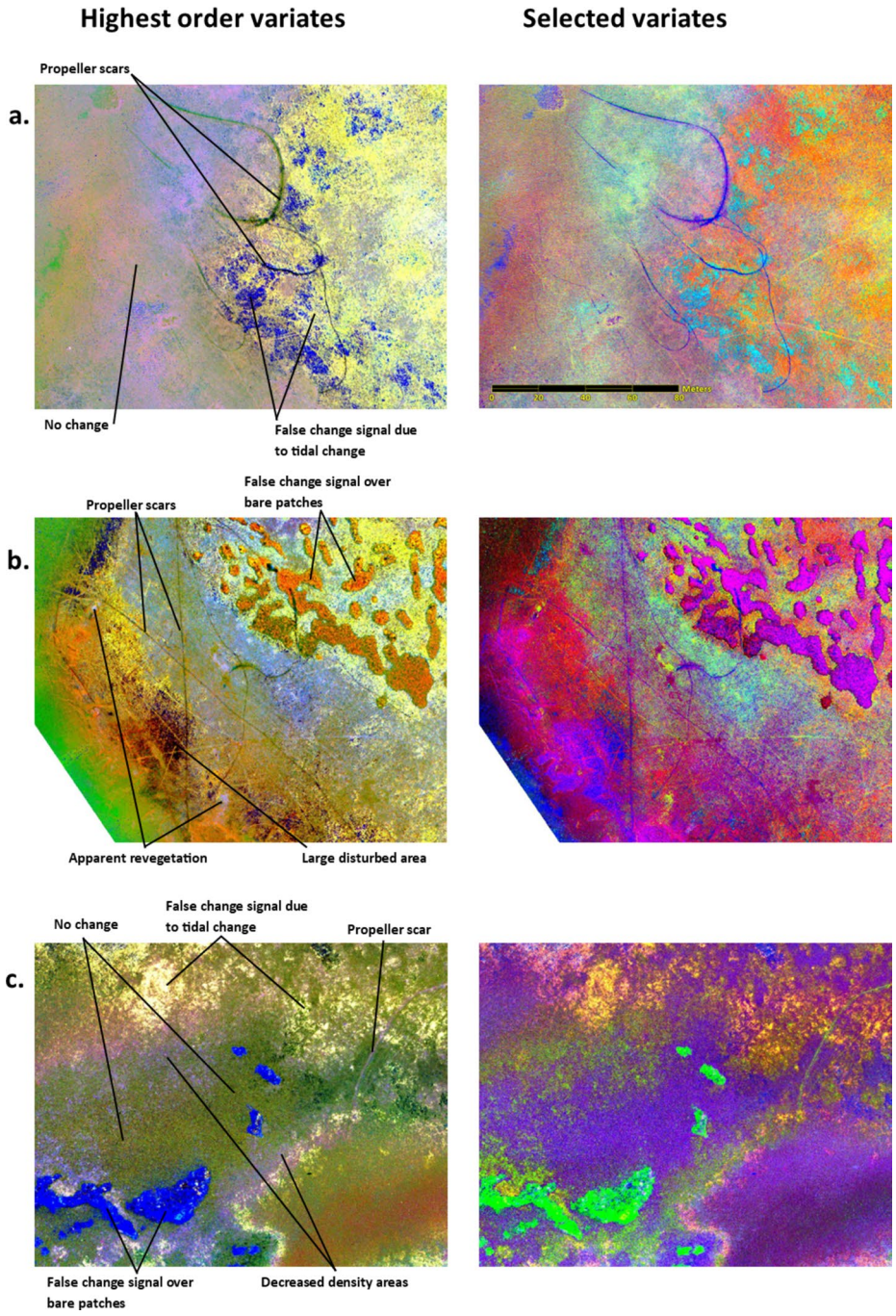

Figure 5. Examples of identified change categories overlayed on false colour change images. Change images were derived using the higher-order MAD variates 10, 9, and 8 (left column), variates 10, 8, and 6 (right column, image (**a**) and (**b**)), and variates 9, 8, and 7 (right column, image (**c**)). Change categories include: (**a**) propeller scars at St Huberts Island, (**b**) a large disturbed area at St Huberts Island, and (**c**) areas of decreased seagrass density at Empire Bay. All variates were derived from bi-temporal images captured by the MX-10 sensor.

both disturbed classes, but showed weaker separability from changes to oyster infrastructure, and the below water unchanged class.

Separability between the two unchanged classes was lower for the two virtual (VIS-6 and RGB) sensors which did not have the red-edge and near-infrared. Submerged unchanged areas and emerged unchanged areas appear more similar in the VIS-6 and RGB sensor IR-MAD outputs data compared to the MX-10 and MX-5 IR-MAD outputs (Fig. 8).

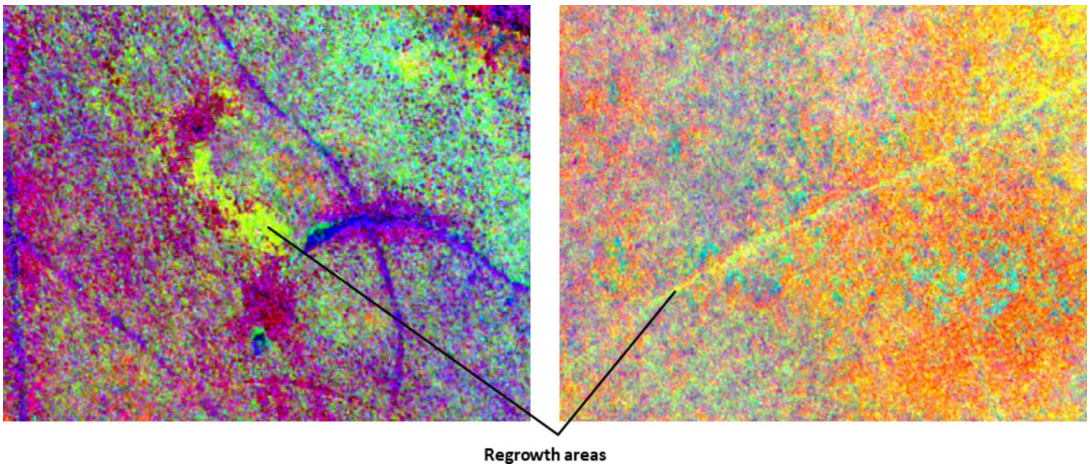

Figure 6. Apparent seagrass regrowth annotated on spatial subsets of false colour images of the IR-MAD outputs (variates 10, 8, and 6) for St Huberts Island (derived from the MX-10 sensor).

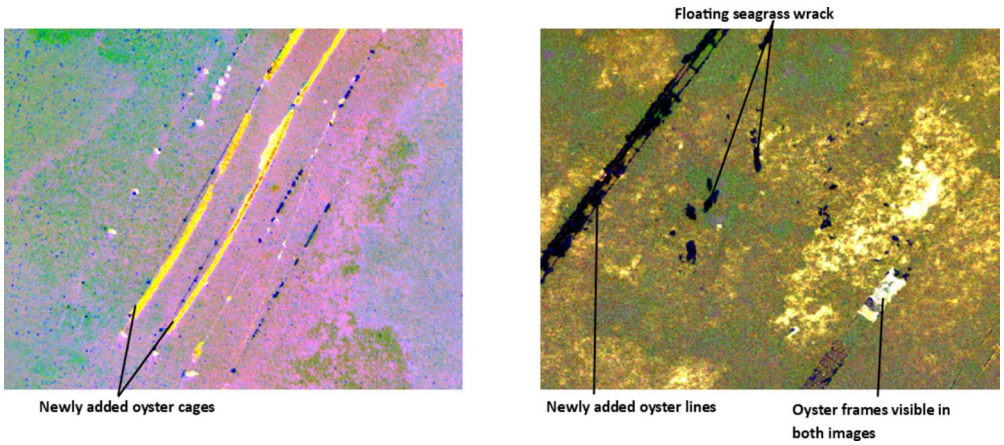

Figure 7. Oyster aquaculture infrastructure changes identified in the IR-MAD outputs for St Huberts Island (left) and Empire Bay (right). Both images were visualised using MAD variates 10, 9, and 8 derived from the bi-temporal image pairs captured by the MX-10 sensor.

Individual band influence on detecting change

The transformed eigenvector weights were used to assess the contribution of each band to the IR-MAD calculations across both study sites for all four alternative sensors (Table 6).

Across the data from the MX-10, VIS-6, and MX-5 sensors, the Green 2 and Red 2 bands had a consistently high influence, while the Blue band was consistently less influential on the IR-MAD results. For the RGB sensor data, the blue band had the highest influence. The NIR band in the MX-10 sensor data also had a relatively large statistical influence on the change signals produced by this sensor. The five MX-10 sensor bands that were not available in the MX-5 sensor data had differing influences on change detection results. The Green 1 band had a relatively small influence, the Red 1 band had a variable influence depending on the image pair, and the Coastal Blue band had a consistently high influence.

Discussion

The IR-MAD method applied to images captured by a UAV was shown to be viable for detecting fine-scale physical disturbances to seagrass beds using the 10-band, 5-band, and 6-band data, and potentially effective for 3-band data. Large areas of disturbed seagrass were visibly identified in IR-MAD results from all sensors and were strongly separable from all other change categories in the 10-band and 5-band data, and from most other change categories in the 6-band and 3-band data. Propeller scars were visible in all IR-MAD outputs, and JM distance results showed moderate to strong separability for propeller scars in the 10- and 5-band data, moderate separability in the 6-band data, and weak to moderate separability in the 3-band data. This study demonstrates the potential of IR-MAD analysis to support seagrass monitoring and management at relevant finer spatio-temporal resolution, especially when multispectral sensors like the Micasense RedEdge-MX Dual sensor are used.

MX-10	Propeller scars	Damaged patches	Apparent regrowth	New oyster infrastructure	Removed oyster infrastructure	Bright sand false positive	Unchanged above water	Unchanged below water
Propeller scars								
Damaged patches	1.40							
Apparent regrowth	1.79	1.99						
New oyster infrastructure	2.00	2.00	1.99					
Removed oyster infrastructure	1.98	2.00	1.99	2.00				
Bright sand false positive	1.69	1.76	1.96	2.00	1.99			
Unchanged above water	1.94	2.00	1.77	1.99	1.99	2.00		
Unchanged below water	1.90	2.00	1.71	2.00	2.00	2.00	1.75	

MX-5	Propeller scars	Damaged patches	Apparent regrowth	New oyster infrastructure	Removed oyster infrastructure	Bright sand false positive	Unchanged above water	Unchanged below water
Propeller scars								
Damaged patches	1.30							
Apparent regrowth	1.74	1.98						
New oyster infrastructure	1.98	1.99	1.94					
Removed oyster infrastructure	1.73	1.92	1.79	1.73				
Bright sand false positive	1.43	1.48	1.94	1.97	1.82			
Unchanged above water	1.90	2.00	1.64	1.91	1.92	2.00		
Unchanged below water	1.82	1.99	1.49	1.99	1.96	1.99	1.62	

VIS-6	Propeller scars	Damaged patches	Apparent regrowth	New oyster infrastructure	Removed oyster infrastructure	Bright sand false positive	Unchanged above water	Unchanged below water
Propeller scars								
Damaged patches	1.21							
Apparent regrowth	1.72	1.95						
New oyster infrastructure	1.79	1.88	1.68					
Removed oyster infrastructure	1.55	1.91	1.40	1.78				
Bright sand false positive	1.57	1.80	1.56	1.19	1.75			
Unchanged above water	1.68	1.97	1.86	1.98	1.81	1.93		
Unchanged below water	1.54	1.96	1.76	1.98	1.76	1.89	0.78	

RGB	Propeller scars	Damaged patches	Apparent regrowth	New oyster infrastructure	Removed oyster infrastructure	Bright sand false positive	Unchanged above water	Unchanged below water
Propeller scars								
Damaged patches	1.13							
Apparent regrowth	1.53	1.93						
New oyster infrastructure	1.55	1.66	1.45					
Removed oyster infrastructure	1.47	1.86	1.10	1.64				
Bright sand false positive	1.20	1.59	1.37	0.46	1.58			
Unchanged above water	1.47	1.95	1.64	1.88	1.67	1.76		
Unchanged below water	1.39	1.96	1.46	1.85	1.61	1.71	0.51	

Table 4. JM distance values between the eight identified change categories for the four sensors: MX-10, MX-5, VIS-6, and RGB. Table cells colour coded from weakest separability (red) to strongest (dark green).

Substantial changes in seagrass cover were identified at both study sites, but they were noticeably different in the IR-MAD results. At St Huberts Island, many propeller scars and other instances of boat damage were identified, clustered towards the western edge of the meadow and near oyster aquaculture infrastructure, where boat traffic is likely to be highest. At Empire Bay, however, the patterns of change were more spatially consistent potentially indicating seasonal trends or environmental conditions such as water quality.

The full set of 10 bands provided by the MX-10 sensor demonstrated advantages for seagrass change detection. The IR-MAD method using images from the MX-10 sensor detected change features more effectively than the

Sensor	Strong	Moderate	Weak
MX-10	21	6	1
MX-5	18	6	4
VIS-6	12	12	4
RGB	6	11	11

Table 5. Number of change category pairs with strong (JM distance > 1.8), moderate (1.8 ≥ JM distance > 1.4), and weak (1.4 ≥ JM distance) separability for each alternative sensor. Based on JM distance calculated from each alternative sensor's IR-MAD results.

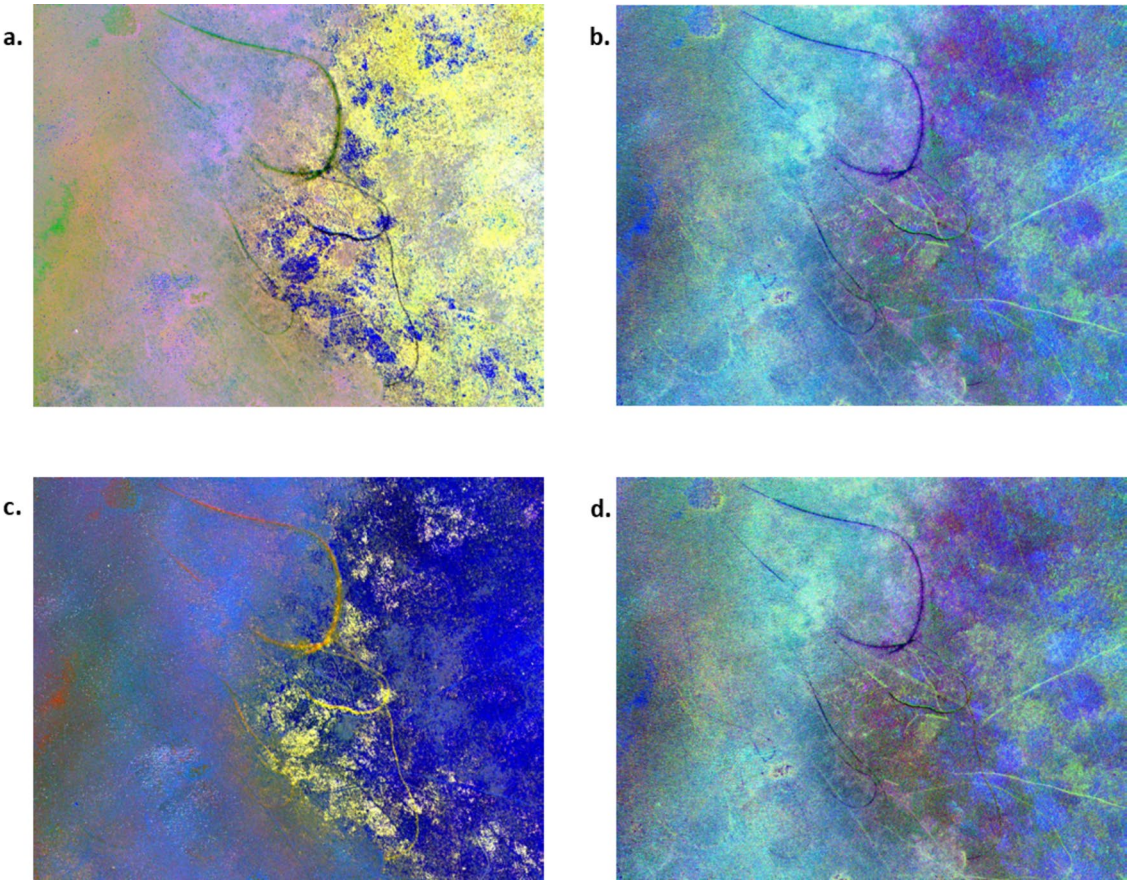

Figure 8. Propeller scars were visibly present at the St Huberts Island in the (**a**) MX-10 sensor IR-MAD outputs visualised with variates 10, 9, and 8, (**b**) VIS-6 sensor IR-MAD output visualised with variates 6, 5, and 4, (**c**) MX-5 sensor IR-MAD output visualised with variates 5, 4, and 3, and (**d**) the RGB sensor IR-MAD output visualised with variates 3, 2, and 1.

other three sensors, with strongly separable JM distance measurements recorded for all eight change categories tested. Outputs from the theoretical VIS-6 sensor also offered improved change detection over the RGB sensor. Two of the additional visible bands included in IR-MAD analysis for the MX-10 and VIS-6 sensors (Coastal Blue and Red 1), had a relatively high weighting, indicating a strong influence on change detection. This suggests that their addition enhances change detection compared to the MX-5 sensor.

The improvement offered by these additional bands is consistent with past research using satellite-borne sensors for characterising seagrass in coastal ecosystems. For example, the Sentinel-2 coastal blue band was shown to improve seagrass classification[53], and analysis of hyperspectral images has shown that the green–red visible range is optimal for predicting seagrass percent cover and related variables[54–56]. Multispectral sensors with additional visible light bands compared with a standard RGB sensors has been demonstrated here and elsewhere[57] to provide improved ability to characterise seagrass ecosystems without necessitating the use of expensive hyperspectral sensors.

Though the full 10 band MX-10 sensor was the most effective in discriminating change classes, the change class separability results suggest that cheaper and simpler sensors may be sufficient for efficient monitoring of seagrass using IR-MAD. The Micasense RedEdge MX sensor (MX-5) is a commonly available sensor which

Band	St Huberts 10-band	Empire Bay 10-band	St Huberts 6-band	Empire Bay 6-band	St Huberts 5-band	Empire Bay 5-band	St Huberts 3-band	Empire Bay 3-band
Coastal Blue	1.24	1.22	1.37	1.1				
Blue	0.73	0.68	0.85	0.73	0.92	1.12	1.16	1.03
Green 1	0.78	0.85	0.69	0.65				
Green 2	1.14	1.28	1.01	0.91	1.04	0.98	0.88	0.94
Red 1	1.29	0.66	0.87	1.02				
Red 2	1.05	1.2	1.2	1.59	1.49	1.15	0.97	1.03
RE 1	0.78	0.97						
RE 2	0.7	0.94			0.80	0.86		
RE 3	1.06	0.86						
NIR	1.23	1.34			0.75	0.90		

Table 6. Transformed weights for each eigenvector element, indicating the influence of each corresponding spectral band on MAD outputs.

can be integrated on consumer UAVs at relatively low cost. For visual analysis of IR-MAD outputs, the 5-band images provided by this sensor has been demonstrated here as sufficient for focused management responses to seagrass disturbance.

The red-edge and near-infrared bands can improve accuracy results in seagrass mapping when leaves are on or near the surface of the water due to the absorption of red and scattering of near-infrared light by photosynthetic vegetation[26]. However, the high absorbance of red-edge and near-infrared light by water can reduce the effectiveness of bands in these regions when seagrass is fully submerged. The IR-MAD analyses in this study which included red-edge and near-infrared bands detected differences in water level between image captures as a distinct category of change which is separable from disturbance events, and this was reflected in the high level of influence that the NIR band had on the MX-10 change result. However, IR-MAD outputs produced without the red-edge and near-infrared bands are easier to interpret visually as the extensive change signals caused by tidal differences are less apparent, highlighting the change signals representing actual seagrass disturbance. This suggests that excluding the red-edge and near-infrared bands before any IR-MAD analysis may improve results and interpretation if there are significant tidal differences between the bi-temporal image pair.

Spatially coherent patterns by seagrass disturbances were visible in the IR-MAD outputs for the simple 3-band RGB sensor, even though the disturbances were only weakly to moderately separable from other categories. This may provide a more accessible remote sensing option by using consumer-grade UAVs with inbuilt RGB cameras to capture and analyse bi-temporal image pairs for seagrass disturbance. Orthorectified RGB images have been used to map seagrass beds, even radiometrically uncalibrated data[28,58,59]. However, the poorer separability values for the RGB data compared to the 6-band VIS-6 sensor demonstrated here highlight the trade-off between achieving improved change detection results using IR-MAD and relative sensor cost and accessibility.

Physical disturbances, especially root-rhizome damage, can lead to further degradation through positive feedback mechanisms as the sediment is destabilised increasing bed exposure to erosion from waves and currents[60–62]. This may lead to the release of stored soil carbon and negative impacts on future carbon sequestration[63,64]. Additionally, physical disturbances to seagrass beds can impact the composition and condition of faunal communities[65–67]. Management interventions, including educating fishers and boaters to reduce propeller damage, restricting activities under certain tidal conditions, or restoring seagrass beds damaged by watercraft can lead to measurable improvements in seagrass condition[21,68,69]. Timely detection of fine-scale physical disturbances such as propeller scars, which are otherwise difficult to detect, is needed to support the implementation of these intervention strategies. Applying IR-MAD to UAV images provides a relatively simple unsupervised method for identifying disturbance.

Effective long-term monitoring is important for the success of seagrass restoration projects[70,71] and monitoring cost effectiveness is particularly crucial for projects limited by financial constraints[72]. The effectiveness of blue carbon restoration projects for generating high-quality and verifiable carbon offsetting services requires robust approaches for identifying and tracking change in biomass extent at ecologically relevant spatio-temporal scales. Although IR-MAD cannot provide quantitative measurements of seagrass blue carbon stocks, in detecting fine scale change from baseline conditions, results can complement existing measurement approaches for project reporting.

Change detection using IR-MAD could be further enhanced by adding pre- or post-processing steps. Water column correction, applied to the UAV images, may assist in reducing change signals caused by differences in tidal level between images. Additionally, changes detected in IR-MAD outputs could be automatically extracted using object-based image analysis methods, image thresholding, or machine learning methods. IR-MAD outputs by themselves, however, offer a valuable resource for coastal managers and scientists due to the unsupervised nature of the process, and the need for no data inputs beyond two coregistered UAV images.

Wider application of IR-MAD for seagrass change detection requires further testing over multi-species seagrass beds and different water optical properties. The study findings are restricted to two temperate water study sites covering predominantly monospecific seagrass beds. Additionally, the band configurations (including band centres and widths) of the two virtual sensors used in this study (VIS-6 and RGB) may not correspond with actual, commercially available sensors. Testing the IR-MAD method using images captured from alternative, commercially available sensors such as a simple RGB sensor commonly integrated on many UAV platforms, may provide further insights into sensor selection considerations for coastal managers.

Conclusions

Seagrasses perform a range of vital ecosystem functions including sediment stabilisation, carbon sequestration, habitat provision and water purification[73]. There is a need for seagrass monitoring techniques that detect disturbances which interfere with these functions. The application of IR-MAD to co-registered, bi-temporal UAV-acquired images offers a relatively cost-effective, unsupervised method of detecting very fine-scale changes to seagrass beds, at the on-demand temporal resolution UAV imaging provides. IR-MAD applied to UAV-acquired multispectral images can be used to distinguish and map multiple forms of change in seagrass beds, including propeller scars, regrowth, and oyster farming. In detecting key fine-scale change features, this method can inform management interventions designed to prevent seagrass degradation, guide restoration efforts, and contribute to blue carbon accounting. Change detection using IR-MAD is unsupervised, can be implemented in open-source software, with consumer-grade computing power, using images from standard off-the-shelf UAV multispectral sensors.

Data availability

The datasets generated and analysed during the current study are available from the corresponding author on request.

Received: 3 April 2024; Accepted: 7 August 2024
Published online: 17 August 2024

References

1. Hossain, M. S. & Hashim, M. Potential of earth observation (EO) technologies for seagrass ecosystem service assessments. *Int. J. Appl. Earth Obs. Geoinf.* **77**, 15–29 (2019).
2. Griffiths, L. L., Connolly, R. M. & Brown, C. J. Critical gaps in seagrass protection reveal the need to address multiple pressures and cumulative impacts. *Ocean Coast. Manag.* https://doi.org/10.1016/j.ocecoaman.2019.104946 (2020).
3. Unsworth, R. K. F., Cullen-Unsworth, L. C., Jones, B. L. H. & Lilley, R. J. The planetary role of seagrass conservation. *Science* **377**, 609–613. https://doi.org/10.1126/science.abq6923 (2022).
4. Waycott, M. *et al.* Accelerating loss of seagrasses across the globe threatens coastal ecosystems. *Proc. Natl. Acad. Sci.* **106**, 12377–12381 (2009).
5. Lovelock, C. E. *et al.* Assessing the risk of carbon dioxide emissions from blue carbon ecosystems. *Front. Ecol. Environ.* **15**, 257–265 (2017).
6. Brondizio, E. S., Settele, J., Diaz, S. & Ngo, H. T. Global assessment report on biodiversity and ecosystem services of the Intergovernmental Science-Policy Platform on Biodiversity and Ecosystem Services (2019).
7. Pendleton, L. *et al.* Estimating global "blue carbon" emissions from conversion and degradation of vegetated coastal ecosystems (2012).
8. O'Brien, K. R. *et al.* Seagrass ecosystem trajectory depends on the relative timescales of resistance, recovery and disturbance. *Mar. Pollut. Bull.* **134**, 166–176 (2018).
9. Orth, R. J. *et al.* Restoration of seagrass habitat leads to rapid recovery of coastal ecosystem services. *Sci. Adv.* **6**, eabc6434 (2020).
10. Beheshti, K. M. *et al.* Rapid enhancement of multiple ecosystem services following the restoration of a coastal foundation species. *Ecol. Appl.* https://doi.org/10.1002/eap.2466 (2022).
11. Barry, S. C., Raskin, K. N., Hazell, J. E., Morera, M. C. & Monaghan, P. F. Evaluation of interventions focused on reducing propeller scarring by recreational boaters in Florida, USA. *Ocean Coast. Manag.* **186**, 105089 (2020).
12. Kilminster, K. *et al.* Unravelling complexity in seagrass systems for management: Australia as a microcosm. *Sci. Total Environ.* **534**, 97–109. https://doi.org/10.1016/j.scitotenv.2015.04.061 (2015).
13. Kirkman, H. Baseline and monitoring methods for seagrass meadows. *J. Environ. Manag.* **47**, 191–201 (1996).
14. Short, F. T., Coles, R. G. & Short, C. M. SeagrassNet manual for scientific monitoring of seagrass habitat (2015).
15. Roelfsema, C. *et al.* Challenges of remote sensing for quantifying changes in large complex seagrass environments. *Estuar. Coast. Shelf Sci.* **133**, 161–171. https://doi.org/10.1016/j.ecss.2013.08.026 (2013).
16. Traganos, D. *et al.* Towards global-scale seagrass mapping and monitoring using sentinel-2 on google earth engine: The case study of the Aegean and Ionian Seas. *Remote Sens.* https://doi.org/10.3390/rs10081227 (2018).
17. Lizcano-Sandoval, L. *et al.* Seagrass distribution, areal cover, and changes (1990–2021) in coastal waters off West-Central Florida, USA. *Estuar. Coast. Shelf Sci.* **279**, 108134 (2022).
18. Coffer, M. M. *et al.* Providing a framework for seagrass mapping in United States coastal ecosystems using high spatial resolution satellite imagery. *J. Environ. Manag.* **337**, 117669 (2023).
19. Fletcher, R. S., Pulich, W. Jr. & Hardegree, B. A semiautomated approach for monitoring landscape changes in Texas seagrass beds from aerial photography. *J. Coast. Res.* **25**, 500–506 (2009).
20. Uhrin, A. V. & Townsend, P. A. Improved seagrass mapping using linear spectral unmixing of aerial photographs. *Estuar. Coast. Shelf Sci.* **171**, 11–22. https://doi.org/10.1016/j.ecss.2016.01.021 (2016).
21. Orth, R. J., Lefcheck, J. S. & Wilcox, D. J. Boat propeller scarring of seagrass beds in lower Chesapeake Bay, USA: Patterns, causes, recovery, and management. *Estuar. Coasts* **40**, 1666–1676 (2017).
22. Mancini, G. *et al.* Detecting trends in seagrass cover through aerial imagery interpretation: Historical dynamics of a *Posidonia oceanica* meadow subjected to anthropogenic disturbance. *Ecol. Indic.* **150**, 110209 (2023).
23. Virnstein, R. W. Seagrass management in Indian River Lagoon, Florida: Dealing with issues of scale. *Pac. Conserv. Biol.* **5**, 299–305 (1999).
24. Kaufman, K. A. & Bell, S. S. The use of imagery and GIS techniques to evaluate and compare seagrass dynamics across multiple spatial and temporal scales. *Estuar. Coasts* **45**, 1028–1044 (2022).

25. Veettil, B. K. *et al.* Opportunities for seagrass research derived from remote sensing: A review of current methods. *Ecol. Indic.* https://doi.org/10.1016/j.ecolind.2020.106560 (2020).
26. James, D. *et al.* Towards better mapping of seagrass meadows using UAV multispectral and topographic data. *J. Coast. Res.* https://doi.org/10.2112/si95-217.1 (2020).
27. Chen, J. & Sasaki, J. Mapping of subtidal and intertidal seagrass meadows via application of the feature pyramid network to unmanned aerial vehicle orthophotos. *Remote Sens.* **13**, 4880 (2021).
28. Tahara, S., Sudo, K., Yamakita, T. & Nakaoka, M. Species level mapping of a seagrass bed using an unmanned aerial vehicle and deep learning technique. *PeerJ* **10**, e14017 (2022).
29. Price, D. M. *et al.* Quantifying the intra-habitat variation of seagrass beds with unoccupied aerial vehicles (UAVs). *Remote Sens.* **14**, 480 (2022).
30. Karang, I. A. *et al.* High-resolution seagrass species mapping and propeller scars detection in Tanjung Benoa, Bali through UAV imagery. *J. Ecol. Eng.* **25**, 161–174 (2024).
31. Martin, R., Ellis, J., Brabyn, L. & Campbell, M. Change-mapping of estuarine intertidal seagrass (*Zostera muelleri*) using multispectral imagery flown by remotely piloted aircraft (RPA) at Wharekawa Harbour, New Zealand. *Estuar. Coast. Shelf Sci.* **246**, 107046 (2020).
32. Krause, J. R., Hinojosa-Corona, A., Gray, A. B. & Burke Watson, E. Emerging sensor platforms allow for seagrass extent mapping in a turbid estuary and from the meadow to ecosystem scale. *Remote Sens.* **13**, 3681 (2021).
33. Aoki, L. R. *et al.* UAV high-resolution imaging and disease surveys combine to quantify climate-related decline in seagrass meadows. *Oceanography* **36**, 38 (2023).
34. Singh, A. Digital change detection techniques using remotely-sensed data. *Int. J. Remote Sens.* **10**, 989–1003 (1989).
35. Nielsen, A. A. The regularized iteratively reweighted MAD method for change detection in multi-and hyperspectral data. *IEEE Trans. Image Process.* **16**, 463–478 (2007).
36. Nielsen, A. A., Conradsen, K. & Simpson, J. J. Multivariate alteration detection (MAD) and MAF postprocessing in multispectral, bitemporal image data: New approaches to change detection studies. *Remote Sens. Environ.* **64**, 1–19 (1998).
37. Liu, Y. *et al.* Discovering potential illegal construction within building roofs from UAV images using semantic segmentation and object-based change detection. *Photogramm. Eng. Remote Sens.* **87**, 263–271 (2021).
38. Román, A., Tovar-Sánchez, A., Olivé, I. & Navarro, G. Using a UAV-mounted multispectral camera for the monitoring of marine macrophytes. *Front. Mar. Sci.* https://doi.org/10.3389/fmars.2021.722698 (2021).
39. Davies, B. F. R. *et al.* Multi- and hyperspectral classification of soft-bottom intertidal vegetation using a spectral library for coastal biodiversity remote sensing. *Remote Sens. Environ.* **290**, 113554. https://doi.org/10.1016/j.rse.2023.113554 (2023).
40. Roy, P. *et al.* Structure and function of south-east Australian estuaries. *Estuar. Coast. Shelf Sci.* **53**, 351–384 (2001).
41. NSW Department of Primary Industries, New South Wales Government. NSW Estuarine Macrophytes. Accessed 22 Feb 2024. https://data.gov.au/data/dataset/estuarine-macrophytes-of-nsw (2022).
42. Jelbart, J. E. & Ross, P. M. *Report for Gosford City Council* (Central Coast, 2006).
43. Macreadie, P. I., Sullivan, B., Evans, S. M. & Smith, T. M. *Seagrasses of Australia: Structure, Ecology, and Conservation* 31–59 (Springer International Publishing AG, 2018).
44. NSW Department of Primary Industries, NSW Priority Oyster Aquaculture Areas, accessed from The Sharing and Enabling Environmental Data Portal. https://datasets.seed.nsw.gov.au/dataset/b643e8ee-d9f6-43ca-9558-c161b166c60d (2024)
45. Davis, J. *et al.* Best practices for incorporating UAS image collection into wetland monitoring efforts: A guide for entry level users (2022).
46. Doukari, M., Katsanevakis, S., Soulakellis, N. & Topouzelis, K. The effect of environmental conditions on the quality of UAS orthophoto-maps in the coastal environment. *ISPRS Int. J. Geo-inf.* **10**, 18 (2021).
47. Canty, M. J. & Nielsen, A. A. Visualization and unsupervised classification of changes in multispectral satellite imagery. *Int. J. Remote Sens.* **27**, 3961–3975. https://doi.org/10.1080/01431160500222608 (2006).
48. Hotelling, H. Relations between two sets of variables. *Biometrika* **28**, 321–377 (1936).
49. Canty, M. J. *Image Analysis, Classification and Change Detection in Remote Sensing, with Algorithms for ENVI/IDL and Python* (Taylor and Francis CRC Press, 2014).
50. Kirk, J. T. *Light and Photosynthesis in Aquatic Ecosystems* (Cambridge University Press, 1994).
51. Wacker, A. & Landgrebe, D. Minimum distance classification in remote sensing. *LARS Technical Reports*, 25 (1972).
52. Richards, J. A. & Richards, J. A. *Remote Sensing Digital Image Analysis* Vol. 5 (Springer, 2022).
53. Poursanidis, D., Traganos, D., Reinartz, P. & Chrysoulakis, N. On the use of Sentinel-2 for coastal habitat mapping and satellite-derived bathymetry estimation using downscaled coastal aerosol band. *Int. J. Appl. Earth Obs. Geoinf.* **80**, 58–70 (2019).
54. Phinn, S., Roelfsema, C., Dekker, A., Brando, V. & Anstee, J. Mapping seagrass species, cover and biomass in shallow waters: An assessment of satellite multi-spectral and airborne hyper-spectral imaging systems in Moreton Bay (Australia). *Remote Sens. Environ.* **112**, 3413–3425. https://doi.org/10.1016/j.rse.2007.09.017 (2008).
55. Pu, R., Bell, S., Meyer, C., Baggett, L. & Zhao, Y. Mapping and assessing seagrass along the western coast of Florida using Landsat TM and EO-1 ALI/Hyperion imagery. *Estuar. Coast. Shelf Sci.* **115**, 234–245 (2012).
56. Valle, M. *et al.* Mapping estuarine habitats using airborne hyperspectral imagery, with special focus on seagrass meadows. *Estuar. Coast. Shelf Sci.* **164**, 433–442. https://doi.org/10.1016/j.ecss.2015.07.034 (2015).
57. Dierssen, H. M. *et al.* Pushing the limits of seagrass remote sensing in the turbid waters of Elkhorn slough, California. *Remote Sens.* https://doi.org/10.3390/rs11141664 (2019).
58. Riniatsih, I., Ambariyanto, A., Yudiati, E., Redjeki, S. & Hartati, R. Monitoring the seagrass ecosystem using the unmanned aerial vehicle (UAV) in coastal water of Jepara. *IOP Conf. Ser. Earth Environ. Sci.* **674**, 012075. https://doi.org/10.1088/1755-1315/674/1/012075 (2021).
59. Hamad, I. Y., Staehr, P. A., Rasmussen, M. B. & Sheikh, M. Drone-based characterization of seagrass habitats in the tropical waters of Zanzibar. *Remote Sens.* **14**, 680 (2022).
60. Larkum, A. W. D. Ecology of botany bay. I. Growth of *Posidonia australis* (Brown) Hook. f. in botany bay and other bays of the Sydney basin. *Mar. Freshw. Res.* **27**, 117–127 (1976).
61. West, R. J. Impact of recreational boating activities on the seagrass posidonia in SE Australia. *Wetlands (Australia)* **26**, 3 (2012).
62. Swadling, D. S., West, G. J., Gibson, P. T., Laird, R. J. & Glasby, T. M. Don't go breaking apart: Anthropogenic disturbances predict meadow fragmentation of an endangered seagrass. *Aquat. Conserv. Mar. Freshw. Ecosyst.* **33**, 56–69. https://doi.org/10.1002/aqc.3905 (2023).
63. Bourque, A. S., Kenworthy, W. J. & Fourqurean, J. W. Impacts of physical disturbance on ecosystem structure in subtropical seagrass meadows. *Mar. Ecol. Prog. Ser.* **540**, 27–41 (2015).
64. Macreadie, P. I. *et al.* Losses and recovery of organic carbon from a seagrass ecosystem following disturbance. *Proc. R. Soc. B Biol. Sci.* **282**, 20151537 (2015).
65. Reed, B. J. & Hovel, K. A. Seagrass habitat disturbance: how loss and fragmentation of eelgrass Zostera marina influences epifaunal abundance and diversity. *Mar. Ecol. Prog. Ser.* **326**, 133–143 (2006).
66. Bell, S. S., Fonseca, M. S. & Kenworthy, W. J. Dynamics of a subtropical seagrass landscape: Links between disturbance and mobile seed banks. *Landsc. Ecol.* **23**, 67–74. https://doi.org/10.1007/s10980-007-9137-z (2008).

67. Iacarella, J. C. *et al.* Anthropogenic disturbance homogenizes seagrass fish communities. *Glob. Change Biol.* **24**, 1904–1918. https://doi.org/10.1111/gcb.14090 (2018).
68. Orth, R. J., Marion, S. R., Moore, K. A. & Wilcox, D. J. Eelgrass (*Zostera marina* L.) in the Chesapeake Bay region of mid-Atlantic coast of the USA: Challenges in conservation and restoration. *Estuar. Coasts* **33**, 139–150 (2010).
69. Rezek, R. J., Furman, B. T., Jung, R. P., Hall, M. O. & Bell, S. S. Long-term performance of seagrass restoration projects in Florida, USA. *Sci. Rep.* **9**, 15514 (2019).
70. Cunha, A. H. *et al.* Changing paradigms in seagrass restoration. *Restor. Ecol.* **20**, 427–430. https://doi.org/10.1111/j.1526-100X.2012.00878.x (2012).
71. Tan, Y. M. *et al.* Seagrass restoration is possible: Insights and lessons from Australia and New Zealand. *Front. Mar. Sci.* https://doi.org/10.3389/fmars.2020.00617 (2020).
72. Macreadie, P. I. *et al.* Operationalizing marketable blue carbon. *One Earth* **5**, 485–492. https://doi.org/10.1016/j.oneear.2022.04.005 (2022).
73. Nordlund, L., Koch, E. W., Barbier, E. B. & Creed, J. C. Seagrass ecosystem services and their variability across genera and geographical regions. *PLoS One* **11**, e0163091. https://doi.org/10.1371/journal.pone.0163091 (2016).

Acknowledgements
We thank Alexandra Jones and Kate Whitton for their fieldwork assistance.

Author contributions
J.S., K.P.D., E.B. and P.B. conceived and designed the study. J.S. and K.P.D. collected data. J.S. prepared the data and ran all data analysis, and K.P.D. supervised data analysis. J.S. prepared the manuscript, and K.P.D., E.B., and P.B. edited the manuscript. E.B. acquired funding for the project. All authors contributed extensively to the work presented.

Funding
This research was funded by the Australian Research Council, grant number IC170100023.

Competing interests
The authors declare no competing interests.

Additional information
Correspondence and requests for materials should be addressed to J.S.

Reprints and permissions information is available at www.nature.com/reprints.

Publisher's note Springer Nature remains neutral with regard to jurisdictional claims in published maps and institutional affiliations.

Appendix B. Presentations and awards

Presentations

Simpson, J. (2021). Mapping 'blue carbon' in heterogeneous seagrass environments. 'Thinking Space' seminar series, School of Geosciences, University of Sydney, September 2021

Simpson, J. (2021). GeoInspire Panel. Panel presentation. Regional Geospatial Youth Forum, Singapore, September 2021

Simpson, J. (2022). Developing a database to support remediation cost estimation with machine learning. Final presentation for Australian Postgraduate Research internship with Senversa Pty. Ltd., Sydney, February 2022

Simpson, J. (2022). Novel technologies in science. Panel presentation. University of Sydney Science HDR Student Conference, University of Sydney, September 2022

Simpson, J. (2022). High resolution UAV-based mapping of seagrass beds. 'Thinking Space' seminar series, School of Geosciences, University of Sydney, November 2022

Simpson, J. (2023). Remote sensing and geospatial science for management of coastal areas. Invited presentation at East Sea Institute, Diplomatic Academy of Vietnam, Hanoi, Vietnam, July 2023

Simpson, J. (2025). High-resolution Seagrass Monitoring Using UAV-deployed Multispectral Sensors. *Australian Marine Science Association conference 2025*, Melbourne, Australia, July 2025

Awards and grants

CUAVA scholarship

Australian Postgraduate Research internship 2021-2022

2021 Esri Young Scholar Australia. Awarded for "The University of Sydney COVID-19 Community Profiles Mapping Tool"

Appendix C. List of papers reviewed (Chapters 2 & 3)

Table C1. List of papers analysed in systematic and synthetic literature reviews (Chapters 2 and 3).

Authors	Title	Journal	Year
Ackleson and Klemas	Remote Sensing of Submerged Aquatic Vegetation in Lower Chesapeake Bay: A comparison of Landsat MSS to TM imagery	Remote Sensing Of Environment	1987
Armstrong	Remote sensing of submerged vegetation canopies for biomass estimation	International Journal Of Remote Sensing	1993
Michalek et al.	Multispectral change vector analysis for monitoring coastal marine environments	Photogrammetric Engineering And Remote Sensing	1993
Ferguson and Korfmacher	Remote sensing and GIS analysis of seagrass meadows in North Carolina, USA	Aquatic Botany	1997
Mumby et al.	Coral reef habitat mapping: how much detail can remote sensing provide?	Marine Biology	1997
Mumby et al.	Measurement of seagrass standing crop using satellite and digital airborne remote sensing	Marine Ecology Progress Series	1997
Ward et al.	Distribution and stability of eelgrass beds at Izembek Lagoon, Alaska	Aquatic Botany	1997
Macleod and Congalton	A quantitative comparison of change-detection algorithms for monitoring eelgrass from remotely sensed data	Photogrammetric Engineering And Remote Sensing	1998
Dahbouh-Guebas et al.	Remote sensing and zonation of seagrasses and algae along the Kenyan coast	Hydrobiologia	1999
Stumpf et al	Variations in water clarity and bottom albedo in Florida Bay from 1985 to 1997	Estuaries	1999
Maeder et al	Classifying and mapping general coral reef structure using IKONOS data	Photogrammetric Engineering And Remote Sensing	2002
Mumby and Edwards	Mapping marine environments with IKONOS imagery: enhanced spatial resolution can deliver greater thematic accuracy	Remote Sensing Of Environment	2002
Bouvet et al	Evaluation of large-scale unsupervised classification of New Caledonia reef ecosystems using Landsat 7 ETM+ imagery	Oceanologica Acta	2003
Call et al	Coral reef habitat discrimination using multivariate spectral analysis and satellite remote sensing	International Journal Of Remote Sensing	2003
Ward et al	Long term change in eelgrass distribution at Bahia San Quintin using satellite imagery	Estuaries	2003
Dekker et al	Retrospective seagrass change detection in a shallow coastal tidal Australia lake	Remote Sensing Of Environment	2005
Mishra et al	High-resolution ocean color remote sensing of benthic habitats: A case study at the Roatan Island, Honduras	Ieee Transactions On Geoscience And Remote Sensing	2005
Pasqualini et al	Use of SPOT 5 for mapping seagrasses: an application to Posidonia oceanica	Remote Sensing Of Environment	2005
Phinn et al	Mapping water quality and substrate cover in optically complex coastal and reef waters: an integrated approach	Marine Pollution Bulletin	2005
Schweizer et al	Remote sensing characterization of benthic habitats and submerged vegetation biomass in Los Roques Archipelago National Park, Venezuela	International Journal Of Remote Sensing	2005
Fornes et al	Mapping Posidonia oceanica from IKONOS	Isprs Journal Of Photogrammetry And Remote Sensing	2006
Gullstrom et al	Assessment of changes in the seagrass-dominated submerged vegetation of tropical Chwaka Bay Zanzibar using satellite remote sensing	Estuarine Coastal And Shelf Science	2006

Mishra et al	Benthic habitat mapping in tropical marine environments using QuickBird multispectral data	Photogrammetric Engineering And Remote Sensing	2006
Roelfsema et al	Monitoring toxic cyanobacteria L. majuscula in Moreton Bay, Australia, by integrating satellite image data and field mapping	Harmful Algae	2006
Shapiro and Rohmann	Mapping changes in submerged aquatic vegetation using Landsat imagery and benthic habitat data	Bulletin Of Marine Science	2006
Wang et al	Terrestrial and submerged aquatic vegetation mapping in Fire Island National Seashore using high spatial resolution remote sensing data	Marine Geodesy	2007
Houk and van Woesik	Dynamics of shallow-water assemblages in the Saipan Lagoon	Marine Ecology Progress Series	2008
Phinn et al	Mapping seagrass species, cover and biomass in shallow waters: an assessment of satellite multi-spectral and airborne hyperspectral imaging systems in Moreton Bay	Remote Sensing Of Environment	2008
Sagawa et al	Mapping seagrass beds using IKONOS satellite image and side scan sonar measurements: a Japanese case study	International Journal Of Remote Sensing	2008
Tripathi et al	Mapping changes in the benthic community of the marine environment of Phu Quoc Island, Vietnam	International Journal Of Geoinformatics	2008
Vela et al	Use of SPOT 5 and IKONOS imagery for mapping biocenoses in a Tunisian Coastal Lagoon	Estuarine Coastal And Shelf Science	2008
Wabnitz et al	Regional-scale seagrass habitat mapping in the Wider Caribbean Region using Landsat sensors	Remote Sensing Of Environment	2008
Howari et al	Field and remote-sensing assessment of mangrove forests and seagrass beds in the Northwestern part of the UAE	Journal Of Coastal Research	2009
Moses et al	Regional estimates of reef carbonate dynamics and productivity using Landsat 7 ETM+, and potential impacts from ocean acidification	Marine Ecology Progress Series	2009
Roelfsema et al	An integrated field and remote sensing approach for mapping seagrass cover, Moreton Bay, Australia	Journal Of Spatial Science	2009
Urbanski et al	Object-oriented classification of QuickBird data for mapping seagrass spatial structure	Oceanological And Hydrobiological Studies	2009
Yang and Yang	Detection of seagrass distribution changes from 1991 to 2007 in Xincun Bay, Hainan with satellite remote sensing	Sensors	2009
Amran	Estimation of seagrass coverage by depth invariant indices on QuickBird imagery	Biotropia	2010
Barille et al	Increase in seagrass distribution and Bourgneuf Bay (France) detected by spatial remote sensing	Aquatic Botany	2010
Dierssen et al	Benthic ecolog from space: optics and NPP in seagrass and benthic algae across the Great Bahama Bank	Marine Ecology Progress Series	2010
Knudby et al	Simple and effective monitoring of historic changes I nearshore environments using the free archive of Landsat imagery	International Journal Of Applied Earth Observation And Geoinformation	2010
Roelfsema and Phinn	Integrating field data with high spatial resolution multispectral satellite imagery for calibration and validation of coral reef benthic community maps	Journal Of Applied Remote Sensing	2010
Sagawa et al	Using bottom surface reflectance to map coastal marine areas	International Journal Of Remote Sensing	2010
Sridhar et al	Assessment of coastal bio-resources of the Palk Bay, India, using IRS-LISS-III data	Journal Of The Indian Society Of Remote Sensing	2010
Knudby and Nordlund	Remote sensing of seagrass in a patchy multi-species environment	International Journal Of Remote Sensing	2011

Lyons et al	Integrating QuickBird multispectral satellite and field data	Remote Sensing	2011
Madden et al	Modern fringing reef carbonates from equatorial SE Asia: An integrated environmental, sediment and satellite characterisation study	Marie Geology	2011
Yang and Huang	Impact of typhoons Tianying and Dawei on seagrass distribution in Xincun Bay	Acta Oceanologica Sinica	2011
Baumstark et al	Alternative spatially enhanced integrative techniques for mapping seagrass in Florida's marine ecosystem	International Journal Of Remote Sensing	2012
Dadhich and Naduoka	Analysis of terrestrial discharge from agricultural watersheds and its impact on nearshore and offshore reefs in Fiji	Journal Of Coastal Research	2012
Hamylton et al	Observations of dugongs at Aldabra Atoll, western Indian ocean	International Journal Of Geographical Information Science	2012
Li et al	A systematic approach toward detection of seagrass patches from hyperspectral images	Marine Geodesy	2012
Lyons et al	Long term land cover and seagrass mapping using Landsat and object-based image analysis from 1972 to 2010	Isprs Journal Of Photogrammetry And Remote Sensing	2012
Meyer and Pu	Seagrass resources assessment using remote sensing methods in St Joseph Sound and Clearwater Harbor, Florida, USA	Environmental Monitoring And Assessment	2012
Nobi and Thangaradjou	Evaluation of the spatial changes in seagrass cover in the lagoons of Lakshadweep Islands, India, using IRS LISS III satellite images	Journal Of The Indian Society Of Remote Sensing	2012
Nobi et al	Estimation of the aerial cover of seagrasses of Lakshadweep Islands (India) using remote sensing satellite (IRS P6 LISS IV)	Geocarto International	2012
Parangit and Nadaoka	Simultaneous estimation of benthic fractional cover and shallow water bathymetry in coral reef areas from high-resolution satellite images	International Journal Of Remote Sensing	2012
Pu et al	Mapping and assessing seagrass along the western coast of Florida using Landsat TM and EO-1 ALI/Hyperion imagery	Estuarine Coastal And Shelf Science	2012
Borfecchia et al	Posidonia oceanica genetic and biometry mapping through high-resolution satellite spectral vegetation indices and sea-truth calibration	International Journal Of Remote Sensing	2013
Lyons et al	Towards understanding temporal and spatial dynamics of seagrass landscapes using time series remote sensing	Estuarine Coastal And Shelf Science	2013
Nobi et al	Integrating Indian remote sensing multispectral satellite and field data to estimate seagrass cover change in the Andaman and Nicobar Islands, India	Marine Geology	2013
O'Neill and Costa	Mapping eelgrass in the Gulf Islands National Park Reserve of Canada using high spatial resolution satellite and airborne imagery	Remote Sensing Of Environment	2013
Pu and Bell	A protocol for improving mapping and assessing of seagrass abundance along the West Central Coast of Florida using Landsat TM and EO-1 ALI/Hyperion images	Isprs Journal Of Photogrammetry And Remote Sensing	2013
Rioja-Nieto et al	Benthic habitat beta-diversity modeling and landscape metrics for the selection of priority conservation areas using a systematic approach	Ocean & Coastal Management	2013
Roelfsema et al	Challenges of remote sensing for quantifying changes in large complex seagrass environments	Estuarine Coastal And Shelf Science	2013
Torres-Pulliza et al	Ecoregional scale seagrass mapping: A tool to support resilient MPA network design in the Coral Triangle	Ocean & Coastal Management	2013
Wicaksono and Hafizt	Mapping seagrass from space: Addressing the complexity of seagrass LAI mapping	European Journal Of Remote Sensing	2013

Cho et al	Evaluating Hyperspectral Imager for the Coastal Ocean (HICO) data for seagrass mapping in Indian River Lagoon, FL	Giscience & Remote Sensing	2014
El-Askary et al	Change detection of coral reef habitat using Landsat-5 TM, Landsat 7 ETM+, and Landsat 8 OLI data in the Red Sea	International Journal Of Remote Sensing	2014
Hogrefe et al	Establishing a baseline for regional scale monitoring of eelgrass (Z. marina) habitat on the lower Alaska Peninsula	Remote Sensing	2014
Mustapha et al	Coral reef and associated habitat mapping using ALOS satellite imagery	Sains Malaysiana	2014
Nguyen et al	Coastal and marine ecological changes and fish cage culture development in Phu Quoc, Vietnam (2001-2011)	Geocarto International	2014
Pu et al	Mapping and assessing seagrass bed changes in Central Florida's west coast using multitemporal Landsat TM imagery	Estuarine Coastal And Shelf Science	2014
Reshitnyk et al	Evaluation of WorldView-2 and acoustic remote sensing for mapping benthic habitats in temperate coastal waters	Remote Sensing Of Environment	2014
Roelfsema et al	Multi-temporal mapping of seagrass cover, species and biomass: A semi-automated object based image analysis approach	Remote Sensing Of Environment	2014
Barrell et al	Evaluating the complementarity of acoustic and satellite remote sensing for seagrass landscape mapping	International Journal Of Remote Sensing	2015
Blakey et al	Supervised classification of benthic reflectance in shallow subtropical waters using a generalised pixel-based classifier across a time series	Remote Sensing	2015
Eugenio et al	High resolution maps of bathymetry and benthic habitats in shallow water environments using multispectral remote sensing imagery	Ieee Transactions On Geoscience And Remote Sensing	2015
Hossain et al	Application of Landsat images to seagrass areal cover change analysis for Lawas, Terengganu and Kelantan of Malaysia	Continental Shelf Research	2015
Jung et al	A multi-sensor approach for detecting the different land covers of tidal flats in the German Wadden Sea - A case study at Norderney	Remote Sensing Of Environment	2015
Kim et al	Observation of typhoon-induced seagrass die-off using remote sensing	Estuarine Coastal And Shelf Science	2015
Lyons et al	Rapid monitoring of seagrass biomass using a simple linear modelling approach in the field and from space	Marine Ecology Progress Series	2015
Sawayama et al	Introduction of geospatial perspective to the ecology of fish-habitat relationships in Indonesian Coral Reefs: A remote sensing approach	Ocean Science Journal	2015
Baumstark et al	Mapping seagrass and colonised hard bottom in Springs Coast, Florida using WorldView-2 satellite imagery	Estuarine Coastal And Shelf Science	2016
Chen et al	Multi-temporal change detection of seagrass beds using integrated Landsat TM/ETM+/OLI imageries in Cam Ranh Bay, Vietnam	Ecological Informatics	2016
Giardino et al	Mapping submerged habitats and mangroves of Lampi Island Marine Park (Myanmar) from in situ and satellite observations	Remote Sensing	2016
Hachini et al	The mapping of Posidonia oceanica (L.) Delile barrier reef meadow in the southeastern Gulf of Tunis (Tunisia)	Journal Of African Earth Sciences	2016
Hoang et al	Identification and mapping of marine submerged aquatic vegetation in shallow coastal waters with WorldView satellite data	Journal Of Coastal Research	2016
Hossain et al	Marine and human habitat mapping for the Coral Triangle Initiative region of Sabah using Landsat and Google Earth imagery	Marine Policy	2016
Kakuta et al	Seaweed and seagrass mapping in Thailand measured using Landsat 8 optical and textural image properties	Journal Of Marine Science And Technology-Taiwan	2016
Koedsin et al	An integrated field and remote sensing method for mapping seagrass species cover and biomass in Southern Thailand	Remote Sensing	2016

Misbari and Hashim	Change detection of submerged seagrass biomass in shallow coastal water	Remote Sensing	2016
Muller et al	Remotely sensing the German Wadden Sea – a new approach to address national and international environmental legislation	Environmental Monitoring And Assessment	2016
Palafox-Juarez and Liceaga-Correa	Spatial diversity of a coastal seascape: Characterization, analysis and application or conservation	Ocean & Coastal Management	2016
Tsujimoto et al	Damage to seagrass and seaweed beds in Matsushima Bay, Japan ,cuased by the huge tsunami of the Great East Japan earthquake of 11 March 2011	International Journal Of Remote Sensing	2016
Wicaksono	Improve the accuracy of multispectral-based benthic habitat mapping using image rotations: the application of Principle Component Analysis and Independent Component Analysis	European Journal Of Remote Sensing	2016
Amran	Mapping seagrass condition using Google Earth imagery	Journal Of Engineering Science And Technology Review	2017
Asner et al	Coral reef atoll assessment in the South China Sea using Planet Dove satellites	Remote Sensing In Ecology And Conservation	2017
Calleja et al	Long-term analysis of Zostera noltei: A retrospective approach for understanding seagrass dynamics	Marine Environmental Research	2017
da Silva et al	Application of ALOS AVNIR-2 for the detection of seaweed and seagrass beds on the northeast of Brazil	International Journal Of Remote Sensing	2017
Elso et al	Genetic description and remote sensing techniques as management tools for Zostera noltii seagrass populations along the Atlantic Moroccan coast	Journal Of Coastal Research	2017
Fauzan et al	Assessing the capability of Sentinel-2A data for mapping seagrass percent cover in Jerowaru, East Lombok	Indonesian Journal Of Geography	2017
Pu and Bell	Mapping seagrass coverage and spatial patterns with high spatial resolution IKONOS imagery	International Journal Of Applied Earth Observation And Geoinformation	2017
Ampou et al	Change detection of Bunaken Island coral reefs using 15 years of very high resolution satellite images: A kaleidoscope of habitat trajectories	Marine Pollution Bulletin	2018
Bramante et al	Decadal biomass and area changes in a multi-species meadow in Singapore: application of multi-resolution satellite imagery	Botanica Marina	2018
Chayhard et al	Multi-temporal mapping of seagrass distribution by using integrated remote sensing data in Kung Kraben Bay (KKB), Chanthaburi Province, Thailand	International Journal Of Agricultural Technology	2018
Geevarghase et al	A comprehensive geospatial assessment of seagrass distribution in India	Ocean & Coastal Management	2018
Harcourt et al	The thin(ning) green line? Investigating changes in Kenya's seagrass coverage	Biology Letters	2018
Helmi et al	Benthic diversity mapping and analysis based on remote sensing and seascape ecology	International Journal Of Civil Engineering And Technology	2018
Kovacs et al	Seagrass habitat mapping: how do Landsat 8 OLI, Sentinel-2, ZY-3A and WorldView-3 perform?	Remote Sensing Letters	2018
Marcello et al	Seabed mapping in coastal shallow waters using high resolution multispectral and hyperspectral imagery	Remote Sensing	2018
McIntyre et al	Mapping shallow nearshore benthic features in a Caribbean marine protected area: assessing the efficacy of using different data types (hydroacoustic versus satellite images) and classification techniques	International Journal Of Remote Sensing	2018

Mohamed et al	Assessment of machine learning algorithms for automatic benthic cover monitoring and mapping using towed underwater video camera and high resolution satellite images	Remote Sensing	2018
Poursanidis et al	Mapping coastal marine habitats and delineating the deep limits of the Neptune's seagrass meadows using very high resolution Earth observation data	International Journal Of Remote Sensing	2018
Roelfsema et al	Use of a semi-automated object based analysis to map benthic composition, Heron Reef, Southern Great Barrier Reef	Remote Sensing Letters	2018
Toupozelis et al	Seagrass mapping in Greek territorial waters using Landsat-8 satellite images	International Journal Of Applied Earth Observation And Geoinformation	2018
Traganos and Reinartz	Machine learning based retrieval of benthic reflectance and Posidonia oceanica seagrass extent using a semi-analytical inversion of Sentinel-2 satellite data	International Journal Of Remote Sensing	2018
Traganos and Reinartz	Mapping Mediterranean seagrass with Sentinel-2 imagery	Marine Pollution Bulletin	2018
Traganos and Reinartz	Interannual change detection of Mediterranean seagrasses using RapidEye image time series	Frontiers In Plant Science	2018
Traganos et al	Towards global scale seagrass mapping and monitoring using Sentinel-2 on Google Earth Engine: The case study of the Aegean and Ionian Seas	Remote Sensing	2018
Wicaksono and Lazuardi	Assessment of PlanetScope images for benthic habitat and seagrass species mapping in a complex optically shallow water environment	International Journal Of Remote Sensing	2018
Zharikov et al	Application of Landsat data for mapping higher aquatic vegetation of the Far East Marine Reserve	Oceanology	2018
Borfecchia et al	Landsat 8 OLI satellite data for mapping of the Posidonia oceanica and benthic habitats of coastal ecosystems	International Journal Of Remote Sensing	2019
Cozza et al	Biomonitoring of Posidonia oceanica beds by a multiscale approach	Aquatic Botany	2019
Forsey et al	Refinements in Eelgrass Mapping at Tabusintac Bay (New Brunswick, Canada): A comparison between random forest and the maximum likelihood classifier	Canadian Journal Of Remote Sensing	2019
Hang et al	Spatial distribution of submerged aquatic vegetation in An Chan coastal waters, Phu Yen province using the PlanetScope satellite image	Vietnam Journal Of Earth Sciences	2019
Leon-Perez et al	Characterisation and distribution of seagrass habitats in a Caribbean Nature Reserve using high-resolution satellite imagery and field sampling	Journal Of Coastal Research	2019
Li et al	Object-based mapping of coral reef habitats using Planet Dove satellites	Remote Sensing	2019
Mclaren et al	Using the random forest algorithm to integrate hydroacoustic data with satellite images to improve the mapping of shallow nearshore benthic features in a marine protected area in Jamaica	Giscience & Remote Sensing	2019
Poursanidis et al	On the use of Sentinel-2 for coastal habitat mapping and satellite derived bathymetry estimation using downscaled coastal aerosol band	International Journal Of Applied Earth Observation And Geoinformation	2019
Su and Huang	Seagrass resource assessment using WorldView-2 imagery in Redfish Bay, Texas	Journal Of Marine Science And Engineering	2019
Wicaksono et al	Benthic habitat mapping model and cross validation using machine learning classification algorithms	Remote Sensing	2019
Wicaksono et al	Analysis of reflectance spectra of tropical seagrass species and their value for mapping using multispectral satellite images	International Journal Of Remote Sensing	2019

Wilson et al	Eelgrass (Zostera marina) and benthic habitat mapping in Atlantic Canada using high resolution SPOT 6/7 satellite imagery	Estuarine Coastal And Shelf Science	2019
Abo Elenin et al	An integrated field survey and remote sensing approach for marine habitat mapping along Hurghada Coast, Red Sea, Egypt	Egyptian Journal Of Aquatic Biology And Fisheries	2020
Ahmed et al	Monitoring benthic habitats using Lyzenga model features from Landsat multi-temporal images in Google Earth Engine	Modeling Earth Systems And Environment	2020
Bakirman and Gumusay	Assessment of machine learning methods for seagrass classification in the Mediterranean	Baltic Journal Of Modern Computing	2020
Bayyana et al	Detection and mapping of seagrass meadows at Ritchie's archipelago using Sentinel-2A satellite imagery	Current Science	2020
Butler et al	A high-resolution remotely sensed benthic habitat map of the Qatari coastal zone	Marine Pollution Bulletin	2020
Cajica et al	Seascape metrics, spatio-temporal change, and intensity of use for the spatial conservation prioritization of a Caribbean marine protected area	Ocean & Coastal Management	2020
Chayhard et al	Multi temporal mapping of seagrass distribution by using integrated remote sensing data in Kung Kraben Bay, Chanthaburi province, Thailand	International Journal Of Agricultural Technology	2020
Coffer et al	Performance across WorldView-2 and RapidEye for reproducible seagrass mapping	Remote Sensing Of Environment	2020
Ha et al	A comparative assessment of ensemble-based machine learning and maximum likelihood methods for mapping seagrass using Sentinel-2 imagery in Tauranga Harbor, New Zealand	Remote Sensing	2020
Kohlus et al	Mapping seagrass (Zostera) by remote sensing in the Schleswig-Holstein Wadden Sea	Estuarine Coastal And Shelf Science	2020
Leon-Perez et al	Seagrass cover expansion off Caja de Muertos Island, Puerto Rico, as determined by long-term analysis fo historical aerial and satellite images (1950-2014)	Ecological Indicators	2020
Mateos-Molina et al	Applying an integrated approach to coastal marine habitat mapping in the north-western United Arab Emirates	Marine Environmental Research	2020
Mohamed et al	Semiautomated mapping of benthic habitats and seagrass species using a convolutional neural network framework in shallow water environments	Remote Sensing	2020
Ni et al	Mapping submerged aquatic vegetation along the central Vietnamese coast using multi-source remote sensing	Isprs International Journal Of Geo-Information	2020
Perez et al	Quantifying seagrass distribution in Coastal Water with Deep Learning Models	Remote Sensing	2020
Poursanidis et al	Cloud-native seascape mapping of Mozambique's Quirimbas National Park with Sentinel-2	Remote Sensing In Ecology And Conservation	2020
Rende et al	Ultra-high resolution mapping of Posidonia oceanica (L.) Delile meadows through acoustic, optical data and object-based image classification	Journal Of Marine Science And Engineering	2020
Santos et al	Implications of macroalgae blooms to the spatial structure of seagrass seascapes: the case of Anadyomene spp. (Chlorophyta) bloom in Biscayne Bay, Florida	Marine Pollution Bulletin	2020
Sievers et al	Non-reef habitats in a tropical seascape affect density and biomass of fishes on coastal reefs	Ecology And Evolution	2020
Strydom et al	Too hot to handle: Unprecedented seagrass depth driven by marine heatwave in a World Heritage Area	Global Change Biology	2020
Tin et al	Decadal dynamics and challenges for seagrass bed management in Cu Lao Cham Marine protected area, Central Vietnam	Environment Development And Sustainability	2020

Upadhyay et al	Random forest based classification of seagrass habitat	Journal Of Information & Optimization Sciences	2020
Vo et al	Satellite image analysis reveals changes in seagrass beds at Van Phong Bay, Vietnam during the last 30 years	Aquatic Living Resources	2020
Wicaksono et al	Assessment of Sentinel-2A multispectral image for benthic habitat composition mapping	Iet Image Processing	2020
Wilson et al	Branching algorithm to identify bottom habitat in the optically complex coastal waters of Atlantic Canada using Sentinel-2 satellite imagery	Frontiers In Environmental Science	2020
Yucel-Gier et al	Evaluation of Posidonia oceanica map generated by Sentinel-2 Image: Gulbahce Bay Test Site	Turkish Journal Of Fisheries And Aquatic Sciences	2020
Zoffoli et al	Sentinel-2 remote sensing of Zostera noltei-dominated intertidal seagrass meadows	Remote Sensing Of Environment	2020
Benmokhtar et al	Mapping and quantification of the Dwarf Eelgrass Zostera noltei using a random forest algorithm on a SPOT 7 satellite image	Isprs International Journal Of Geo-Information	2021
Borfecchia et al	Satellite multi/hyper spectral HR sensors for mapping Posidonia oceanica in the South Mediterranean Islands	Sustainability	2021
Butler et al	A benthic habitat sensitivity analysis of Qatar's coastal zone	Marine Pollution Bulletin	2021
Cuevas et al	Spatial configuration of seagrass community attributes in a stressed coastal lagoon, southeastern Gulf of Mexico	Regional Studies In Marine Science	2021
Da Silveira et al	Coral reef mapping with remote sensing and machine learning: A nurture and nature analysis in marine protected areas	Remote Sensing	2021
Fauzan et al	Characterizing Derawan seagrass cover change with time-series Sentinel-2 images	Regional Studies In Marine Science	2021
Fernandes et al	Landsat historical records reveal large-scale dynamics and enduring recovery of seagrasses in an impacted seascape	Science Of The Total Environment	2021
Ha et al	The use of radar and optical satellite imagery combined with advanced machine learning and metaheuristic optimization techniques to detect and quantify above ground biomass of intertidal seagrass in a New Zealand estuary	International Journal Of Remote Sensing	2021
Ha et al	Detecting multi-decadal changes in seagrass cover in Tauranga Harbour, New Zealand, using Landsat imagery and boosting ensemble classification techniques	Isprs International Journal Of Geo-Information	2021
Hafizt et al	Change Detection of Benthic Habitat Communities using Landsat Imageries in Wakatobi Islands from 1990 to 2017	Indonesian Journal Of Geography	2021
Hartoko et al	Seagrass cholorophyll-a, biomass and carbon algorithms based on the field and sentinel-2a satellite data at Karimunjawa Island, Indonesia	Science And Technology Indonesia	2021
Hashim et al	Appraisal of seagrass aboveground biomass changes using satellite data within the tropical coastline of Peninsular Malaysia	Geocarto International	2021
Hedley et al	Seagrass Depth distribution mirrors coastal development in the Mexican Caribbean – An automated analysis of 800 satellite images	Frontiers In Marine Science	2021
Huber et al	Novel approach to large-scale monitoring of submerged aquatic vegetation: A nationwide example from Sweden	Integrated Environmental Assessment And Management	2021
Kartikasari et al	Representative benthic habitat mapping on Lovina coral reefs in northern Bali, Indonesia	Biodiversitas	2021
Krause et al	Emerging sensor platforms allow for seagrass extent mapping in a turbid estuary and from the meadow to ecosystem scale	Remote Sensing	2021
Kuhwald et al	How can Sentinel-2 contribute to seagrass mapping in shallow, turbid Baltic Sea waters?	Remote Sensing In Ecology And Conservation	2021

Leblanc et al	Using Landsat time series to monitor and inform seagrass dynamics: A case study in the Tabusintac Estuary, New Brunswick, Canada	Canadian Journal Of Remote Sensing	2021
Maruta et al	Monitoring oyster culture rafts and seagrass meadows in Nagatsura-ura Lagoon, Sanriku Coast, Japan before and after the 2011 tsunami by remote sensing	Peerj	2021
Nguyen et al	Update of seagrass cover and species diversity in Southern Vietnam using remote sensing data and molecular analyses	Regional Studies In Marine Science	2021
Pottier et al	Mapping coast marine ecosystems of the National park of Banc d'Arguin in Mauritania using Sentinel-2 imagery	International Journal Of Applied Earth Observation And Geoinformation	2021
Sabilah et al	Comparison of seagrass cover classification based on SVM and fuzzy algorithms using multi-scale imagery in Kodingareng Lompo Island	Jurnal Ilmu Dan Teknologi Kelautan Tropis	2021
Schill et al	Regional High-Resolution Benthic Habitat Data from Planet Dove Imagery for conservation decision-making and marine planning	Remote Sensing	2021
Singh et al	Benthic resource baseline mapping of Cakaunisasi and Yarawa reef ecosystem in the Ba region of Fiji	Water	2021
Stankovic et al	Two decades of seagrass area change: Organic carbon sources and stock	Marine Pollution Bulletin	2021
Tu et al	Impacts of urbanization and land transitions on seagrass beds ion tropical lagoon in central Vietnam	Regional Studies In Marine Science	2021
Turissa et al	Evaluation methods of change detection of seagrass beds in the waters of Pajenekang and Gusung Selayar	Trends In Sciences	2021
Vahtmae et al	Mapping spatial distribution, percent cover and biomass of benthic vegetation in optically complex coastal waters using hyperspectral CASI and multispectral Sentinel-2 sensors	International Journal Of Applied Earth Observation And Geoinformation	2021
Wicaksono et al	Sentinel-2 images deliver possibilities for accurate and consistent multi-temporal benthic habitat maps in optically shallow water	Remote Sensing Applications: Society And Environment	2021
Zoffoli et al	Decadal increase in the ecological status of a North Atlantic intertidal seagrass meadow observed with multi-mission satellite time-series	Ecological Indicators	2021
Carpenter et al	Using UAVs to map seagrass cover from Sentinel-2 imagery	Remote Sensing	2022
Haro et al	Microphytobenthos spatio-temporal dynamics across an intertidal gradient using Random Forest classification and Sentinel-2 imagery	Science Of The Total Environment	2022
Kovacs et al	Cloud processing for simultaneous mapping of seagrass meadows in optically complex and varied water	Remote Sensing	2022
Lebrasse et al	Temporal stability of seagrass extent, leaf area, and carbon storage in St Joseph Bay, Florida: a Semi-automated remote sensing analysis	Estuaries And Coasts	2022
Mizouchi et al	Multi-band bottom index: A novel approach for coastal environmental monitoring using hyperspectral data	Remote Sensing Applications: Society And Environment	2022
Nguyen et al	Establishing distribution maps and structural analysis of seagrass communities based on high-resolution remote sensing images and field surveys: a case study at Nam Yet Island, Truong Sa Archipelago, Vietnam	Landscape And Ecological Engineering	2022
Nurdin et al	Estimation of seagrass biomass by in situ measurement and remote sensing technology on Small Islands, Indonesia	Ocean Science Journal	2022
Suryanti et al	Multi-temporal mapping and recent structures of seagrass community in Panjang Island	Aquaculture, Aquarium,	2022

		Conservation & Legislation	
Wang et al	Satellite retrieval of benthic reflectance by combining lidar and passive high-resolution imagery: Case-I water	Remote Sensing Of Environment	2022
Wicaksono et al	Multitemporal seagrass carbon assimilation and aboveground carbon stock mapping using Sentinel-2 in Labuan Bajo 2019-2020	Remote Sensing Applications: Society And Environment	2022
Wilson et al	Comparing Sentinel-2 and WorldView-3 Imagery for coastal bottom habitat mapping in Atlantic Canada	Remote Sensing	2022
Xu et al	Long-term changes in the unique and largest seagrass meadows in the Bohai Sea (China) using satellite (1974-2019) and Sonar data: Implications for conservation and restoration	Remote Sensing	2022

Appendix D. Quadrat field data (Chapter 5)

Table D1. Quadrat ground truth data used in Chapter 5. Includes field data collection data, overall quadrat number (across the entire study), quadrat number for that day, depth measured with depth gauge, and cover estimate derived from quadrat photographs.

Quadrat date	Overall quadrat number	Day quadrat number	Uncorrected depth (cm)	Cover (%)
4/12/2023	1	1	10	100
4/12/2023	2	2	5	100
4/12/2023	3	3	25	75
4/12/2023	4	4	25	85
4/12/2023	5	5	40	90
4/12/2023	6	6	40	90
4/12/2023	7	7	50	50
4/12/2023	8	8	40	80
4/12/2023	9	9	45	80
4/12/2023	10	10	30	95
4/12/2023	11	11	25	15
4/12/2023	12	12	30	75
4/12/2023	13	13	35	82
4/12/2023	14	14	25	0
4/12/2023	15	15	30	40
4/12/2023	16	16	35	95
4/12/2023	17	17	35	10
4/12/2023	18	18	30	0
4/12/2023	19	19	25	100
4/12/2023	20	20	35	75
5/12/2023	21	1	22	88
5/12/2023	22	2	22	60
5/12/2023	23	3	23	83
5/12/2023	24	4	28	70
5/12/2023	25	5	20	92
5/12/2023	26	6	25	6
5/12/2023	27	7	25	46
5/12/2023	28	8	15	51
5/12/2023	29	9	30	84
5/12/2023	30	10	20	19
5/12/2023	31	11	15	76
5/12/2023	32	12	15	58
5/12/2023	33	13	15	60
5/12/2023	34	14	28	86
5/12/2023	35	15	20	54
5/12/2023	36	16	25	8
5/12/2023	37	17	15	0
5/12/2023	38	18	10	36

5/12/2023	39	19	20	89
5/12/2023	40	20	10	96
6/12/2023	41	1	23	95
6/12/2023	42	2	15	45
6/12/2023	43	3	25	91
6/12/2023	44	4	25	100
6/12/2023	45	5	15	85
6/12/2023	46	6	15	91
6/12/2023	47	7	15	75
6/12/2023	48	8	30	89
6/12/2023	49	9	30	60
6/12/2023	50	10	15	100
6/12/2023	51	11	18	92
6/12/2023	52	12	22	100
6/12/2023	53	13	5	26
6/12/2023	54	14	15	95
6/12/2023	55	15	6	39
6/12/2023	56	16	12	78
6/12/2023	57	17	10	76
6/12/2023	58	18	20	94
6/12/2023	59	19	0	0
6/12/2023	60	20	10	93
7/12/2023	61	1	36	80
7/12/2023	62	2	40	70
7/12/2023	63	3	37	29
7/12/2023	64	4	28	86
7/12/2023	65	5	20	87
7/12/2023	66	6	22	65
7/12/2023	67	7	15	94
7/12/2023	68	8	37	100
7/12/2023	69	9	20	8
7/12/2023	70	10	22	60
7/12/2023	71	11	5	0
7/12/2023	72	12	22	94
7/12/2023	73	13	10	95
7/12/2023	74	14	37	65
7/12/2023	75	15	15	33
7/12/2023	76	16	10	50
7/12/2023	77	17	22	100
7/12/2023	78	18	12	88
7/12/2023	79	19	33	38
7/12/2023	80	20	10	89
8/12/2023	81	1	40	95
8/12/2023	82	2	40	82
8/12/2023	83	3	60	99

8/12/2023	84	4	30	100
8/12/2023	85	5	20	84
8/12/2023	86	6	20	97
8/12/2023	87	7	20	93
8/12/2023	88	8	15	65
8/12/2023	89	9	24	55
8/12/2023	90	10	40	96
8/12/2023	91	11	40	91
8/12/2023	92	12	30	78
8/12/2023	93	13	30	56
8/12/2023	94	14	30	82
8/12/2023	95	15	35	78
8/12/2023	96	16	25	97
8/12/2023	97	17	55	100
8/12/2023	98	18	25	84
8/12/2023	99	19	35	100
8/12/2023	100	20	20	0

Appendix E. Agisoft Metashape processing parameters (Chapter 5)

Accuracy: Highest

Key point limit: 40,000

Tie point limit: 10,000

Generic preselection: on

Reference preselection: on

Exclude stationary tie points: on

Camera alignment parameters: f, cx, cy, b1, b2, k1, k2, k3

Point cloud quality: Ultra high

Depth filtering: Mild

DEM source: Point cloud

Interpolation: Enabled

Orthomosaic surface: DEM

Enable hole filling: on

Refine seamlines: on

Appendix F. Uncorrected vs. corrected RENDI (Chapter 5)

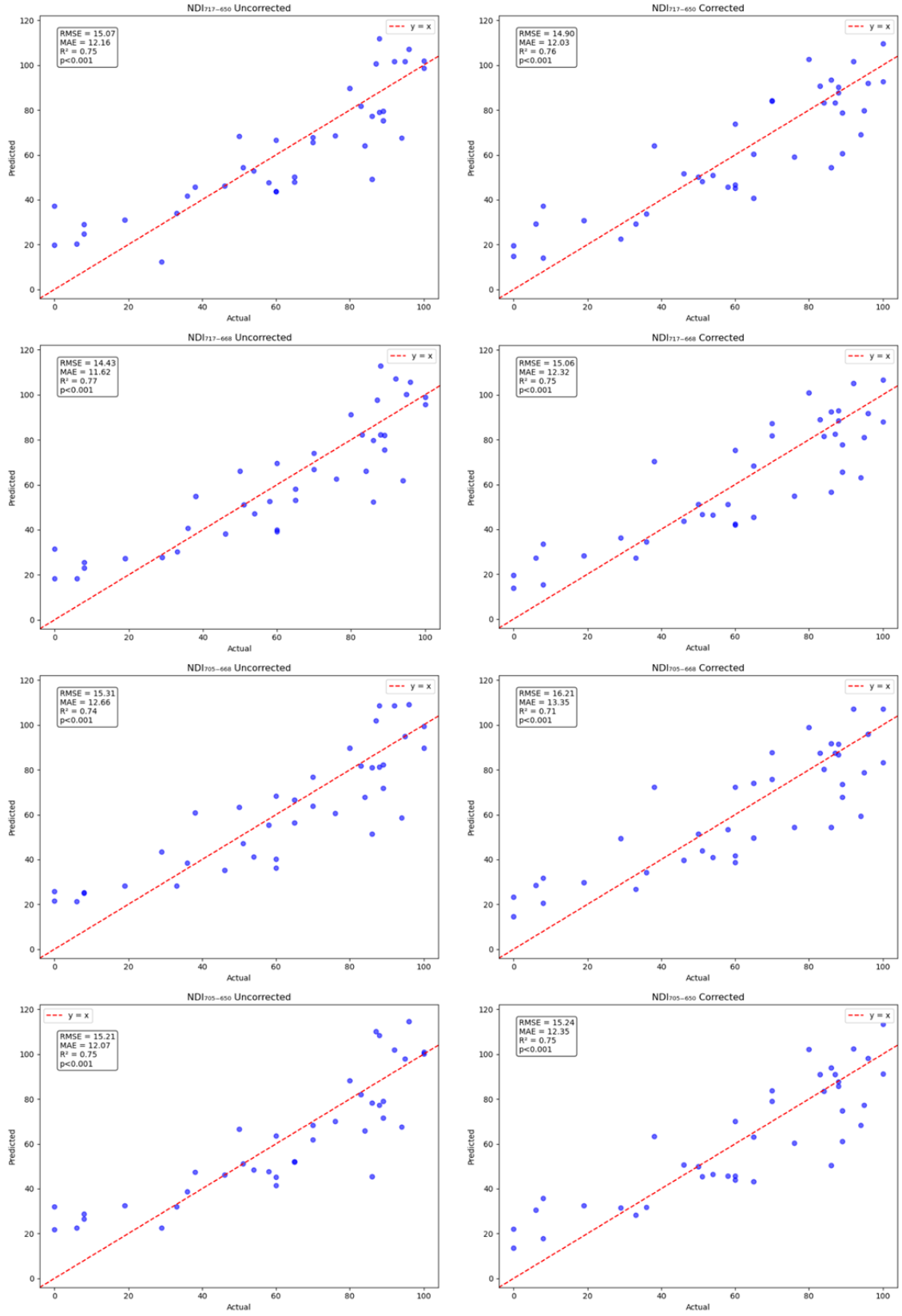

Figure F1. Red-edge normalised difference index for predicting seagrass cover with data uncorrected and corrected for water column interference. Data for St Huberts Island, 5/12/23.

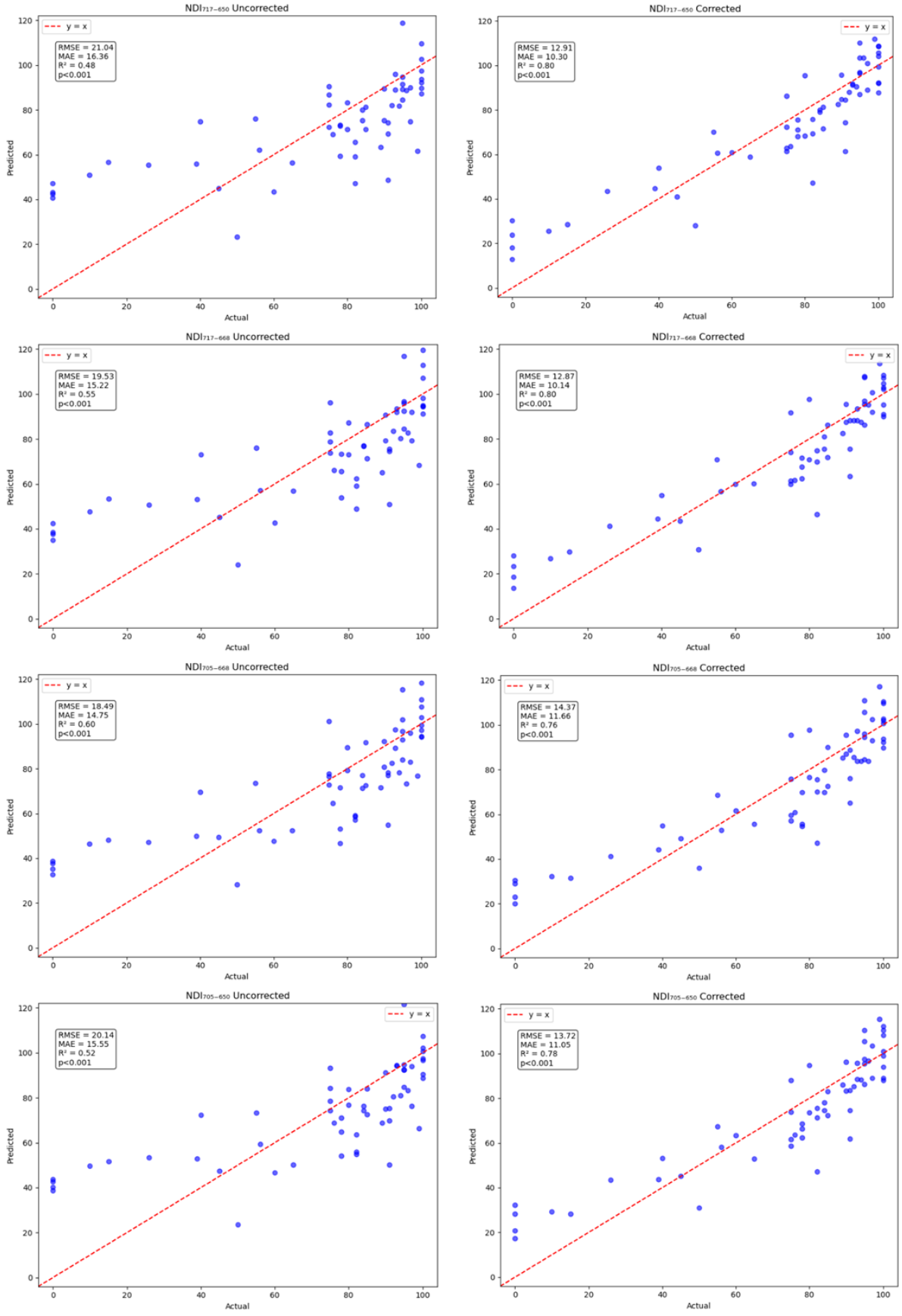

Figure F2. Red-edge normalised difference index for predicting seagrass cover with data uncorrected and corrected for water column interference. Data for Empire Bay, 6/12/23.

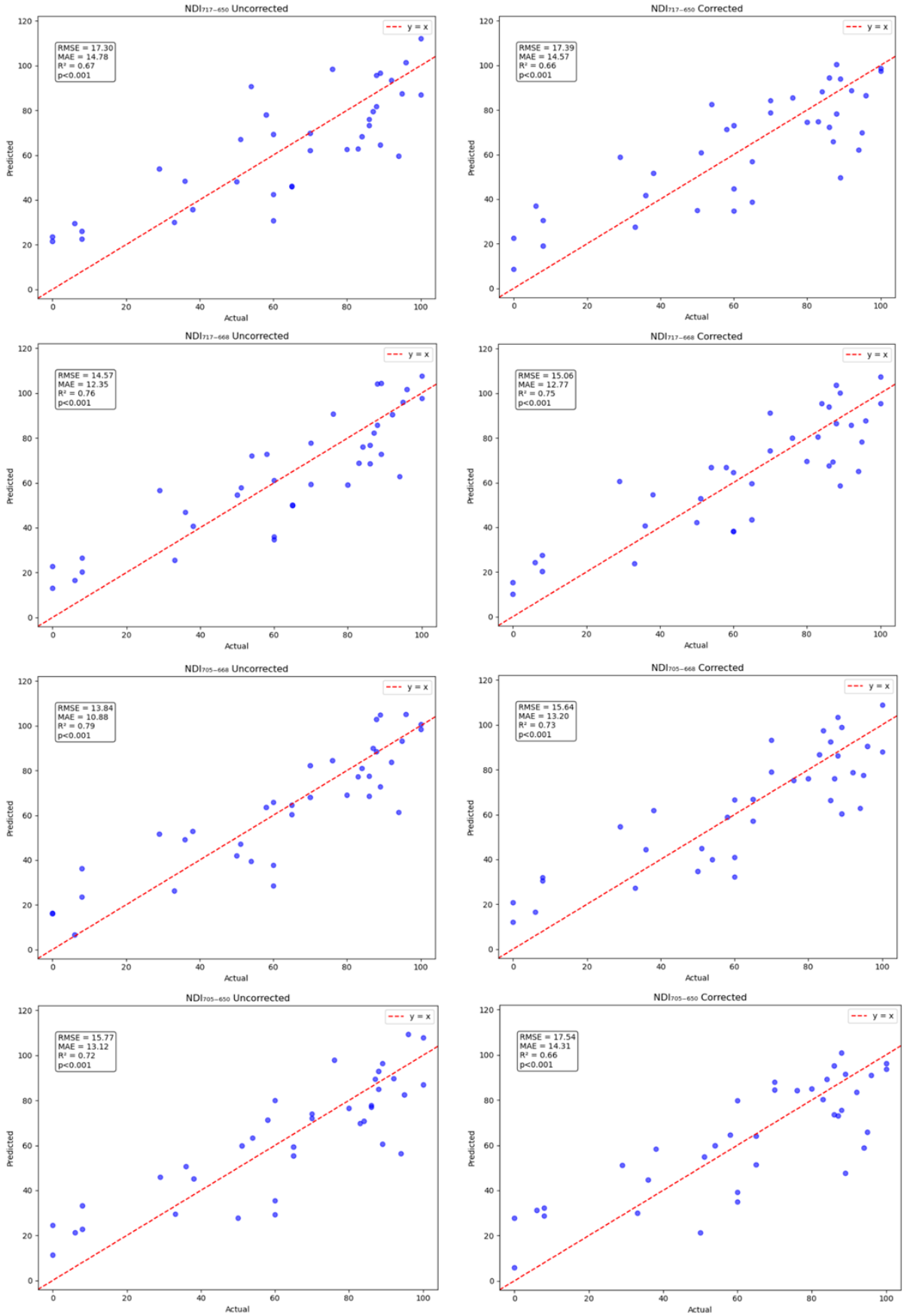

Figure F3. Red-edge normalised difference index for predicting seagrass cover with data uncorrected and corrected for water column interference. Data for St Huberts Island, 7/12/23.

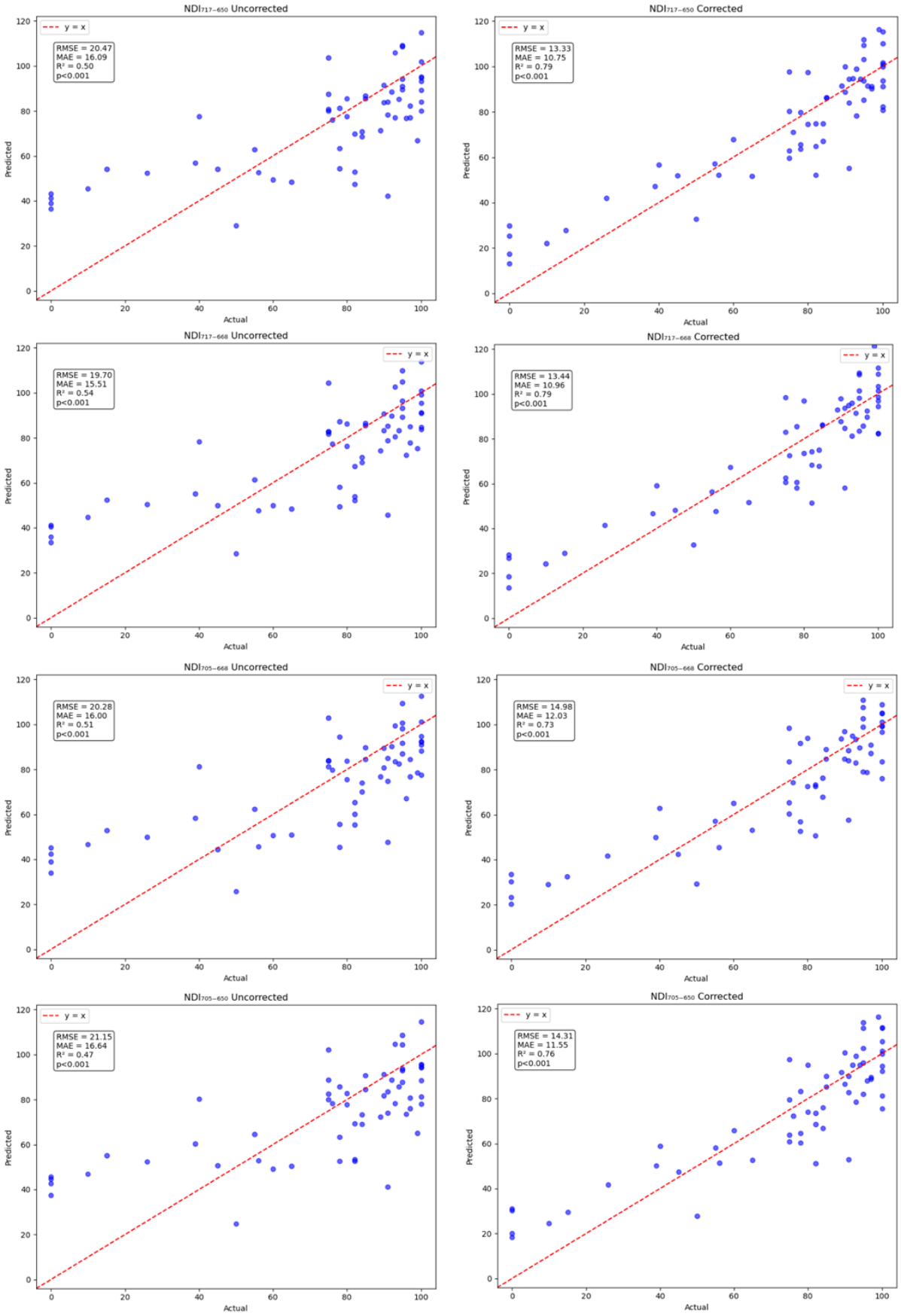

Figure F4. Red-edge normalised difference index for predicting seagrass cover with data uncorrected and corrected for water column interference. Data for Empire Bay, 8/12/23.

Appendix G. Turbidity threshold testing (Chapter 6)

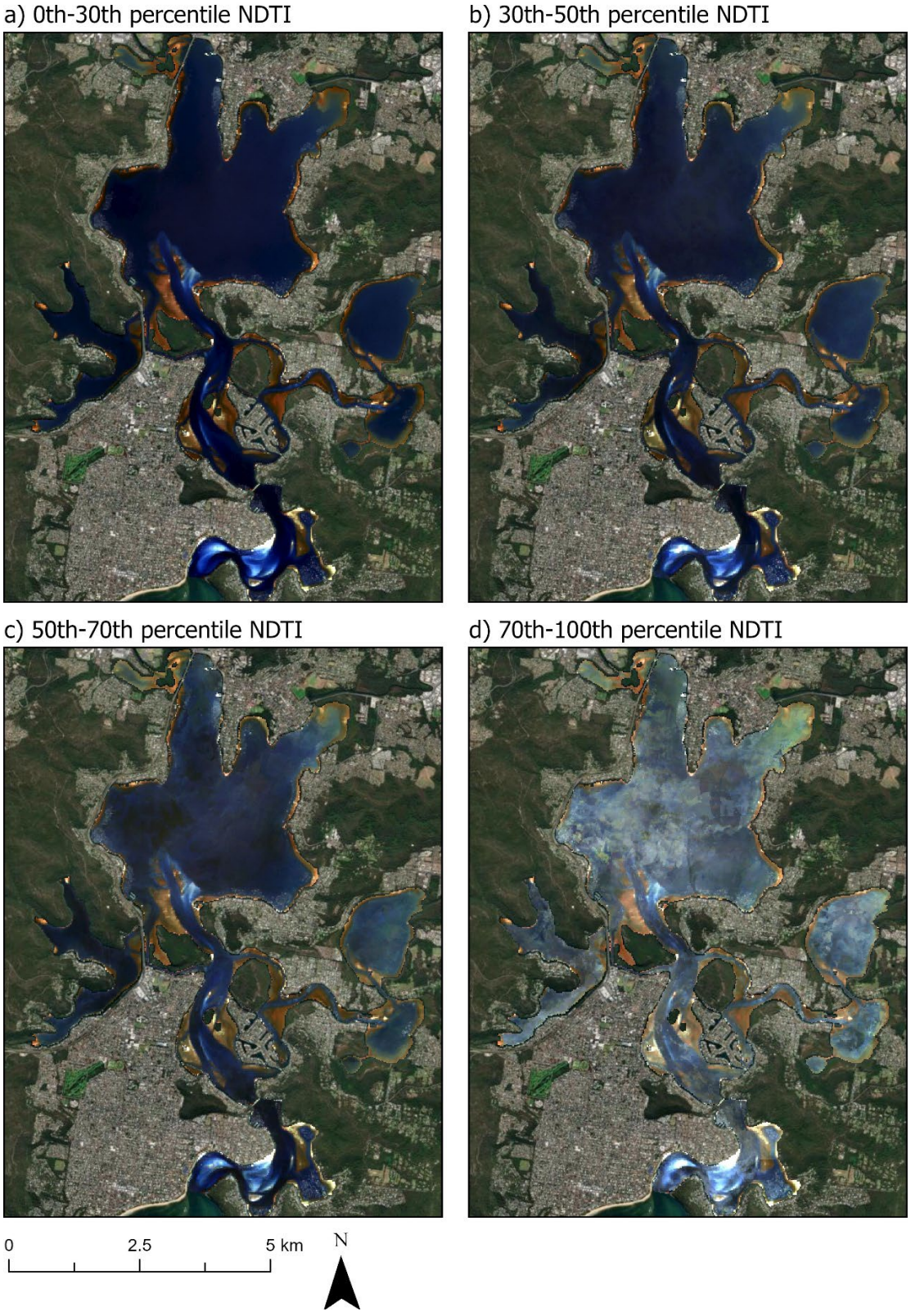

Figure G1. Median images of NDTI ranges for Brisbane Water, in red-edge false colour (RGB = RE, red, green). a) 0^{th}-30^{th} percentile NDTI, b) 30^{th}-50^{th} percentile NDTI, c) 50^{th}-70^{th} percentile NDTI, d) 70^{th}-100^{th} percentile NDTI

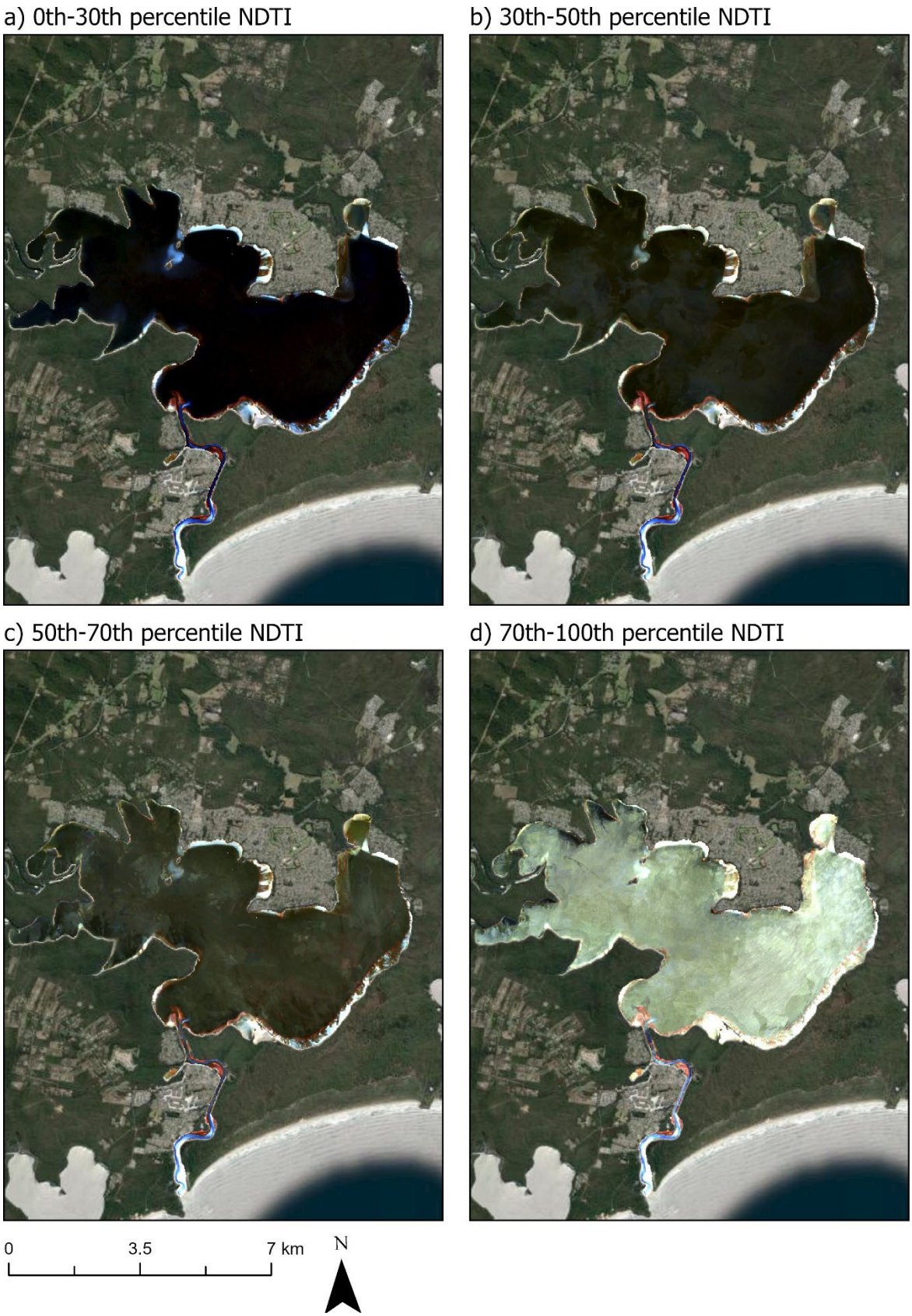

Figure G2. Median images of NDTI ranges for St Georges Basin, in red-edge false colour (RGB = RE, red, green). a) 0^{th}-30^{th} percentile NDTI, b) 30^{th}-50^{th} percentile NDTI, c) 50^{th}-70^{th} percentile NDTI, d) 70^{th}-100^{th} percentile NDTI

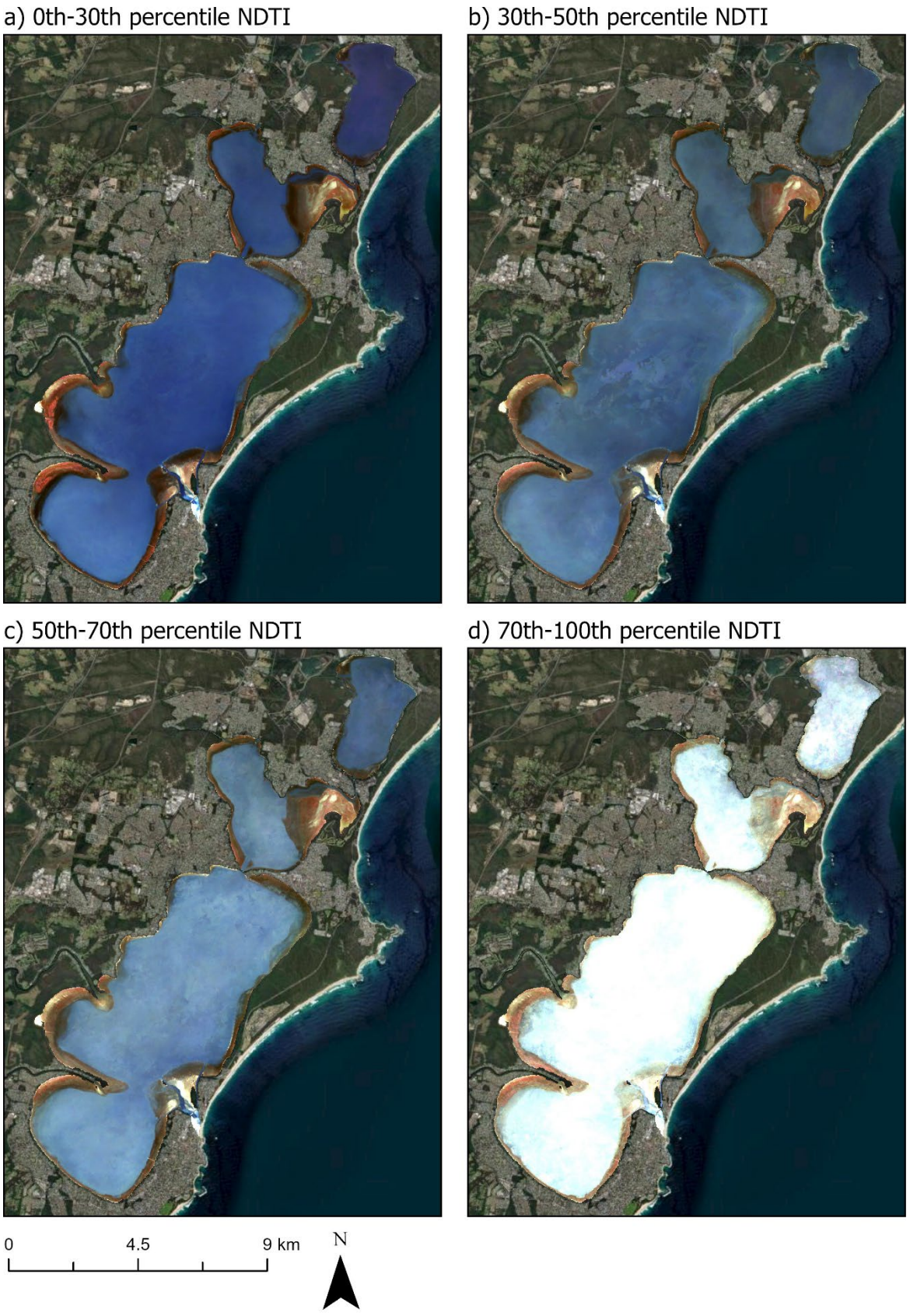

Figure G3. Median images of NDTI ranges for Tuggerah Lakes, in red-edge false colour (RGB = RE, red, green). a) 0^{th}-30^{th} percentile NDTI, b) 30^{th}-50^{th} percentile NDTI, c) 50^{th}-70^{th} percentile NDTI, d) 70^{th}-100^{th} percentile NDTI

Appendix H. Cover and cover variability maps (Chapter 6)

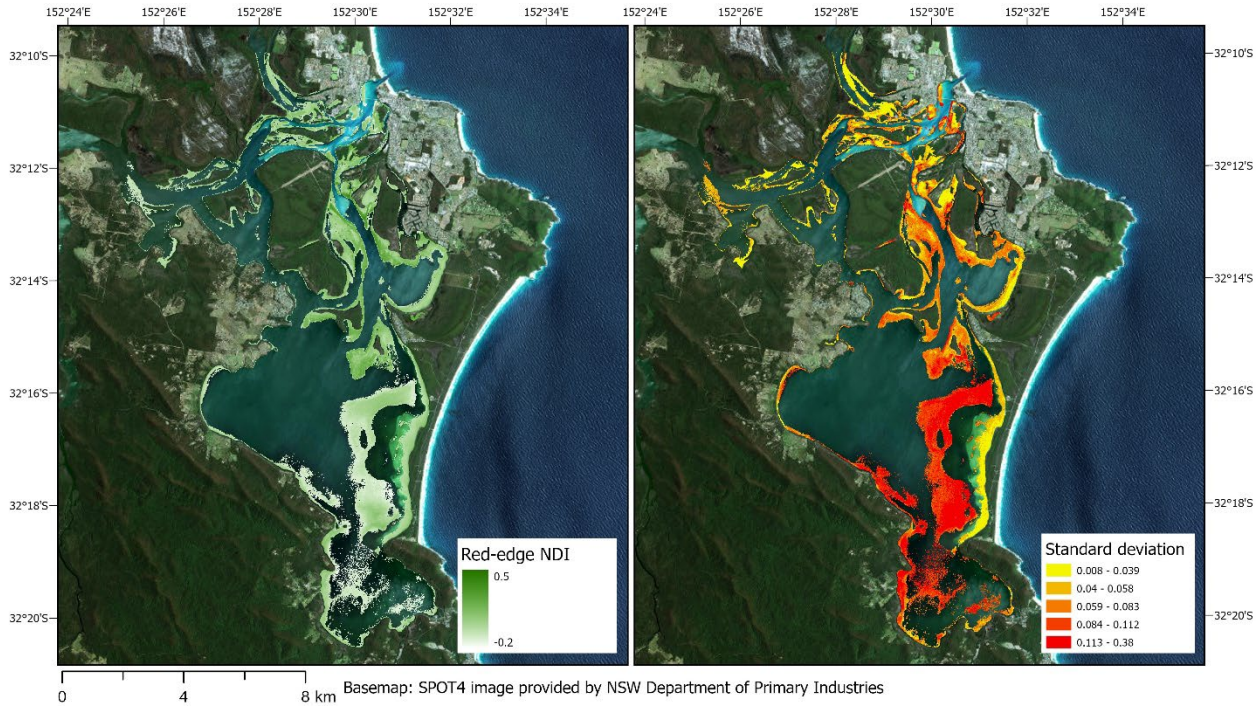

Figure H1. Maps of mean red-edge normalised difference index and standard deviation over the time series for Wallis Lake. RENDI is visualised as a continuous scale between -0.2 and 0.5. Standard deviation is visualised in quintiles.

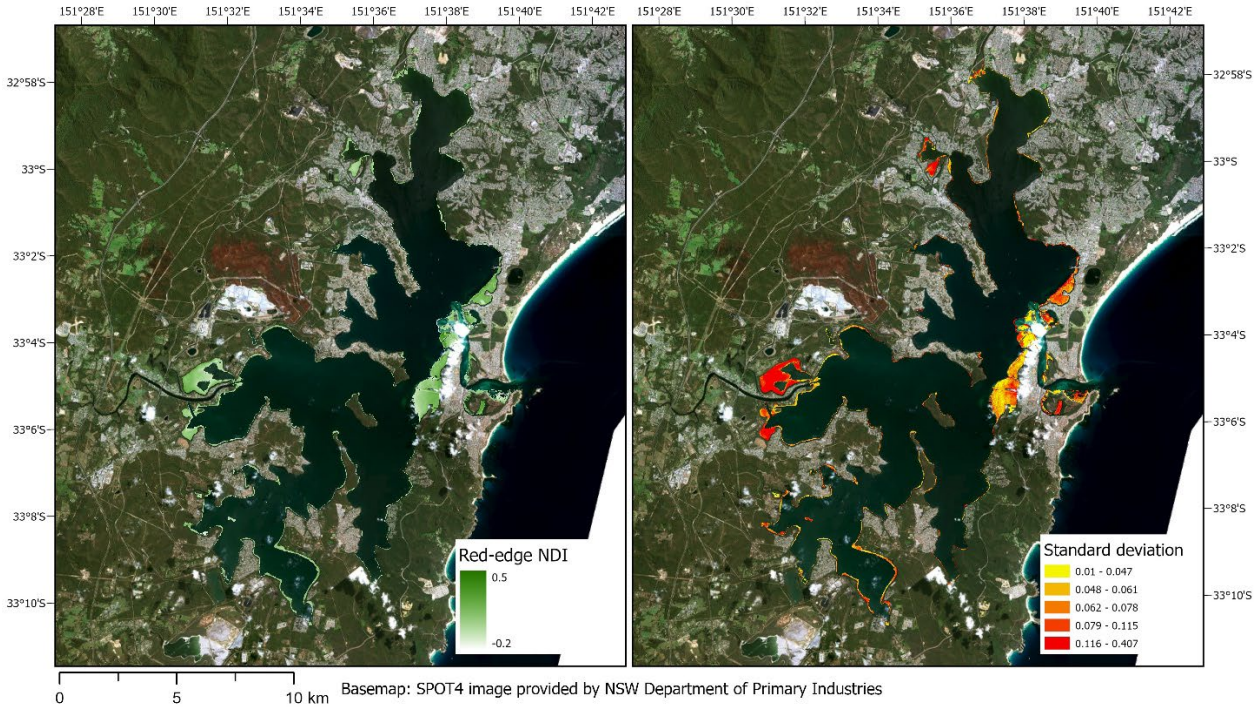

Figure H2. Maps of mean red-edge normalised difference index and standard deviation over the time series for Lake Macquarie. RENDI is visualised as a continuous scale between -0.2 and 0.5. Standard deviation is visualised in quintiles.

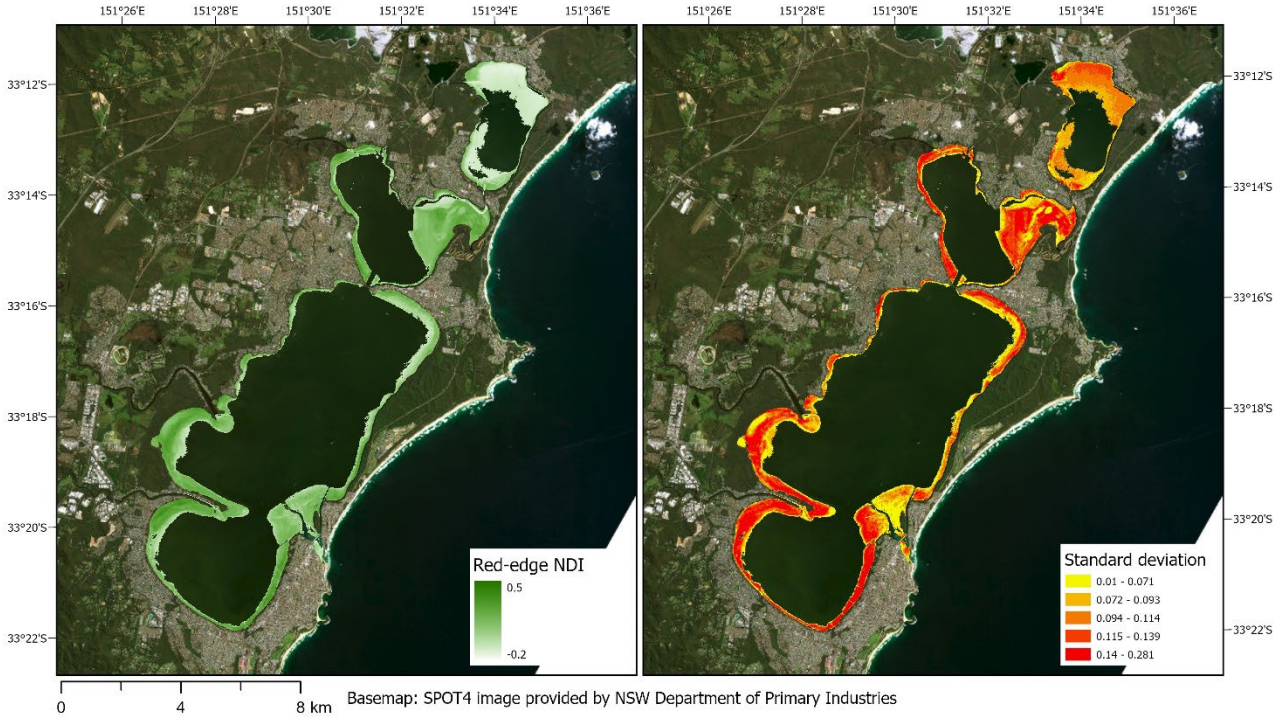

Figure H3. Maps of mean red-edge normalised difference index and standard deviation over the time series for Tuggerah Lakes. RENDI is visualised as a continuous scale between -0.2 and 0.5. Standard deviation is visualised in quintiles.

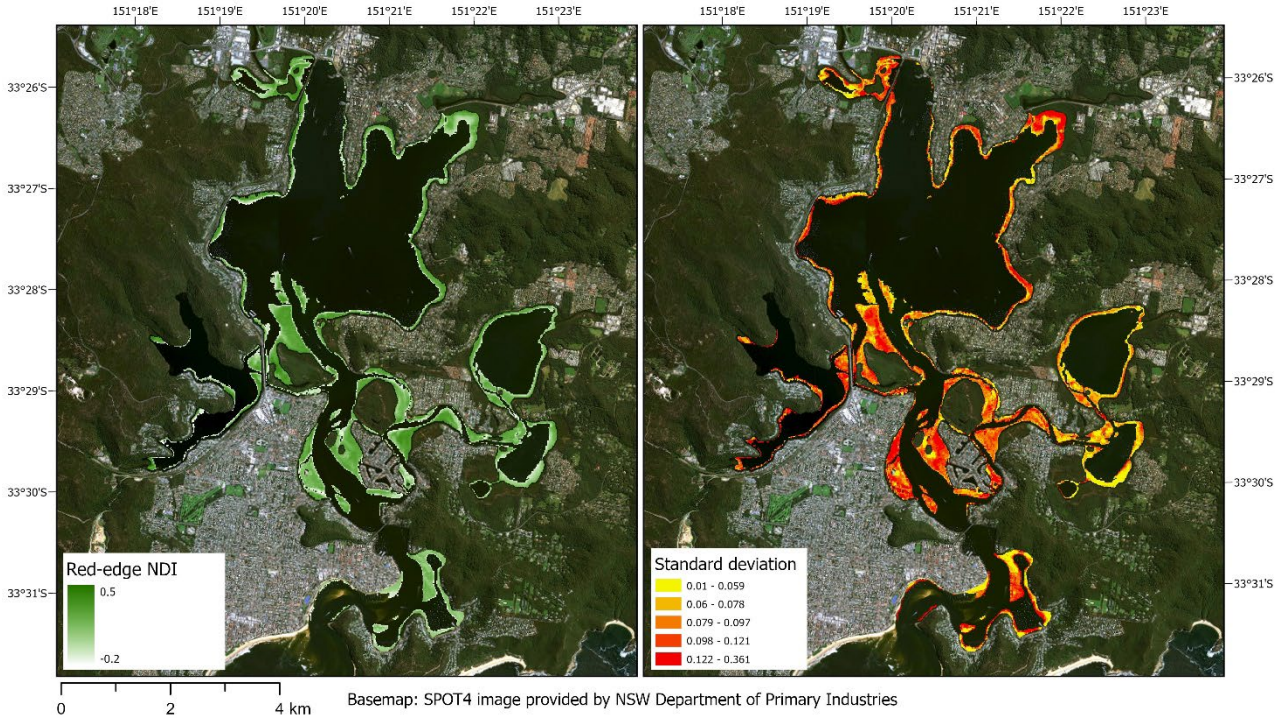

Figure H4. Maps of mean red-edge normalised difference index and standard deviation over the time series for Brisbane Water. RENDI is visualised as a continuous scale between -0.2 and 0.5. Standard deviation is visualised in quintiles.

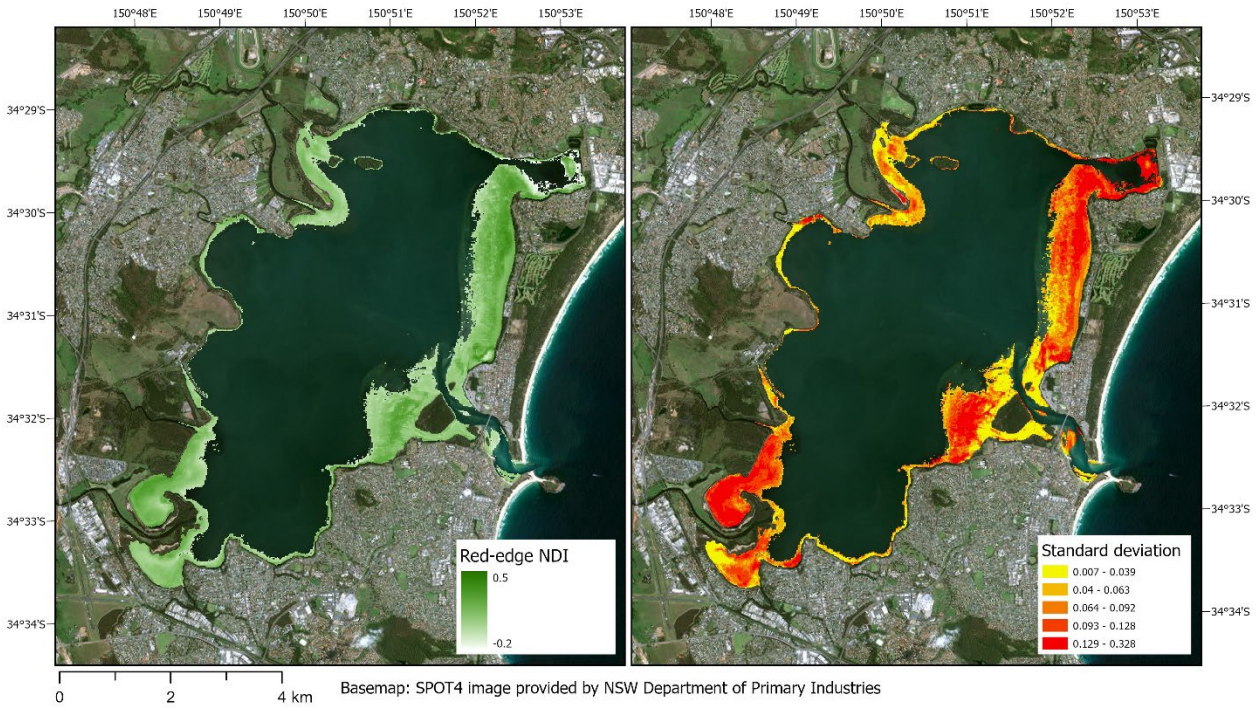

Figure H5. Maps of mean red-edge normalised difference index and standard deviation over the time series for Lake Illawarra. RENDI is visualised as a continuous scale between -0.2 and 0.5. Standard deviation is visualised in quintiles.

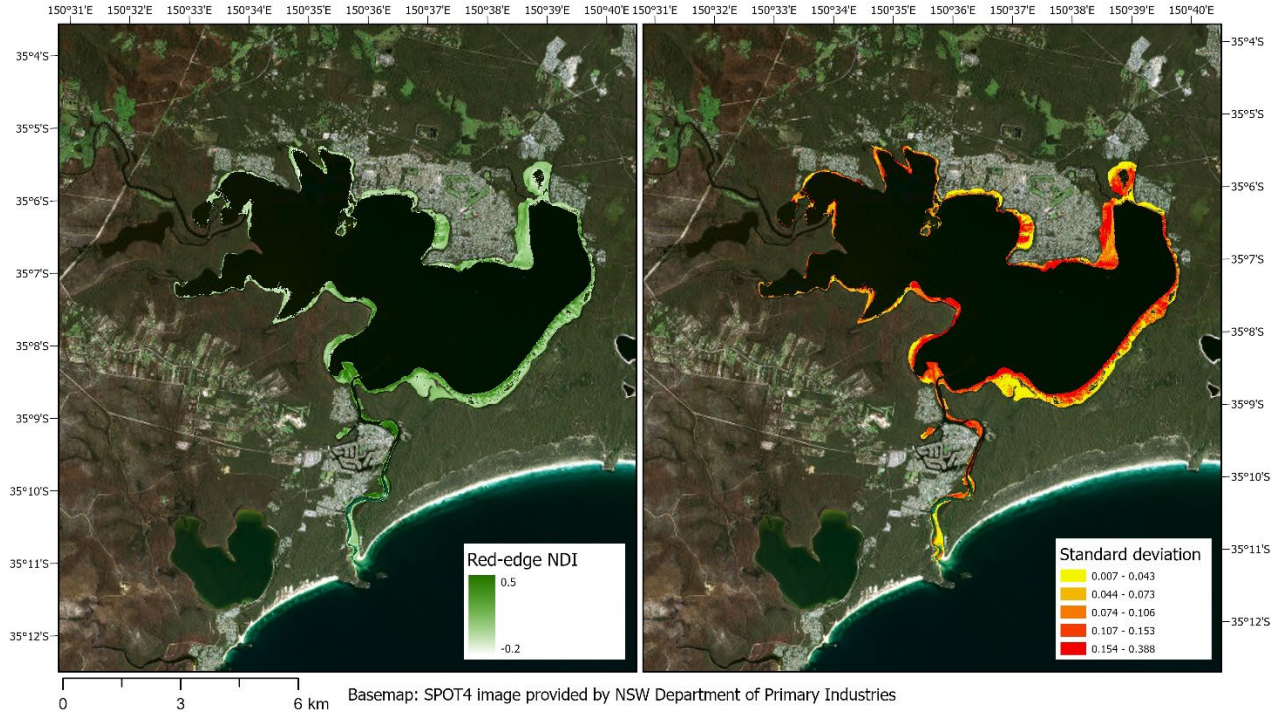

Figure H6. Maps of mean red-edge normalised difference index and standard deviation over the time series for St Georges Basin. RENDI is visualised as a continuous scale between -0.2 and 0.5. Standard deviation is visualised in quintiles.

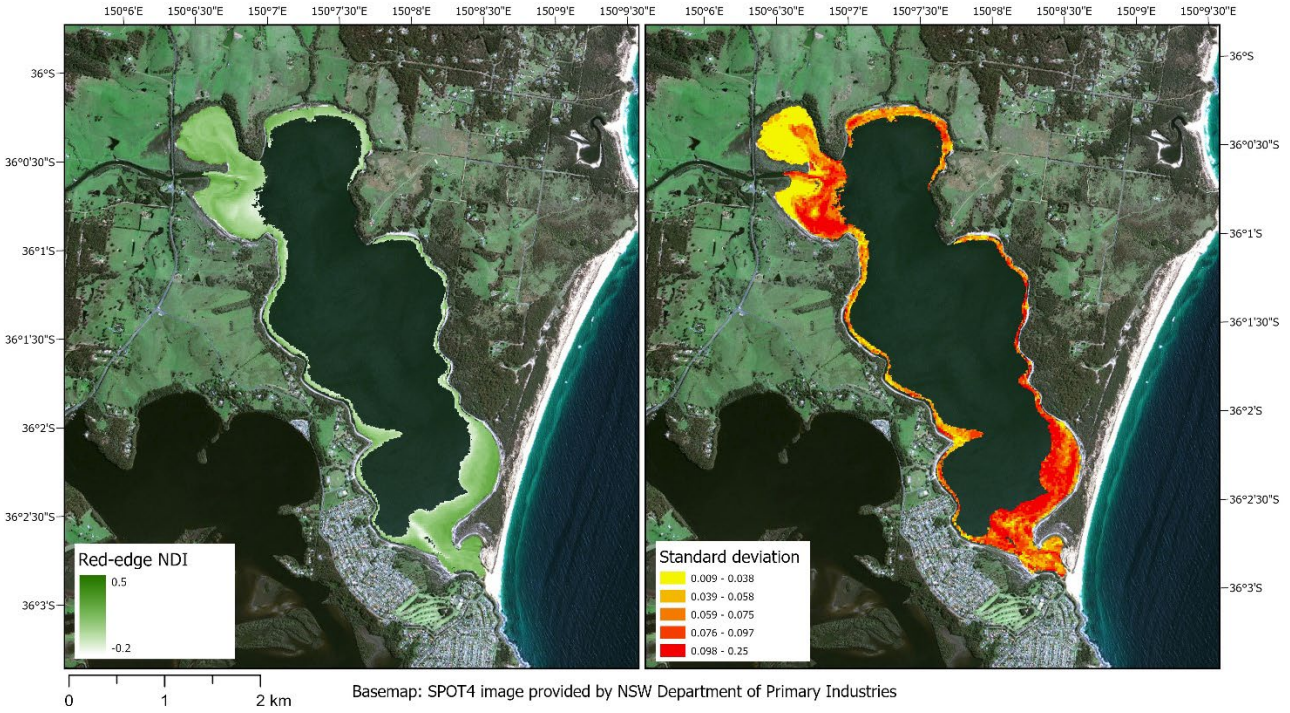

Figure H7. Maps of mean red-edge normalised difference index and standard deviation over the time series for Coila Lake. RENDI is visualised as a continuous scale between -0.2 and 0.5. Standard deviation is visualised in quintiles.

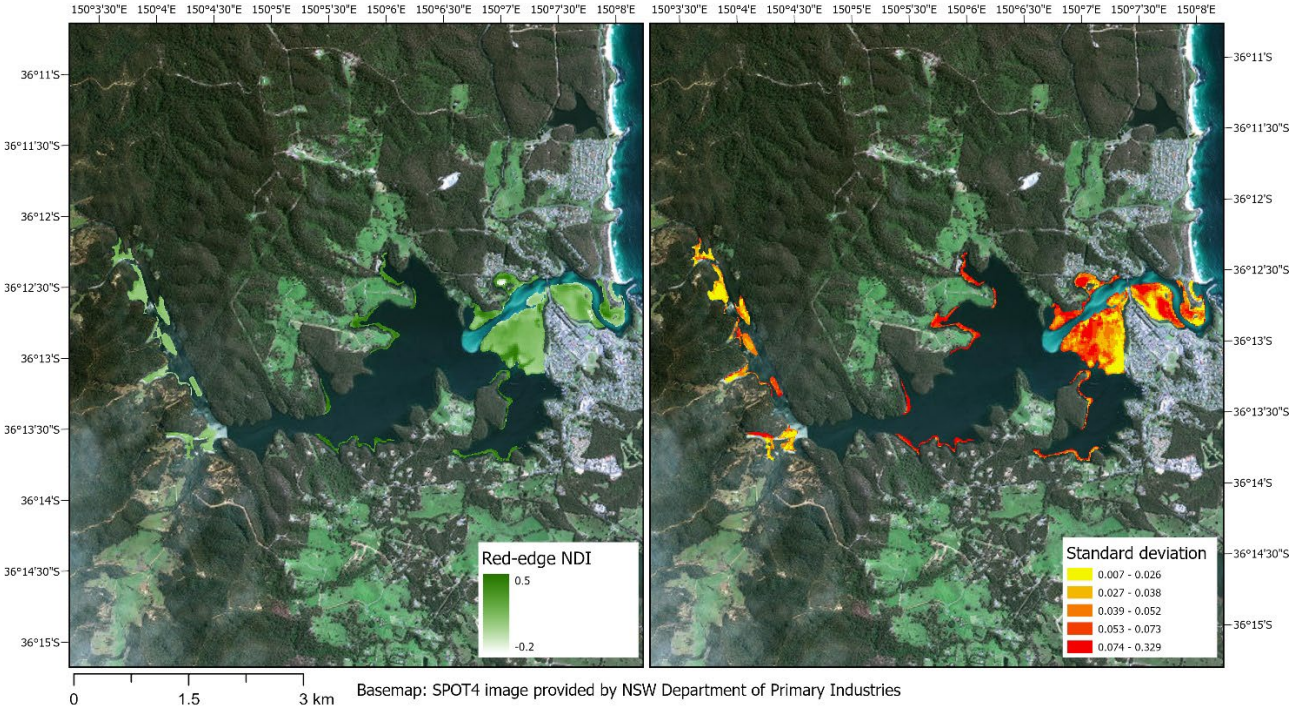

Figure H8. Maps of mean red-edge normalised difference index and standard deviation over the time series for Wagonga Inlet. RENDI is visualised as a continuous scale between -0.2 and 0.5. Standard deviation is visualised in quintiles.

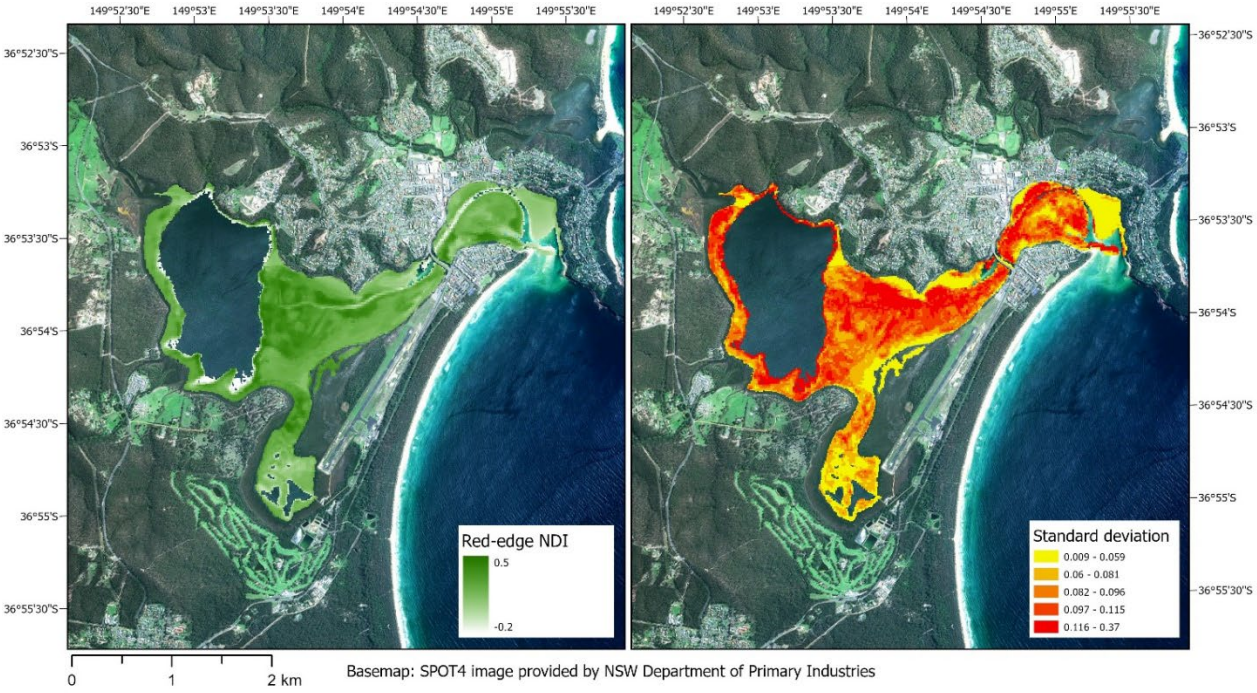

Figure H9. Maps of mean red-edge normalised difference index and standard deviation over the time series for Merimbula Lake. RENDI is visualised as a continuous scale between -0.2 and 0.5. Standard deviation is visualised in quintiles.